

IMPERIAL COLLEGE LONDON
NATURAL HISTORY MUSEUM, LONDON

PHD THESIS

UNDERSTANDING THE ORIGIN OF
METEORITIC MAGNETISM:
IMPLICATIONS FOR PROTOPLANETARY
DISK ACCRETION

Jay Shah

Supervised by

Dr Adrian R. MUXWORTHY

Dr Matthew J. GENGE

Prof Sara S. RUSSELL (NHM)

Submitted for the degree of Doctor of Philosophy at Imperial College London

Imperial College
London

N NATURAL
HISTORY
MUSEUM

December 8, 2017

Declaration of originality

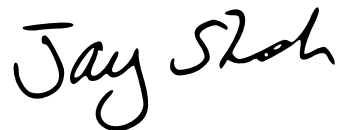
The work submitted in this thesis has been wholly produced by myself, and any supporting material or collaboration has been cited accordingly.

A handwritten signature in black ink that reads "Jay Shah". The letters are cursive and fluid, with the 'J' and 'S' being particularly prominent.

Jay Shah

Copyright declaration

The copyright of this thesis rests with the author and is made available under a Creative Commons Attribution Non-Commercial No Derivatives licence. Researchers are free to copy, distribute or transmit the thesis on the condition that they attribute it, that they do not use it for commercial purposes and that they do not alter, transform or build upon it. For any reuse or redistribution, researchers must make clear to others the licence terms of this work.

A handwritten signature in black ink that reads "Jay Shah". The letters are cursive and fluid, with the 'J' and 'S' being particularly prominent.

Jay Shah

Acknowledgements

I would first like to thank my supervisors Adrian Muxworthy, Matt Genge, and Sara Russell for providing continual support and encouragement throughout my PhD. I am especially thankful to Adrian for introducing me to rock magnetism all those years ago, and for the knowledge, time, and sage advice that he has given me since.

I thank Trevor Almeida, Ecaterina Ware, Mahmood Ardakani, and Catriona McGilvery at Imperial College London for teaching me how to use FIBs and TEMs, and Anton Kearsley, John Spratt, and Tomasz Goral at the NHM for teaching me how to use SEMs. I thank Trevor Almeida, Andras Kovács, Chris Boothroyd, Vadim Migunov, Martial Duchamp, Patrick Diehle, Jan Caron, Florian Winkler, Rafal Dunin-Borkowski for teaching and helping me with electron holography during my time at the Forschungszentrum Jülich, as well as Pascha, Asta, Magdalena, Sebastian, Arya, Helena, Baxter, Janghjun, and the Cool Kids of Jülich for making it some of the most enjoyable six months of my PhD. The work that I have done that stems from my time in Jülich in combination with the modelling, which I received invaluable help with from Wyn Williams, Lesleis Nagy, Pádraig Ó Conbhuí, and Miguel Valdez-Grijalva, has been something I am endlessly enthused by. I thank Wyn Williams for spending his own time and HPC facility time to conduct the high-temperature micromagnetic simulations presented in this thesis.

I am grateful to Farah Ahmed for granting me CT time, and Rebecca Summerfield, Dan Sykes, and Natasha Almeida at the Natural History Museum for their assistance with imaging, analysis, and pumping some great lab music. The CT project gave me the opportunity to supervise Helena Bates, who was possibly the best MSci student one could ask for. I also had the privilege of being apart of the Meteorites group at the NHM, and while as a palaeomagician it can often feel like you're preaching a dark art to the meteoriticists, the group at the NHM were always understanding and inquisitive. I thank Natasha Stephen, Natasha Almeida, Ashley King, Jenny Claydon, Penny Wozniakiewicz, and Epi Vaccaro for showing me the ropes in the early days and back at my first MetSoc meeting. I thank Sara Russell,

Caroline Smith, and Natasha Almeida for kindly spending time digging through the collections to loan me the best samples in the Solar System.

I thank Richard Harrison, Ioan Lascu, and the rest of the Nanopaleomagnetism group at the University of Cambridge for allowing me to visit and measure Bishunpur with their MTJ microscope. Unfortunately we were unable to invert the data, and I hope to be able to revisit this in the future. I thank Chuang Xuan and Tim van Peer at the University of Southampton for allowing me to use their SQUID magnetometer. I thank Conal Mac Niocaill at the University of Oxford for allowing me to use their SQUID magnetometer.

From Sam Taylor, Nick Wainwright, Jack Ashley, and Sally Scourfield just before I started my PhD to Trevor Almeida, Susie Maidment, Mathias van Ginneken, Anita di Chiara, Arne Dossing, Rabiul Abubakhar, Sarah Dodd, Tom Berndt, Miguel Valdez-Grijalva, Aike Supakulapos, Sope Badejo, and Charlie Penny since, the Natural Magnetism Group has seen a lot of people go through it during my seemingly eternal time at Imperial. They have always been happy to help, motivate, and inspire; magnetism does indeed attract the best bunch.

Huge credit to my officemates Alistair, twowine, Tom, Mosayeb, Rabia, and Martin for maintaining such an entertaining and caffeinated pod. It is thanks to my endless stint at Imperial that I have had the chance to meet so many stimulating minds, with whom I have had countless productive discussions (usually at Fribes). Thanks to Matt Loader for birthing Fribes, and especially to Tom Phillips and Alex Perrin; together we took it to unprecedented heights.

The people outside of my office and lab have played as important a role throughout my PhD by always being supportive and ensuring spirits are high. I'm especially thankful to Chris, Chris, yza, Ron, Niko, Jack, pyg, James, Tom, Amelia, Archie, Nat, Megan, Grace, Pez, Natasha, Trevor, Phil, John, Craig, Carl, Janice, Miriam, Pete, Naomi, Tim, Omar, and my sax teacher Greg. I'm grateful for Oakley, Mirabel, and Colehill, and all those that have made them such sanctuaries.

I thank my family for being supportive and encouraging throughout.

Abstract

Chondritic meteorites largely formed 4.6 billion years ago, and can range from being metamorphosed as a result of processing on their asteroid parent bodies to entirely unaltered since their formation in the protoplanetary disk. The magnetic grains within these meteorites can potentially record and retain the magnetic conditions on the parent body and the conditions in the protoplanetary disk during the formation of our planetary system. However, the complex history of these meteorites can make their magnetic records difficult to interpret, and their age prompts the question of whether a magnetic remanence can be retained for so long.

In this thesis, to help identify the origin of the magnetic remanence, a new method for the palaeomagnetic conglomerate test that uses micro-CT scans to accurately mutually orient chondrules from chondrites was developed. When applied to Vigarano (CV3) and Bjurböle (L/LL4), a more in-depth understanding of parent body processing was achieved that provides evidence for magnetic dynamo activity on their parent bodies.

To understand the magnetic record of CK chondrites, a palaeomagnetic analysis of Karoonda (CK4) was conducted, and found no evidence of a significant magnetic field recording, supporting the solar radiative heating model for the CV-CK chondrites.

To determine whether magnetic remanence can be retained from the early Solar System, the high thermal stability of single and multi-vortex kamacite grains from Bishunpur (LL3.1) was demonstrated by performing in-situ temperature-dependent nanometric magnetic measurements using electron holography and numerical micromagnetic energy barrier calculations. This study found that the majority of kamacite grains in dusty olivines are capable of retaining magnetic field information from the early Solar System, a key finding in our quest to understand the formation of our Solar System.

Thesis contents

List of Figures	8
List of Tables	10
1 Introduction to meteorites and magnetism	11
1.1 Introduction to the thesis	11
1.2 Meteorites	12
1.2.1 Meteorite parent bodies	12
1.2.2 Chondrules	15
1.2.3 Chondrule formation processes	16
1.2.4 Parent body accretion	24
1.3 Palaeomagnetism and rock magnetism	27
1.3.1 Ferromagnetism	27
1.3.2 Domain theory	28
1.3.3 Magnetic relaxation	29
1.3.4 Magnetic remanence	31
1.3.5 Magnetic hysteresis	34
1.4 Meteoritic magnetism	36
1.4.1 Magnetic properties of meteorites	36
1.4.2 Determining the magnetic mineralogy	37
1.4.3 Palaeointensity determination for meteorites	38
1.4.4 Dusty olivine	40
1.4.5 Origin of meteorite magnetic remanence	46
1.4.6 Brief history of meteoritic magnetism	49
1.5 Thesis objectives and layout	52
2 The natural remanence of metamorphosed chondrite Karoonda	54
2.1 Introduction	54
2.2 Methods	61
2.2.1 Rock magnetic measurements	62
2.2.2 Magnetic remanence measurements	62
2.3 Results	63
2.3.1 Rock magnetic measurements	63
2.3.2 Magnetic remanence measurements	63
2.4 Discussion	65
2.4.1 Natural and anhysteretic remanence properties	65
2.4.2 Implications for the origin of Karoonda's magnetisation	67
2.5 Conclusion	70
2.5.1 Acknowledgements and contributions	71
3 Long-lived magnetism on chondrite parent bodies	72
3.1 Introduction	73
3.2 Samples	75
3.2.1 Bjurböle (L/LL4)	75
3.2.2 Vigarano (CV3)	77
3.3 Methods	79

3.3.1	Meteorite disaggregation	80
3.3.2	Microcomputed X-ray tomography	80
3.3.3	Magnetic measurements	82
3.4	Results	84
3.4.1	Micro-CT scanning and in-situ alignment	84
3.4.2	Rock magnetic properties	84
3.4.3	Magnetic remanence measurements	87
3.5	Discussion	91
3.5.1	Conglomerate test	91
3.5.2	Origin of Bjurböle’s remanent magnetisation	93
3.5.3	Origin of Vigarano’s remanent magnetisation	95
3.5.4	Implications for parent body magnetism	97
3.5.5	Conclusions	99
3.5.6	Acknowledgements and contributions	101
4	Nanomagnetic imaging of dusty olivine	102
4.1	Introduction	102
4.1.1	Bishunpur	105
4.2	Methods and sample preparation	105
4.2.1	Scanning electron microscopy	106
4.2.2	Focused ion beam scanning electron microscopy	107
4.2.3	Transmission electron microscopy	109
4.2.4	Off-axis electron holography	110
4.2.5	Numerical modelling	116
4.3	Results	116
4.3.1	Chemical analysis	116
4.3.2	Room-temperature off-axis electron holography	118
4.3.3	Temperature-dependent off-axis electron holography	120
4.4	Discussion	124
4.4.1	Chemical and physical properties of Bishunpur dusty olivine	125
4.4.2	Electron holography	126
4.5	Conclusions	128
4.5.1	Acknowledgements and contributions	130
5	Micromagnetic modelling of dusty olivine	131
5.1	Introduction	131
5.2	Methods	135
5.3	Results	137
5.3.1	Local energy minima for iron	137
5.3.2	Nudged elastic band modelling iron	140
5.4	Discussion	143
5.4.1	Uniform magnetisation	144
5.4.2	Non-uniform magnetisation	145
5.4.3	Dusty olivine as a credible recorder of pre-accretionary remanence	147
5.4.4	Implications for protoplanetary disk magnetic fields	148
5.5	Conclusions	149
5.5.1	Acknowledgements and contributions	150
6	Conclusions and future research	151
6.1	Conclusions and summary	151
6.2	Future research	155
	Bibliography	159

List of Figures

1.1	An early model of a meteorite parent body.	13
1.2	Models of meteorite parent bodies.	15
1.3	Schematic of chondrule textures and corresponding formation mechanisms.	16
1.4	Schematic of chondrule formation mechanisms.	18
1.5	Ferromagnetism and ferrimagnetism.	28
1.6	Schematic diagrams of domain structures.	29
1.7	Example of a hysteresis loop.	34
1.8	The construction of first-order reversal curves.	35
1.9	Dusty olivine in Semarkona.	41
1.10	Synthetic dusty olivine.	42
1.11	Dusty olivine in Bishunpur.	42
1.12	Hysteresis loop and FORC diagram of synthetic dusty olivine.	43
1.13	Magnetic induction maps for synthetic dusty olivine.	44
1.14	Remanence states for Semarkona dusty olivine kamacite calculated using micromagnetic modelling.	46
1.15	Domain state transitions for magnetite and iron.	46
1.16	A timeline for the early Solar System development.	53
2.1	Schematic of the CV-CK partially differentiated parent body model.	55
2.2	Demagnetisation of Karoonda.	57
2.3	NRM-ARM plot for Karoonda.	59
2.4	First-order reversal curve for Karoonda.	60
2.5	Hysteresis loop for a sub-sample of KR02 from Karoonda.	63
2.6	First-order reversal curve for Karoonda.	64
2.7	Demagnetisation of Karoonda's NRM and ARM.	66
3.1	Schematic of a conglomerate magnetised pre- and post-accretion.	75
3.2	Formation history of Vigarano.	79
3.3	Schematic diagram of micro-CT data acquisition.	81
3.4	micro-CT scan slice of Bjurböle.	85
3.5	Day plot for Bjurböle and Vigarano chondrules.	88
3.6	Representative FORC diagrams for Bjurböle and Vigarano chondrules.	88
3.7	Demagnetisation plots for Bjurböle and Vigarano chondrules.	90
3.8	Equal-area projections of ChRM directions for Bjurböle and Vigarano chondrules.	91
3.9	Schematic formation scenario for Bjurböle.	95
3.10	Schematic formation scenario for Vigarano.	98
4.1	SEM image of Bishunpur.	107
4.2	SEM image of dusty olivine in Bishunpur.	108
4.3	SEM image of dusty olivine in Bishunpur.	109
4.4	FIB-milling procedure to prepare TEM lamellae.	110
4.5	FIB-milling procedure to prepare TEM lamellae for <i>in-situ</i> heating.	111

4.6	The excavated site after preparation of a TEM lamella from Bishunpur dusty olivine.	112
4.7	Schematic diagram of a TEM equipped to perform off-axis electron holography.	113
4.8	The procedure for creating magnetic induction maps using the Semper image processing program.	115
4.9	Chemical analysis of Bishunpur dusty olivine.	117
4.10	Magnetic induction map of a kamacite grain from Bishunpur dusty olivine.	118
4.11	Magnetic induction maps of a kamacite grains from Bishunpur dusty olivine.	119
4.12	Temperature-dependent electron holography of Bishunpur dusty olivine kamacite.	121
4.13	Chemical alteration of Bishunpur dusty olivine.	122
4.14	Micromagnetic modelling of high-temperature dusty olivine kamacite multi-vortex magnetisation structures.	123
4.15	Energy barrier between modelled high-temperature dusty olivine kamacite multi-vortex magnetisation states.	124
5.1	Magnetic induction maps and micromagnetic solutions for iron nanocubes.	133
5.2	Domain state phase diagram for parallelepipeds of metallic iron.	135
5.3	Magnetisation states for iron nanocubes determined by micromagnetic modelling.	138
5.4	Magnetisation states for iron parallelepipeds of 1.5 axial ratio determined by micromagnetic modelling.	139
5.5	Magnetisation states for iron parallelepipeds of 1.7 axial ratio determined by micromagnetic modelling.	139
5.6	The energy along the path between two global energy minimum (GEM) magnetisation states.	141
5.7	Relaxation times for iron parallelepipeds determined by micromagnetic modelling.	142

List of Tables

1.1	Chondrite physical properties.	17
2.1	Mass, NRM, ARM, and MDF for Karoonda.	65
3.1	Hysteresis parameters for Bjurböle and Vigarano chondrules.	86
3.2	Remanence data and palaeointensity estimates for Bjurböle and Vigarano chondrules.	92
5.1	Relaxation times and GEM magnetisation states for iron parallelepipeds.	140

Chapter 1

Introduction to meteorites and magnetism

1.1 Introduction to the thesis

It was once standard procedure to identify meteorites in the field using a hand magnet, however, modern meteorite collection methods typically try to preserve the natural remanent magnetisation carried by meteorites (Weiss et al., 2010b). The age and origin of the natural magnetic remanence carried by these extraterrestrial materials is often far more complex than that which is found in terrestrial rocks, which are normally well understood in terms of their origin and formation histories (Fu et al., 2014a; Dodd et al., 2015; Muxworthy et al., 2017). Our understanding of early Solar System dynamics and the degree of planetesimal differentiation is still limited (Elkins-Tanton et al., 2011; Sterenborg and Crowley, 2013; Scheinberg et al., 2016), and there are numerous conflicting theories attempting to explain these ancient processes, which are typically difficult to comprehend (Mann et al., 2016; Matsumoto et al., 2017; Wakita et al., 2017). The magnetic record in meteorites develops our understanding of both early Solar System dynamics and the planetary bodies they sample (Fu et al., 2014b; Gattacceca et al., 2016; Wang et al., 2017). However, there are limited palaeomagnetic data for meteorites, and magnetic evidence of-

ten contradicts geochemical evidence for the history of planetesimal differentiation (Carpurzen et al., 2011b; Dunn et al., 2016); more robust data is required, as well as a greater understanding of the origin and nature of magnetisation acquisition. In this thesis, the origin of magnetic remanence observed in common chondritic meteorites is analysed and scrutinised for credibility and recording fidelity by combining a variety of interdisciplinary techniques that include microcomputed tomography, electron microscopy and micromagnetic modelling in conjunction with traditional palaeomagnetic techniques that analyse magnetic remanence and rock magnetic properties.

1.2 Meteorites

1.2.1 Meteorite parent bodies

Early meteoriticists hypothesised that all meteorites originated from a single, or a few Moon-sized partially differentiated parent bodies (Fig. 1.1, 1.2a) (Wahl, 1952; Wood, 1958). Wahl (1952) studied several polymict breccias containing chondritic and achondritic clasts, and suggested through petrographic evidence that all constituents of the breccia originated from the same parent body, and Wood (1958) conducted an extensive geological and geochemical analysis of chondritic, achondritic, stony-iron, and iron meteorites to deduce a single-parent body origin for meteorites of different classes. Based on observations that meteorites were largely analogous to terrestrially formed rocks, Wood (1958) hypothesised a ‘central-heating model’: a 1000-2000 km (slightly smaller than the Moon) homogeneous sphere composed of chondrules and dust at a high temperature due to impacts during accretion (Fig. 1.1). Subsequent outward cooling and internal heating driven by radioactive decay results in melting of the interior 50% of the body, and separating out a central liquid iron phase, an overlying liquid troilite phase, and a liquid silicate phase between that and an unmelted chondritic ‘crust’. Following a period of cooling, crystallisation of silicate magmas as olivines and pyroxenes, forming thick chassignite

(later found to be a Martian meteorite (Smith et al., 1984)) and diogenite (HED meteorites) left the remaining liquid of eucritic composition. Iron meteorites are explained in the model by crystallisation of the iron core, and eucrites are intruded into faulted chondritic crust as dikes.

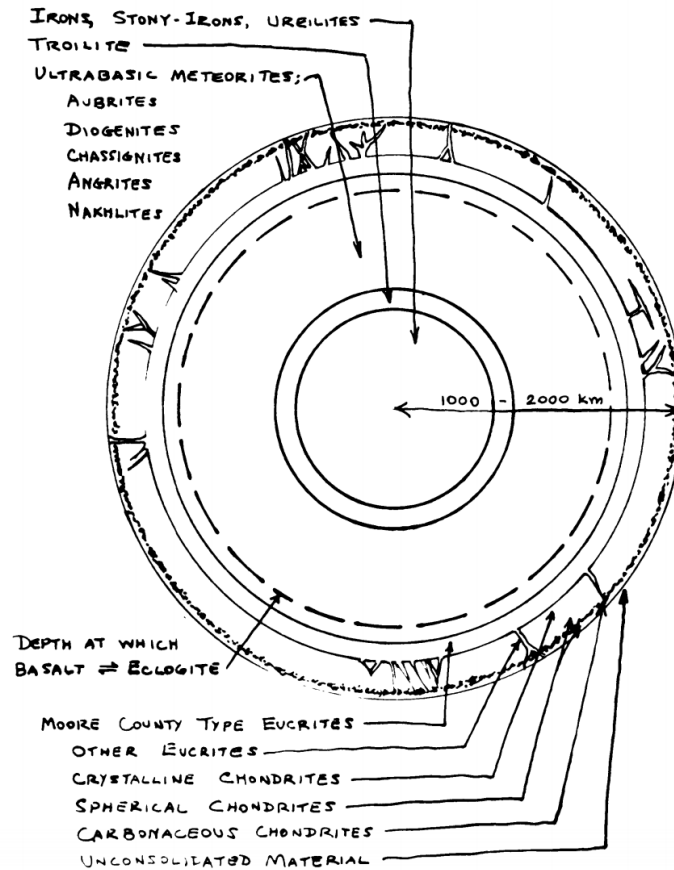


Figure 1.1: Model of the parent body for the various types of meteorites studied by (Wood, 1958). From (Wood, 1958).

There are flaws to the single-body origin, however, for example, Wood (1958) is unable to fit a variety of meteorite types into the single-parent central-heating model, such as enstatite chondrites and stony-irons. Unified parent body theories have since fallen out of favour with mounting geochemical and petrological evidence for heterogeneous meteorite origins. Substantially differing isotopic compositions in meteorite breccias (Clayton and Mayeda, 1978), and that the breccias are associated with shock processes (Bischoff and Stöfler, 1992) indicated that the meteorite breccias like those observed by Wahl (1952) are unlikely to have originated from a single parent body. The variation in the isotopic compositions of meteorites is

significant in itself; the variation between the different meteorite classes present in our record is not continuous, and this is the case for most physical and chemical properties of meteorites (e.g. discrete variation between classes in Table 1.1). Anders (1964) considered the unlikelihood of certain ‘difficult’ transformations, such as the possibility of a Type 1 carbonaceous chondrite being able to transform to a hypersthene chondrite on a single planetary body. For this transformation to occur, water, sulphur, carbon, 30% of Fe, 15% of Mg, and 80% of 10 to 15 trace elements must all be lost, Pb, Bi, and Tl must be depleted by a factor of 1000, and depletions of heavy isotopes of carbon by 3‰ and oxygen by 13‰ (Anders, 1964). Given the numerous studies that present the geochemical and petrologic heterogeneity and variety amongst meteorite classes, it seems unlikely that meteorites originated from one or two Moon-sized planetesimals.

Further evidence from spectral reflectivity indicates that meteorites originate from multiple asteroids (McCord et al., 1970). Five of the ~ 135 meteorite classes have been related to probable parent bodies (Fieber-Beyer and Gaffey, 2014): (4) Vesta (HEDs), (3103) Eger (enstatite achondrites/aubrites), (6) Hebe (H chondrites and IIE iron meteorites), and the Maria Asteroid Family (mesosiderites) (McCord et al., 1970; Gaffey et al., 1992; Gaffey and Gilbert, 1998; Fieber-Beyer et al., 2011). Recent work by Fieber-Beyer and Gaffey (2014), extending the work by Vilas and McFadden (1992) suggests that (1722) Goffin is a possible parent body for the L-type ordinary chondrites.

The spectral diversity amongst the asteroid belt arising from mineralogical variations indicates that these asteroid meteorite parent bodies are predicted to be either differentiated, partially differentiated, or entirely undifferentiated. The degree of differentiation depends upon formation age and accretion rate, which control the short-lived radiogenic isotope ^{26}Al content necessary for heating (Urey, 1955). Meteorite isotope systems have evidenced rapid accretion and differentiation occurring in bodies forming early in the early Solar System, when ^{26}Al was most abundant (Lee and Halliday, 1996; Baker et al., 2005). The magnetism recorded by chondrite

and achondrite classes such as the CV chondrites and the angrites evidence possible magnetic activity on their parent bodies, which would suggest that they were partially differentiated (Weiss et al., 2008; Elkins-Tanton et al., 2011; Gattacceca et al., 2016).

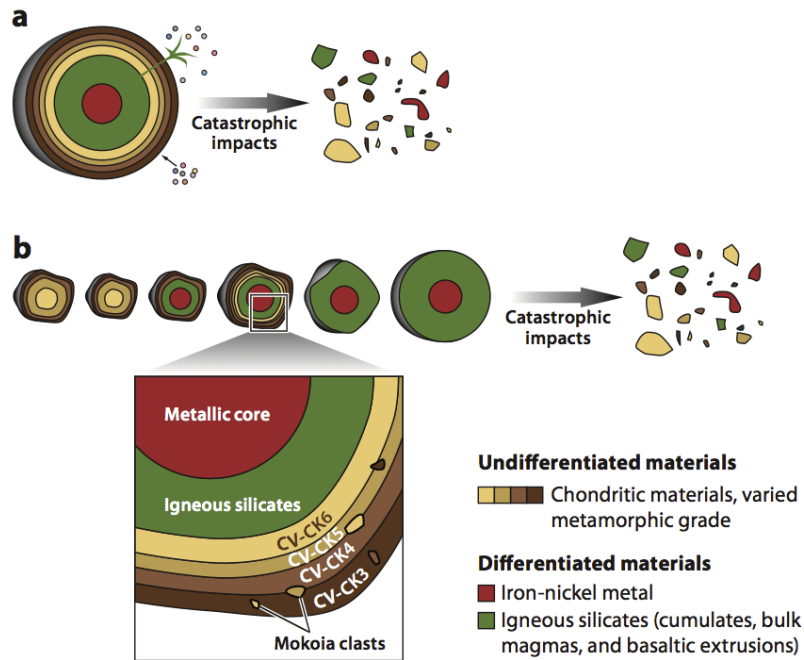


Figure 1.2: Models of meteorite parent bodies. (a) All meteorites originated from one or a few Moon-sized partially differentiated planetesimals (Wood, 1958). (b) All meteorites originated from multiple asteroid-sized fully and partially differentiated, and fully undifferentiated bodies (Anders and Goles, 1961). From Weiss and Elkins-Tanton (2013)

1.2.2 Chondrules

Chondrules, mm-scale spherical particles, are one of the main constituents within meteorites, with abundances of up to 75% in some chondrite classes (Table 1.1). They are largely composed of olivine and pyroxene in a glass matrix, and can also contain metallic Fe alloys and sulphides. In order to begin understanding Solar System formation processes and conditions, we must first understand how chondrules were formed in the early Solar System. There is a lack of a consensus amongst the scientific community for a chondrule formation mechanism, and there are in excess of 60 theories to which there is an almost infinite number of variants (Sears, 2004). There are various constraints on conditions that would have been required to form

chondrules: heating a precursor of the 1 mm-scale from 1000 K to approximately 1800 K, and then cooling at rates of 100-1000 K h⁻¹ (Hewins and Radomsky, 1990); heating to approximately 2000 K and then cooling at rates of 5000 K h⁻¹ to 1500-1800 K to form barred olivine textures (Tsuchiyama et al., 2004); Alexander et al. (2008) observed that the presence of Na and volatiles in chondrules requires a low starting temperature of approximately 650 K, and high densities of solids and rapid processing to not deplete them (McNally et al., 2013). Fig. 1.3 illustrates various chondrule textures and possible mechanisms for their formation. We are able to determine these constraints through analysis of physical chondrule samples and mathematical models of the early Solar System, and theories on chondrule formation are generally split into nebular processes or impact melt processes to attempt to fit these requirements. These theories have similar respective underlying principles, which I review here, in Section 1.2.3.

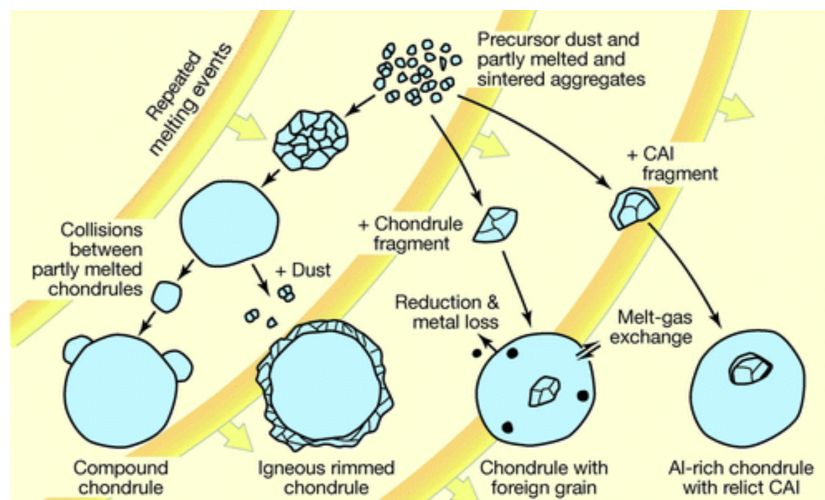


Figure 1.3: Schematic diagram of the melting events necessary to result in various chondrule textures. From Scott (2007).

1.2.3 Chondrule formation processes

Method 1: Nebular shock

Chondrule formation by a nebular shock mechanism (Fig. 1.4a) to flash heat nebular dust is a popular theory, and may be the most plausible theory, however the mechanism to produce shock waves is still debated.

Table 1.1: Physical and compositional properties of enstatite, ordinary, and carbonaceous chondrite classes. Table from Sears (2004).

	EH	EL	H	L	LL	R	CK	CV	CO	CH	CR	CM	CI
Physical properties													
Chondrule diam.	0.2-0.6	0.8	0.3	0.7	0.9	0.4	0.7	1	0.2-0.3	<0.1	0.8	0.3	-
Metal grain size	-	-	0.2	0.18	0.14	-	-	-	-	6	-	-	-
Chondrule abund.	20-40	0-40	65-75	65-75	65-75	≥40	15	35-45	35-40	~70	52	~15	0
Metal abund.	22	18	16	6	2	0.1	<0.01	0-7	0-5	20	6.3	0	0
Matrix abund.	<5	<5	10-15	10-15	10-15	35	75	40-50	30-40	5	44	~60	100
Compositional properties													
Carbon	0.42	0.32	0.11	0.12	0.22	-	0.1	0.43	0.38	-	1.97	1.82	2.8
Water	1.9	1.6	0.22	0.46	0.71	-	1.6	0.25	3.3	-	7.11	10.4	16.9
Fe _m /Fe _t	0.76	0.83	0.58	0.29	0.11	~0	~0	0-0.3	0-0.2	0.95	0.22	0	0
Mg/Si	0.77	0.83	0.96	0.93	0.94	-	1.13	1.07	1.05	1.02	1.06	1.05	1.05
Ca/Si	0.035	0.038	0.05	0.046	0.049	-	0.068	0.084	0.067	0.017	0.06	0.068	0.064
δ ¹⁷ O	3	2.7	2.9	3.5	3.9	5.27	-5	~4.0	~5.1	~1.3	~-0.7	~4.0	~8.8
δ ¹⁸ O	5.6	5.3	4.1	4.6	4.9	4.74	-1	~0	~-1.1	~0	~2	~12.2	~16.4

Units: chondrule diameter and metal grain size, mm; chondrule and matrix abundance, vol. %; metal, carbon, and water abundance, wt %; Fe_m/Fe_t, Mg/Si, and Ca/Si, atom ratio; δ¹⁷O and δ¹⁸O, per mil.

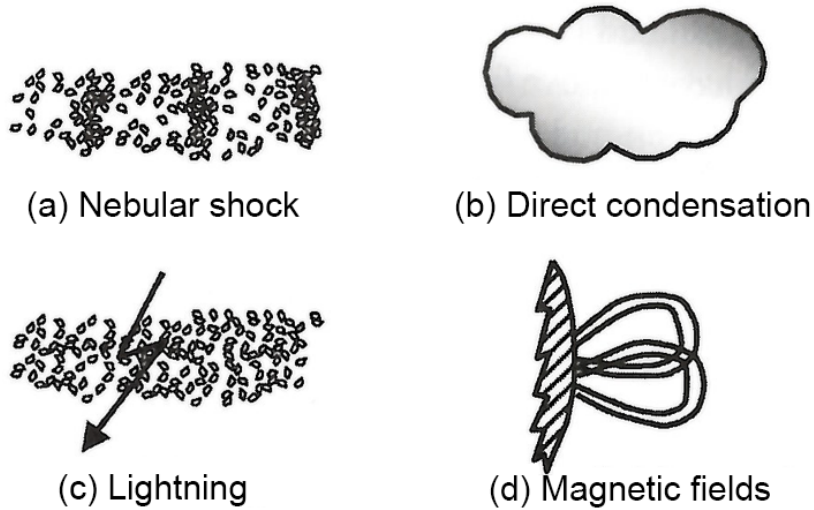


Figure 1.4: Models of chondrule formation processes in the Solar Nebula. (a) Chondrules formed as a result of shock processes in the Solar Nebula (Hood and Horanyi, 1991). (b) Chondrules formed due to solar gas condensing (Wood, 1963). (c) Chondrules formed from dust in the Solar Nebula melted by discharges of lightning (Whipple, 1966). (d) Chondrules formed due to processes driven by magnetic fields (Shu et al., 1996). From Sears (2004).

X-ray flares are generated frequently during the young, high-energy T-Tauri phase of a star, and Feigelson and Montmerle (1999) suggested that these may be responsible for chondrule melting. The activity of these X-ray flares with energy sufficient to form chondrules has been observed in young T-Tauri stars as 10^4 to 10^7 years (Feigelson et al., 2002), which is in line with chondrule formation ages (0-3 Myr after CAI formation (Connelly et al., 2012b)). Developing this idea further, Nakamoto et al. (1996) numerically simulate X-ray flares and subsequent expanding magnetic bubbles to show that shock waves sufficient to form chondrules are generated in the upper region of the disk. Their numerical simulation models X-ray flares with very high luminosities (10^{25} W) resulting in a gas density of 10^{19-20} m^{-3} and shock wave front propagations of 100 km s^{-1} , which are too strong to form chondrules. However, at the lower energy range of their model, some X-ray flares produced shock wave fronts of 25 km s^{-1} with a gas density of 10^{18} m^{-3} , which would be suitable for chondrule formation (Nakamoto et al., 1996; Miura and Nakamoto, 2005). Over the past decade less attention has been paid towards X-ray flare generated shock waves, focus has moved towards other mechanisms: gravitational instabilities and planetesimal bow shocks.

Hood and Horanyi (1991) suggested nebula shock as a chondrule formation mech-

anism, and proposed gravitational instabilities, planetesimal bow shocks, and processes external to the nebula as sources for shock. The gravitational instability theory was more favoured over planetesimal bow shock, as the observed abundance of chondrules did not seem feasible if they did not begin forming prior to the existence of planetesimals (Cameron, 1973; Hood and Horanyi, 1991). The gravitational instability concept follows that as the nebula evolved, interstellar material was collapsing onto the disk, which grew in mass to the point of gravitational instability (Wood, 1996). A loss of axial symmetry of the disk follows this, and spiral arms form in order to distribute disk mass inwards and angular momentum outwards to prevent further increase in the disk/star mass ratio (Wood, 1996). Simulations have shown that protoplanetary disks large enough to form gas giants such as Jupiter would go into or be close to gravitational instability (Boss, 2002; Pickett et al., 2003). In a protoplanetary disk capable of forming Jupiter, gravitational instability at and beyond Jupiter’s orbit would produce shock fronts spiralling inwards with speeds of approximately 10 km s^{-1} , which would be sufficient to form chondrules (Boss and Durisen, 2005).

In a recent model, Boley et al. (2013) were able to simulate mechanisms for barred and radial chondrule textures to form, as well as porphyritic chondrules. They model nebula shocks as a product of bow shocks formed by planetesimals and planetary embryos on eccentric orbits moving supersonically through the disk gas (Boley et al., 2013). Excited bodies in an eccentric or inclined orbit can move supersonically relative to gas, and strong bow shocks are generated as a result (Boley et al., 2013). Therefore, the planetesimal bow shock model requires that large planetary bodies had existed before chondrule formation, and this is substantiated by the chronology of the early Solar System. Scherstén et al. (2006) presented Hf/W isotope data that suggests iron meteorite parent body core formation occurred within 1.5 Myr of CAI formation, which is also early enough for ^{26}Al decay to have been an important source of heat for melting of the parent body interior, and evidence that chondrules, or at least those observed today, formed in the presence of large plan-

etary bodies with iron cores. Further isotope research on Mars again using Hf/W ratios showed that the planetary embryo of Mars ($< 50\%$ current mass) accreted in the first $1.8_{-1.0}^{+0.9}$ million years of the Solar System (Dauphas and Pourmand, 2011). If planetary embryos of Moon-to-Mars-size were the main bodies in the eccentric orbit, more realistic cooling rates for chondrules can be modelled (Morris et al., 2012). Mann et al. (2016) modelled the formation of bow shocks in a dusty early solar system orbited by planetary embryos, given that the planetary embryo of Mars is predicted to already have formed before the first chondrules. Consistency with experimental petrology constraints could be met with some of the model's conditions, and the models may have found a mechanism for terrestrial volatile loss by atmosphere stripping, however, most model conditions found cooling rates to be too high to be consistent with observations.

There are still questions left unanswered by the bow shock process, for example, it is not certain whether there was a sufficient population of planetesimals widespread enough to result in the high abundance of chondrules we observe today (Hood and Weidenschilling, 2012). Numerical models need further development in both experimental and numerical aspects; further study of whether the cooling trends observed in the models are consistent with experimentally derived cooling trends is required (Boley et al., 2013; Mann et al., 2016; Imae and Isobe, 2017).

Method 2: Direct condensation

Wood (1963) suggested that chondrules formed by direct condensation from solar gas (Fig. 1.4b). Analysis of olivine from the Renazzo (CR) chondrite showed almost pure forsterite composition, which is permitted to condensate at high pressure and temperature; the T-Tauri Sun was believed to experience large-scale mass ejections capable of influencing conditions of high temperatures and pressures (Wood, 1963). Continuing to pursue condensation of chondrules, McSween (1977) suggested that chondrule diversity is a result of local variations of gas/dust proportions. They discuss the theory that chondrules are formed in areas of enhanced gas/dust ratios, and

that transient high energy events resulted in heating of gas and vaporisation of dust, elevating that ratio. Models suggest that direct condensation is a possible method for chondrule formation, however the observations of relict grains within chondrules strongly suggest that solid materials in the Solar Nebula were melted and incorporated into chondrules (Nagahara, 1981; Rambaldi, 1981; Jones and Danielson, 1997).

Method 3: Lightning

Later, Whipple (1966) suggested that chondrules were produced by lightning discharges melting dust in the primitive Solar Nebula (Fig. 1.4c). Cameron (1966) soon after attempted to develop Whipple's lightning theory quantitatively, and found that lightning discharges would form chondrules of the size range we observe, as larger volumes would not melt, and smaller volumes would be vaporised. Lightning as a formation process has been pursued since, but recent estimates of early Solar System magnetic fields suggest it is an unlikely candidate for chondrule formation. Fu et al. (2014b) report findings of early nebular magnetic fields recorded by dusty olivine in primitive L3.0 Semarkona. They conclude that the weak palaeofields ($54 \pm 21 \mu\text{T}$) recorded by the dusty olivine bearing chondrules dismiss the likelihood of chondrule formation events that would result in the generation of strong magnetic fields.

Method 4: X-wind and magnetic reconnection

The X-wind model proposes that chondrules originated 0.06 au from the Sun, and were then thrown out to 2.5 au from the Sun by magnetocentrifugally driven winds (Fig. 1.4d), or, 'X-winds' (Shu et al., 1996). The initial close proximity to the Sun is in order to explain the melting observed in chondrules, and the expulsion to 2.5 au is where the chondrules would have accreted with ambient dust to form larger chondritic bodies near the 3:1 resonance with Jupiter, where collisional fragments are thrown into Earth's orbit (Shu et al., 1996). The magnetic reconnection model suggests that energy from nebular magnetic flares was sufficient enough to melt dust

balls to form chondrules (Levy and Araki, 1989). As for the lightning model, the magnetic field estimates reported by Fu et al. (2014b) are too weak to be consistent with these models; Levy and Araki (1989) suggested that flares occurring in the presence of a $> 500 \mu\text{T}$ magnetic field would result in the short-lived $> 1700 \text{ K}$ heating events required for chondrule formation. Also applying to the lightning model, further theoretical work is necessary to determine whether the intensity of the magnetic fields remains high as the chondrule cools through its Curie temperature (approximately 760°C) (Fu et al., 2014b), as well as further theoretical and experimental study to obtain more accurate estimates of the nebular magnetic fields. Recently, significant doubt is now cast upon this theory. The proximity to the Sun required to melt the chondrules is too close to avoid accreting onto the Sun, observations have shown that there is no solid material $< 0.1 \text{ au}$, and if there was, collisions at $< 0.1 \text{ au}$ would destroy them (Desch et al., 2010).

Method 5: Volcanism and volcanism-related processes

As chondrules were once molten droplets, the theory that they were erupted from volcanoes on the parent body and then accumulated as terrestrial tuffs seems possible. von Tschermak and Wood (1964) noted the tuff-like nature of meteorites, and that chondrules are rapidly cooled molten droplets, and Fish et al. (1960) noted the presence of pigeonite and glass as quenching process indicators, with terrestrial pigeonite and glass as analogues for volcanic activity. Wood (1963) highlighted the serious flaw in their theories: volcanism on the parent body as an origin for chondrules is unlikely to result in the solar proportion of metals, as the magma would fractionate between metal and silicate phases. Ringwood (1959) believed that chondrules were formed on the parent body planet, and dehydration of upwelling magma resulted in rapid crystallisation of chondrules. Wood (1963) listed a series of criticisms with the model, and it has been universally rejected. Anders and Goles (1961) note that the energy produced by the collision and breakup of these two planets would be enough to vaporise them. The formation of chondrules

by hypervelocity impacts has been since rethought, and recent numerical models demonstrate that it was likely a mechanism that resulted in chondrule formation (see below) (Johnson et al., 2015; Wakita et al., 2017).

Method 6: Planetesimal collisions and impact-jetting

Impact-jetting (ejection and melting of material due to hypervelocity impact, (Johnson et al., 2015)) occurs during planetesimal collisions at speeds greater than 2.5 km s^{-1} . Impact-jetting has emerged as a viable mechanism for chondrule formation that fulfils the Solar Nebula magnetic field intensity estimated by Fu et al. (2014b). Numerical analyses predict that planetesimal collisions during the first five million years of the Solar System would generate enough chondrules to account for the mass of the present day asteroid belt (Johnson et al., 2015). A recent study found further compelling evidence for planetesimal collisions being the formation mechanism for chondrules by numerical analysis, with models forming chondrules of similar size ranges (Wakita et al., 2017). Composition of chondrules formed was found to be dependent on the impacting planetesimals (Wakita et al., 2017). An area worth further exploration is the inevitable formation of larger unmelted ejecta as products of the impacts, as these may potentially play into the size-filtering process that results in purely chondritic lithologies, and may explain how some meteorite breccias contain unmelted lithologies, e.g. Stöffler et al. (1991) (Wakita et al., 2017).

Review of mechanisms

There are many theories for how chondrules formed, and there is still a lack of a widespread consensus amongst the scientific community. Of the six methods described above, planetesimal bow shocks propagated through the nebula and impact-jetting seem to be the most viable mechanisms for chondrule formation. The experimental formation of chondrules with accurate textures and compositions by shock processes (Imae and Isobe, 2017) clearly shows that bow shocks are capable of forming chondrules if the shocks could be generated. Recent models of bow shocks

generated in nebulae populated by planetary embryos (Mann et al., 2016) and of chondrules formed by planetesimal collisions by impact-jetting (Johnson et al., 2015; Wakita et al., 2017) suggest that it is realistic for the chondrule forming environment to have been populated by large planetesimals and planetary embryos that had already formed, as indicated by isotopic data for Mars and iron meteorites (Scherstén et al., 2006; Dauphas and Pourmand, 2011). Chondrules are likely a product of the planet-forming process as well as being key constituents to planetary bodies. More research is essential to further develop the current models (Boley et al., 2013; Johnson et al., 2015; Mann et al., 2016; Wakita et al., 2017).

The palaeomagnetism of meteorites can provide insights in to Solar Nebula conditions and apply constraints to chondrule formation models and Solar System evolution, as evident by the work of Fu et al. (2014b); Cournede et al. (2015); Wang et al. (2017). Accurate and reliable palaeofield information is necessary to accomplish this, which requires a detailed understanding of the magnetic minerals in the meteorite. I investigate the magnetic properties of grains likely to have recorded early Solar System magnetic fields in Chapters 4 and 5 to better understand their magnetic recording properties and stabilities.

1.2.4 Parent body accretion

Chondrule accretion

The constraints for chondrule formation processes, such as magnetic field intensity in the Solar Nebula, are fulfilled by the impact-jetting mechanism (Johnson et al., 2015; Hasegawa et al., 2016). The nature of the impact-jetting mechanism requires for planetesimals already to exist in the chondrule forming region (2.5 au) to collide at hypervelocity ($> 2.5 \text{ kms}^{-1}$) in the first two to three million years of the Solar System's existence. Given that the first CAIs, i.e. solids, formed three million years prior to chondrule formation (Connelly et al., 2012a), it is not inconceivable to postulate that planetesimals also existed (Matsumoto et al., 2017). Dauphas and Pourmand (2011) reported Hf-W data that indicate Mars had already formed

its planetary embryo (half its present size) $1.8_{-1.0}^{+0.9}$ million years after CAIs. It is therefore likely that protoplanets may have been in an ‘ocean’ of chondrules and dust in the protoplanetary disk.

Johansen et al. (2015) modelled planetesimal accretion within an ocean of pre-existing chondrules, and found that planetary embryos of the size of Mars can be formed within $1.8_{-1.0}^{+0.9}$ Myr, agreeing with the isotopic evidence from Mars (Dauphas and Pourmand, 2011). A recent model of chondrule accretion in the protoplanetary disk populated by planetesimals and protoplanets, Matsumoto et al. (2017) predicted that the planetesimals accrete chondrules as a surface layer, and only accrete enough chondrules to represent chondritic meteorite if chondrites sample these layers specifically. Incremental accretion models (Elkins-Tanton et al., 2011; Sahijpal and Gupta, 2011), in which an initial accretion of enough material rich in Al^{26} and Fe^{60} results in large-scale melting and differentiation followed by a subsequent accretion of a surface chondrule layer may agree with the chondrule-veneer modelled by Matsumoto et al. (2017) and the observed magnetic remanence in chondrites, e.g. Gattacceca et al. (2016). Johansen et al. (2015) predicted that planetesimals less than 100 km radius are inefficient at accreting chondrules, and are likely to only have a thin veneer (dozens of kilometres) of chondrules accreted upon the primordial planetesimal, likely differentiated as a result of radionuclide decay. Planetesimals larger than 100 km are expected to grow mainly by accreting chondrules; planetesimal 100 - 200 km in size are expected to be the most size sorted and internally heterogeneous as is observed amongst the Eos family of asteroids, which Allende is expected to originate from (Mothé-Diniz et al., 2008).

Magnetic field contributions to accretion

It was reported by Hayashi (1981), that the magnetic effects in the protoplanetary disk were likely to be significant for the formation of ice giants Uranus and Neptune, but they can be ignored for the terrestrial planets as they decay faster than they grow. However, Hayashi (1981) also notes that it is difficult to estimate the mag-

netic field effects due to the evolving conditions of the nebula influencing growth and decay of magnetic fields with varying degrees of ionisation. Hence, reliable experimental palaeomagnetic data that can estimate the magnetic field influence in the protoplanetary disk are essential to accurately model formation and accretion processes.

Although planetesimals are considered to be the building blocks of terrestrial planets and the cores of ice giants, accretion of solid bodies to larger than a kilometre in size is an inefficient process that is difficult to explain both theoretically and experimentally (Lambrechts and Johansen, 2012). Accretion by coagulation is inefficient to sizes larger than a centimetre due to processes such as destructive collisions (Brauer et al., 2007; Blum and Wurm, 2008; Windmark et al., 2012). Windmark et al. (2012) found that larger than centimetre-sized seeds are required for planetesimals to form merely by coagulation.

Magnetorotational instabilities (MRI) can induce turbulence that can form dust trap regions for enhanced growth due to the resulting localised pressure bumps, which can lead to the formation of planetesimal seeds (Balbus and Hawley, 1991; Johansen et al., 2009). Turbulence can also be induced by streamline instabilities, which cause instability as a result of the aerodynamic drag between the gas and dust interaction, and this can also result in the formation of planetesimal seeds Youdin and Goodman (2005); Johansen and Youdin (2007); Bai and Stone (2010). The vertical extent of chondrules relative to the disk is an important parameter for the accretion of chondrules, and it is affected by turbulence (Levison et al., 2015). At the time of the models conducted by Johansen et al. (2015), the magnetic field intensity in the Solar Nebula estimated by Fu et al. (2014b) had only just been made and not incorporated into their study; they note the importance of a well-constrained nebular magnetic field intensity. Matsumoto et al. (2017) incorporate the likely turbulence as a result of MRI into their models based upon the estimate of a Solar Nebula magnetic field strength of $54 \pm 21 \mu\text{T}$ from Semarkona (Fu et al., 2014b). This study, based upon six data points, is informing the majority of contemporary

models that include the effects of magnetic fields, yet the reliability and stability of the magnetic vortex states that populate the remanence carriers of Semarkona dusty olivine is still unknown. In Chapter 4 and 5 the thermomagnetic properties and stability of remanence in dusty olivine is determined.

Given that both magnetic and non-magnetic processes can feasibly produce similar effects, reliable palaeomagnetic data from meteorites are necessary to determine the degree of magnetic effects to the transport of momentum and turbulence to accurately constrain models of the early Solar System.

1.3 Palaeomagnetism and rock magnetism

Palaeomagnetism is the science of determining and interpreting ancient magnetic fields recorded by rocks as a remanent magnetisation, whereas rock magnetism focuses on acquisition processes and reliability for application to palaeomagnetism.

1.3.1 Ferromagnetism

Magnetic materials contain atoms with permanent magnetic moments. In palaeomagnetism, we are interested in ferro/ferrimagnetic materials such as iron and magnetite, as they retain a magnetisation after an applied field is removed due to long-range ordering of magnetic moments below a critical temperature (Bertotti, 1998). This is referred to as a remanent magnetisation, or remanence. Remanence can be remagnetised by new fields in part or entirely wiping the original magnetisation.

Ferromagnetism arises due to the quantum mechanical effect of electron spin (Stacey and Banerjee, 1974). In addition to the charge properties of electrons, electrons also have a quantum spin in either ‘up’ or ‘down’ configuration. The majority of materials have complete electron orbital shells with coupled ‘up’ and ‘down’ spins producing no net spin. However, ferromagnetic (Fig. 1.5a) (and ferrimagnetic (Fig. 1.5b)) materials, such as iron, nickel and cobalt (magnetite is ferrimagnetic), have unfilled electron shells that lead to an unpaired electron spin; the accumulation

of unpaired electron spins may align with an external field to produce a net magnetisation (Fig. 1.5). In the absence of an external field, the alignment of spins is expected to produce a net magnetisation, referred to as spontaneous magnetisation.

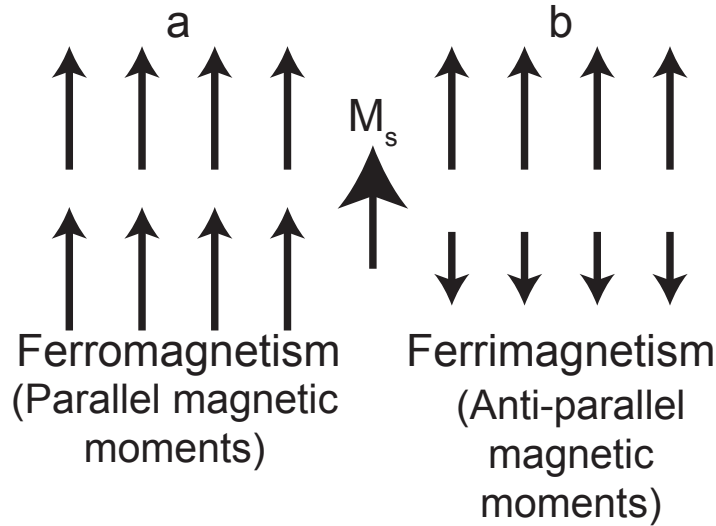


Figure 1.5: Schematic diagrams of the exchange couplings that lead to (a) ferromagnetism and (b) ferrimagnetism. The net magnetisation of the ferrimagnetic material is indicated by M_s .

1.3.2 Domain theory

Ferromagnetic materials have contributions to magnetic energy that control their magnetisation. The magnetic grain configures its magnetisation and domain structure to minimise its magnetostatic energy (Butler, 1998). As magnetic grains become larger, their self-magnetostatic energy increases such that they develop domain walls to reduce it (Butler, 1998). Hence, individual magnetic crystals are subdivided into regions called magnetic domains. A magnetic domain is a region within a magnetic grain that has its magnetic moments mutually aligned, i.e., uniformly magnetised. The grain size of the magnetic crystal is an important factor, as this controls its magnetic domain state.

Classical domain theory has stated that the most stable magnetic recorder of remanence is the single domain (SD) state (Kittel, 1949). This is a state in which the magnetisation flows through the ferromagnetic grain uniformly, as in Figure 1.6. Ferromagnetic grains change their magnetic domain structure depending on their

volume, with non-uniform vortex magnetisation structures forming once uniform structures are no longer the least-energy structure (Williams and Dunlop, 1989). Larger non-uniformly magnetised grains form domain walls once volume increases to a certain limit in order to minimise magnetostatic energy (Kittel, 1949; Williams and Wright, 1998). Non-uniformly magnetised grains have long been assumed to be less stable recorders of magnetic remanence than uniformly magnetised grains; I investigate the thermomagnetic stability and relaxation times (see below) for non-uniformly magnetised grains abundant in meteorites in Chapters 4 and 5 to determine their fidelity for recording and retaining magnetic remanence from the early Solar System.

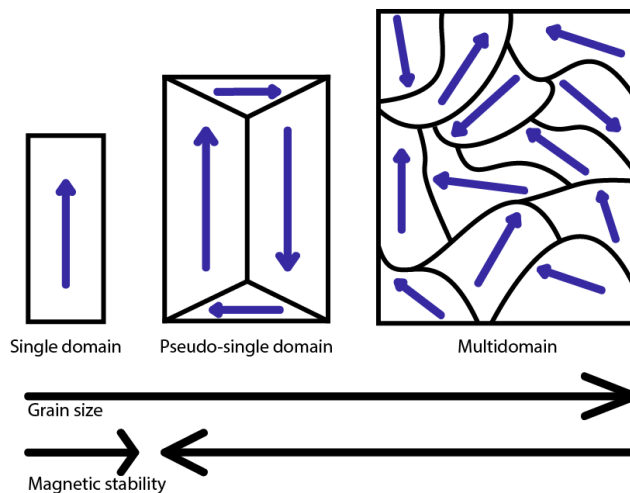


Figure 1.6: Schematic diagrams of single domain (SD), pseudo-single domain (PSD), and multi-domain (MD) particles, showing that transition between domain states is a function of grain size and effects magnetic stability.

1.3.3 Magnetic relaxation

‘Stable magnetisations’ are carried by ensembles of magnetic grains large enough to apply to Maxwell-Boltzmann statistics, i.e., statistical thermodynamics, and are long-lived on observable timescales (Berndt et al., 2016). However these stable magnetic states are never truly stable, as the equilibrium state for an ensemble of magnetic grains is zero or near zero net magnetisation in the absence of a biasing field. Hence, the equilibrium state is achieved when the magnetic moments of these grains are randomly oriented. Thermal energy at any temperature will

attempt to ‘relax’ the magnetisation to this state. This is not an abrupt process, and individual grain magnetic moments are reversed gradually at random due to thermal energy excitations having a statistical Maxwell-Boltzmann distribution of magnitudes. Hence, the time for relaxation, τ , can be determined, given by the Néel-Arrhenius equation (Néel, 1949):

$$\tau = \frac{1}{C} e^{\frac{\Delta E}{k_B T}} \quad (1.1)$$

where C is the atomic switching frequency ($10^{-9} s$), k_B is Boltzmann’s constant, T is the temperature, and E is the energy barrier. The relaxation time is directly related to the stability of the magnetisation state, and was proposed by Néel (1949) as an explanation for remanent magnetisation in rocks carrying ancient magnetic field information.

Based upon equation 1.1, it has been calculated that uniformly magnetised SD grains above a certain size are capable of carrying remanence for the billion-year timescales that are of interest to meteoritic (and terrestrial) palaeomagnetic (Néel, 1949; Butler and Banerjee, 1975; Muxworthy and Williams, 2015). As such, great effort has been put into determining the grain size thresholds for SD behaviour Morrish and Yu (1955); Evans and McElhinny (1969); Schabes and Bertram (1988); Williams and Dunlop (1989); Winklhofer et al. (1997); Gatel et al. (2015); Muxworthy and Williams (2015). The size range for SD metallic Fe is between 8 nm and 23 nm (experimentally determined; (Kneller and Luborsky, 1963)), and between 17 nm and 24 nm (theoretically determined; (Muxworthy and Williams, 2015)). The lower limit is defined by the volume at which energy barriers are so small that they can be overcome by room-temperature thermal energy fluctuations within a short timescale, i.e., < 100 seconds; grains in this size range are classified as being in ‘superparamagnetic’ state (Bean and Livingston, 1959). Above the SD size range, the grains are in a non-uniformly magnetised pseudo-single domain (PSD) state, which have been observed to behave similarly to SD grains (Almeida et al., 2014b), yet have a non-uniform, e.g., vortex, magnetic structure (Fig. 1.6). As

grain size increases further, domain walls develop and grains are considered to be in multi-domain (MD) state (Fig. 1.6). These larger grains with more complex magnetisation structures have long been assumed to be unstable and poor recorders of ancient magnetic fields. Difficulty arises when attempting to experimentally estimate palaeointensity from MD and PSD grains, as estimation protocols are based upon Néel's theory for uniformly magnetised grains (Néel, 1949), and hence do not model the thermomagnetic behaviour of non-uniformly magnetised grains; the MD model proposed by Néel (1955a) is not consistent with experimental observations of MD grains, e.g. Pike et al. (2001). This is problematic, as the naturally logarithmic grain size distribution in rocks results in the majority of grains being of PSD and MD size (Robertson and France, 1994; Kruiver et al., 2001). In Chapter 4 and Chapter 5, the experimental technique of off-axis electron holography coupled with numerical micromagnetic modelling are applied to meteorites to challenge these assumptions about the stability and recording fidelity of pseudo-single domain and multi-domain grains.

1.3.4 Magnetic remanence

Thermoremanent magnetisation

At elevated temperatures, the relaxation time decreases (Eq. 1.1). Above the Curie temperature, T_c , grains are paramagnetic, and thermal energy randomises the orientation of magnetic moments in the absence of a field (Dunlop and Özdemir, 2001). In the presence of a field, the magnetic moment orientations will be biased by the field. As the grain cools below the Curie temperature, it will lock (block) in its magnetic moment orientations, which, if biased by an ambient field, will record a thermoremanent magnetisation (TRM). In the absence of a field as the grain cool, the randomised magnetic moment orientations will average out to zero.

Chemical remanent magnetisation

Chemical remanent magnetisation (CRM) is due to the crystallisation of a new ferromagnetic (*sensu lato*) grain, and the newly crystallised daughter phase has been observed to acquire a magnetic remanence biased by the ambient field present at the time of crystallisation (Johnson and Merrill, 1972; Fu et al., 2014a) and a remanence that is inherited from the parent phase (Johnson and Merrill, 1974). The process has been found to be dependent upon the domain structures of the altered grains and is also complicated by both the ambient field and the magnetostatic interaction between the daughter and parent phases (Özdemir and Dunlop, 1985; Heider and Dunlop, 1987; Dunlop and Özdemir, 2001). Typically CRM is considered a contamination of the natural remanence, as it can be often difficult to date the secondary mineralisation and determine whether the remanence has been inherited from the parent phase or affected by an ambient magnetic field. However, chemical alteration on the parent body of a meteorite can be analysed to understand magnetic field conditions on the parent body at the time of alteration, e.g., Fu et al. (2014a); Cournede et al. (2015).

Isothermal remanent magnetisation

Isothermal remanent magnetisation (IRM) is acquired at a constant temperature due to application of strong magnetic fields, and is commonly applied to samples to analyse the constituent magnetic components. A saturating field can produce a more stable remanence (SIRM; saturation isothermal remanent magnetisation), and can occur in nature due to lightning strikes, or during sample handling or collection due to contact with a strong hand magnet. Saturation remanence is less stable than thermoremanence (Rimbert, 1959; Dunlop and West, 1969), and is typically considered a contamination to the NRM.

Anhysteretic remanent magnetisation

Anhysteretic remanent magnetisation (ARM) is acquired when an ambient biasing magnetic field is present while alternating fields are being applied to a sample. The alternating fields demagnetise pre-existing remanence, and result in the acquisition of an ARM in the direction of the biasing field (Dunlop and Özdemir, 2001). ARM can contaminate the demagnetisation spectrum if it is unwanted, i.e. the Earth's magnetic field is not shielded during demagnetisation. ARM can only be applied in the laboratory to a sample and is often considered analogous remanence to a thermoremanence, such that the ancient magnetising field can be estimated from the comparison of the ARM and TRM (Banerjee and Mellema, 1974; Stephenson and Collinson, 1974).

Viscous remanent magnetisation

Viscous magnetisation is a thermally activated process that occurs at constant temperature over a period of time greater than the relaxation time (Dunlop and Özdemir, 2001). Many grains in a natural sample will have relaxation times that are much longer than geological timescales, so magnetic viscosity will not affect them; there would be no palaeomagnetic remanence otherwise. However, a small fraction of grains will have relaxation times similar to the time since formation, or in the case for meteorites, time since landing on Earth and residing in Earth's magnetic field. For these grains, the natural remanence will be overprinted by a viscous remanent magnetisation (VRM), which is usually considered a contamination. As this process typically affects grains of low coercivity, small alternating fields (AF) (< 20 mT) can be applied to the sample in the laboratory to demagnetise the VRM overprint.

Shock remanent magnetisation

Shock remanent magnetisation (SRM) is typically associated with hypervelocity impacts, which have been abundant throughout the history of the Solar System. For

SD grains, the induced stresses due to the shock can supply magnetoelastic energy sufficient to exceed the anisotropy energy, which can result in a remagnetisation in the presence of an ambient field (Cisowski and Fuller, 1978; Tikoo et al., 2015). For MD grains, the induced stresses can supply enough magnetoelastic energy to rearrange domain walls, resulting in an SRM remagnetisation in the presence of an ambient field (Cisowski and Fuller, 1978; Tikoo et al., 2015). In the absence of an ambient field, the shock process has been shown to demagnetise the natural remanence (Gattacceca et al., 2010b).

1.3.5 Magnetic hysteresis

Hysteresis loops (Fig. 1.7) are generated in experiments to observe the response of particles to the application of external fields (Tauxe, 2010). Hysteresis loops are quick measurements that can yield the coercivity H_c , saturation field H_{sat} , saturation magnetisation M_s , and saturation remanence M_{rs} . These hysteresis parameters can be used to make an approximation of the domain states present in the sample (Day et al., 1977). The coercivity, or coercive field, is the magnetic field required to reduce the magnetisation of an assemblage of particles to zero (Dunlop and Özdemir, 2001). Magnetic grains are typically classed as hard or soft depending on the magnitude of coercive field necessary to magnetise or demagnetise the assemblage of grains.

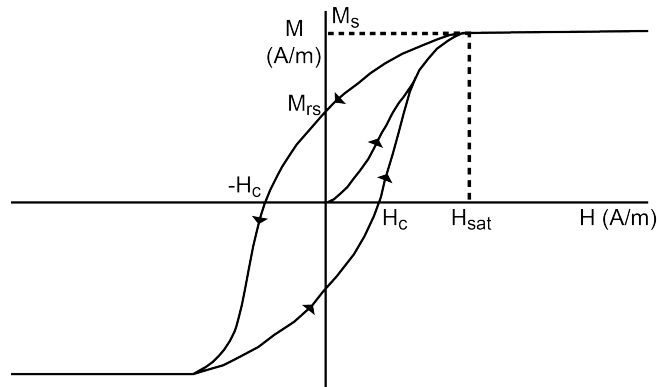


Figure 1.7: An example of a hysteresis loop, with hysteresis parameters coercivity H_c , saturation field H_{sat} , saturation magnetisation M_s , and saturation remanence M_r labelled.

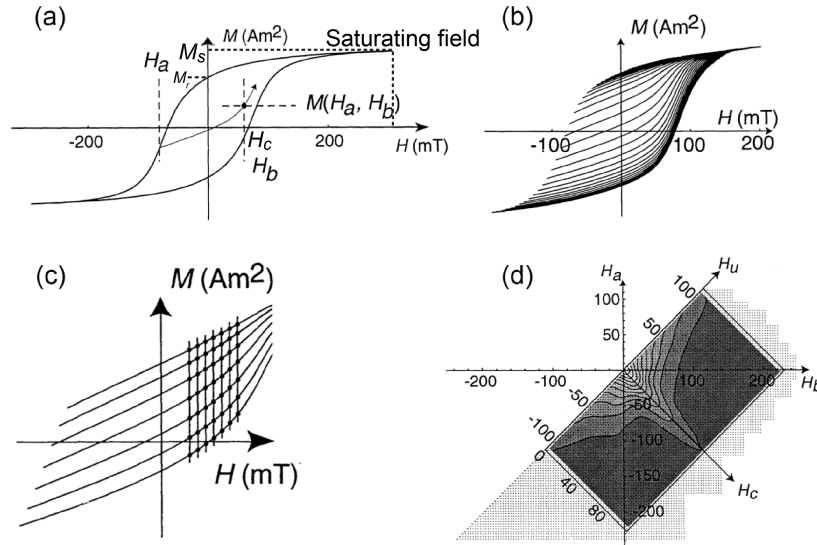


Figure 1.8: The construction of a first-order reversal curve (FORC) diagram. (a) An example of a hysteresis loop, with the reversal point H_a labelled. FORCs begin at H_a and proceed to saturation. (b) Multiple FORCs for a series of different H_a values. (c) A subset of FORCs with evenly spaced H_a and H_b data points circled. (d) A plot of a FORC diagram, with H_u and H_c axes superimposed upon the H_a and H_b plot. H_u and H_c represent magnetic interactions and coercivity respectively, and are functions of H_a and H_b . Adapted after Roberts et al. (2000).

Pike and Fernandez (1999) and Roberts et al. (2000) presented a method that can identify individual magnetic components in a mixed mineral assemblage in minutes, represented visually and quantitatively in a first-order reversal curve (FORC) diagram (Fig. 1.8). FORC diagrams are calculated from a suite of partial hysteresis curves, referred to as first-order reversal curves (FORCs) (Mayergoyz, 1986). Measurement of individual FORCs involves saturating the sample with a large positive field, and then decreasing the field to a reversal field H_a (Fig. 1.8a). The field is then increased back to saturation from H_a , and the FORC is defined as the magnetisation curve that results from this saturation. Multiple FORCs are produced by repeating this procedure for different H_a values (Fig. 1.8b and c). A FORC diagram is produced by plotting the distribution of consecutive FORCs, with vertical axis H_u , representing magnetic interactions, and horizontal axis H_c , representing the coercivity distribution (Fig. 1.8d) (Pike and Fernandez, 1999; Roberts et al., 2000).

1.4 Meteoritic magnetism

1.4.1 Magnetic properties of meteorites

High-temperature measurements

Heating a meteorite sample can determine the unblocking spectrum for magnetic remanence and the Curie temperatures of the magnetic phases within the sample; the Curie temperature can be diagnostic of the magnetic phases present in the sample, e.g. iron has a T_C of 760°C and magnetite has a T_C of 585°C (Bozorth, 1951; Stacey et al., 1961; Herndon et al., 1976). Thermomagnetic analyses of meteorites are problematic, however, as meteorites are prone to thermochemical alteration; oxidation readily occurs due to the reduced composition of many of the magnetic carriers (Herndon et al., 1976). Also common magnetic carriers within meteorites such as tetrataenite should not be analysed for palaeomagnetic data by heating methods, as tetrataenite undergoes a phase transformation to taenite upon heating above 320°C (Dos Santos et al., 2015).

Room-temperature measurements

Given that meteorites chemically alter with ease when heating and that the value and scarcity of meteorites requires experimental methods to be non-destructive when possible, room-temperature methods of analysing rock magnetic properties are often employed to avoid altering the meteorite. Magnetic susceptibility is the ratio of induced magnetisation to the inducing field. An extensive study of the magnetic susceptibility of 971 ordinary chondrites demonstrated that it is a parameter that can quickly and non-destructively characterise and classify the amount of metal within the sample (Rochette and Sagnotti, 2003). As the metal abundance is distinctly variable between different chondrite classes (Table 1.1), meteorite classification is possible. Complementary follow-up studies on non-ordinary chondrites and achondrites have also since been conducted (Rochette et al., 2008, 2009).

Magnetic susceptibility can vary according to measurement direction; anisotropic

magnetic minerals with a preferred orientation will have an anisotropic magnetic susceptibility on the bulk rock scale (Jackson and Aubourg, 1992). The anisotropy of magnetic susceptibility (AMS) is another magnetic property that can be non-destructively measured. AMS can determine whether there is any preferred orientation within a rock, and the intensity of that fabric (Jackson and Aubourg, 1992). A preferred orientation fabric could be the result of an impact-related shock inducing compaction of loose material, for example (Gattacceca et al., 2005). AMS can accurately and quantitatively distinguish between S1-S3 shock stages (S3-S6 shock stages deform metallic grains completely) (Gattacceca et al., 2005).

Hysteresis loops, direct current back-field demagnetisation, and FORCs are commonly used to analyse the magnetic grains within a sample and to determine the likely domain states present (Acton et al., 2007; Uehara et al., 2011; Gattacceca et al., 2014) (see below).

1.4.2 Determining the magnetic mineralogy

The magnetic phases of meteorites are important for determining what is of palaeomagnetic significance, and should be known before interpreting palaeomagnetic data. Through the analysis of 91 ordinary chondrite falls, Gattacceca et al. (2014) demonstrated that the hysteresis properties of meteorites can be diagnostic for the magnetic phases present in meteorites, however, hysteresis does not give unique solutions. Analysis by techniques such as electron microscopy energy dispersive X-ray spectroscopy (EDS), electron and X-ray diffraction, and Mössbauer spectroscopy, can accurately determine the composition of the magnetic minerals (Bland et al., 2004; Menzies et al., 2005; Uehara et al., 2011; Howard et al., 2010).

Unequilibrated chondrites, which represent the most primitive of the chondrites (less than petrologic type 3.5 (Huss et al., 2006)), have FeNi alloys kamacite and martensite that may retain palaeomagnetic remanence (Gattacceca et al., 2014). Kamacite is the single-domain FeNi phase found in dusty olivine. Magnetite and cohenite have also been found in Semarkona and some other very primitive chon-

drites (Hutchinson et al., 1987; Krot et al., 1997).

Equilibrated chondrites have undergone metamorphism sufficient to alter the magnetic grains present, for example, taenite undergoes atomic reordering upon slow cooling below 320 °C to become tetrataenite (Clarke and Scott, 1980). Tetrataenite has a very high coercivity and can occur in single-domain state in the cloudy zone of a zoned taenite grain (Bryson et al., 2014). As slow cooling below 400 °C in the subsolidus temperature range is a requirement, abundance of tetrataenite is controlled by the thermal history of the meteorite (Gattacceca et al., 2014). Tetrataenite is formed by transformation from taenite, and while it was once considered to possibly retain the TRM of taenite (Nagata and Funaki, 1982; Wasilewski, 1988), this is not the case. Taenite is ferromagnetic only below 400 °C (rim), and 350 °C (cloudy zone); it is paramagnetic above these temperatures (Uehara et al., 2011). Therefore, the only TRM retained from the taenite in the tetrataenite could be the TRM acquired when cooling from 400 °C to 320 °C and 350 °C to 320 °C for the rim and cloudy zone respectively (Gattacceca et al., 2014). Hence, it is only possible to determine the remanent magnetisation from cooling from these temperatures, and not from before that. This would provide information about whether the parent body had an active magnetic field at the time of cooling.

1.4.3 Palaeointensity determination for meteorites

The palaeointensity (ancient field intensity) of meteorites can provide valuable information about the evolution of the early Solar System and meteorite parent bodies. It is commonly assumed that the magnetisation acquired is a TRM, which is the magnetisation the meteorite would have been subject to when cooling through its Curie point, which is, for example, 760 °C for Ni_{3%} kamacite (Garrick-Bethell and Weiss, 2010).

Palaeointensity determination from a rock follows the principle that the NRM (M_{NRM}) of the sample is linearly proportional to the ancient magnetic field ($B_{ancient}$) (Equation 1.2). This principle also applies for a magnetic field applied in the lab-

oratory, where M_{lab} is proportional to B_{lab} (Equation 1.3). As $v_{ancient}$ and v_{lab} are constants of the proportional relationship, it can be assumed that $v_{ancient} = v_{lab}$, allowing the $B_{ancient}$ to be determined by Equation 1.4 (Koenigsberger, 1930).

$$M_{NRM} = v_{ancient} B_{ancient} \quad (1.2)$$

$$M_{lab} = v_{lab} B_{lab} \quad (1.3)$$

$$B_{ancient} = \frac{M_{NRM}}{M_{lab}} B_{lab} \quad (1.4)$$

In theory, palaeointensity acquisition is therefore simple, and it can be determined by applying a lab field and measuring the induced magnetisation. However, in practice complications arise due to complex magnetic properties of natural rock samples. Presence of MD and PSD grains can lead to erroneous palaeointensity values, as unblocking and blocking temperatures will be different, so recreating NRM acquisition conditions will be difficult. Specimen anisotropy can lead to the the proportionality constants being significantly different if the laboratory field direction is different to the ancient field direction. In practice $v_{ancient}$ may not be a constant as the NRM may not have been acquired linearly, and v_{lab} may be different to $v_{ancient}$ if the sample's capacity to acquire remanence has changed due to chemical alteration or weathering (Tauxe, 2010). Capacity for remanence could be altered during experimentation due to thermochemical alteration; meteorites are particularly susceptible to this (Westphal, 1986), thus non-heating palaeointensity protocols have been developed. These protocols (REM (Gattacceca and Rochette, 2004), ARM (Banerjee and Mellema, 1974; Stephenson and Collinson, 1974), and Preisach (Muxworthy and Heslop, 2011)) compare the natural remanent magnetisation (NRM) of the sample with laboratory applied at room temperature, e.g., ARM or SIRM and use a calibration constant to estimate a palaeointensity. The Preisach method determines a calibration factor from the FORC distribution measured from

the sample. However, there is not a widely accepted value for the calibration constants for the REM and ARM methods, and they have changed significantly since the methods were first proposed, e.g., the most recent determination for the REM calibration constant (for magnetite bearing samples) Lerner et al. (2017) is half that of Gattacceca and Rochette (2004). These methods also assume that the NRM of the sample is entirely a TRM, which is often not the case, e.g., Fu et al. (2014a); Cournede et al. (2015).

In addition to determining the palaeointensity, it is important to identify particles that are likely to retain a primary remanence. Metamorphism and/or hydrothermal alteration would result in alteration of the pre-existing minerals that carried the original TRM, for example, kamacite can transform to taenite, which has different magnetic properties, and would acquire a changed remanence (Stacey, 1976; Yang et al., 1997); this is referred to as a thermochemical remanent magnetisation (TCRM). The TRM of a meteorite may have been wiped by shock due to asteroid impacts on the parent body, which would mean the NRM is a shock remanent magnetisation (SRM) (Louzada et al., 2007). Exposure to magnetic fields can induce a viscous remanent magnetisation (VRM), however this is easily removed by applying a weak alternating field (AF) demagnetisation to the sample. More significant overprints are IRM, where short term exposure to strong magnetic fields, for example using a hand magnet when collecting meteorites can remagnetise the sample.

1.4.4 Dusty olivine

Dusty olivine is forsteritic olivine with low-Ni kamacite (\sim metallic Fe) inclusions causing the ‘dusty’ appearance (Fig. 1.9), and grains of dusty olivine are found within chondrules of ordinary, carbonaceous, and enstatite chondrites (Nagahara, 1981; Prinz et al., 1985). As chondrules formed prior to the accretion of the meteorite it is common practise to study them individually to gain insight into pre-accretionary conditions as well as parent-body conditions (Lanoix and Strangway, 1978; Sugiura

et al., 1979; Wasilewski, 1982; Acton et al., 2007).

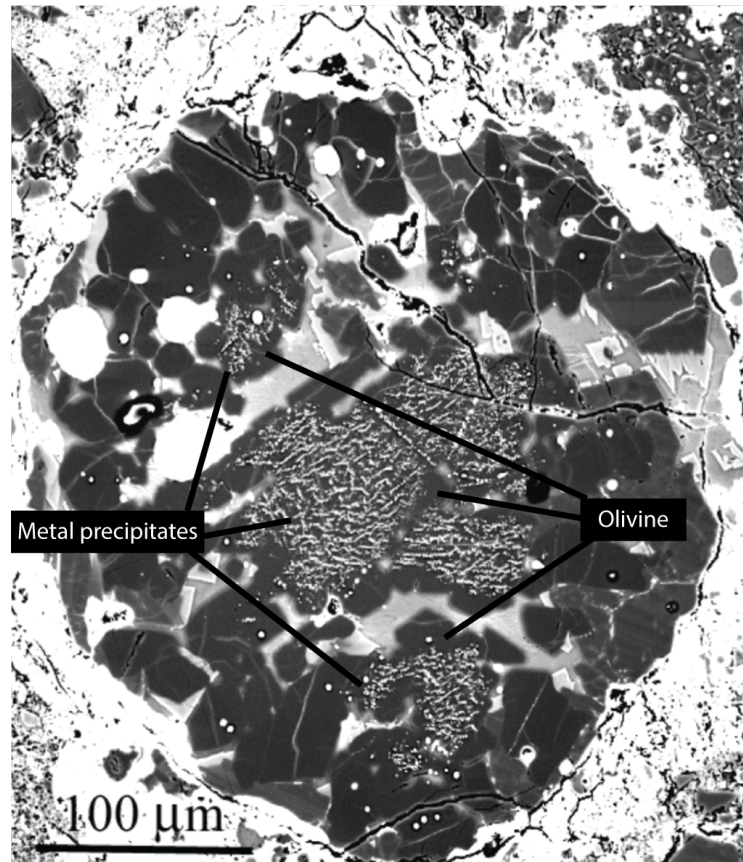
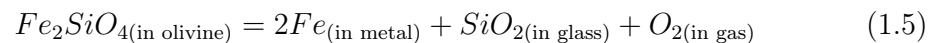


Figure 1.9: SEM image of dusty olivine in the Semarkona ordinary chondrite (LL3.0). The ‘dusty’ low-Ni kamacite inclusions are evident largely in the centre of olivines. Modified after Leroux et al. (2003).

Due to its chemical and physical properties, dusty olivine presents an excellent opportunity to estimate the magnetic fields present in the chondrule forming region of the Solar Nebula (Uehara and Nakamura, 2006). Leroux et al. (2003) studied the formation process of dusty olivine in unequilibrated ordinary chondrite Bishunpur (LL3.1) and synthetic dusty olivine, and proposed that forsteritic dusty olivine formed from fayalitic olivine by the reduction reaction:



During the analytical TEM study of the synthetic dusty olivine (Fig. 1.10), the metal to glass ratio exceeded the proportions expected in the reaction (Leroux et al., 2003). They explained that for this reaction to occur, high temperatures are required, at which SiO_2 may exist as a melt and/or vapour. Other experiments to determine

the formation processes of dusty olivine indicated that heating in the presence of carbon to achieve reducing conditions is necessary (Connolly Jr. et al., 1994; Libourel and Chaussidon, 1995; Uehara and Nakamura, 2006). The requirement of high temperatures suggest the Fe inclusions were formed during the flash-heating chondrule formation event (Zanda, 1996), and the remanent magnetisation recorded by them is a TRM from the time of chondrule formation (Uehara and Nakamura, 2006).

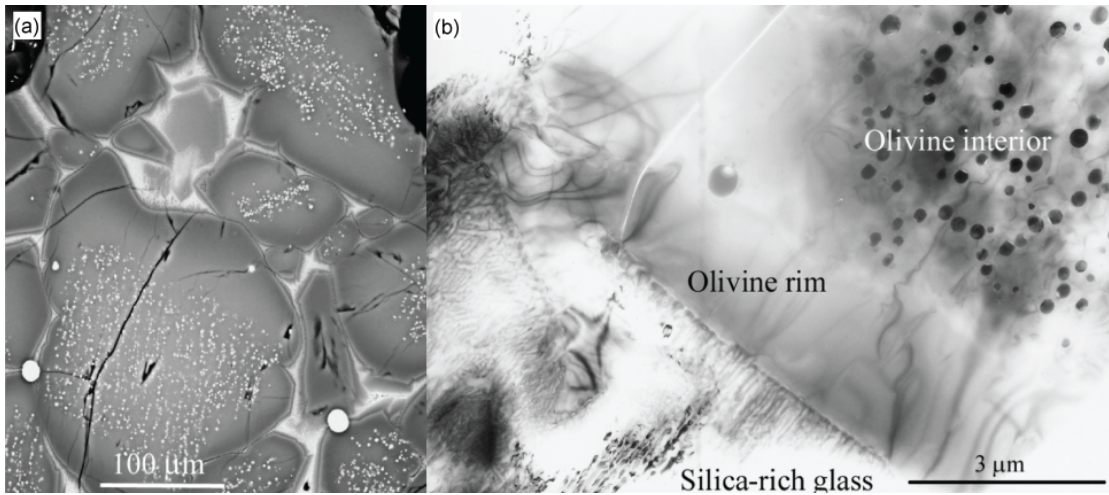


Figure 1.10: SEM images of synthetically produced dusty olivine by reduction of San Carlos olivine. From Leroux et al. (2003).

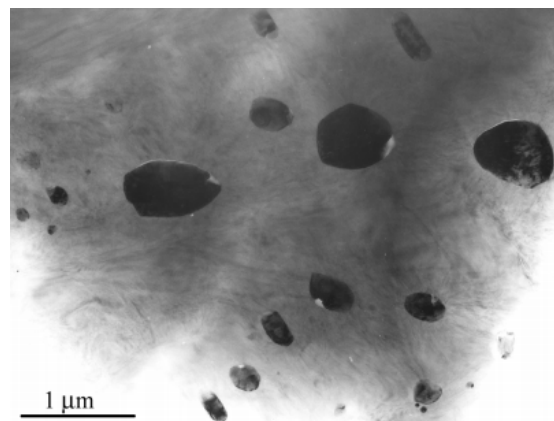


Figure 1.11: TEM image of the metallic FeNi inclusions within dusty olivine in the Bishunpur ordinary chondrite (LL3.1). From Leroux et al. (2003).

Magnetic properties of dusty olivine

Research into the mineral magnetic properties of synthetic dusty olivine suggested that it is a credible recorder of pre-accretionary remanence in chondrules (Uehara and Nakamura, 2006). The low-Ni kamacite inclusions found in synthetic dusty olivine (Fig. 1.11) are non-interacting (Fig. 1.12, 1.13), sub- μm -sized, single domain and single vortex grains with high coercivity (Fig. 1.12, 1.13) in a silicate-glass matrix (Lappe et al., 2011). It was suggested that these kamacite grains can possibly carry a stable thermoremanent magnetisation for up to 4.6 Ga (Lappe et al., 2011). The olivine acts to protect the FeNi inclusions from oxidation and shock remagnetisation, which is similar to some terrestrial examples, where fine-grained magnetite and/or titanomagnetite are encased in silicates such as plagioclase, and the plagioclase crystal has prevented the magnetic grains from being altered or oxidised (Cottrell and Tarduno, 1999; Feinberg et al., 2005, 2006; Uehara and Nakamura, 2006).

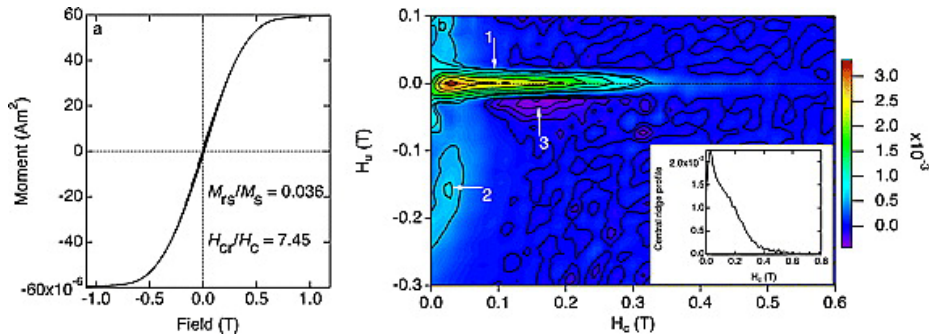


Figure 1.12: Hysteresis loop and FORC diagram of synthetic dusty olivine grains. The hysteresis parameters ($M_{RS}/M_S = 0.036$ and $H_{CR}/H_C = 7.45$) are typically associated with multidomain behaviour if plotted on a Day plot (Day et al., 1977), however the FORC diagram (Pike and Fernandez, 1999) is showing evidence for an assemblage of non-interacting single domain grains (central ridge, (1)) and single vortex grains (broad negative (2) and positive (3) peaks). From Lappe et al. (2011).

The mineral magnetic properties of synthetic dusty olivine suggesting that it is an exemplary source for pre-accretionary magnetic field estimation compared to past attempts at estimating pre-accretionary magnetic fields from chondrules and bulk meteorite measurements, e.g., Butler (1972); Strangway and Sugiura (1982); Sugiura and Strangway (1983). Fu et al. (2014b) analysed the chondrules from Semarkona to determine the palaeointensity from its dusty olivine bearing chondrules. Using

highly sensitive superconducting magnetic microscopes, Fu et al. (2014b) compared the natural remanence of six dusty olivine bearing chondrules carefully extracted from Semarkona with an anhysteretic remanence imparted under controlled conditions in the laboratory to estimate the palaeointensity as $54 \pm 21 \mu\text{T}$. This estimate is used as the reference for magnetic field conditions in the chondrule forming region (2.5 astronomical units (au)) of Solar Nebula within the first three million years of the Solar System's history.

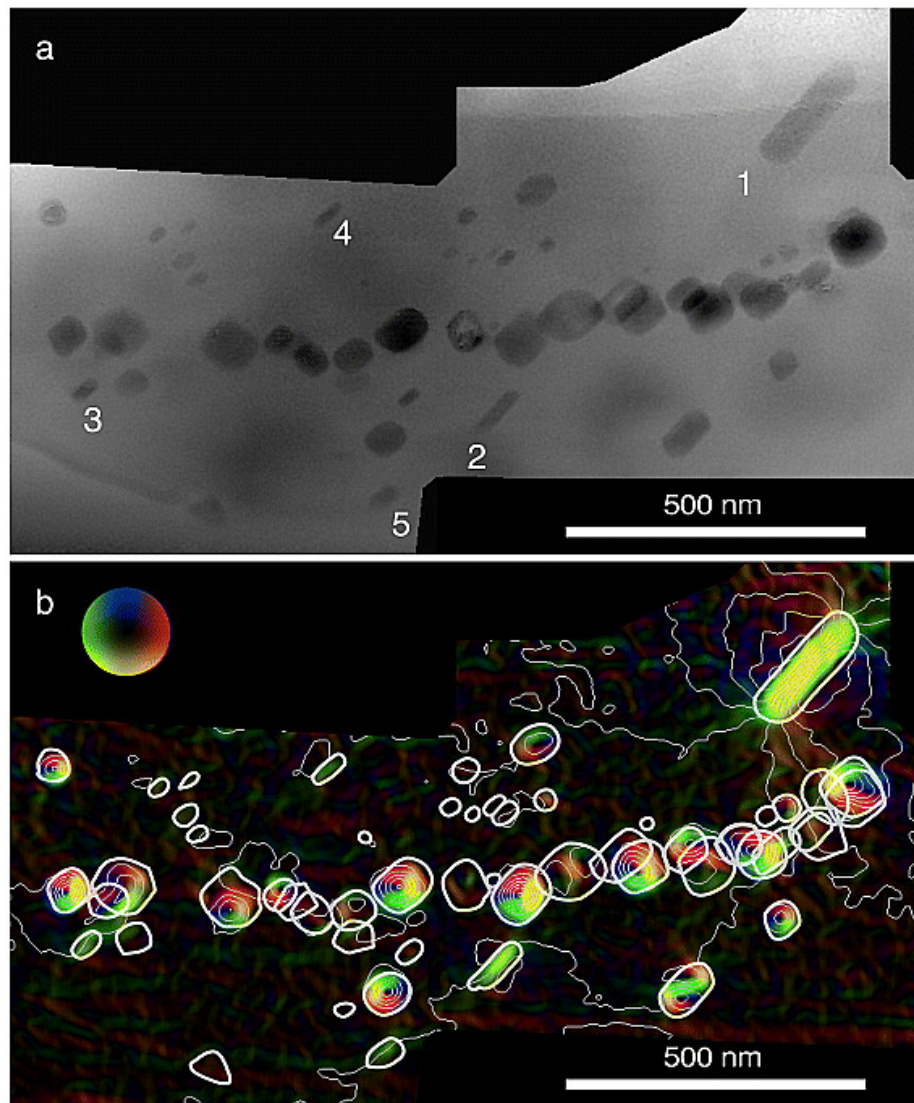


Figure 1.13: (a) A TEM image of synthetic dusty olivine analysed using the technique of off-axis electron holography to observe the nanometric magnetic properties of its constituent kamacite grains. (b) Magnetic induction map of the grains imaged in (a) produced from electron holograms acquired at room temperature. More information on the methods of off-axis electron holography can be found in Chapter 4. The colour wheel in (b) indicates the direction of projected in-plane magnetic induction. Contours indicate magnitude of magnetic induction. The grains are seen to be strongly magnetic and typically non-interaction. The large grain (1) appears to be in single domain state, however this could also be an in-plane magnetic vortex structure. The majority of the other particles (2-5) are in single vortex state. From Lappe et al. (2011).

As stated previously, the palaeointensity estimate from Semarkona dusty olivine (Fu et al., 2014b) is made under the assumption that the remanence has remained stable for 4.6 Ga given that it has a largely single domain grain assemblage. The requirement for single domain (referred to in this thesis as uniformly magnetised) grains is due to palaeomagnetic theory and the theory for thermal relaxation (Néel, 1949), which only applies to single domain, or uniformly magnetised, grains. From the magnetic induction maps acquired by electron holography of synthetic dusty olivine and the micromagnetic solutions for typical remanence states of kamacite grains observed in Semarkona, however, it is clear that a large proportion of these grains are non-uniformly magnetised in single or multi-vortex states (Fig. 1.13, 1.14). Despite efforts in the past to understand thermomagnetic properties of vortex states (Winklhofer et al., 1997; Muxworthy et al., 2003), it is still unknown whether they are capable of retaining magnetic remanence for Solar System timescales. The formation of grains from igneous processes typically results in a logarithmic distribution of grain sizes, with the majority of grains typically being in magnetite's size range for pseudo-single domain state (Robertson and France, 1994; Kruiver et al., 2001). The size range and threshold for single domain behaviour is narrower and smaller for iron than it is for magnetite (Fig. 1.15) (Muxworthy and Williams, 2006, 2015). Thus, it is of great importance to both terrestrial and extraterrestrial palaeomagnetism to determine whether magnetic vortex states are credible recorders of palaeomagnetic remanence, and especially whether meteoritic iron, which is far more likely to be in vortex state, can retain remanence for 4.6 billion years.

Chapter 4 of this thesis considers the recording fidelity of dusty olivine from the unequilibrated ordinary chondrite Bishunpur, e.g. Fig. 1.11, using the advanced TEM technique of off-axis electron holography, e.g., Fig. 1.13, at room temperature and high temperature to observe the thermomagnetic properties of dusty olivine kamacite. Chapter 5 is a numerical study of the magnetic states and stabilities of meteoritic iron, i.e. dusty olivine.

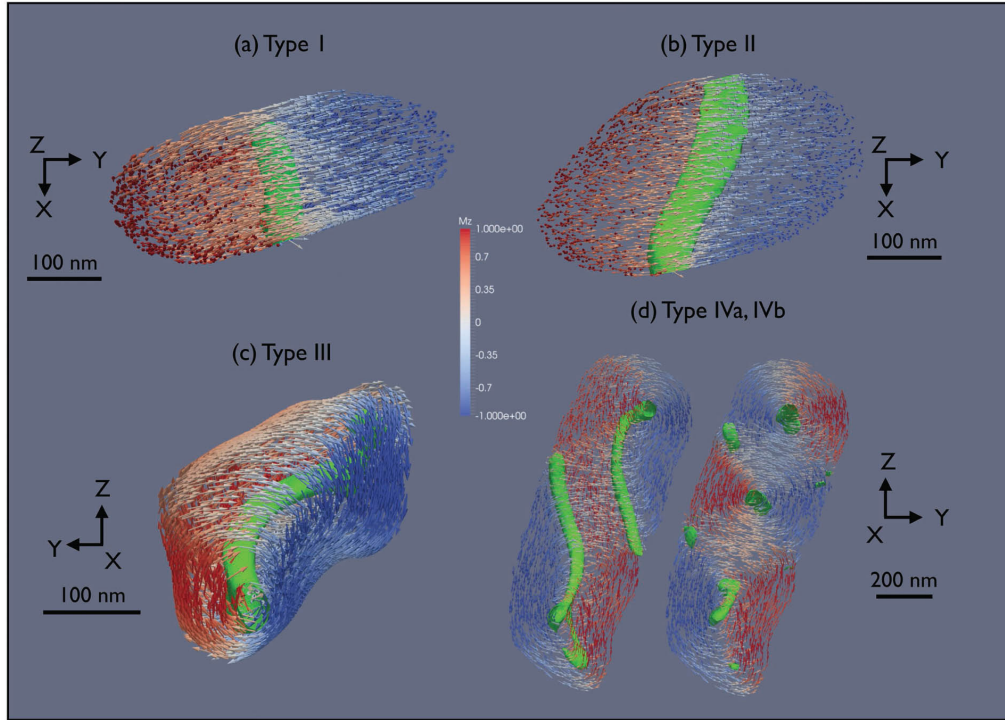


Figure 1.14: Typical remanence states of kamacite grains meshed for micromagnetic simulation after 3D tomographic images of Semarkona dusty olivine kamacite observed using the FIB ‘slice and view’ technique (see Einsle et al. (2016) for more information about methods). Micromagnetic simulations assign a random magnetisation to each cell of the meshed grain, and then MERRILL (see Chapter 5) is used to determine least energy states, i.e. states likely to occur in nature. The typical states observed are in single or multi-vortex state. The areas highlighted in green are vortex cores determined by calculating the helicity of the magnetisation vectors. From Einsle et al. (2016).

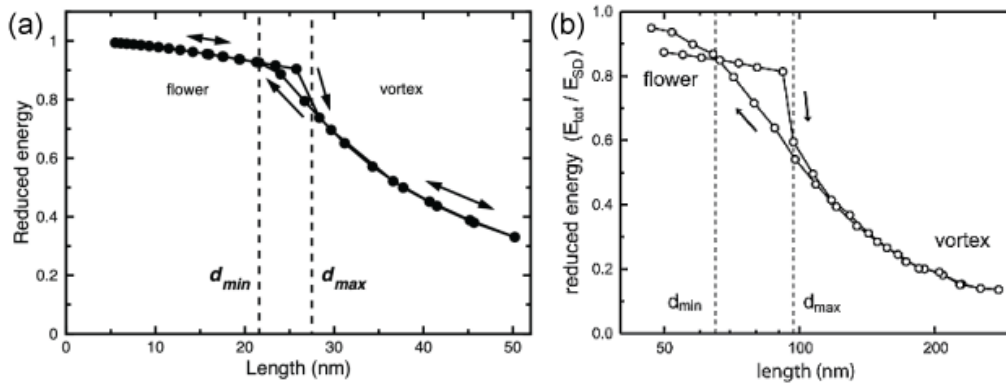


Figure 1.15: The domain state transitions for iron (a) and magnetite (b) determined by finite difference method micromagnetic models by starting with an initial single domain (flower) solution and increasing grain volume (length, x-axis) until a vortex state is energetically favourable, and then decreasing in size until a flower state is favourable. Iron transitions to vortex state at smaller grain volumes than magnetite. Adapted after (a) Muxworthy and Williams (2015) and (b) Muxworthy and Williams (2006).

1.4.5 Origin of meteorite magnetic remanence

Pre- or post-accretionary remanence

The magnetic properties of meteorites have been studied for over fifty years, with primary aims of understanding more about the parent body from which the mete-

orite originated from, and to better understand the protoplanetary disk, as certain meteorites have the potential to retain remanent magnetisation since their formation 4.6 billion years ago. Minerals such as dusty olivine have been suggested as being capable of retaining magnetic remanence since their formation 4.6 billion years ago (Uehara and Nakamura, 2006; Lappe et al., 2011; Fu et al., 2014b). In Chapter 4 and 5 I investigate the possibility of dusty olivine having retained a pre-accretionary magnetic remanence.

A secondary magnetisation on the parent body could be induced by re-heating, which would reset the magnetisation in the presence of a field, or demagnetise it in the absence of a field. Chemical alteration of the magnetic minerals, or growth of new magnetic minerals during hydrothermal alteration or metamorphism on the parent body would induce a post-accretional magnetisation. Post-accretional magnetisation can be analysed to give insight into the parent body of the meteorite, such as whether it had developed a dynamo, and size of the parent body can be modelled from the palaeointensity of the meteorite (Weiss et al., 2008).

Terrestrial ‘contamination’ of remanence

It is possible for meteorites to acquire a magnetisation of terrestrial origin, and this must be identified if present. Upon atmospheric entry stony meteorites experience heat sufficient to melt the outer few-mm of the meteorite, this is widely known as the ‘fusion crust’. A fusion crust is very distinct, as it is glassy, and its magnetisation will be of terrestrial origin (Butler, 1972). Lovering et al. (1960) modelled iron meteorite mass loss due to ablation upon atmospheric entry, with an approximate ablation of 0.18 cm s^{-1} from the surface. As well as this, removal of material by ablation is more rapid than the inward diffusion of heat, so only the outer few-mm of stony meteorites would be remagnetised due to their lower thermal conductivity (Lovering et al., 1960). Therefore, the interior of the meteorite sample should have preserved pre-terrestrial magnetic remanence.

Remagnetisation of meteorites can also occur when they come in contact with

hand magnets, a common practise when identifying and collecting meteorites. Gattacceca and Rochette (2004) argued that artificial contamination of magnetic remanence with strong hand magnets can be identified by Zijderveld plots that have curved demagnetisation paths.

The formation of newly mineralised magnetic phases whilst residing on Earth can result in a meteorite acquiring a terrestrial chemical remanent magnetisation corresponding to the Earth's magnetic field that will contaminate the natural remanence (Uehara et al., 2012). Hence, it is desirable to analyse meteorites that are observed falls and collected before the opportunity for terrestrial alteration.

Impact origin of remanence

It has been suggested that the magnetisation present in meteorites could be a result of magnetic fields generated by very large impacts with the Earth (Crawford and Schultz, 1999; Carporzen et al., 2005). Carporzen et al. (2012) analysed the rocks below the surface of the Vredefort impact crater with two 10 m boreholes and determined that the previously identified surface random magnetisation (Carporzen et al., 2005) is a near-surface feature caused by lightning strikes. Such signals are ubiquitous in ancient terranes like those found in Africa, e.g., Biggin et al. (2011); Dodd et al. (2015).

The observed difference between the magnetic remanences of the interior of the meteorite and the near-surface fusion crust indicates that the near-surface remanence is usually of terrestrial origin, i.e., the Earth's magnetic field, and the interior remanence usually pre-dates atmospheric entry (Weiss et al., 2010b). Over the recent decades it has been established that the magnetisation observed in the interior of meteorites is usually of extraterrestrial origin, and while we must be wary of terrestrial contamination of the remanent magnetisation, it can be analysed to aid our understanding of early Solar System processes and meteorite parent bodies.

1.4.6 Brief history of meteoritic magnetism

Reliability of magnetisation identified in early studies

Lovering (1959) conducted one of the first extraterrestrial magnetic analyses on the Moore County eucritic meteorite. Thermomagnetic analysis suggested the meteorite had experienced a minimum temperature of at least 560 °C, and a magnetic field was present on the parent body. It is clear now, however, the interpretations of the remanence in these early studies often suffered from alteration of the remanence carriers contaminating results; meteorites are typically heavily reduced and more prone to thermal alteration than is typical for terrestrial rocks (Herndon et al., 1976; Dos Santos et al., 2015); modern palaeomagnetic techniques aim to avoid heating (Gattacceca and Rochette, 2004; Lappe et al., 2013).

The CV-CK parent body dynamo hypothesis

Cosmic ray exposure ages and spectral reflectance analyses predict that the CV-CK clan of carbonaceous chondrites originate from the same heterogeneous, and possibly thermally stratified, asteroid (Greenwood et al., 2010). It has been proposed that the unequilibrated CV chondrites sample the crust of the asteroid, and the metamorphosed CK chondrites sample the thermally stratified interior (Weiss and Elkins-Tanton, 2013).

Allende has been one of the most magnetically analysed meteorites since its fall, e.g., Butler (1972); Sugiura et al. (1979); Acton et al. (2007); Kletetschka et al. (2010); Fu et al. (2014a); Muxworthy et al. (2017). Early work attempted to estimate pre-accretionary magnetic fields from Allende (Sugiura et al., 1979), however, more recent studies have demonstrated that the magnetic remanence carried by Allende is complex and multi-component, and it is clear now that the chondrules and matrix must be analysed separately, as they have significantly different magnetic histories (Fu et al., 2014a; Bland et al., 2014; Muxworthy et al., 2017).

Carporzen et al. (2011b) presented evidence for uniform magnetisation amongst mutually oriented Allende bulk subsamples, indicating a post-accretional rema-

nence, and arguing that the parent body had undergone partial differentiation with a sustained magnetic dynamo. Further analysis of Allende's chondrules by Emmer-ton et al. (2011) agreed that Allende's magnetisation is post-accretional, and that it may have retained a possibly pre-accretionary high-temperature primary magneti-sation component, however, the most recent study of Allende's chondrules proposed that their magnetic remanences have no nebular origin due to hydrothermal aqueous alteration of the chondrules' magnetic carriers on the parent body in the absence of a magnetic field (Fu et al., 2014a). Kaba, a meteorite thought to be from the same parent body as Allende has shown evidence for a magnetic field on the CV parent body existing in the first 6 Myr since its accretion (Gattacceca et al., 2016). The palaeomagnetic data from Allende limits the upper bounds of the suggested CV-dynamo at 40 million years since accretion (no ambient field present during aqueous alteration of Allende (Fu et al., 2014a)).

The aforementioned CV-CK parent body dynamo debate (see section 1.2.1) has been ongoing as a result of a lack of agreement between the geochemical evidence and the palaeomagnetic evidence (Elkins-Tanton, 2010; Greenwood et al., 2010; Carporzen et al., 2011b; Fu et al., 2014a; Dunn et al., 2016). There are however, also discrepancies in the palaeomagnetic data that are presented.

Brecher and Arrhenius (1974) found that Karoonda, a CK4 chondrite, does not carry any remanence of palaeomagnetic significance; this would be unlikely had it been subjected to an ambient field due to the CV-CK-dynamo as it cooled. The remanence of Karoonda is analysed in this thesis in Chapter 2 to revisit the CV-CK parent body dynamo debate. A recent palaeomagnetic study of the meteorite Kaba (CV3) found evidence for the existence of a magnetic dynamo on its parent body more than 6 million years after formation of the Solar System (Gattacceca et al., 2016).

The most recent study on Allende focused on its matrix rather than the chon-drules, and suggested that a parent body dynamo was not necessary to impart the magnetisation observed in its matrix (Muxworthy et al., 2017). This study looks

at an impact compaction process that is capable of rapidly heating the matrix to high-temperatures while leaving little evidence for shock (Bland et al., 2014), which results in the acquisition of a parent-body TRM by the matrix magnetic carriers. The unlithified parent body implies that the matrix TRM acquisition pre-dates the initiation of the CV-CK dynamo proposed by Gattacceca et al. (2016). No significant remanence was recorded in the high-temperature end of the magnetic blocking spectrum of Kaba, indicating that no ambient field ($< 0.3 \mu\text{T}$) was present 4 to 6 million years after formation of the Solar System, and that the CV parent body dynamo was not active during this time (Gattacceca et al., 2016). More palaeomagnetic data from CV chondrites are required, hence the remanences of Vigarano (CV3) chondrules are analysed in Chapter 3 to observe the possible evidence for a parent body dynamo recorded by CV chondrites.

Magnetism after the Solar Nebula

As magnetic fields present in the Solar Nebula are likely a result of a gaseous nebula, a lack of a nebular field suggests a lack of a gaseous nebula, i.e. the lower limit for the age of the Solar Nebula can be constrained by nebular magnetic field palaeointensity data (Fig. 1.16). Magnetic remanence imparted after the decay of nebular magnetic fields may potentially originate from the onset of a meteorite's parent body dynamo, e.g., Wang et al. (2017) found that the dynamo for the Angrite parent body did not initiate until between 4 to 11 million years after the beginning of the Solar System (Fig 1.16). The timing for parent body dynamo onset has been debated, with Weiss et al. (2008) and Elkins-Tanton et al. (2011) proposing a rapid onset following large-scale melting, and Sterenborg and Crowley (2013) proposing a delay in onset of more than 10 million years being likely; dynamos may persist for longer periods of time than those suggested by Elkins-Tanton et al. (2011). However, melting and differentiation do not always lead to the formation of a planetesimal magnetic dynamo, as was observed in the magnetic record of ungrouped achondrite NWA 7325 (Weiss et al., 2017). The lack of a magnetic record in NWA 7325 (palaeointensity

$< 1.7 \mu\text{T}$) agrees with a decayed nebular magnetic field 4 million years after Solar System formation (NWA 7325 Al-Mg dated to be 4563.09 ± 0.26 Myr old).

Magnetism in the Solar Nebula

Nebular magnetic field data that indicate the presence of ambient magnetic fields can therefore also constrain the lifetime of the Solar Nebula. Prior to the study of Wang et al. (2017), from the same research group at the Massachusetts Institute of Technology, Fu et al. (2014b) reported a palaeointensity estimate attributed to nebular magnetic fields present during the first three million years of the Solar System. Used to distinguish between the chondrule formation mechanisms discussed previously in this chapter (see section 1.2.3), the palaeointensity estimate of $54 \pm 21 \mu\text{T}$ suggested against theories that require strong magnetic fields such as X-winds (Shu et al., 1997) and magnetic reconnection (Levy and Araki, 1989). The palaeointensity has brought the theories of chondrule formation by the nebular shock (Desch et al., 2012) and planetesimal collision (Wakita et al., 2017) to prominence as they fulfil the Solar Nebula magnetic field requirements suggested by Semarkona dusty olivine.

1.5 Thesis objectives and layout

The following chapters of this thesis will use experimental and numerical data to consider the origin and reliability of magnetic remanence carried by various chondritic meteorites, determine whether the remanence originates from before or after the Solar Nebula, and how these records of remanent magnetisation can inform us about the history of the meteorite from formation 4.6 billion years ago to the present day.

In chapter 2, the natural remanence carried by the carbonaceous chondrite Ka-roonda (CK4) is scrutinized to determine whether it has any palaeomagnetic significance, as has been implied by various recent studies.

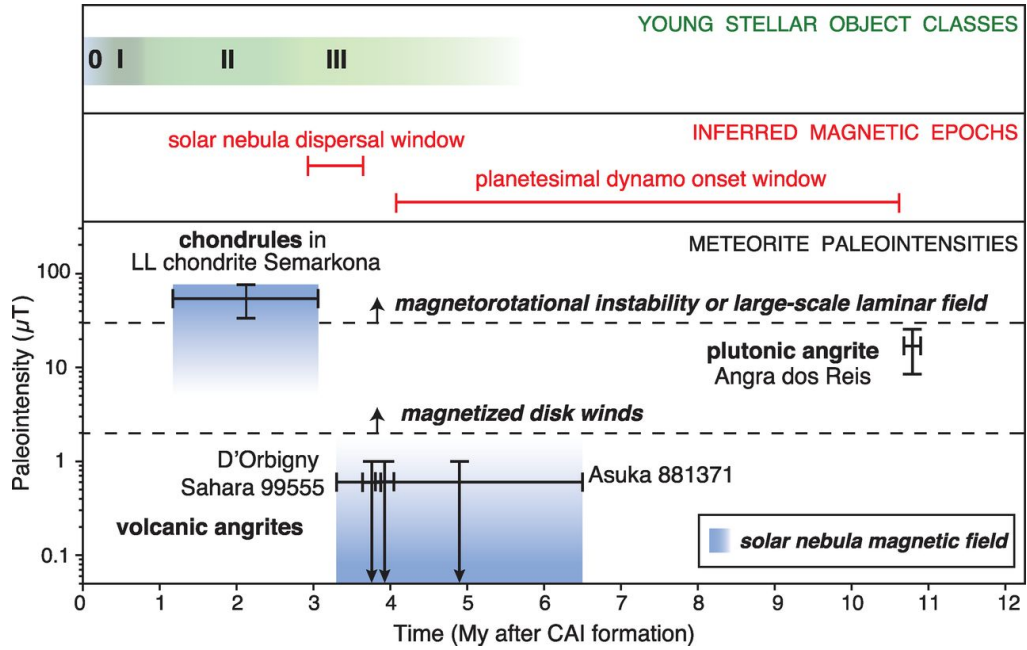


Figure 1.16: A timeline for the early Solar System development constrained by palaeointensity estimates from Semarkona (Fu et al., 2014b) and volcanic and plutonic Angrites (Wang et al., 2017). Time zero is in reference to the formation of the oldest known CAI (Connelly et al., 2012a). Dashed lines mark the lower limits of two nebular angular momentum transport mechanisms: magnetorotational instability (MRI) and magnetised disk winds.

Given the difficulty to determine the origins of remanence, a micro-CT conglomerate test of chondrites is developed in Chapter 3 and applied on chondrites Vigarano (CV3) and Bjurböle (L/LL4) to constrain the timing of remanence acquisition.

In Chapter 4, the origin of remanence in unequilibrated ordinary chondrite Bishunpur (LL3.1) is observed experimentally using electron microscopic techniques, which motivated the study recounted in Chapter 5; a micromagnetic modelling campaign analysing meteoritic iron to determine its recording fidelity, and the feasibility of retaining remanence from the early Solar System.

Conclusions of the findings in this thesis and avenues for future research motivated by them are discussed in Chapter 6.

Chapter 2

The natural remanence of metamorphosed chondrite Karoonda

2.1 Introduction

Geological and geophysical analyses of meteorites can develop understanding of the history of the meteorites' parent body, and depending on the extent of parent body alteration, potentially the pre-accretionary conditions of the early Solar System. Recent studies (Carpözen et al., 2011a; Elkins-Tanton et al., 2011; Weiss and Elkins-Tanton, 2013) have suggested that the CV chondritic meteorites, which are typically unequilibrated, and the CK chondritic meteorites, which have undergone metamorphism, originate from the same thermally stratified asteroid; the unequilibrated CV chondrites sample the crust, and the metamorphosed CK chondrites originate from deeper within the body (Fig. 2.1). Cosmic ray exposure ages and spectral reflectance analysis link the CV and CK chondrites and the Eos family of asteroids, suggesting they were once a single asteroid (Greenwood et al., 2010). Elkins-Tanton et al. (2011) propose that the parent body would have formed an Earth-like magnetic dynamo due to partial differentiation. The CV-CK magnetic dynamo hypothesis was initially based upon palaeomagnetic data from Allende (Carpözen et al., 2011a); more CV chondrites have since shown evidence of magnetic remanence which may

be due to a parent body magnetic dynamo, e.g., Kaba (Gattacceca et al., 2016).

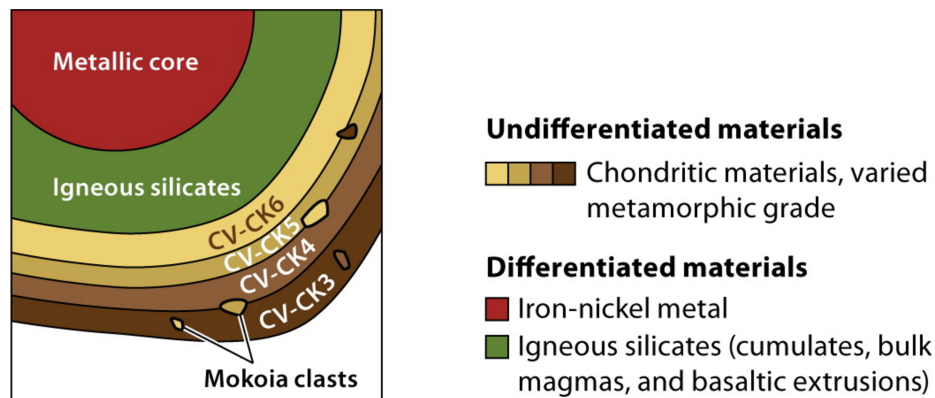


Figure 2.1: A schematic diagram from Weiss and Elkins-Tanton (2013) to show the single partially differentiated parent body that accounts for the CV and CK chondritic meteorites proposed by Weiss and Elkins-Tanton (2013) due to the petrologic and magnetic properties of the CV and CK chondrites.

This parent body magnetic dynamo signature could be recorded by the metamorphosed CK chondrites. The peak metamorphic temperatures reached by CK4 chondrites is broadly constrained due to the variation in techniques used. Clayton et al. (1977) estimate a peak-temperature of 525°C based on the distribution of pre-solar grains in Karoonda. An estimate of 545°C to 645°C was made by Geiger and Bischoff (1991) based on the chemical composition of coexisting pyroxenes; however, these estimates should be considered with caution due to the abundance of Al₂O₃ in CK4 pyroxenes (Noguchi, 1993), which is not taken into account by the method, which is intended for natural pyroxenes with low contents of Al (Lindsley and Andersen, 1983; Chaumard and Devouard, 2016). Olivine-spinel thermometry and pyroxene compositions suggest a peak-temperature of 745°C to 845°C (Noguchi, 1993). ¹⁸O/¹⁶O fractionation of major CK4 minerals indicate temperatures of 585°C to 625°C (Clayton and Mayeda, 1999). Analysis of petrology and Al-Mg isotopes of coarse calcium-aluminium-inclusions in TNZ 057 (CK4) suggest peak-temperatures of 535°C to 795°C for CK4 chondrites (Chaumard et al., 2014). Although these temperature estimates are varying, critically they exceed the majority of the (un)blocking spectrum for magnetite, the primary magnetic carrier in Karoonda, exceeding or near to the Curie point for magnetite, 585°C. Therefore, the temperatures reached by Karoonda would be sufficient to completely overprint pre-

accretionary magnetic remanence, and acquire a thermoremanence of an ambient field. The duration of metamorphism for a thermally stratified parent body heated by radionuclide decay is expected to be on the order of 1 to 100 Myr (Ghosh and McSween Jr., 1998; Henke et al., 2013). However, recent analysis of Fe/Mg interdiffusion of zoned olivines found chondrules of CK chondrites suggest much shorter peak-metamorphic durations of 50 to 70000 years (Chaumard and Devouard, 2016). These timescales suggest either impacts or a radiative heating model (Chaumard et al., 2012) as likely mechanisms for metamorphism. Given the lack of polymict meteorite breccias with both CV and CK material and lack of correlation between petrologic type and shock stage, impacts are unlikely to be the process for heating and metamorphism (Rubin, 1992; Tomeoka et al., 2001; Ohnishi et al., 2007). The radiative heating model proposes an initial CV-type parent body, with metamorphism occurring to the meteoroids during close orbit to the Sun at perihelia of < 0.15 au (Chaumard et al., 2012; Chaumard and Devouard, 2016). The function of heating and duration of heating, and the resulting variation in petrologic type is controlled by size of the meteoroid and the distance and duration of orbit (Chaumard et al., 2012; Chaumard and Devouard, 2016). The radiative heating model can account for the duration and variable heating observed amongst the CV and CK chondrites, and the lack of correlation between shock stage and petrologic type (Chaumard and Devouard, 2016).

As metamorphism is likely to have completely overwritten the remanent magnetisation of the CK chondrites, the record of remanent magnetisation remaining reflects upon the metamorphic conditions. As the interplanetary magnetic field is reported to have decayed to < 1.7 μT after the accretion of the CV-CK parent body (Jogo et al., 2009; Doyle et al., 2016; Weiss et al., 2017), a record of remanent magnetisation owing to an ambient field could indicate a parent body dynamo magnetic field. Given the weak interplanetary magnetic field, a lack of a remanent magnetisation supports a radiative heating model or a parent body with no active dynamo.

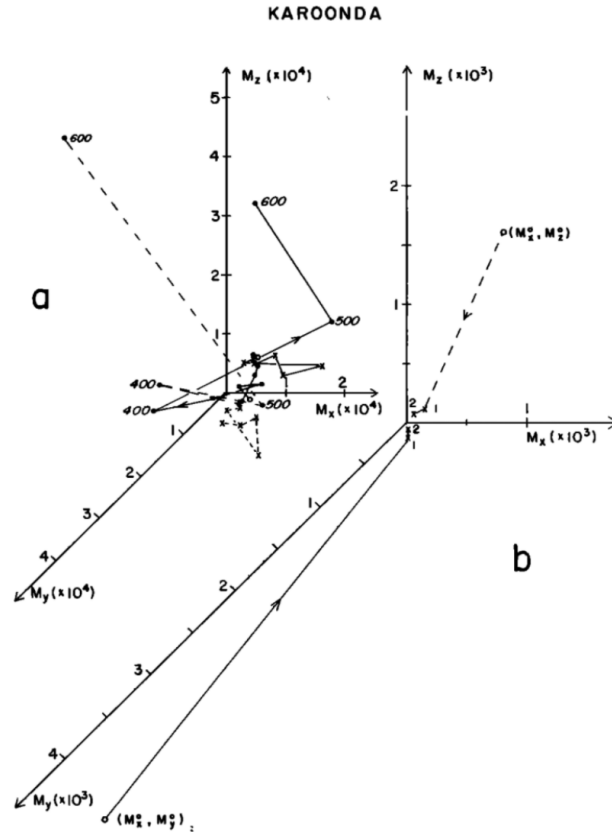


Figure 2.2: A demagnetisation plot of Karoonda from Brecher and Arrhenius (1974), showing that 95% of remanence is lost after one cycle; Karoonda is easily demagnetised.

Conflicting reports of the magnetic record of Karoonda, a CK chondrite that was an observed fall in Australia in 1930 (Mason and Wiik, 1962) make it difficult to distinguish between these two possibilities. Immediate recovery makes this an ideal CK chondrite to study both chemically and magnetically. Mineralogical analyses find approximately 80% of the magnetic mineralogy in Karoonda is large (5-10 μm) magnetite, and 20% of the mineralogy is fine-grained magnetite, which has the potential to carry a stable natural remanent magnetisation (NRM) (Mason and Wiik, 1962; Ramdohr, 1963). Brecher and Arrhenius (1974) analysed the NRM of Karoonda and found that the stable component of magnetisation did not carry a significant palaeomagnetic signal (Fig. 2.2). This suggests that Karoonda did not acquire a significant TRM when it cooled. Petrological evidence for heterogeneous silicate darkening of matrix and chondrule mesostases in Karoonda suggest that it has been subject to significant shock at high temperature, resulting in the melting

and recrystallisation of some non-vesicular olivine grains as olivine with vesicles (< 10 to 100 nm) and opaque inclusions (0.1 to 3 μm magnetite and (non-magnetic) pentlandite) (Ohnishi et al., 2007). There is also evidence for dislocations subsequent to vesicular olivine crystallisation and heating of these later dislocations, indicating multiple events of shock and annealing (Ohnishi et al., 2007). The rapid heating and cooling experienced by Karoonda would have remagnetised the magnetite with a thermoremanence depending on the ambient magnetic field conditions and the degree of shock remanence overprinting.

Early magnetic studies of Karoonda found that the intensity and stability of the NRM carried by Karoonda is almost identical to the intensity and stability of a pTRM imparted cooling to room temperature from 300°C in an ambient field of 50 μT (Sugiura, 1977). This suggests the NRM of Karoonda may be a pTRM blocked up to 300°C in an ambient field of 89 μT , as later quantified by Nagata (1979). Anhysteretic remanent magnetisation (ARM) has been used as an analogue to TRM (for single domain grains) (Lappe et al., 2013; Lerner et al., 2017), however it is not a perfect analogue (Dunlop and Argyle, 1997). Concave plots of the NRM-ARM demagnetisation spectra for Karoonda suggest that the NRM is not carried by the high-coercivity remanence carriers (Fig. 2.3) (Sugiura, 1977).

Thermomagnetic curves measured for Karoonda by Herndon et al. (1976) were reversible on cooling after heating to the 580°C Curie temperature, showing chemical stability with heating and that pure magnetite is the primary magnetic phase in Karoonda. Sugiura (1977) demonstrated that Karoonda is chemically stable with heating by comparing ARM demagnetisation spectra before and after heating. However, there are significant limitations to the Sugiura (1977) study, which should preclude their palaeointensity estimate from being reliable. Checks for chemical alteration when the pTRM is being applied, i.e., pTRM checks, are essential to ensure that the sample has not been altered during the laboratory repeated heatings. Sugiura (1977) did not conduct pTRM checks as they were imparting the laboratory pTRM. Further, the palaeointensity estimate is based upon one sample, which is

not sufficient for statistical significance. The palaeointensity estimates are unlikely to achieve a single score if using a palaeointensity quality check such as Q_{PI} (Biggin and Paterson, 2014), which typically requires a score of at least 4 to be considered a reliable palaeointensity estimate. Although Karoonda has exhibited thermomagnetic stability (Herndon et al., 1976), I was not able to heat the sample studied in this chapter due to curation restrictions. It is not always possible to heat rare meteoritic material due to curation restrictions or their susceptibility to chemical alteration.

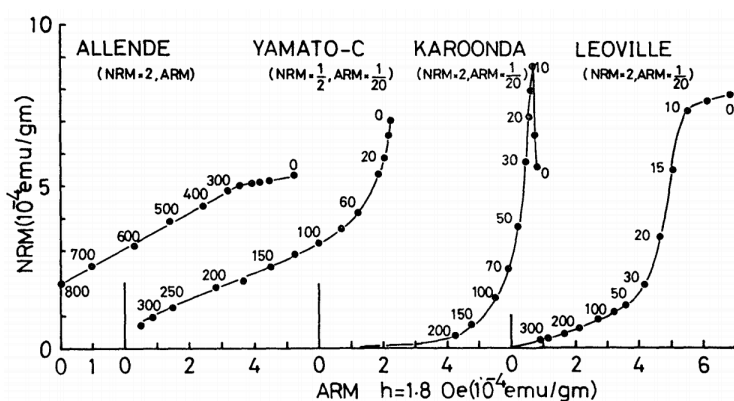


Figure 2.3: A plot of the alternating field (AF) demagnetisation of the NRM plotted against the AF demagnetisation of a laboratory applied ARM for various carbonaceous chondrites. From Sugiura (1977). The third plot shows the demagnetisation behaviour of Karoonda. The concave shape of the Karoonda plot demonstrates that the NRM is more efficiently removed than the ARM, indicating that the NRM is carried by low-coercivity grains, and that the high-coercivity grains do not carry NRM.

Acton et al. (2007) presented a non-heating palaeointensity study of various chondrites, including Karoonda. Acton et al. (2007) investigated chondrules from Karoonda, and found that the magnetite is in pseudo-single domain (PSD) state (Fig. 2.4), a magnetisation structure that has recently been found to be remarkably stable over Solar System timescales (Almeida et al., 2016; Nagy et al., 2017; Chapter 5). The remanence carried by the PSD magnetite, therefore, is unlikely to have relaxed since it was imparted. Acton et al. (2007) attributed an ancient magnetic field of 4.6 ± 1.0 μ T intensity to its remanence using the ratio of equivalent magnetisation (REMc) palaeointensity proxy (Acton et al., 2007). The REMc proxy is calibrated by and assumes a TRM as the origin of remanence (Gattacceca and Rochette, 2004), and Acton et al. (2007) used a calibration factor of 3000, which has since seen refinement to 1900 (Muxworthy and Heslop, 2011), lowering their

estimate to $2.9 \pm 0.6 \mu\text{T}$. The palaeointensity estimate of Acton et al. (2007) is significantly weaker than the $89 \mu\text{T}$ estimate made by Sugiura (1977) and Nagata (1979). The ARM demagnetisation spectra of Karoonda were not found to relate to the NRM demagnetisation spectra (Acton et al., 2007), agreeing with the concave NRM-ARM plots of Sugiura (1977). This indicates that the high-coercivity remanence carriers do not carry remanence, and may suggest that Karoonda has recorded a low temperature pTRM as reported by Sugiura (1977) and Nagata (1979). A different mode of acquisition could be the origin of magnetic remanence in Karoonda, e.g., shock remanent magnetisation (SRM), which has been shown to affect only the low-coercivity remanence carriers (Gattacceca et al., 2008, 2010b; Tikoo et al., 2015).

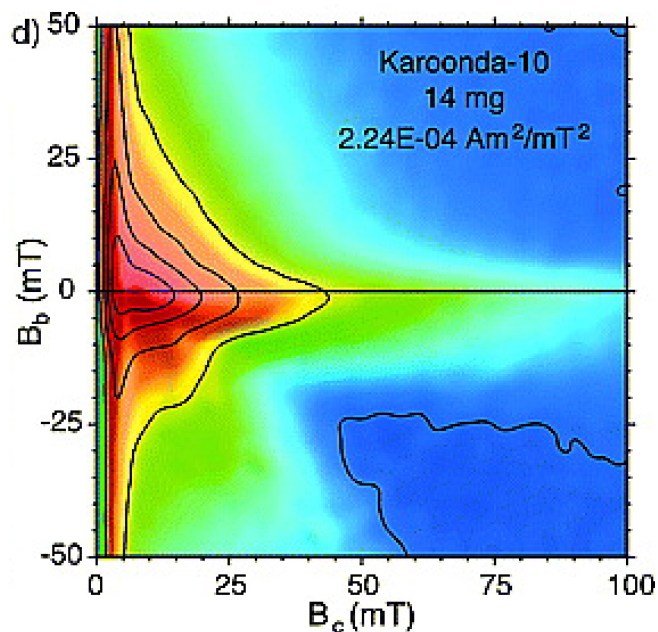


Figure 2.4: A first order reversal curve (FORC) for a sample of Karoonda. From Acton et al. (2007).

The significant difference between palaeointensity estimates for Karoonda may reflect the bulk matrix and chondrule analysis of Sugiura (1977) compared to the individual chondrule analysis of Acton et al. (2007). However, this is unlikely given that Karoonda is an equilibrated meteorite. The variation in estimates may also be due to the different estimation methods employed. The thermal demagnetisation analysis of Sugiura (1977) presents evidence for a 300°C peak temperature pTRM

of approximately 89 μT , however they did not conduct pTRM checks, and the estimate is based upon only one sample. The alternating field (AF) demagnetisation analysis of Acton et al. (2007) demagnetised the NRM of Karoonda chondrules at low alternating fields (MDF \ll 20 mT), while the palaeointensity protocols employed analysed NRM after demagnetisation to 20 mT for the REMc protocol, and 12-35 mT, 18-35 mT, 18-50 mT for the REM' protocol. These demagnetisation fields may target partially demagnetised low coercivity magnetic remanence carriers and the higher coercivity grains predicted by Sugiura (1977) and Acton et al. (2007) to not carry magnetic remanence (Fig. 2.3), and thus result in low palaeointensity estimates.

In this chapter new NRM and ARM demagnetisation spectra and rock magnetic analysis of Karoonda are presented in order to consider its origin of magnetic remanence and its status as a carrier of parent body dynamo palaeomagnetism.

2.2 Methods

The Karoonda samples were prepared from four fragments of Karoonda, KR01, KR02, KR03 and KR04. The samples were taken from the interior of the bulk meteorite to avoid any fusion crust contribution. Five sub-samples were taken from KR01, four from KR02, and KR03 and KR04 were not sub-sampled, totalling 11 samples of Karoonda containing both chondrules and matrix for alternating-field (AF) demagnetisation (Table 2.1). An 18 mg fragment from KR02 was used for rock magnetic characterisation. Samples were loaned from the Natural History Museum, London. Sub-sampling was conducted by the meteorite collection curators at the Natural History Museum, London. It was not possible to mutually orient the sub-samples.

2.2.1 Rock magnetic measurements

To characterize the magnetic carriers in Karoonda, hysteresis loops, backfield remanence curves and first-order reversal curves (FORCs) were measured using a Princeton Measurements Vibrating Sample magnetometer at Imperial College London. FORCs were measured following the Irregular FORC measurement protocol (Zhao et al., 2015), which determines an irregular grid for variable resolution measurements from an initial hysteresis loop measurement; larger magnetisation gradients are measured at higher resolution and smaller magnetisation gradients are measured at lower resolution. Irregular FORCs were measured over two hours, with 80 individual curves, which has been shown to produce results similar to standard FORCs of up to 300 individual curves (Zhao et al., 2015).

2.2.2 Magnetic remanence measurements

Before the FORC measurements, the NRM of the sub-samples from Karoonda was step-wise alternating field (AF) demagnetised with logarithmically increasing field strength to accurately model the logarithmic coercivity spectrum (Robertson and France, 1994; Kruiver et al., 2001) until each sample appeared to be fully demagnetised, i.e. displayed erratic behaviour. Samples were demagnetised with a Molspin Tumbling AF Demagnetizer and magnetisation was measured with an Agico JR-5 at Imperial College London. After demagnetisation of the NRM, an ARM was applied to the sub-samples using an ASC Scientific D-2000 AF Demagnetizer at Imperial College London. A bias field of 30 μT was applied, with a peak AF of 80 mT and a decay rate of 0.001 mT per half-cycle. The ARM was subsequently AF demagnetised as described above for the NRM. Demagnetisation data were processed and presented using PuffinPlot (Lurcock and Wilson, 2012).

2.3 Results

2.3.1 Rock magnetic measurements

The hysteresis loops, e.g., Figure 2.5, indicate a coercivity of 14 mT and FORCs, e.g., Figure 2.6, indicate a coercivity of up to 40 mT. The FORCs indicate that the grain assemblage contains both uniformly and non-uniformly magnetised grains, classically referred to as single domain and pseudo-single domain respectively. Micromagnetic simulations have shown that cubic single domain grains are manifested as the 135° ridge in FORC diagrams, similar to Figure 2.6 (Valdez-Grijalva, personal communication). Such a grain assemblage of magnetite has been shown to be capable of carrying and retaining palaeomagnetic remanence over geological timescales (Almeida et al., 2016a). The spreading of the ridge vertically at the origin suggests a possible contribution from superparamagnetic (SP) grains.

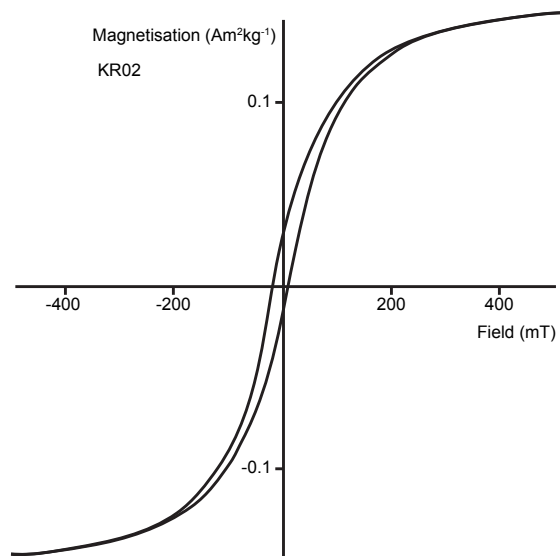


Figure 2.5: Hysteresis loop for a sub-sample of KR02 from Karoonda.

2.3.2 Magnetic remanence measurements

Zijderveld plots (Zijderveld, 1967) with inset equal-area projects of the NRM demagnetisation and inset demagnetisation spectra of the NRM and ARM for four representative Karoonda samples are presented in Figure 2.7. The mass normalised NRM

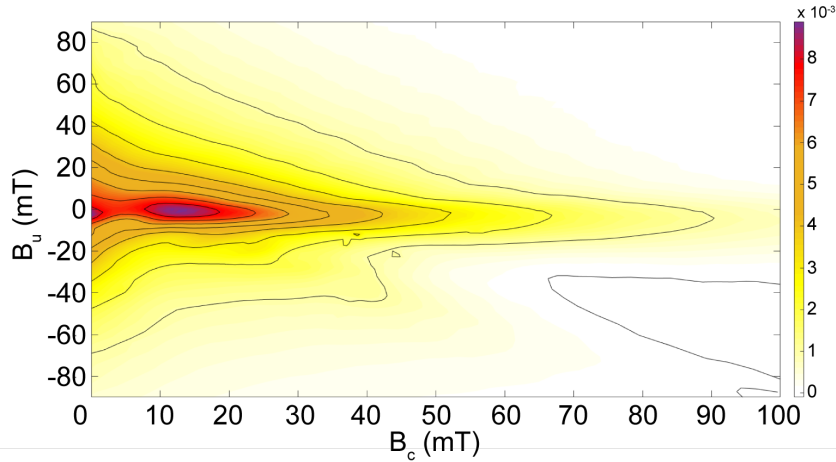


Figure 2.6: First order reversal curve (FORC) (Roberts et al., 2000) for sample KR02 measured over two hours using the Irregular FORC measurement protocol (Zhao et al., 2015), with 80 individual curves and processed with a smoothing factor (SF) of two.

intensities of all 11 Karoonda samples are of the range of 0.671 to $23.4 \text{ mAm}^2\text{kg}^{-1}$, with an average of $12 \pm 8 \text{ mAm}^2\text{kg}^{-1}$ (Table 2.1). The median destructive field (MDF) ranges from 2.2 to 9.1 mT with an average of $3.8 \pm 1.8 \text{ mT}$ (Table 2.1). These AF demagnetisation spectra do not resemble the spectra for the AF demagnetisation of the ARM applied (Fig. 2.7). The mass normalised ARM intensities of the 11 Karoonda samples are of the range of 1.39 to $2.26 \text{ mAm}^2\text{kg}^{-1}$ with an average of $1.7 \pm 0.25 \text{ mAm}^2\text{kg}^{-1}$ (Table 2.1). The MDF ranges from 11 to 16 mT with an average of $14 \pm 1.2 \text{ mT}$ (Table 2.1).

The NRM of the sub-sampled fragments is significantly higher (average of $15 \pm 6.0 \text{ mAm}^2\text{kg}^{-1}$) than that of KR03 and KR04 (average of $1.3 \pm 0.63 \text{ mAm}^2\text{kg}^{-1}$), which were not sub-sampled. The NRM of the sub-samples is also significantly higher than the NRM of the KR01 ($1.6 \text{ mAm}^2\text{kg}^{-1}$) and KR02 ($3.0 \text{ mAm}^2\text{kg}^{-1}$) samples, which was measured prior to sub-sampling. Sub-sampling was conducted with non-magnetic equipment to reduce the chance of contamination during sub-sampling. However the substantial difference between the intensity of magnetisation and the demagnetisation spectra of the sub-sampled fragments compared to KR03 and KR04 (Fig. 2.7) suggests that they have been magnetically contaminated through the sub-sampling process.

Table 2.1: A table showing the mass, natural remanent magnetisation (NRM), anhysteretic remanent magnetisation (ARM), and the median destructive field (MDF) for the AF demagnetisation of the NRM and ARM for each sample of Karoonda studied in this chapter.

Sample	Mass (mg)	NRM ($\text{mAm}^2\text{kg}^{-1}$)	ARM ($\text{mAm}^2\text{kg}^{-1}$)	NRM MDF (mT)	ARM MDF (mT)
KR01Aa	168	8.83	1.91	9.1	14
KR01Ab	192	17.8	1.94	2.8	15
KR01Ba	70.1	17.9	1.52	2.7	15
KR01Bb	73.9	15.6	1.49	2.8	16
KR01Bc	95.4	23.4	1.57	4.3	14
KR02A	56.4	7.44	1.52	3.3	14
KR02B	148	14	1.39	3.1	14
KR02C	88.6	6.43	1.46	4.3	14
KR02D	43.6	23.4	1.67	3.2	14
KR03	90.1	0.671	2.26	2.2	11
KR04	134	1.93	1.48	4.2	13

2.4 Discussion

2.4.1 Natural and anhysteretic remanence properties

The ARM acquisition and demagnetisation was similar for all the samples of Karoonda, reflecting the equilibration of the meteorite’s mineralogy. This is in contrast to the NRM of the samples, which is significantly higher for the KR01 and KR02 sub-samples than for KR03 and KR04, which were not sub-sampled. The equipment used to sub-sample was non-magnetic, and all the samples were kept in the same containers and inside a non-magnetic Faraday cage except during their storage in the Natural History Museum and transporting between the Natural History Museum and Imperial College London. While the demagnetisation spectra do not follow a curved path as is typical for samples magnetised with an artificial strong field (Fig. 2.7) (Gattacceca and Rochette, 2004), the intensities are significantly stronger than those observed in previous studies (Sugiura, 1977; Acton et al., 2007) and in KR03 and KR04, suggesting that they may have been artificially remagnetised through the sub-sampling process.

The AF demagnetisation of the NRM of all the Karoonda samples was achieved at very low alternating fields. The samples were typically almost entirely demagnetised (approximately 10 to 20% remaining) with alternating fields as low as 6 mT (Fig. 2.7). The efficient AF demagnetisation of the samples is also reflected in the low values for the MDF (average of 3.8 ± 1.8 mT). This is in contrast to the AF

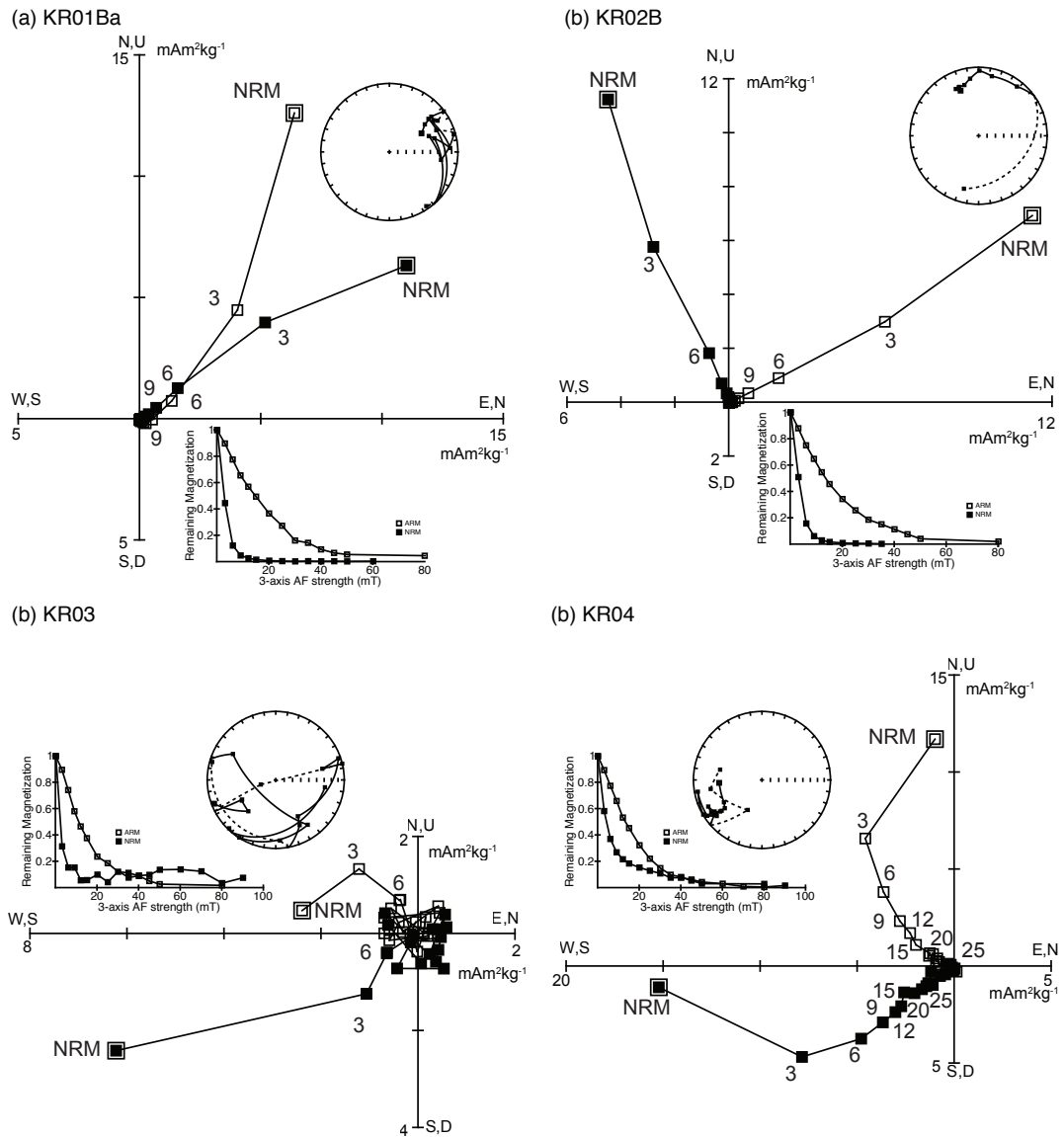


Figure 2.7: Representative Zijderveld plots and equal area projections of the sample set for the AF demagnetisation of Karoonda. The Zijderveld plots and equal area projections are for the demagnetisation of the natural remanent magnetisation (NRM) of Karoonda samples. Both NRM and anhysteretic remanent magnetisation (ARM) are plotted on the demagnetisation plot insets, which are normalised to the initial NRM and ARM. Demagnetising field steps are labelled on the Zijderveld plots in mT, and magnetisation is in $\text{mA}\cdot\text{m}^2\cdot\text{kg}^{-1}$

demagnetisation of the 30 μT ARM applied to the sample. The ARM MDF average of 13.9 ± 1.15 mT is more than three times greater than the MDF for the NRM; the NRM is largely carried by grains of low-coercivity. This is in agreement with the findings of Sugiura (1977). ARM acquisition is analogous to a TRM acquisition (Lappe et al., 2013; Lerner et al., 2017), which suggests that no thermoremanence is

carried by the higher-coercivity grains; a parent-body field has not been recorded by the magnetite in Karoonda. A palaeointensity estimate was not attempted in this study due to the difference between the NRM and ARM demagnetisation spectra; there was no plateau to compare the two remanences, as is necessary with remanence ratio methods (Muxworthy and Heslop, 2011; Lappe et al., 2013). The ease of demagnetisation at fields typically used for cleaning of viscous remanence may suggest that Karoonda's remanence is largely a VRM due to residing on Earth with the ambient field of the geodynamo present, however Brecher and Arrhenius (1974); Sugiura (1977) demonstrated that Karoonda does not acquire a significant VRM. Gattacceca et al. (2010a) found a similar range of NRM and ARM MDF values (2 to 5 mT and 4 to 37 mT respectively) for lunar lithologies determined to have a shock origin of remanence.

2.4.2 Implications for the origin of Karoonda's magnetisation

A shock origin of remanence would require that Karoonda has experienced shock on the order of > 5 to 20 GPa (Sugiura, 1977; Gattacceca et al., 2008, 2010b). Scott et al. (1992) classify Karoonda as shock stage 1 (S1), however, which corresponds to < 5 GPa. The silicate darkening observed in Karoonda, which is due to the presence of vesicular olivine in both the matrix and chondrules, indicates that it has undergone heterogeneous partial melting of olivines and recrystallisation after accretion (Ohnishi et al., 2007). A mild impact event while the meteorite was at $> 600^{\circ}\text{C}$, i.e., syn-metamorphic shock, may have resulted in heterogeneous heating in excess of 1600°C ; the bulk meteorite was not heated to 1600°C . The new crystallisation of > 100 nm magnetite suggests that these recrystallised grains are the single domain high coercivity remanence carriers predicted to not carry NRM. The dislocations also evident in Karoonda chondrules and matrix post-dating the vesicular olivine formation indicate a late stage shock event also occurred (Ohnishi et al., 2007). These dislocations show evidence of being thermal annealed, indicating that an even later heating event after this secondary shock event occurred

(Ohnishi et al., 2007). The high resolution observations of silicate darkening and dislocations motivate Ohnishi et al. (2007) to reclassify Karoonda as shock stage 2 (S2), corresponding to up to 10 GPa shock pressures. Syn-metamorphic shock has been observed in ordinary chondrites to suggest that an optically assigned shock stage cannot indicate an absence of shock (Ruzicka et al., 2015).

The efficient AF demagnetisation of the NRM here, in Sugiura (1977), and Acton et al. (2007) suggests that the NRM has been influenced by shock, and any TRM that may have been carried has likely been overprinted by an SRM. Sugiura (1977) present evidence for the NRM in Karoonda being of pTRM origin, however they also propose SRM as a possible origin of remanence if Karoonda experienced > 5 GPa impacts in the presence of an ambient field. Shock remanence typically affects the low-coercivity grains (Cisowski et al., 1983; Tikoo et al., 2012), which suggests that a lack of remanence at higher alternating fields is due to a lack of a significant ambient field recording when the vesicular olivine magnetites cooled. However, given that Karoonda experienced thermal annealing subsequent to the shock-induced formation of vesicular olivine, this may be the thermal event that resulted in the recording of remanent magnetisation, which could suggest that Karoonda's NRM is a pTRM, as proposed by Sugiura (1977) and Nagata (1979).

The lack of a high-temperature magnetic remanence suggests that metamorphism and formation of vesicular olivines occurred in the absence of an ambient magnetic field, which suggests that there was not an active magnetic dynamo on Karoonda's parent body during metamorphism and final cooling. An alternative theory for the processing of CV and CK chondrites to account for both the similarities and the variation amongst them is by thermal processing due to variable heliocentric distances from the Sun prior to atmospheric entry (Chaumard et al., 2012). The radiative heating from the Sun can account for the peak-temperatures reached to account for the metamorphism as well as the observed silicate darkening. An impact event > 5 GPa subsequent to the formation of the vesicular olivines is necessary, as the observed dislocations would not survive the heating (Tomeoka

et al., 2001; Ohnishi et al., 2007; Chaumard et al., 2012). Impacts of magnitude > 5 GPa are severe enough to result in overprinting the NRM with a shock remanence (Cisowski et al., 1983; Tikoo et al., 2012). The magnitude of the magnetic field of the Solar Wind after the first 4 Myr since Solar System formation is argued to be < 1.7 μT (Weiss et al., 2017), so a radiative heating model would result in a weak palaeofield recording, which is consistent with Acton et al. (2007), however inconsistent with Sugiura (1977) and Nagata (1979).

The evidence for an 89 μT palaeofield recorded by Karoonda as a pTRM (Sugiura, 1977; Nagata, 1979) is not of high enough quality. Palaeointensity estimates are typically unreliable unless sufficient quality control checks are incorporated into the experimentation protocol. The conclusion drawn by Brecher and Arrhenius (1974) and Sugiura (1977) agrees with this study: there is no significant remanence in the high-coercivity magnetic carriers. These were identified as 20% of the magnetite grains (Brecher and Arrhenius, 1974); these are likely formed as a result of the melting and rapid recrystallisation of vesicular olivine containing magnetite and (non-magnetic) pentlandite inclusions of 0.1 to 3 μm size (Ohnishi et al., 2007). The dissimilarity between the NRM and ARM AF demagnetisation spectra found in Karoonda by Sugiura (1977) and Acton et al. (2007) agrees with the AF demagnetisation spectra observed in this study: there is no significant high-coercivity thermoremanence carried by Karoonda. Considering the high resolution transmission electron microscopy analysis of Ohnishi et al. (2007), it is most likely that Karoonda was remagnetised (or demagnetised) by the thermal annealing event subsequent to the shocks that proceeded the formation of the vesicular olivines. The palaeointensity estimate made by Acton et al. (2007), however, should be reduced to 2.9 ± 0.6 μT according to the recalibration of the REM method calibration constant (Muxworthy and Heslop, 2011). The estimate should still be approached with caution, as the estimation protocol targeted the demagnetised low-coercivity grains and higher-coercivity grains predicted to not carry magnetic remanence.

2.5 Conclusion

This study aimed to determine the origin and type of remanence present in Karoonda. The natural remanent magnetisations of the Karoonda sub-samples of KR01 and KR02 are more intense than the magnetisations of KR01 and KR02 measured prior to sub-sampling. This may indicate that the cutting of the samples resulted in contamination of the natural remanence. Previous publications have reported palaeointensity estimates for Karoonda as 89 μT and $2.9 \pm 0.6 \mu\text{T}$ (Sugiura, 1977; Nagata, 1979; Acton et al., 2007). However, the 89 μT estimate made by Sugiura (1977) and Nagata (1979) should not be considered to be reliable estimates due to insufficient quality checks during the experimental protocol. Previous studies also report no significant palaeomagnetic remanence in the higher end of the coercivity spectrum (Brecher and Arrhenius, 1974; Sugiura, 1977; Acton et al., 2007). The anhysteretic remanence was found to not replicate the natural remanence, and indicates that no NRM is carried by the high-coercivity magnetic carriers, agreeing with previous studies (Sugiura, 1977; Acton et al., 2007). Further, a new value for the calibration constant for the REMc protocol reduces the palaeointensity estimated by Acton et al. (2007) to $2.9 \pm 0.6 \mu\text{T}$.

The rock magnetic measurements presented here agree with those previously published, and indicate that a remanence would be recorded and preserved to the present day. The demagnetisation of the natural remanence suggests that there is no remanence carried by the medium to high end of the coercivity spectrum. This suggests that no ambient field was recorded, or the magnetic remanence was not retained, from the event that resulted in the formation of vesicular olivine and associated fine-grained magnetite (Ohnishi et al., 2007).

The remanent magnetisation of Karoonda likely originates from the thermal annealing event subsequent to the shocks that resulted in the dislocations that postdate the formation of vesicular olivine. The formation of vesicular olivine would have occurred in the absence of a significant ambient field, given that Karoonda does not appear to carry any high-coercivity remanence, and the high-coercivity

remanence carriers are likely to have been formed during this event (Sugiura, 1977; Acton et al., 2007; Ohnishi et al., 2007).

Acquisition of a remanence in interplanetary orbit agrees with the palaeomagnetic evidence that suggests no stable ambient field has been recorded. Chaumard et al. (2012) suggest that the petrologic variation observed amongst CV and CK chondrites is a result of heating of initially homogeneous meteoroids at variable heliocentric distances from the Sun. Solar radiative heating combined with impacts is sufficient to produce the silicate darkening, and would remagnetise the magnetic carriers in Karoonda while in interplanetary orbit subsequent to any processing that occurred on the parent body.

The magnetic remanence of Karoonda suggests that it was heated in the absence of an ambient magnetic field, which supports a solar radiative heating mechanism for CV-CK metamorphism. These events could have taken place on the CK parent body in the absence of a magnetic dynamo. Further study to determine the age of the vesicular olivine and final cooling would help to determine whether these events took place on the CK parent body or in interplanetary orbit.

2.5.1 Acknowledgements and contributions

I conducted the magnetic measurements and analysis, and Sope Badejo helped with the Irregular FORC protocol. Caroline Smith and Natasha V. Almeida conducted the sub-sampling of the original Karoonda sample at the Natural History Museum, London who supplied the meteorite sample. I wrote the chapter with the help of Adrian R. Muxworthy, who had the original idea for the project. This work was funded by the STFC (grant number grant number ST/N000803/1).

Chapter 3

Long-lived magnetism on chondrite parent bodies

The work presented in this chapter has been published in the peer-reviewed journal *Earth and Planetary Science Letters*: Shah, J., Bates, H.C., Muxworthy, A.R., Hezel, D.C., Russell, S.S., Genge, M.J., Long-lived magnetism on chondrite parent bodies. *Earth Planet. Sci. Lett.* 475, pp. 106-118.

The previous chapter considered the origin of magnetisation carried by Karoonda, a metamorphosed carbonaceous chondrite (CK4) assumed to be from the same parent body as the CV chondrites. The CV chondrites are typically unmetamorphosed and as such, can potentially record and retain pre-accretionary magnetic remanence from the early Solar System. However, mild heating and aqueous alteration has affected the CV chondrites, resulting in the magnetic record being altered whilst residing upon the parent body; the CV chondrites can detail the ambient field conditions on the parent body. As discussed in the previous chapter, a parent body dynamo has been proposed for the CV-CK parent body (e.g. (Elkins-Tanton et al., 2011; Gattacceca et al., 2016)). While no dynamo appears to have been recorded by Karoonda (see Chapter 2), the chondrules of CV chondrites affected by parent body processing provide an opportunity to find evidence for an ambient field on the parent body by employing the conglomerate test (Graham, 1949) routinely used

in terrestrial studies to distinguish between pre- and post-accretionary remanence. This chapter reports a new micro-conglomerate test applied to chondrules from Vigarano, a CV3 chondrite, to continue the analysis of the CV-CK parent body, as well as chondrules from Bjurböle, a L/LL4 chondrite that is particularly friable, and hence ideally suited for the initial pilot study of the new method developed in this chapter.

3.1 Introduction

Chondrites formed mainly by accreting up to millimetre-sized chondrules, micrometre-sized fine-grained dust, millimetre-sized calcium-aluminium rich inclusions (CAIs) and opaque phases approximately 4.6 Ga ago (e.g. Scott (2007); Connelly et al. (2012a)). Chondrules are thought to have formed in the presence of magnetic fields before accretion of the parent asteroid, and have the potential to record pre-accretionary magnetic remanences that can be used to estimate the role of magnetic fields in early Solar System momentum transport and chondrule formation (Desch et al., 2012; Fu et al., 2014b). However, many primitive and unequilibrated chondritic meteorites show some evidence of secondary alteration on their parent bodies (Butler, 1972; Krot et al., 1995; Gattacceca et al., 2016). Such alteration could have affected the magnetic carriers, thereby resetting or contaminating pre-accretionary magnetisations. It is, therefore, highly important to unequivocally determine whether the chondrules carry a pre- or post-accretionary magnetic remanence, and to determine the origin of remanence in the case of the latter (Shah et al., 2017).

The so called ‘conglomerate test’ (Graham, 1949) is a palaeomagnetic test to determine the timing of magnetisation for an accreted body (Fig. 3.1), and has been used before in several meteoritic studies, e.g., Allende (CV3) (Butler, 1972; Sugiura et al., 1979; Carporzen et al., 2011b; Fu et al., 2014a), Bjurböle (L/LL4) (Strangway and Sugiura, 1982; Wasilewski et al., 2002), and Vigarano (CV3) (Weiss

et al., 2010a). These studies have found both random and aligned palaeomagnetic directions amongst sub-samples, suggesting, in the former, a pre-accretionary remanence, and in the latter, complex parent-body processing. However, there are some inconsistencies: for some meteorites both types of magnetisation have been reported, e.g., Butler (1972) found a homogeneous magnetisation amongst sub-samples of Allende, then Sugiura et al. (1979) found inhomogeneous magnetisation and finally Carporzen et al. (2011b) again found homogeneous magnetisations. Some of these inconsistencies could lie in the difficulty of performing conglomerate tests on the sub-millimetre scale: sampling, orienting and measuring smaller than standard samples ($\sim 11 \text{ cm}^3$ in terrestrial studies) leads to greater angular-dispersion errors as well as sampling both chondrule and matrix material together into individual samples (Butler, 1972; Strangway and Sugiura, 1982; Böhnell et al., 2009; Böhnell and Schnepf, 2014). Chondrules are particularly small, with volumes of $\sim 0.0005 \text{ cm}^3$ (Table 1.1). Physical disaggregation and reorientation of individual chondrules from a chondrite by hand is likely to introduce errors that are difficult to quantify and, due to scarcity of material, cannot be reduced by simply measuring more samples as is the case for most terrestrial studies (Böhnell and Schnepf, 2014). In a recent palaeomagnetic study of CV chondrite Kaba, Gattacceca et al. (2016) were not able to mutually orient their sub-samples owing to small initial sample sizes (masses up to 220 mg). Accurate reorientations ($< 5^\circ$ error) of chondrule samples have been achieved by working with cut-sections of material (Carporzen et al., 2011b; Fu et al., 2014b,a), however these studies worked with sample sections, and not with whole chondrule samples (Shah et al., 2017).

X-ray micro-computed tomography (micro-CT) has been a successful technique for the 3D volumetric non-destructive characterisation of meteorites, and is widely being incorporated into the curation procedure for meteorites (Hezel et al., 2013; Smith et al., 2013; Zeigler et al., 2015; Shah et al., 2017).

In this chapter a new sub-millimetre-scale method for the palaeomagnetic conglomerate test is presented that uses X-ray micro-computed tomography (micro-CT)

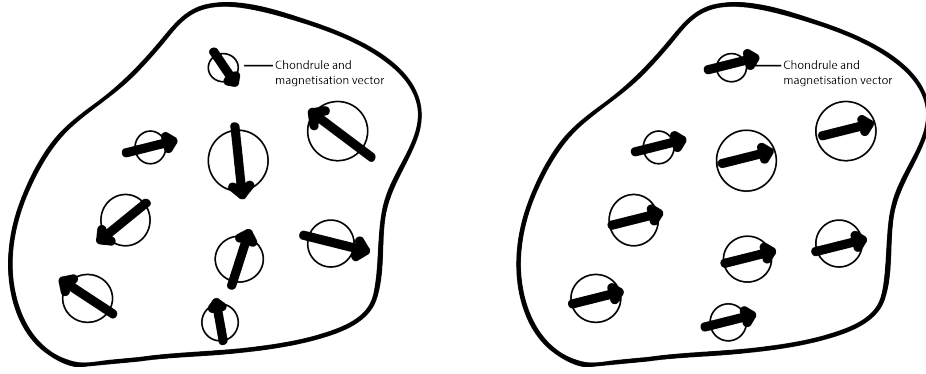


Figure 3.1: Illustration of a conglomerate with its clasts magnetised prior to accretion (left) and post-accretion (right).

images with the aid of computer software to rotate the ex-situ chondrules to their in-situ positions, allowing their palaeodirections to be determined at an accuracy equal to that of routine terrestrial palaeomagnetic measurements. This technique has been developed and applied to chondrules from two meteorites: Bjurböle (L/LL4) and Vigarano (CV3). The relative orientation of the remanent magnetisation of the constituent chondrules of these two meteorites has been determined (Shah et al., 2017).

3.2 Samples

3.2.1 Bjurböle (L/LL4)

A 686 mg fragment of Bjurböle bulk sample was borrowed from the Natural History Museum, London, from which chondrules were extracted for micro-CT scanning and magnetic measurements. To avoid contamination of the magnetisation during atmospheric entry of the meteorite, the sample is from the interior of the fallen meteorite, with no fusion crust present. Bjurböle is an ordinary chondrite (L/LL4) that fell in Bjurböle Borga, Nyland, Finland in 1899, with a 330 kg approximate recovered weight in total (Grady, 2000). Bjurböle was selected for this study due to its friability, which allows chondrules to be easily disaggregated, however magnetically it was not ideal (see Section 3.4.3). Chondrule abundance in Bjurböle is approximately 66 vol.% and their median diameter is 0.688 ± 0.003 mm (Hughes, 1978). The average

diameter of Bjurböle chondrules used in this study was $820 \pm 330 \mu\text{m}$, which is larger than the average found by Hughes (1978), as larger chondrules were preferentially selected for simpler volumetric characterisation (Shah et al., 2017).

The dominant magnetic mineral in Bjurböle chondrules has been reported as tetrataenite, a magnetically hard mineral, with a high coercivity of up to 600 mT (Wasilewski, 1988). Coercivity can be directly related to palaeomagnetic stability; therefore, Bjurböle's tetrataenite phase is unlikely to have acquired a magnetic overprint since its formation. Tetrataenite transformed from taenite during cooling to below 320°C on the parent body, so any remanent magnetisation it carries will have originated from cooling to below 320°C (Gattacceca et al., 2014). Transmission electron microscope (TEM) observations of equilibrated ordinary chondrites found the tetrataenite occurring in plessite grains consisting of $> 1 \mu\text{m}$ tetrataenite in a kamacite matrix and a high-coercivity cloudy zone of 25-250 nm tetrataenite in zoned taenite, with a rim of 1-14 μm tetrataenite grains (Uehara et al., 2011). The disordering of tetrataenite to taenite upon heating above 320°C has been thoroughly investigated experimentally by Dos Santos et al., (2015); our sample was not thermally demagnetised to prevent this. The presence of tetrataenite also indicates the meteorite did not undergo heating to greater than 320°C after peak metamorphism (Collinson, 1989; Shah et al., 2017).

Uehara et al. (2011) reported tetrataenite in the cloudy zone of individual taenite grains have homogeneous crystallographic orientations; the crystallographic orientation of tetrataenite is significant, as tetrataenite has such a strong magnetocrystalline anisotropy that can result in remanence directions that can diverge by up to 90° from the palaeofield direction (Collinson, 1989). In a general conglomerate test, divergence of greater than 90° from a palaeofield direction would usually suggest post-metamorphic brecciation of Bjurböle. It is expected that tetrataenite would carry no remanent magnetisation if the transformation occurred under zero-field conditions (Uehara et al., 2011). If the transformation occurred in the presence of a magnetic field, the tetrataenite may carry a phase transformation remanent

magnetisation (PhTRM) due to the bias field (Bryson et al., 2014). The dynamics and length-scales of PhTRM acquisition in tetrataenite are uncertain, however, and alignment of the remanence to the crystallographic axes may result in scatter of the recorded palaeodirections (Gattacceca et al., 2014; Bryson et al., 2014; Shah et al., 2017).

Strangway and Sugiura (1982) briefly report a conglomerate test on Bjurböle, in which they find inhomogeneous magnetisations amongst chondrule and matrix sub-samples; however the directions were not entirely random as they are on the same hemisphere as the natural remanent magnetisation (NRM) of the whole meteorite, i.e., the chondrules and matrix. Another conglomerate test on 83 mutually oriented sub-samples of chondrules, matrix, metal, and bulk material from Bjurböle found directions completely scattered on the equal-area projection, with no hemispheric trend, although the sub-sample type is not labelled on the projection (Wasilewski et al., 2002). The random scatter found by Strangway and Sugiura (1982) does not preclude scatter introduced due to anisotropy, however the findings reported by Wasilewski et al. (2002) and chemical anomalies amongst Bjurböle chondrules reported by Scott et al. (1985) suggest Bjurböle underwent brecciation post-metamorphism. These conglomerate tests did not elaborate on disaggregation and mutual alignment methods in great detail (Shah et al., 2017).

3.2.2 Vigarano (CV3)

A 405 mg fragment of Vigarano bulk sample was borrowed from the Natural History Museum, London, from which chondrules were extracted for micro-CT scanning and magnetic measurements. To avoid contamination of the magnetisation during atmospheric entry of the meteorite, the sample was from the interior of the fallen meteorite, with no fusion crust present. Vigarano is a carbonaceous chondrite (CV3) that fell in the Emilia-Romagna region of Italy in 1910 with a total recovered mass of 15 kg (Grady, 2000). Vigarano was selected for this study to explore the theory of a self-exciting magnetic dynamo existing on the CV3 parent body (see Chapter 1.2,

and to further develop the sub-millimetre-scale conglomerate test method using a less friable meteorite, requiring freeze-thaw disaggregation to liberate chondrules (Shah et al., 2017).

The magnetic mineralogy of the chondrules in Vigarano is largely Fe-Ni metal in the form of kamacite, and the matrix is magnetically dominated by magnetite (Brecher and Arrhenius, 1974). Vigarano is believed to be a regolith breccia of the CV chondrite parent body (Kojima et al., 1993; Bischoff et al., 2006) having originated from an aqueously altered precursor chondrite that was subject to impacts of 10 to 20 GPa and transported to re-accrete as Vigarano (Jogo et al., 2009). Vigarano likely underwent its secondary accretion in an anhydrous environment, so a second phase of aqueous alteration is ruled out (Krot et al., 2000; Tomeoka and Tanimura, 2000). The aqueous alteration product fayalite has been $^{53}\text{Mn}/^{53}\text{Cr}$ dated by Jogo et al. (2009) and recalibrated by Doyle et al. (2016) to date the alteration as 4563 ± 1 Myr ago and brecciation of the precursor chondrite approximately 5 Myr later. There is petrographic evidence for peak metamorphic temperatures of 400-500°C (Lee et al., 1996), which could have resulted in a partial thermoremanent magnetisation (pTRM) in the presence of a bias field. Secondary alteration occurred prior to the final accretion of the Vigarano breccia (Jogo et al., 2009), so would not be evident in a conglomerate test as a homogeneous magnetisation. As Vigarano underwent at least two accretions on the parent body 4565 and 4558 Myr ago (Fig. 3.2), both, parent body alteration prior to final accretion and a retained Solar Nebula remanence would be manifested as a random distribution. A shock remanent magnetisation (SRM) is most likely the origin of remanence in Vigarano, considering its 10 to 20 GPa impact history during brecciation. SRM can be identified by AF (alternating field) demagnetisation with small AF, i.e., efficient AF demagnetisation, as the SRM typically affects the low-coercivity grains (Funaki and Syono, 2010; Gattacceca et al., 2010b; Tikoo et al., 2015), and if induced during brecciation of the precursor chondrite, it would likely be observed as a random distribution by the conglomerate test due to the re-accretion of Vigarano. For a Solar

Nebula remanence to be retained through the brecciation process, the magnetic carriers need to have a high coercivity (e.g. dusty olivine (Lappe et al., 2013; Fu et al., 2014b; Einsle et al., 2016; Shah et al., 2017)).

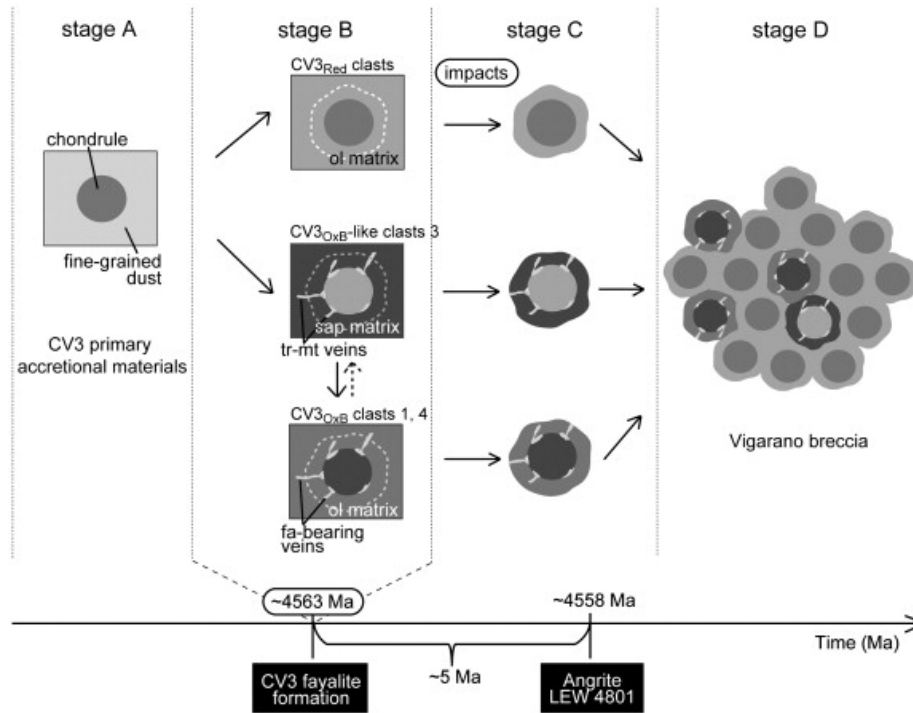


Figure 3.2: The formation history of the meteorite breccia Vigarano, indicating initial accretion on the CV parent body followed by subsequent heterogeneous aqueous alteration on the CV parent body and the later brecciation and reaccrion of unaltered and altered chondritic materials that make the present day Vigarano breccia. Both the absolute and relative ages were calculated by Jogo et al. (2009) based on the $^{53}\text{Mn}/^{55}\text{Mn}$ and Pb-Pb ages of Angrite LEW 4801. From Jogo et al. (2009)

Weiss et al. (2010a) briefly report a conglomerate test on three bulk samples of Vigarano, finding an unstable non-unidirectional high-coercivity component, however, they note that their sample has a suspected isothermal remanent magnetisation (IRM) contamination due to a hand magnet; the natural remanence of their sample has been overprinted since the meteorite landed on Earth by artificial strong magnetic fields (Shah et al., 2017).

3.3 Methods

By micro-CT scanning the bulk meteorite prior to disaggregation, and micro-CT scanning disaggregated chondrules, it is possible to relate the ex-situ and in-situ volumes to each other, and computationally determine the rotation matrix necessary

to compare the magnetic measurements as if they are mutually in-situ. To test for internal consistency and completeness, complementary rock magnetic experiments and palaeointensity (ancient field intensity) estimates were also conducted (Shah et al., 2017).

3.3.1 Meteorite disaggregation

In order to measure the magnetisation of individual chondrules, they must be disaggregated from the bulk meteorite. Bjurböle’s chondrules were easily separated by hand from the matrix due to its high friability. However, Vigarano is significantly more lithified, and freeze-thaw disaggregation following Butterworth et al. (2004) was necessary to separate the chondrules. The Vigarano sample was submerged in 1 ml of distilled water in a 5 ml volume Pyrex container. Following initial degassing using a vacuum pump, the sample was put through 138 cycles of freeze-thaw disaggregation: submerging the base of the container in liquid nitrogen until the water surrounding the sample is frozen, and then melting using an ultrasound bath. The permeating and expanding frozen water slowly disaggregates the sample, and chondrules were extracted using a stereoscopic microscope. A thermocouple was used to ensure the sample’s temperature remained above 122 K, the Verwey transition for magnetite (Verwey, 1939; Shah et al., 2017).

3.3.2 Microcomputed X-ray tomography

X-ray micro-computed tomography (micro-CT) is a non-destructive technique allowing the 3D visualisation of a scanned object by reconstructing the X-ray attenuation of the object (Ebel, 2006; Elliott and Dover, 2011; Hezel et al., 2013) (Fig. 3.3). The magnetic field inside the CT scanner is < 2 mT (Nikon Metrology Ltd., personal communication), which is not strong enough to contaminate the NRM of the meteorite. The volume can be imaged as a result of variable attenuation intensities due to density contrasts (Ketcham, 2005; Elangovan et al., 2012; Griffin et al., 2012). The bulk meteorite sample and the individual chondrules extracted from it were

measured using the X-Tek HMX ST 225 CT System at the Natural History Museum, London. A 0.25 mm copper filter was used to remove low-energy X-rays. Once the chondrules were extracted, they were mounted on carbon stubs of 11 mm height and 6 mm diameter in the centre. A fine etch was made into the stubs so that the position of the chondrules maintained the same during micro-CT and magnetic measurements. Scanning in batches of four, 40 chondrules from Bjurböle and 19 chondrules from Vigarano were imaged. An additional benefit of volumetric characterisation of the sample prior to disaggregation is that the disaggregation process can be targeted towards constituents of interest, such as those with denser and unique identifying features, and thus preserving more material from the destructive disaggregation process (Shah et al., 2017).

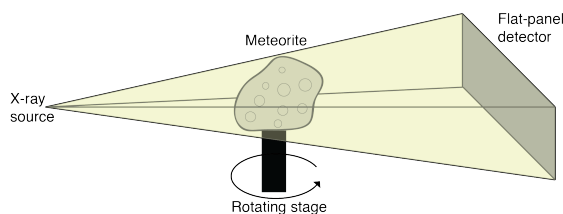


Figure 3.3: A schematic diagram (not to scale) to illustrate the acquisition of a series of X-ray density contrast images of a rotating meteorite to be later reconstructed into a 3D volumetric image of the meteorite at the micron scale.

The raw micro-CT data were converted to bitmap image stacks using the VGStudio MAX software, and the image stacks were viewed in ImageJ (Schneider et al., 2012) to match ex-situ chondrules to in-situ chondrules from the scan of the bulk specimen. Once chondrules were identified, the ex-situ and in-situ volumes were loaded into AvizoFire (VSG Inc., USA) to determine the reorientation. Unique and dense features such as barred olivine, Fe-Ni and sulphides within the chondrules and the size and shape of the chondrules were used to determine the rotation for a mutual in-situ alignment applied to the remanent magnetisation directions of the chondrules. The ‘Register Images function’ on the AvizoFire software can in theory be used to automatically align a chondrule to the bulk-reference orientation; however, this function was found to be unreliable and it was only successful with one sample (BJB37). The other re-orientations were achieved by manually rotating the

3D volume, with accuracy greater than $\sim 1^\circ$.

3.3.3 Magnetic measurements

Magnetic remanence measurements

To determine the magnetic remanence direction, the chondrules were mounted on carbon stubs of 11 mm height and 6 mm diameter and placed in palaeomagnetic sample boxes of size 22 x 22 x 22 mm, such that the chondrule was in the centre of the box. The chondrules from Bjurböle were alternating-field (AF) demagnetised up to 120 mT using a 2G Enterprises SQUID magnetometer, with an in-line AF demagnetizer at The National Oceanography Centre, University of Southampton, and then further AF demagnetised up to 200 mT field using an ASC Scientific D-2000 AF Demagnetizer at Imperial College London. We followed the same procedure for Vigarano, except using the 2G Enterprises SQUID magnetometer at the University of Oxford (Shah et al., 2017).

After AF demagnetisation of the NRM, an isothermal remanent magnetisation (IRM) of 900 mT was applied using a pulse magnetizer and then subsequently AF demagnetised and measured. These data were used to determine the palaeointensity (see Section 3.3.3) (Shah et al., 2017). Magnetic remanence data were processed and presented using PuffinPlot (Lurcock and Wilson, 2012).

Rock magnetic measurements

Hysteresis loops, backfield curves and first-order reversal curves (FORCs) (Roberts et al., 2000) were measured using a Princeton Measurements Alternating Gradient magnetometer (AGM) at Imperial College London for characterisation and to produce an input distribution to determine the palaeointensity of the chondrules with the Preisach palaeointensity method (see below) (Shah et al., 2017).

Palaeointensity estimation

Standard palaeointensity estimation protocols such as the Thellier and IZZI methods require heating of the specimens to replicate the remanence acquisition process under laboratory conditions (Yu and Tauxe, 2005). The magnetic carriers in meteorites are typically heavily reduced, and laboratory heating results in significant thermal alteration of the remanence carriers, and a loss of the palaeomagnetic information stored, e.g. troilite oxidizing to magnetite and tetrataenite disordering to taenite (Herndon et al., 1976; Dos Santos et al., 2015). In order to estimate the palaeointensity without altering the specimens, non-heating methods such as the Ratio of Equivalent Magnetisation (REM) methods (Kletetschka and Kohout, 2003; Gattacceca and Rochette, 2004), and the Preisach method (Muxworthy and Heslop, 2011) have been developed. The REM method estimates the palaeointensity by normalizing the NRM of the sample by its saturation isothermal magnetisation (SIRM), and by multiplying by an experimentally determined calibration factor f , i.e., the palaeointensity is determined such that palaeofield $B = f * (NRM/SIRM)$. To allow for multicomponent magnetisations the REM' (Gattacceca and Rochette, 2004) method compares the magnetisation of the NRM and SIRM after AF demagnetisation isolates the characteristic remanent magnetisation (ChRM). The Preisach protocol also compares the AF demagnetisation data of the NRM and SIRM, however, it uses the FORC distribution of the sample to generate a Preisach distribution to more accurately determine f for each sample (Muxworthy and Heslop, 2011). Of these non-heating palaeointensity protocols, the Preisach method has been demonstrated to be the most accurate (Emmerton et al., 2011; Muxworthy and Heslop, 2011). Lappe et al. (2013) note it may not be accurate when studying a sample dominated by single vortex (SV) state grains, however, no methods accommodate such behaviour. To determine f in this study, a minor modification to the outline described in Muxworthy and Heslop (2011) was made: f is only determined for the part of the AF demagnetisation spectrum for which the palaeointensity estimate is relatively constant (with variation $< 30\%$); this is similar to the REM' approach

(Shah et al., 2017).

3.4 Results

3.4.1 Micro-CT scanning and in-situ alignment

The bulk volume of Bjurböle was micro-CT scanned at a resolution of $6.2\ \mu\text{m}$ (Fig. 3.4), and subsequently 40 chondrules ranging in mass from 0.1 mg to 7.7 mg were extracted. Due to the friability and ease of disaggregation of Bjurböle, the chondrules from Bjurböle had no matrix material attached to them. Individual chondrules were imaged at resolutions between 6 and $12\ \mu\text{m}$, which was sufficient to identify individual chondrules and their positions in-situ. Of the initial 40 chondrules, 16 chondrules were too weakly magnetic to constrain magnetic directions, and were discounted from the alignment process. Magnetic data is presented on 19 chondrules, of which seven could be re-oriented (Shah et al., 2017).

The bulk volume of Vigarano was micro-CT scanned at a resolution of $6.4\ \mu\text{m}$. Using the freeze-thaw disaggregation method we extracted 19 chondrules from Vigarano with masses between 0.1 and 5.3 mg. The chondrules were imaged at resolutions of 7 to $12\ \mu\text{m}$, which was sufficient to identify individual chondrules and their positions in-situ. Of the 19 chondrules, ten were identified in the bulk volume, and eight had sufficient distinctive constituents to accurately rotate to in-situ positions (Shah et al., 2017).

3.4.2 Rock magnetic properties

It was possible to saturate the magnetisation of the chondrules from Vigarano in a field of 1 T to accurately record hysteresis loops and FORC diagrams. However, for Bjurböle it was not possible to achieve true saturation. A Day plot (Day et al., 1977) of the hysteresis parameters for measured samples is presented in Figure 3.5 and Table 3.1, with regions associated with single domain (SD), pseudo-single domain (PSD) and multi-domain (MD) behaviour labelled. Single-domain grains are small

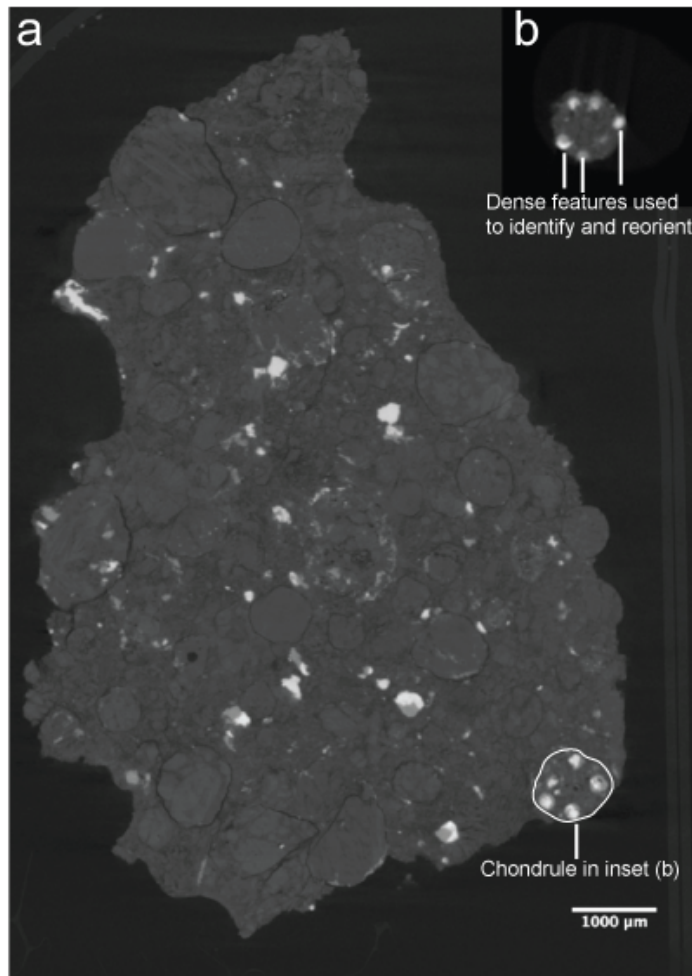


Figure 3.4: (a) a micro-CT scan slice of Bjurböle prior to disaggregation. (b) a slice of the micro-CT scan of the individual chondrule, circled in-situ in (a), after disaggregation. Image is in a greyscale to represent material density, with denser features such as Fe-metal and sulphides appearing brighter. Size and dense features within chondrules are used to locate ex-situ chondrules in their original position prior to disaggregation in the bulk meteorite before loading the 3D volume into AvizoFire (VSG Inc., USA) to determine the reorientation rotation matrix. From Shah et al. (2017).

(< 100 nm for magnetite), uniformly magnetised and considered stable recorders of magnetic fields over geologic timescales. Between the SD and MD size range are the PSD grains, which are typically the size of grains found in rocks (~100 - 1000 nm), and have recently been shown in magnetite to be reliable recorders of remanence over geological timescales (Almeida et al., 2016a) (see Chapter 5 for more on stability of PSD grains). MD grains are large, non-uniformly magnetised and considered to be poor magnetic recorders (Shah et al., 2017).

An ideal sample will have an assemblage of SD or PSD grains. The majority of the chondrules, and all of those that were reoriented plot within the region associated

Table 3.1: A table of hysteresis parameters plotted as M_{RS}/M_S and B_{CR}/B_C in the Day plot (Day et al., 1977) in Figure 3.5. Parameters are defined as coercivity (B_C), coercivity of remanence (B_{CR}), saturation magnetization (M_S) and saturation remanence (M_{RS})

Sample	B_C (mT)	B_{CR} (mT)	M_S (10^{-3} Am ² kg ⁻¹)	M_{RS} (10^{-3} Am ² kg ⁻¹)
Bjurböle				
BJB7	23	280	1.1	0.11
BJB17	51	340	1.5	0.26
BJB22	61	230	0.36	0.084
BJB31	100	130	0.0072	0.0021
BJB34	180	620	0.093	0.043
BJB35	110	620	0.034	0.017
BJB36	7	360	12	0.41
BJB37	33	120	3.6	0.34
BJB38	65	310	0.34	0.077
Vigarano				
VG01	23	57	4.4	0.93
VG02	11	240	3.7	0.21
VG03	16	230	1.6	0.16
VG04	16	67	0.13	0.02
VG06	14	110	1.5	0.14
VG07	15	44	2.5	0.44
VG08	38	160	0.04	0.013
VG09	27	63	0.22	0.055
VG10	28	75	0.63	0.17
VG11	12	68	0.4	0.033
VG12	28	66	0.49	0.14
VG13	17	52	26	4.5
VG14	28	68	8	2
VG15	32	100	8.1	1.7
VG16	29	81	10	2.3
VG17	25	110	21	2.9
VG18	18	54	13	2.5

with PSD behaviour, except for VG02, which plots in the region associated with MD behaviour (Fig. 3.5). The chondrules are grouped into FORC diagram groups A, B and C (Fig. 3.6). Group A represents chondrules with a central peak on the FORC diagram that extends from 20 to 40 mT (Fig. 3.6a). The FORC diagrams in group A indicate a SD grain assemblage similar to that seen in Roberts et al., (2000). The average coercivity of Group A chondrules is 26 mT. Group B represents chondrules with a central peak near the origin that extends up to 60 mT in some samples (Fig. 3.6b), and also includes BJB17. The FORC diagrams in group B indicate a PSD grain assemblage similar to that seen in Roberts et al., (2000). The average coercivity of Group B chondrules is 19 mT. Group C represents chondrule VG02 and nine of the ten Bjurböle chondrules chosen for FORC analysis. These chondrules have no defined peak in their FORC diagrams (Fig. 3.6c). Group C chondrules have an average coercivity of 66 mT (Shah et al., 2017).

3.4.3 Magnetic remanence measurements

AF demagnetisation

In a maximum AF field of 200 mT, the majority of the Bjurböle chondrules were only demagnetised to 40 to 70 % of their NRM, likely due to the tetrataenite component of magnetisation (Fig. 3.7). Some chondrules increased in remanence during demagnetisation (e.g. Fig. 3.7b), which is likely due to low-coercivity remanence carriers being demagnetised, isolating the high-coercivity tetrataenite. Of the 40 extracted chondrules, I was able to determine a ChRM in 24 chondrules using principal component analysis (PCA) (Kirschvink, 1980) (Fig. 3.7a and b). The remaining chondrules were magnetically weak, and no clear direction could be identified (Shah et al., 2017).

Ten of the Vigarano chondrules behaved in a similar way to Bjurböle, in that approximately only 50% of the remanence could be demagnetised by AF fields up to 200 mT (e.g. Fig. 3.7). The other nine, including most of the chondrules for which a reorientation was possible (except VG02 and VG15) had two magnetic components;

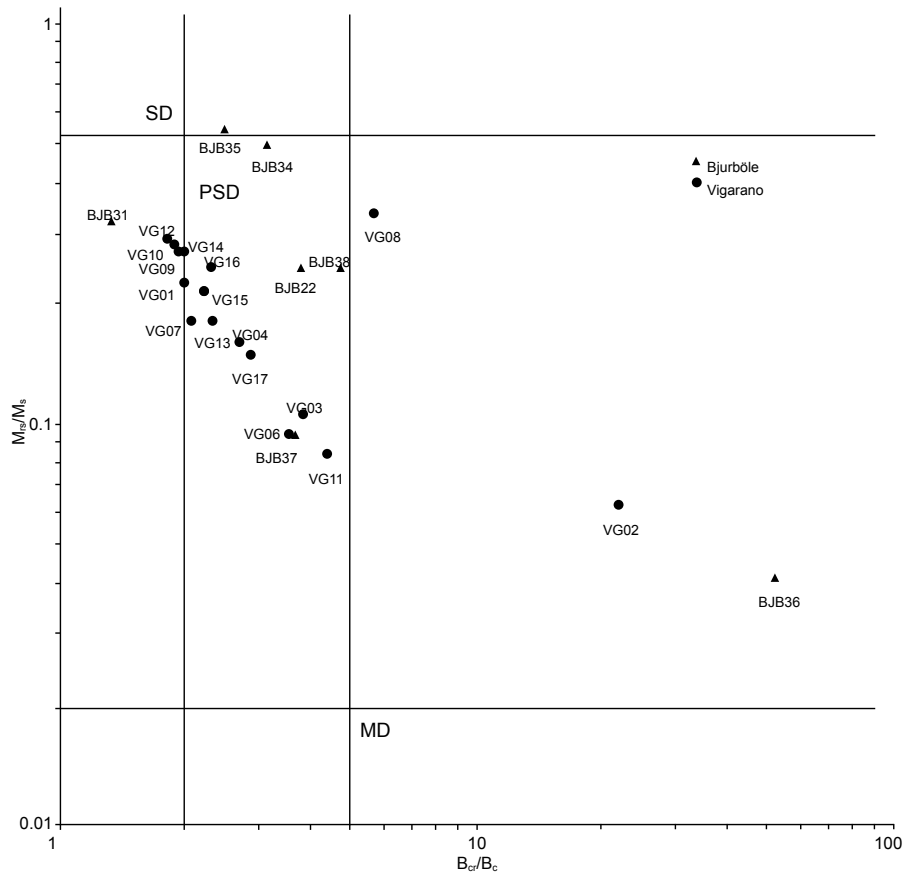


Figure 3.5: A Day plot (Day et al., 1977) with hysteresis parameters coercivity (B_C), coercivity of remanence (B_{CR}), saturation magnetisation (M_S) and saturation remanence (M_{RS}) labelled and plotted as M_{RS}/M_S versus B_{CR}/B_C . Regions associated with single domain (SD), pseudo-single domain (PSD) and multi-domain (MD) are labelled. From Shah et al. (2017).

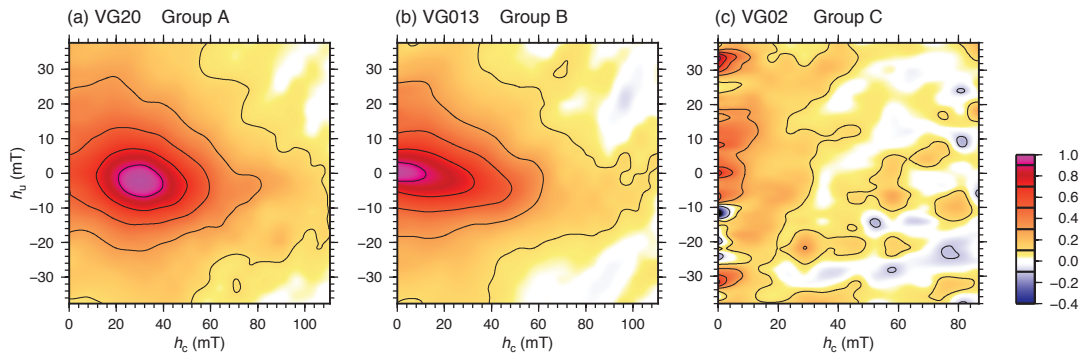


Figure 3.6: Representative first-order reversal curve (FORC) diagrams for the sample set (a, b, c). The chondrules are grouped into A, B and C type FORC diagrams. FORCs were measured over 50 to 60 minutes, and a smoothing factor (SF) of 5 was used when processing the FORCS. From Shah et al. (2017).

a soft component that was demagnetised by AF peak-fields of 6 mT, and a ChRM that was demagnetised in peak fields of 50 mT (Fig. 3.7d). The soft component is likely a (low-coercivity) overprint due to the terrestrial magnetic field, referred

to as a viscous remanent magnetisation (VRM). For the ChRM, 17 chondrules had identifiable stable palaeomagnetic directions (Fig. 3.7c and d), which shows the in-situ NRM directions for VG02 and VG18 on orthogonal-projection plots and equal area projections. VG02 retained 44% of its magnetisation (Fig. 3.7c), VG15 retained 26% of its magnetisation; the rest of the reoriented chondrules were demagnetised to < 10% of NRM, e.g. Fig. 3.7d. The median destructive field (MDF) of the NRM AF demagnetisation spectra ranged from 6.5 to 90 mT with a median of 16 mT, and for the SIRM the MDF was 16 to 61 mT with a median of 28 mT (Shah et al., 2017).

Palaeointensity estimates

Preisach and REM' palaeointensity values for 19 chondrules each from Bjurböle and Vigarano are tabulated in Table 3.2. A calibration factor of 1600 μT was used for the REM' method as determined for synthetic meteoritic samples by Lappe et al. (2013); usually a value of 3000 μT is used (Gattacceca and Rochette, 2004). For Bjurböle, the range of palaeointensities determined by the REM' method is 1.9 - 54 μT with a median of 9.2 μT and mean weighted by the variance of 8.7 ± 1.0 μT . The majority of these estimates are larger than the 3.2 ± 0.2 μT for Bjurböle chondrules reported by Acton et al. (2007), who used the REMc method. It is possible that the palaeofield has been overestimated, as the IRM acquisition of 900 mT would not have saturated the tetrataenite magnetisation of the chondrules. The FORC diagrams of Bjurböle were not of high enough quality to determine Preisach palaeointensities; and it was not possible to saturate the tetrataenite phase. For Vigarano, ten samples were selected for the Preisach method based on the quality of their orthogonal-projection plots and FORC diagrams. The range of palaeointensities determined by the REM' and Preisach methods is 1.7 - 150 μT and 1.1 - 91 μT respectively, with medians of 14 μT and 6.7 μT . The means (weighted by the variance) of the REM' and Preisach estimates are 4.4 ± 0.04 μT and 3.6 ± 1.0 μT (Shah et al., 2017).

Currently all palaeointensity protocols, including the non-heating REM' and

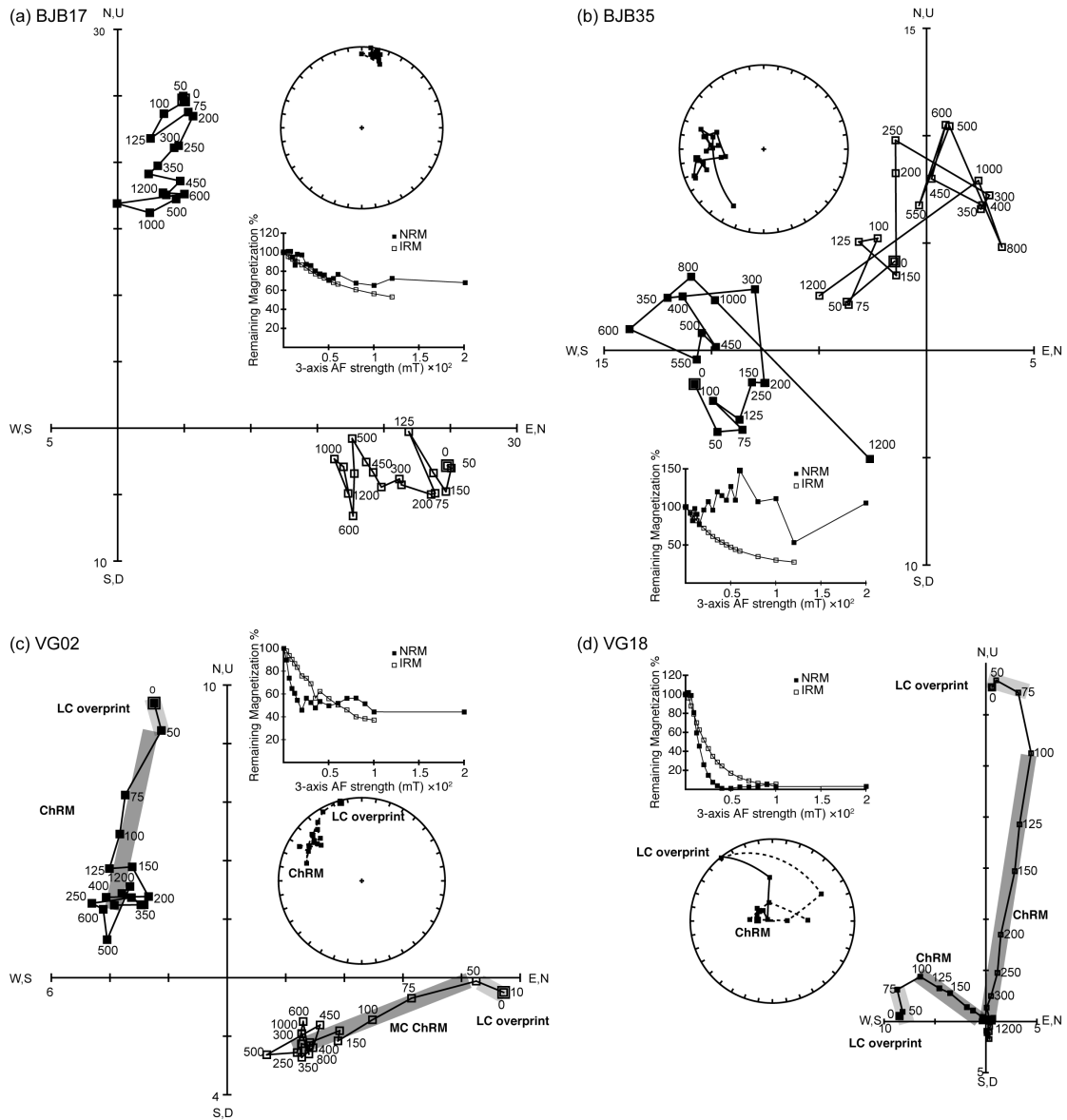


Figure 3.7: Representative Zijderveld plots and equal area projections of the sample set for the AF demagnetisation of (a, b) Bjurböle, and (c, d) Vigarano. Both natural remanent magnetisation (NRM) and isothermal remanent magnetisation (IRM) are plotted on the demagnetisation plot insets, which are normalized to the initial NRM and IRM. Low-coercivity (LC) overprint and characteristic remanent magnetisation (ChRM) components of Vigarano chondrules' remanence have been highlighted and labelled. From Shah et al. (2017).

Preisach protocols, assume a thermoremanent origin of magnetisation (TRM). With regards to Bjurböle, the phase transformation of the tetraetaenite is poorly understood, introducing an additional error to consider when calibrating between PhTRM and TRM acquisition mechanisms. With regards to Vigarano, a shock origin of remanence (SRM) has been shown to be 10% of the recording efficiency of a TRM for pressures up to 1.8 GPa (Cisowski and Fuller, 1978; Tikoo et al., 2015). Hence, the palaeointensity estimation could underestimate the palaeofield strength - if a SRM

- by up to an order of magnitude. Hypervelocity impacts on planetary surfaces in the presence of an ambient field have been shown to result in significant crustal remanence recordings (Gattacceca et al., 2008). The Vigarano chondrules may have recorded remanence at a greater efficiency than 10% given they were subjected to 10 to 20 GPa brecciating impacts, and recording efficiency increases with greater shock pressure (Gattacceca et al., 2008). Hence, the palaeointensity estimates of the Bjurböle and Vigarano chondrules may have an understated error. All theories used for palaeointensity protocols also assume magnetically uniform single domain (SD) assemblages. These assumptions are rarely fulfilled. This is also true for meteoritic materials containing FeNi, as the SD threshold size is very small (< 30 nm) (Muxworthy and Williams, 2015). Therefore, all palaeointensity estimates need to be interpreted very cautiously (Shah et al., 2017).

3.5 Discussion

3.5.1 Conglomerate test

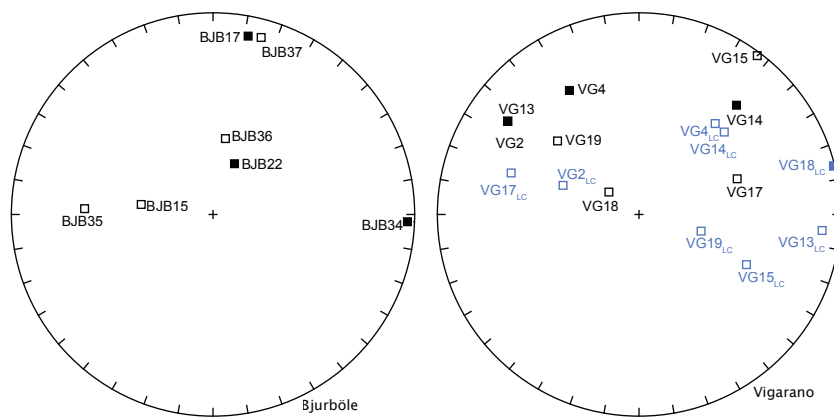


Figure 3.8: Equal-area projections of the ChRM magnetic directions for the chondrules that were reoriented from Bjurböle (a) and Vigarano (b). Directions representing individual samples were determined by principle component analysis of their demagnetisation spectra. The low-coercivity components of magnetisation for Vigarano's chondrules are labelled and plotted in blue. Adapted after Shah et al. (2017).

The reorientation of the ChRM directions to their relative in-situ positions (Fig. 3.8) allows for a statistical determination of whether they are aligned or not us-

Table 3.2: A table of the natural remanent magnetization (NRM), saturation isothermal remanent magnetization (SIRM), mass, palaeointensity estimates by the REM' and Preisach methods and FORC type for Bjurböle and Vigarano chondrules. A calibration factor of 1600 T was used for the REM' method as determined by (Lappe et al., 2013). From Shah et al. (2017).

Sample	Mass (mg)	NRM (mAm ² /kg)	SIRM (mAm ² /kg)	REM' (μT)	Preisach (μT)	FORC type
BJB1	0.8	0.22	98	4.4 ± 2.9
BJB2	0.9	0.38	110	5.5 ± 0.8
BJB5	3.7	0.085	33	2.9 ± 1.2
BJB7	0.9	0.5	140	11 ± 1	...	C
BJB9	0.9	0.64	67	21 ± 3.4
BJB10	4.8	0.18	42	1.9 ± 2.7
BJB13	0.7	0.49	110	9.9 ± 3.3
BJB14	2.6	1.2	84	32 ± 2
BJB15	0.4	0.55	28	54 ± 7
BJB17	2.3	0.85	340	3.9 ± 0.5	...	B
BJB18	0.3	2.3	83	40 ± 5
BJB22	7.7	0.19	33	9.2 ± 0.3	...	C
BJB24	1.2	0.19	11	28 ± 6.3
BJB29	0.8	0.21	20	5.9 ± 13
BJB31	0.1	3.3	530	2.9 ± 2.4	...	C
BJB34	2.1	0.28	70	7 ± 1	...	C
BJB35	1.5	0.18	29	11 ± 0.5	...	C
BJB36	4.5	0.64	130	12 ± 5	...	C
BJB37	1.8	3.2	620	8.6 ± 0.3	...	C
VG1	1.2	1.7	920	3.1 ± 0.7	5.0 ± 0.3	A
VG2	2.4	0.98	130	6.8 ± 3.7	...	C
VG3	1.5	0.81	130	14 ± 2	15 ± 3	B
VG4	0.05	56	880	150 ± 25	...	A
VG6	0.2	54	1700	24 ± 3	91 ± 9	B
VG7	0.3	32	1700	54 ± 2	8.5 ± 1.9	B
VG8	0.1	3.5	430	21 ± 14	...	B
VG9	0.7	0.99	130	61 ± 19	...	A
VG10	0.1	13	2600	8.9 ± 1.8	12 ± 2	A
VG11	0.2	10	300	52 ± 12	55 ± 5	B
VG12	1	3	550	18 ± 4	...	A
VG13	5.3	2.4	990	6.5 ± 1.5	4.1 ± 0.8	B
VG14	2.3	6.4	1000	28 ± 6	1.5 ± 0.4	A
VG15	2.6	1.7	760	3.9 ± 0.4	...	A
VG16	3.9	4	720	5 ± 0.5	2.2 ± 0.0	A
VG17	4.1	5	730	3.1 ± 1.3	...	A
VG18	2.2	40	1200	95 ± 6	...	B
VG19	3	2.9	870	1.7 ± 0.2	...	A
VG20	2.3	2	1200	4.4 ± 0.1	2.1 ± 0.4	A

ing the Watson test for randomness (95% confidence) (Watson, 1956). For Bjurböle, the randomness of the ChRM directions cannot be disproved at the 95% confidence interval, i.e., Bjurböle is said to have passed the conglomerate test, and indicates that the chondrules have random magnetic directions. This is in agreement with the previous conglomerate test on Bjurböle, which also found scattered palaeodirections from seven chondrules (Strangway and Sugiura, 1982; Shah et al., 2017).

For Vigarano, the randomness of the ChRM directions cannot be disproved at the 95% confidence interval, i.e., Vigarano has also passed the conglomerate test, and chondrules carry random magnetic directions. This is in agreement with previous findings by Weiss et al. (2010a) on three oriented bulk samples of Vigarano. The low-coercivity (LC) components of the Vigarano chondrules' magnetisations (< 6mT peak AF fields) fail the conglomerate test, indicating that they are not from a random distribution (Fig. 3.8b). It is very likely the LC components are a terrestrial magnetisation (a viscous remanent magnetisation) (Brecher and Arrhenius, 1974), and thus would be expected to be aligned. The non-random Vigarano LC components validate the reorientation procedure (Shah et al., 2017).

3.5.2 Origin of Bjurböle's remanent magnetisation

The demagnetisation data presented in Figure 3.7 and b indicate that the chondrules in Bjurböle carry a remanent magnetisation, and the inability to demagnetize the magnetisation with peak AF fields of 200 mT or saturate in fields of 1 T during hysteresis suggests it is carried by high-coercivity tetrataenite. I present a schematic to illustrate the likely history of the magnetisation of Bjurböle's chondrules in Figure 3.9. Pre-accretionary remanence carrying chondrules (Fig. 3.9) are heated on the L/LL parent body and cooled, undergoing phase transformation to the final ferromagnetic tetrataenite, with ferromagnetic taenite as its precursor (Uehara et al., 2011) (Fig. 3.9b). The remanence of the tetrataenite in Bjurböle is unlikely to have been overprinted since formation due to its very high coercivity, and probably represents an ambient magnetic field at the time of cooling on the parent body to below

320°C (Uehara et al., 2011; Bryson et al., 2015) (Fig. 3.9c). Given the 1 to 2 cm length scale of the samples the chondrules originated from, an ambient field on the parent body at the time of cooling would result in a mutual alignment of the chondrules' magnetic moments within 180° (Collinson, 1989) (Fig. 3.9c). The palaeodirections of Bjurböle fall within 180° of each other (Fig. 3.8a), so an anisotropy scattered record of an ambient field cannot be precluded (Fig. 3.9c). However, the palaeointensity estimates range from 1.9 - 54 μT , which is a comparatively high-level of variability, thereby supporting inhomogeneity. The inhomogeneity found in this study, by Strangway and Sugiura (1982) and by Wasilewski et al. (2002), suggest that Bjurböle was brecciated post-metamorphism (Fig. 3.9c). Bjurböle has been previously suggested as a breccia due to chemical anomalies (Scott et al., 1985). Shock typically affects the low-coercivity spectrum of grains (Yu et al., 2011; Tikoo et al., 2015), so the brecciation process is unlikely to alter the remanence carried by the high-coercivity tetrataenite grains (Shah et al., 2017).

The palaeointensities and tetrataenite remanence require the existence of an external magnetic field at the time of tetrataenite formation (Fig. 3.9c). Peak metamorphism on the L/LL parent body has been estimated to have prolonged for 0.5 to 5 Myr (Seitz et al., 2016). Thermochronometry suggests that Bjurböle cooled at a rate of 2°C/Myr, which means it would have taken up to 80 to 140 Myr to cool to 320°C (Willis and Goldstein, 1982), transforming its taenite phases to tetrataenite phases (Fig. 3.9b). Phase-transformation remanent magnetisation (PhTRM) is not well understood, and it may be possible that tetrataenite inherits remanence from its precursor taenite. If tetrataenite does acquire a new PhTRM upon transformation, it is unlikely to be due to the solar wind (interplanetary magnetic field). The solar wind would not have been stable relative to the rotating L/LL parent body on the Myr timescale to acquire a PhTRM, and the magnetic field of the solar wind is predicted to have decayed to $< 1.7 \mu\text{T}$ by 3.8 Myr after Solar System formation (Wang et al., 2017). The possibility of a planetesimal sustaining magnetic activity more than 50 Myr after accretion has been suggested based upon observations of the

tetrataenite cloudy zones found within pallasites (Bryson et al., 2015). It may be possible that the L/LL parent body began core solidification to sustain a magnetic dynamo, similar to as has been suggested for long-sustained magnetic activity on the pallasite parent body (Bryson et al., 2015; Nichols et al., 2016). An active magnetic dynamo could produce an ambient field, which was recorded as a PhTRM by the Bjurböle chondrules (Shah et al., 2017).

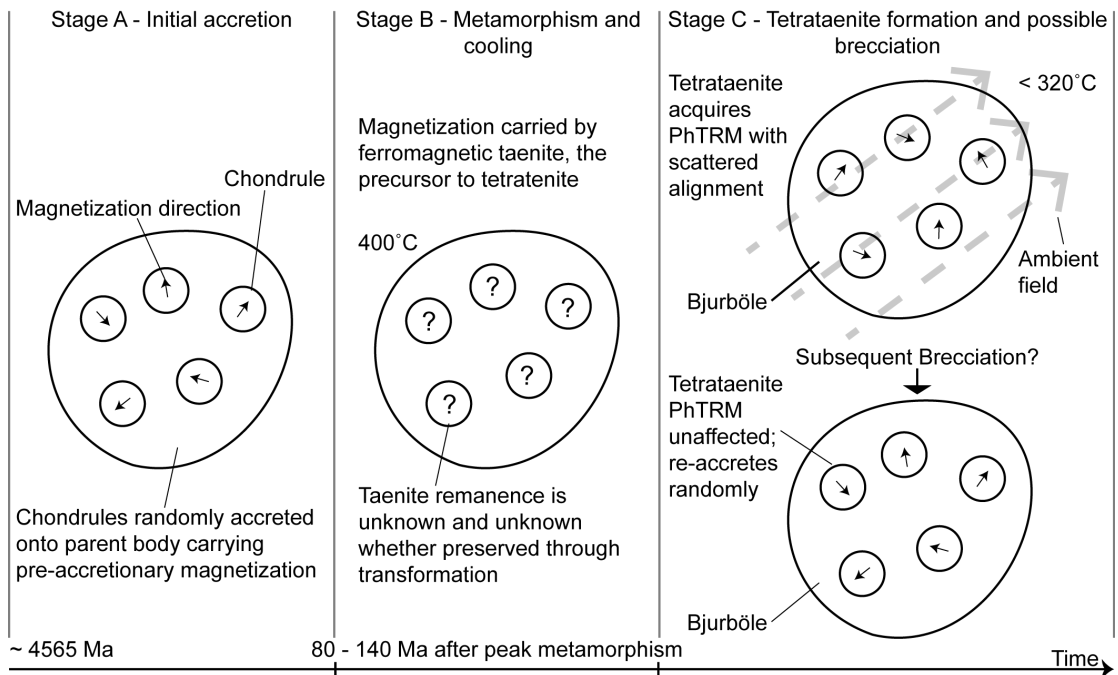


Figure 3.9: A schematic formation scenario for Bjurböle. Initially chondrules acquire a pre-accretionary thermoremanent magnetisation (TRM) and are accreted as a random distribution on the Bjurböle parent body (a). The TRM is subsequently erased due to thermal metamorphism (b). Cooling of the body over 80 to 140 Myr (Willis and Goldstein, 1982) to 320°C results in the formation of ferromagnetic tetrataenite as a phase-transformation remanent magnetisation (PhTRM) (c). It is unknown whether the remanence of the ferromagnetic taenite (b), the precursor to tetrataenite, retains any of its remanence. The random magnetisation distribution of chondrules in Bjurböle (see Fig. 5a) is either due to PhTRM of an ambient field by the anisotropic tetrataenite when Bjurböle cooled to below 320°C, or a PhTRM of the ambient field by the chondrules that are then brecciated and re-accreted (c). From Shah et al. (2017).

3.5.3 Origin of Vigarano's remanent magnetisation

The demagnetisation spectra of the chondrules from Vigarano (Fig. 3.7) indicate that they each carry a low-coercivity (LC) as well as a medium-coercivity (MC) component of remanence. The directions of the LC components align and are demagnetised with peak-AF fields of up to 6 mT, suggesting they are an overprint acquired on Earth due to the geodynamo. The MC components are different to the

LC terrestrial components and have a random magnetisation distribution, indicating that they originated prior to the accretion of the Vigarano breccia (Shah et al., 2017).

A schematic after Jogo et al. (2009) illustrates the likely history of the magnetisation in Vigarano's chondrules in Figure 3.10. Pre-accretionary remanence carrying chondrules were accreted onto the CV parent body (Fig. 3.10a), which underwent heterogeneous aqueous alteration (Fig. 3.10b). The magnetic remanence observed in Vigarano's chondrules may result from the impacts that brecciated the oxidised and reduced CV-type clasts (Fig. 3.10c). The efficient AF demagnetisation of the NRM MC component compared to the demagnetisation of the IRM (Fig. 3.7,d), evident in the comparison between their MDFs (the peak AF required to remove 50% of remanence; see section 3.4.3) suggests that the NRM is likely of shock origin (SRM) (Tikoo et al., 2015). A previous conglomerate test on basalts imparted with an SRM suggests that a remanence proportional to the ambient field and homogeneous in intensity and direction on the millimetre-cubed scale would be acquired (Gattacceca et al., 2010b). Subsequent transport and re-accretion of shocked clasts would then result in a heterogeneous remanence distribution (Fig. 3.10d) (Shah et al., 2017).

There are no previously published palaeointensity estimates for Vigarano that I am aware of. The palaeointensity estimates display variability, particularly when plotted on the equal-area projection of ChRMs for oriented chondrules, suggesting that the inducing field was not the same for chondrules with similar directions (for example VG13 and VG18: Table 3.2, Fig. 3.8). This supports the positive conglomerate test, i.e. the remanence was induced prior to final accretion. If the ChRM is an SRM in origin, the reliability of the palaeointensity estimates is reduced; the estimates assume a TRM origin. An ambient field up to ten times as intense as estimated is required, however, Tikoo et al. (2015) only tested pressure up to 1.8 GPa, so this may not correlate for Vigarano's more intensely shocked chondrules (Shah et al., 2017).

Here I argue that the SRM is unlikely to be a recording of an ambient field due to

solar wind at the time of impact (Tarduno et al., 2016); the present-day field due to the solar wind is on the nanotesla-scale at 1 au (Tarduno et al., 2014). The surface magnetic field, rotational period and mass loss rate of the young Sun has been modelled and observed in comparable stars and suggests the solar wind’s magnetic field to have been not significantly greater than the present day value (Wood et al., 2014). The ~ 50 μT field present during the first 2 to 3 Myr of the Solar System (Fu et al., 2014b) has been observed in angrites and Kaba to have decayed to < 1.7 μT by 4 Myr after CAI formation (Wang et al., 2015; Gattacceca et al., 2016; Shah et al., 2017; Wang et al., 2017).

I argue that the remanence is more likely to be a recording of an ambient field due to a magnetic dynamo generated on Vigarano’s parent body. Given the low recording efficiency of SRM, the palaeofield would have been approximately 40 μT , which is of the order expected for planetary dynamos (Selkin and Tauxe, 2000; Tikoo et al., 2015). The brecciation and associated SRM acquisition occurred between 4563 to 4558 Myr ago (Jogo et al., 2009) (Fig. 3.10), which chronologically agrees with the dynamo identified on the CV parent body of Kaba (Gattacceca et al., 2016; Shah et al., 2017).

3.5.4 Implications for parent body magnetism

Asteroid bodies can feasibly sustain magnetic dynamos for the first 50 Myr of the Solar System due to their thermal structure, and much later once they have cooled enough to initiate core solidification (Elkins-Tanton et al., 2011; Laneuville et al., 2014; Scheinberg et al., 2016; Shah et al., 2017).

Vigarano originates from the CV parent body, and recent investigations of the CV3 chondrite Kaba have interpreted its magnetic remanence as due to an Earth-like magnetic dynamo on the CV parent body that was active > 6 Myr after CV CAI formation (Gattacceca et al., 2016). However, Nagashima et al. (2017) dispute this interpretation; they claim that the initial abundance of ^{26}Al that has been measured in CV chondrules is insufficient to have melted the interior of their parent

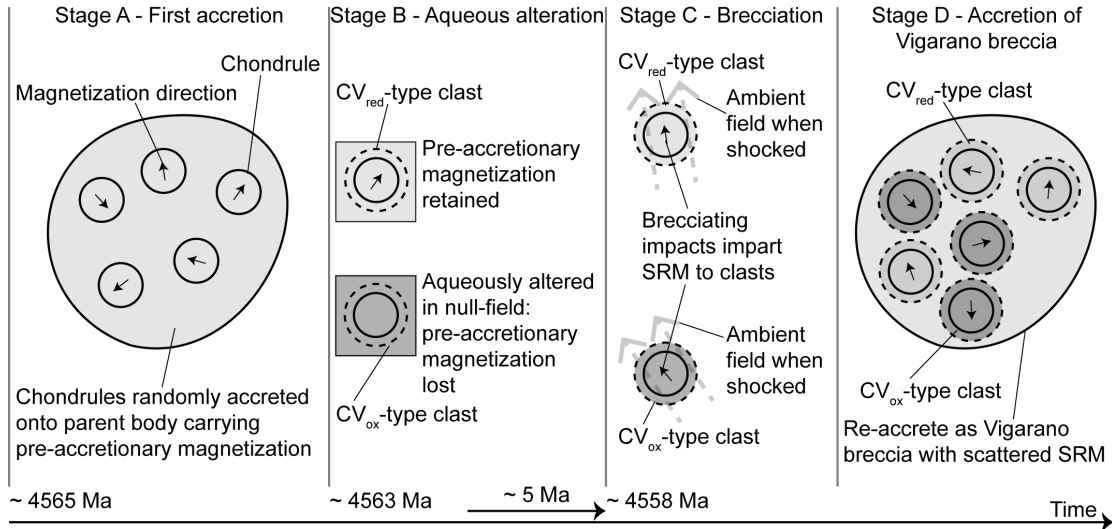


Figure 3.10: A schematic formation scenario for Vigarano with the ages determined by Jogo et al. (2009) and recalibrated by Doyle et al. (2016). Annotations indicate the proposed remanent magnetisation carried by the chondrules of Vigarano during the formation process of the breccia. The chondrules initially carry a pre-accretionary remanent magnetisation (a), which is overprinted by a chemical remanent magnetisation (CRM) if the chondrules were subsequently oxidized (b). These pre-accretionary and chemical remanences are later overprinted by a shock-remanent magnetisation (SRM) due to the breakup of the precursor chondrite (c). The final assembly of the Vigarano breccia results in this SRM have an inhomogeneous distribution at the millimetre to centimetre scale (d). From Shah et al. (2017).

body, thereby suggesting dynamo could not have existed on chondrite parent bodies. The lack of sufficient ^{26}Al to melt the interior of a CV parent body does not preclude the possibility of an incrementally accreted parent body, with undifferentiated CV chondritic material accreting onto an already existing differentiated planetesimal (Nagashima et al., 2017). The Mo isotope relationship between certain groups of magmatic iron meteorites and carbonaceous chondrites suggests they formed in the same region (Budde et al., 2016). The incremental accretion models proposed by Elkins-Tanton et al. (2011) and Sahijpal and Gupta (2011) may describe the formation mechanism of the CV parent body, and how it could have had a differentiated interior with an undifferentiated crust (Shah et al., 2017).

The remanence in the Bjurböle chondrules is carried by high-coercivity tetrataenite, so regardless of whether it is a breccia or not, it acquired a PhTRM at least 80 to 140 Myr after peak metamorphism. A parent body dynamo active for greater than 80 Myr would require a radius of 800 to 1000 km, or smaller if the recorded dynamo activity is due to core solidification, which can extend the lifetime of the planetesimal dynamo by up to 10 Myr (Sternborg and Crowley, 2013; Scheinberg et al.,

2016). The chondrules in Bjurböle are the first non-pallasite indication of late-stage parent body magnetism that may be due to core solidification (Shah et al., 2017).

Asteroids can, therefore, sustain at least three periods of magnetic dynamo activity: (i) one early stage dynamo active < 50 Myr (e.g. Elkins-Tanton et al. (2011); Gattacceca et al. (2016), this study), (ii) a period of quiescence or potentially impact-driven remanences (e.g. Nichols et al. (2016)) and (iii) once the body has cooled sufficiently for compositional convection to sustain a dynamo (e.g. Tarduno et al. (2012); Bryson et al. (2015); Shah et al. (2017)).

3.5.5 Conclusions

This chapter presents a new micron-scale method for the palaeomagnetic conglomerate test that utilizes micro-CT scanning to generate a rotation matrix for disaggregated sub-millimetre clasts from a conglomerate. I applied this method to two chondritic meteorites (Bjurböle (L/LL4) and Vigarano (CV3)) to understand the origin of the magnetisation of the chondrules. The alignment of the reoriented low-coercivity components of Vigarano's chondrules' magnetisations clearly demonstrates that the reorientation protocol was successful. I estimate that the reorientation is accurate to $< 1^\circ$, that is, the directional error in this protocol is the same as that of a standard palaeomagnetic measurement, e.g., a 1-inch core (Shah et al., 2017).

Bjurböle has a non-unidirectional magnetisation distribution amongst its chondrules. I argue that the chondrules in Bjurböle, initially carrying a pre-accretionary magnetisation, recorded a phase-transformation remanent magnetisation (PhTRM) on the parent body after cooling from peak-metamorphism to 320°C over 80 to 140 Ma. After this PhTRM acquisition, I cannot preclude that the scattered palaeodirections are due to an ambient field being recorded by the highly anisotropic tetrataenite. However, the variable palaeointensities, scatter in palaeodirections and previously found chemical anomalies suggest Bjurböle formed as a breccia from a brecciated precursor chondrite (Shah et al., 2017).

Vigarano has a non-unidirectional magnetisation distribution amongst its chondrules. Given that Vigarano formed by re-accreting chondrules and matrix material that had been brecciated by 10 to 20 GPa impacts on the parent body and its demagnetisation behaviour; it is most likely that its NRM is a shock remanence overprint due to impacts. The harder, non-viscous component of remanence (MC), suggests these brecciating impacts occurred in the presence of an ambient field prior to the accretion of the Vigarano breccia 4558 Myr ago (Shah et al., 2017).

Vigarano chondrules evidence the early-stage magnetic activity (ca. 10 Myr after Solar System formation) on asteroid bodies driven by their thermal structure, and the remanence in the Bjurböle chondrules is an indication of late-stage parent body magnetism (> 80 to 140 Myr after Solar System formation) likely due to core solidification. The results of our study support earlier findings of Elkins-Tanton et al. (2011) and Gattacceca et al. (2016) that primitive chondrites originate from asteroids that likely sustained a dynamo magnetic field. It seems ever more evident that primitive chondrites need not to have originated from entirely primitive, never molten and/or differentiated parent bodies. Rather, parent bodies of primitive meteorites consisted of a differentiated interior, encrusted by a layer of incrementally accreted primitive meteoritic material. The difference in magnetic activity between the carbonaceous chondrite Vigarano and the ordinary chondrite Bjurböle might indicate a general difference between carbonaceous and ordinary chondrite parent bodies, and/or formation location in the Solar Nebula (e.g. Budde et al. (2016)). However, this needs to be confirmed by additional studies.

The conclusions presented here are likely to be controversial amongst meteoriticists who do not support a chondrite parent body magnetic dynamo hypothesis. A greater understanding of shock remanence and phase transformation remanences is required, as well as how to determine the palaeointensity from these remanence acquisition mechanisms. Along with further palaeomagnetic data, this greater understanding would help to better understand the history of chondrite parent bodies.

3.5.6 Acknowledgements and contributions

I conducted the sample preparation, micro-CT measurements, micro-CT realignment, and magnetic measurements on Bjurböle. I designed the Vigarano micro-CT project and supervised MSci student Helena C. Bates, who conducted the freeze-thaw disaggregation, sample preparation, micro-CT measurements, micro-CT realignment, and magnetic measurements on Vigarano. I conducted the analyses and wrote this chapter with the help of Adrian R. Muxworthy, Dominik C. Hezel, Sara S. Russell, Matthew J. Genge, and Helena C. Bates. Adrian R. Muxworthy had the original idea for the project.

I would like to thank D. Zenteno Gomez at Imperial College London for assistance with freeze-thaw disaggregation. I thank F. Ahmed, D. Sykes, R. Summerfield and N.V. Almeida at the Natural History Museum, London and P. Lai at Imperial College London for assistance with micro-CT scanning and analysis. I thank T. van Peer, and C. Xuan at the National Oceanography Centre, Southampton and C. Mac Niocaill at the University of Oxford for use of their 2G SQUID magnetometers. Meteorite samples were supplied by the Natural History Museum, London. This work was funded by the STFC (grant number ST/N000803/1).

Chapter 4

Nanomagnetic imaging of dusty olivine

4.1 Introduction

The background that motivates the study presented in this chapter is established in Section 1.3, 1.2 and 1.4.4. Following a brief introduction and explanation of the methods used, experimental data to test the credibility of ‘dusty olivine’ as a recorder of pre-accretionary remanence is presented and discussed. The following chapter complements the experimental analysis of this chapter with micromagnetic modelling analysis of iron, the magnetic carrier within dusty olivine.

Dusty olivine and early Solar System magnetic fields

Accretionary dynamics of protoplanetary disks are thought to be crucially influenced by magnetic fields (Hayashi, 1981; Blandford and Payne, 1982). Unlike the thermochemically altered meteorites analysed in the previous chapters of this thesis, the pristine unequilibrated meteorites originating from our own Solar Nebula present an excellent opportunity to understand the extent of the nebular magnetic field present during the first few million years of the Solar System. The most likely mineral to have retained this field information is dusty olivine: assemblages of nanometric

low-Ni kamacite (FeNi) grains found in the chondrules of unequilibrated primitive chondrites that have not been heated significantly since accretion, and are protected from chemical alteration by their host olivine crystal (Leroux et al., 2003; Uehara and Nakamura, 2006). A recent estimate of the ancient-magnetic-field-intensity (palaeointensity) from dusty olivine in Semarkona (Fu et al., 2014b) has provided an upper bound for the vertical magnetic field present in the chondrule forming region (2.5 AU) of the protoplanetary disk during its first two to three million years (Kita et al., 2000; Nyquist et al., 2001). This recent estimate has been widely used in models for chondrule formation (Hasegawa et al., 2016; Wakita et al., 2017) and for the accretionary dynamics of the Solar Nebula (Gressel et al., 2015; Bai et al., 2016).

However, the low-Ni kamacite (\sim metallic iron) grains that dominate dusty olivine's magnetic remanence are $\gg 25$ nm, and thus are non-uniformly magnetised (Butler and Banerjee, 1975; Lappe et al., 2011; Muxworthy and Williams, 2015; Einsle et al., 2016). Despite efforts to understand non-uniform magnetic vortex structures (Dunlop, 1977), little is known about their thermal or temporal stability; it is unknown whether non-uniformly magnetised grains can retain a remanence for Solar System timescales (i.e. 4.6 Ga). It is therefore imperative to establish whether non-uniform magnetisation structures can theoretically retain remanence imparted by the magnetic fields present in the Solar Nebula billions of years ago.

The advanced TEM technique of off-axis electron holography has seen increasing implementation in the Earth sciences to visually and quantitatively observe the magnetisation structures of individual grains at the nanometric scale (Harrison et al., 2002; Lappe et al., 2011; Almeida et al., 2016a). Following from a study observing magnetotactic bacteria to develop the understanding of magnetotaxis in organisms (Dunin Borkowski et al., 1998), electron holography was initially utilised in geoscience to observe the magnetic interactions between natural titanomagnetites, and was recognised as a tool to develop understanding of grains at the single-domain to pseudo-single-domain boundary (Harrison et al., 2002). The

high resolution of the technique allows for the detailed breakdown of complex microstructures on the nanometric scale: Feinberg et al. (2006) were able to observe the influence of shape anisotropy and magnetic interactions on the macroscopic remanence of silicate hosted nanometric titanomagnetites. Direct application to meteoritic studies was first made by Lappe et al. (2011), in a study of synthetic dusty olivine. The study found strongly magnetised non-interacting grains in both uniform and non-uniform magnetisation states; the presence of uniform states encased in protective olivine supported the proposal that dusty olivine is a credible carrier of magnetic remanence originating from the Solar Nebula (Uehara and Nakamura, 2006; Lappe et al., 2011). However, the majority of remanence carriers in both terrestrial rocks and meteorites are non-uniformly magnetised, and until recent studies (Almeida et al., 2014b, 2016a), these were poorly understood, and assumed to be less magnetically stable than uniformly magnetised grains. Almeida et al. (2016a) applied *in-situ* temperature-dependent holography to synthetic magnetite grains to demonstrate that the vortex magnetisation structure is stable to heating up to magnetite’s Curie temperature (T_C), with a similar thermoremanent magnetisation structure recovered upon cooling from beyond T_C ; non-uniformly magnetised grains can recover both intensity and directional information. The temperature-dependent off-axis electron holography employed by Almeida et al. (2016b) follows the same methodology as for dusty olivine in this chapter (see Section 4.2.4).

However, the magnetic recording fidelity of these vortex states is still poorly understood; can they retain remanences for billions of years like SD grains (Néel, 1949; Garrick-Bethell and Weiss, 2010)? To answer this question, I employ the advanced transmission electron microscopy (TEM) technique of *in-situ* temperature-dependent off-axis electron holography to observe the behaviour of the magnetisation states of chondrule dusty olivine kamacite with respect to heating. To supplement the experimental observations of the behaviour of dusty olivine magnetisation at high-temperature, a numerical micromagnetic modelling analysis of the heated grain is presented in Section 4.3.3. A more in-depth micromagnetic analysis of metal-

lic iron (*sensu lato*) is presented in the following chapter to determine whether dusty olivine can retain a record of the magnetic field from the early Solar System.

4.1.1 Bishunpur

Chondrules from the unequilibrated ordinary chondrite Bishunpur (LL3.1) are considered for this study. Bishunpur has been previously observed to contain dusty olivine, and has been studied to develop understanding of the formation mechanism of dusty olivine (Leroux et al., 2003). It was found that dusty olivine formed owing to a reduction process acting upon chondrule olivine grains in the presence of graphitic carbon in the early Solar Nebula, leaving a product of forsteritic (Mg-rich) olivine encasing nanometric metallic iron precipitates (Leroux et al., 2003; Uehara and Nakamura, 2006).

The material was obtained from the Natural History Museum, London, as it had already been prepared as two thick-sections for a study in collaboration with and initiated by Dr Richard Harrison at the University of Cambridge. Bishunpur is believed to have experienced heating to at most 300 to 350°C after accretion (Rambaldi and Wasson, 1981). The Curie temperature, T_C , of metallic iron, the magnetic carrier in dusty olivine, which is abundant in Bishunpur, is 760°C (Bozorth, 1951); the initial preaccretionary thermoremanent magnetisation (TRM) is thought unlikely to have been thermally demagnetised.

4.2 Methods and sample preparation

The methods in this chapter are largely electron microscopy based. Initial optical and scanning electron microscopy (SEM) analyses were necessary to constrain areas of interest, followed by focused ion beam scanning electron microscopy (FIB-SEM) to prepare samples for transmission electron microscopy and off-axis electron holography at room temperature and variable temperature.

4.2.1 Scanning electron microscopy

A scanning electron microscope (SEM) (Goldstein et al., 2013) operates by using electromagnetic lenses to direct a beam of electrons from a source to the sample. Detectors are used to observe the interactions between the electrons and the surface of the sample. Separate detectors are used to observe electrons that are back-scattered (BSE), and the secondary electrons (SE) released from the sample due to the interaction with the primary electrons. These are examples of elastic and inelastic scattering respectively. SEMs can image at resolutions of the order of tens of nanometres, and topography of the sample can be clearly seen when observing the SEs due to topographically influenced points of least and most electron escape. SEMs can also perform chemical analyses of the sample surface at micron resolution by energy dispersive X-ray spectroscopy (EDS) with the use of an X-ray detector. A high-energy beam of electrons or protons is fired at the sample surface such that inner shell electrons are excited and ejected, resulting in outer shell electrons replacing the electrons in a process that releases X-rays owing to the energy difference between the inner-low-energy and outer-high-energy electrons (Goldstein et al., 2013). The X-rays, which are characteristic and diagnostic of the atomic structure of the element, are collected at the X-ray detector and an elemental map of the sample surface is generated.

A benefit of scanning electron microscopes is the relatively easier sample preparation compared to that of TEM, which is more costly and time consuming, requiring techniques such as focused ion beam milling. Training in operating an SEM and analysing the data was conducted at the Natural History Museum, London. The SEM analysis presented in this chapter was conducted at the Natural History Museum, London.

An initial survey for dusty olivine-bearing chondrules with an SEM was necessary (Fig. 4.1, 4.2, 4.3). Sample preparation involved polishing a surface of the sample flat, which in this case is the ordinary chondrite Bishunpur (LL3.1) (Grady, 2000). The sample was polished and prepared by the Imaging and Analysis Centre at the

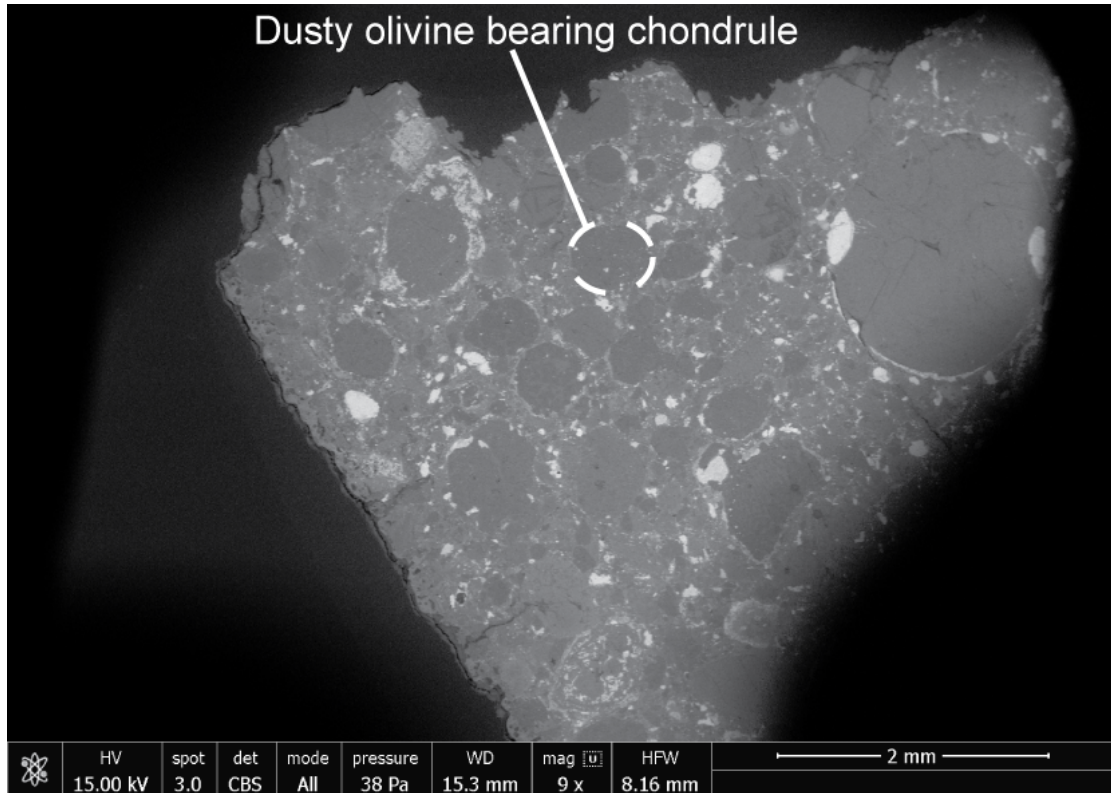


Figure 4.1: A scanning electron microscope image of the polished section of Bishunpur at low magnification to identify dusty olivine bearing chondrules.

Natural History Museum, London.

4.2.2 Focused ion beam scanning electron microscopy

Focused ion beam (FIB) SEMs are used to prepare sections for transmission electron microscopy (TEM) analysis. The bulk sample is prepared as it would be for an SEM. Inside the FIB/SEM, the region of interest (Fig. 4.4a) is initially coated in a protective layer of carbon or platinum (Fig. 4.4b). Carbon is preferable, as it is electron transparent such that the electron beam may pass through it. A beam of Ga ions is then targeted at the sample to mill out a section approximately 50 to 100 nm thick (Fig. 4.4c) to be mounted onto an Omniprobe TEM sample grid (Fig. 4.4d). For temperature-dependent TEM experiments, an even smaller lamella is necessary, as it must be mounted onto a silicon nitride EMheaterchip (Fig. 4.5).

The sample preparation for TEM experiments of rock samples is time consuming and costly, as it is necessary to use the FIB/SEM to prepare an electron-transparent

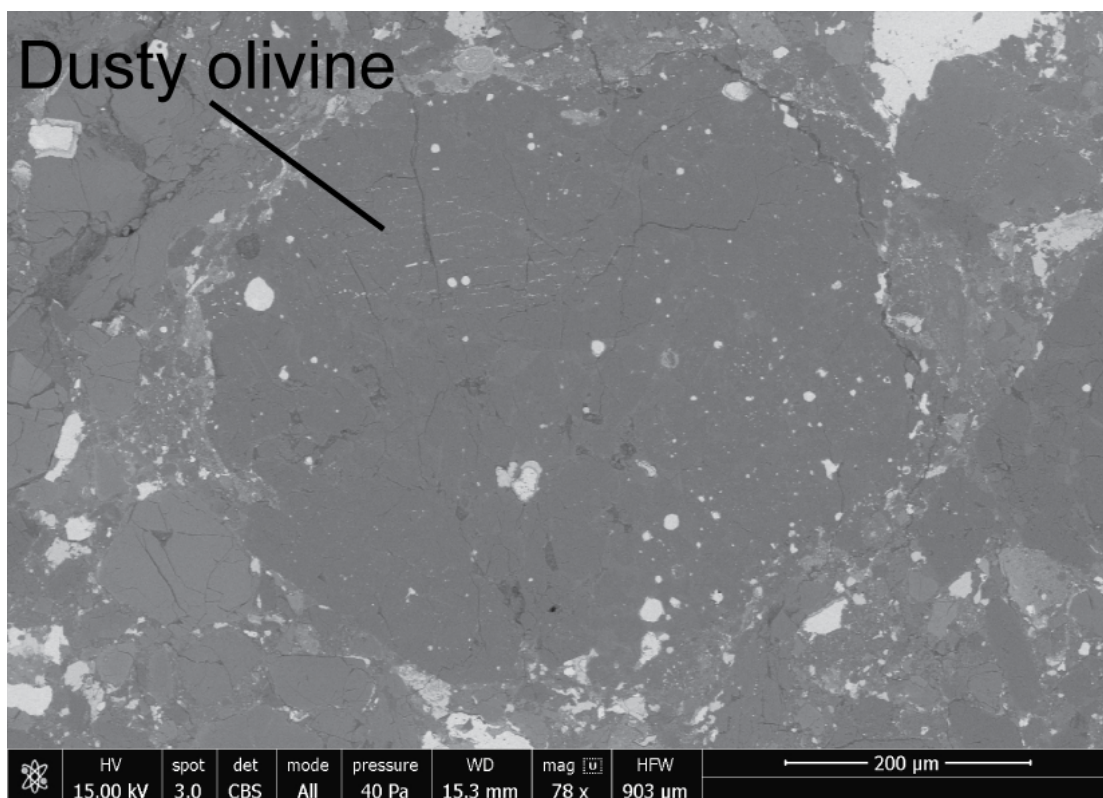


Figure 4.2: A scanning electron microscope image of a chondrule from the polished section Bishunpur that bears numerous dusty olivine grains.

lamella. The process is also error-prone, with the possibility of failed lamellae lift-outs and successful lamellae lift-outs that do not bear any features of interest; this is more prevalent with samples for temperature-dependent analysis, as the lamellae must be half the size of Omniprobe grid lamellae ($5\ \mu\text{m}$ by $2.5\ \mu\text{m}$ compared to $10\ \mu\text{m}$ by $5\ \mu\text{m}$, Fig. 4.4, 4.5). I was trained to operate a FIB and lift-out TEM lamellae in the Department of Materials at Imperial College London, and prepared one lamella of Bishunpur dusty olivine, Bish01, for off-axis electron holography training at the Forschungszentrum Jülich in November 2014. The site of the FIB-milling post-lift-out is presented in Figure 4.6, showing the trenches around the lifted-out section in the centre. As the majority of TEM analysis was conducted during a five-month visit to the ER-C in Jülich, during which new samples needed to be produced, the subsequent samples for TEM analysis were prepared by Doris Meertens at the ER-C in Jülich due to their strict user requirements. A sequence of snapshots of the preparation procedure is presented in Figures 4.4 and 4.5.

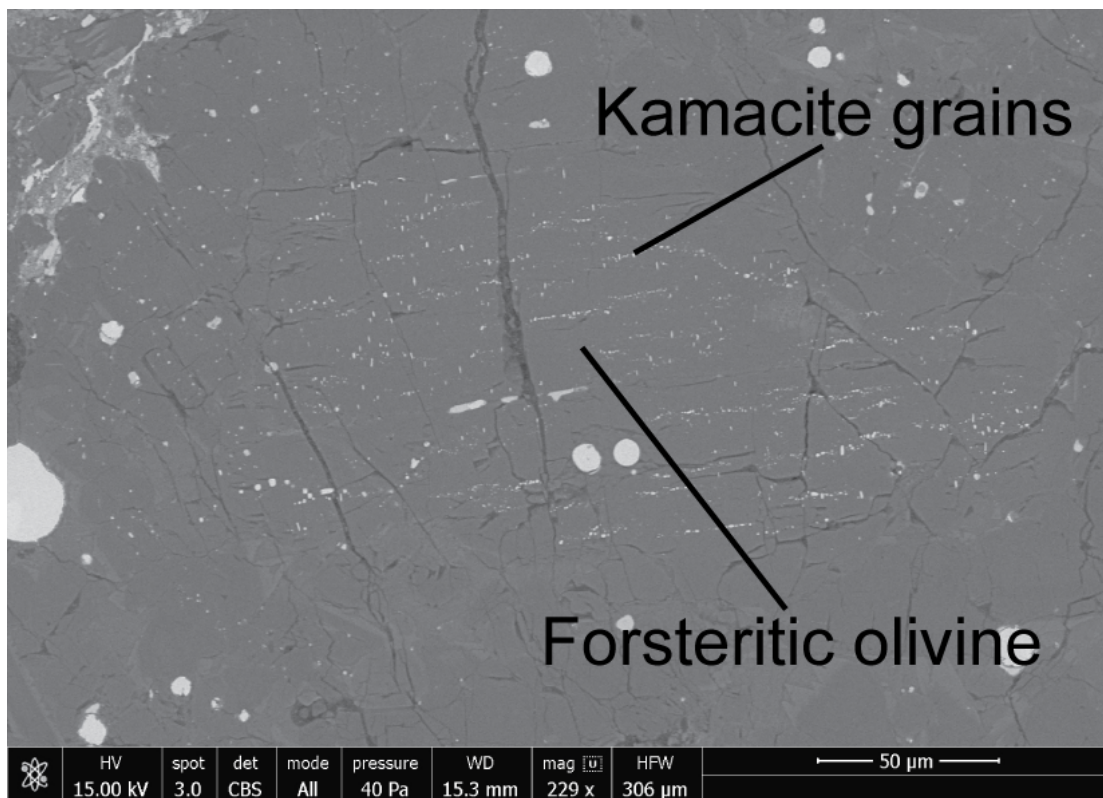


Figure 4.3: A scanning electron microscope image of the polished section of a chondrule from Bishunpur that bears numerous dusty olivine grains.

4.2.3 Transmission electron microscopy

Transmission electron microscopy (TEM) operates in principle similarly to transmission optical microscopy, however, instead of optical lenses it uses electromagnetic lenses, and a beam of high energy (80-300 keV) electrons instead of a beam of light. By utilising the small wavelength of electrons, high-end TEMs can achieve sub-Å spatial resolution. As well as high resolution spatial imaging, TEM is capable of producing diffraction patterns and spectroscopic information allowing accurate determination of the material's chemical composition and physical properties. In this chapter, scanning transmission electron microscopy (STEM) was used to perform 2 nm resolution chemical maps with EDX and to determine sample thickness using the electron energy loss spectroscopy (EELS) technique, which detects the energy loss of electrons owing to inelastic scattering with an electron spectrometer.

TEM's main importance to this project is that it provides the unique opportunity to quantitatively and visually image the magnetic properties of a material at the

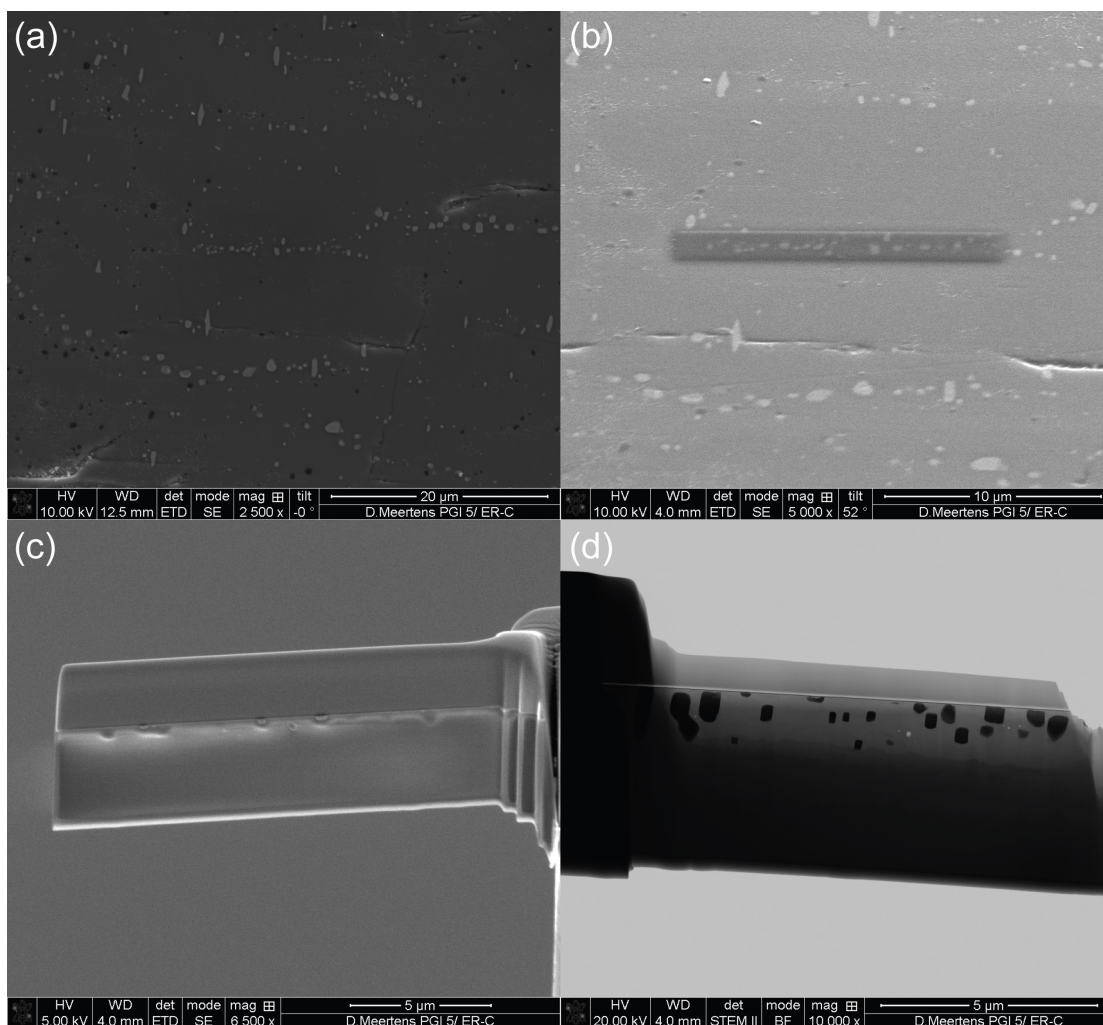


Figure 4.4: Images taken by Doris Meertens on the focused ion beam scanning electron microscope (FIB/SEM) at the Ernst Ruska Centre for Microscopy and Spectroscopy with Electrons in Jülich of the preparation of a lamella of Bishunpur, Bish02, for TEM analysis. (a) The selected site for FIB-milling, (b) the layer of carbon deposited onto the milling site to protect the surface of the excavated section from being effected by the Ga ion beam, (c) the excavated section from the sample surface attached to the lift-out probe, and (d) the TEM lamella attached to the Omniprobe grid and thinned by further sputtering to between 60 and 200 nm in thickness.

nanoscale by using the off-axis electron holography technique (see below).

4.2.4 Off-axis electron holography

Off-axis electron holography (hereafter holography) is a TEM technique that has gained feasibility in recent years with the commercial availability of coherent and brilliant field emission gun (FEG) electron sources (Midgley and Dunin Borkowski, 2009). Electron holography is a technique originally developed to correct for lens aberration in TEMs more than fifty years ago (Gabor, 1949). Correction for the lens aberration by performing wave optical image processing of the amplitude and phase

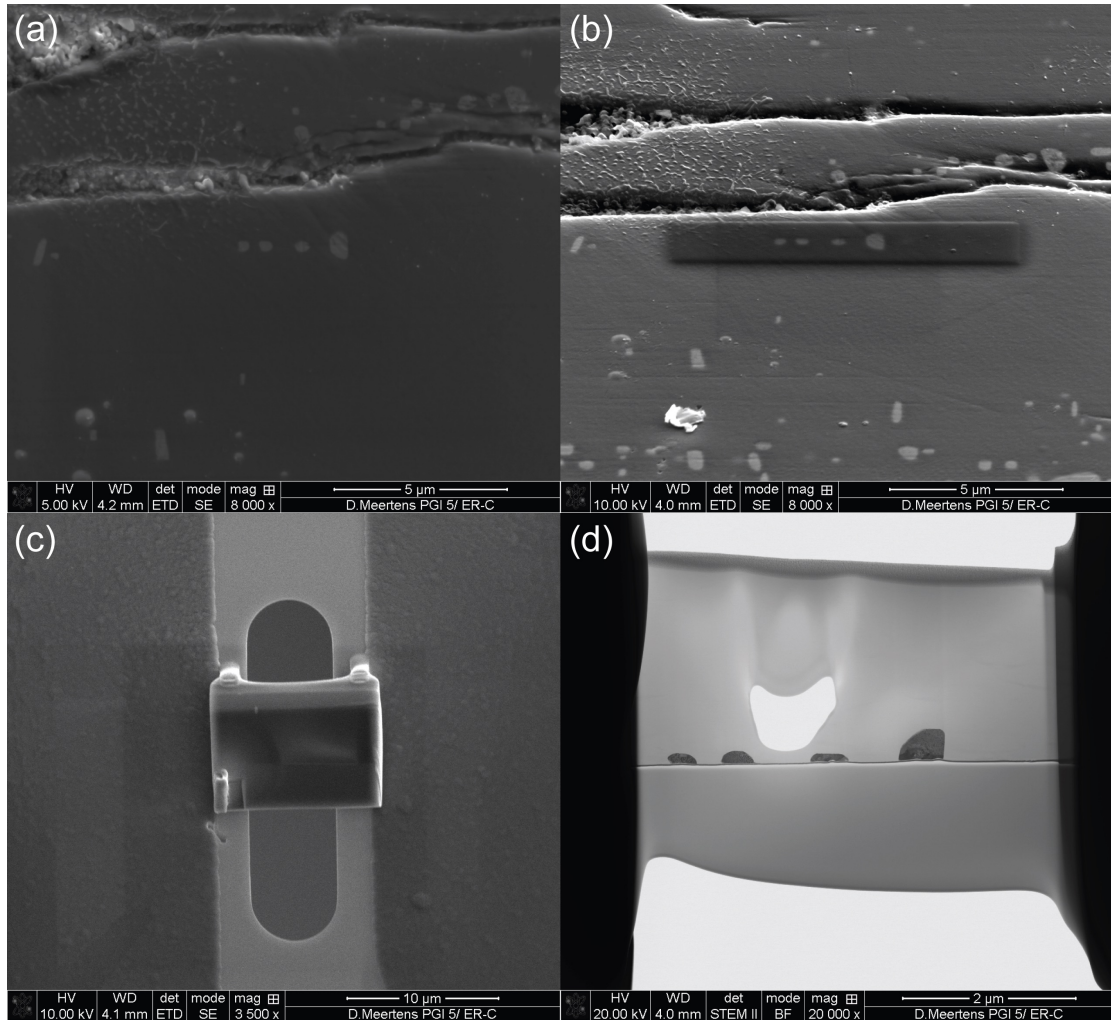


Figure 4.5: Images taken by Doris Meertens on the focused ion beam scanning electron microscope (FIB/SEM) at the Ernst Ruska Centre for Microscopy and Spectroscopy with Electrons in Jülich of the preparation of a lamella, Bish04, from Bishunpur for temperature-dependent TEM analysis. (a) The selected site for FIB-milling, (b) the layer of carbon deposited onto the milling site to protect the surface of the excavated section from being effected by the Ga ion beam, (c) the excavated section from the sample surface attached across a window of the EMheaterchip, and (d) the TEM lamella attached to the EMheaterchip and thinned by further sputtering, estimated to be between 60 and 200 nm in thickness.

information recorded by the electron hologram greatly increased TEM resolution (Orchowski et al., 1995). In typical operation of a TEM, only a spatial distribution of electron energy is recorded, but through electron holography, the phase change of the electron beam after passing through the sample is also recorded (Midgley and Dunin Borkowski, 2009; Kasama et al., 2011). This is achieved by using an electrostatic biprism (typically a $<1 \mu\text{m}$ gold coated quartz wire), through which a voltage is applied to generate a reference electron wave (Midgley and Dunin Borkowski, 2009; Kasama et al., 2011). Provided the electron beam source is highly coherent, the interferences produced through the interaction with the reference electron wave

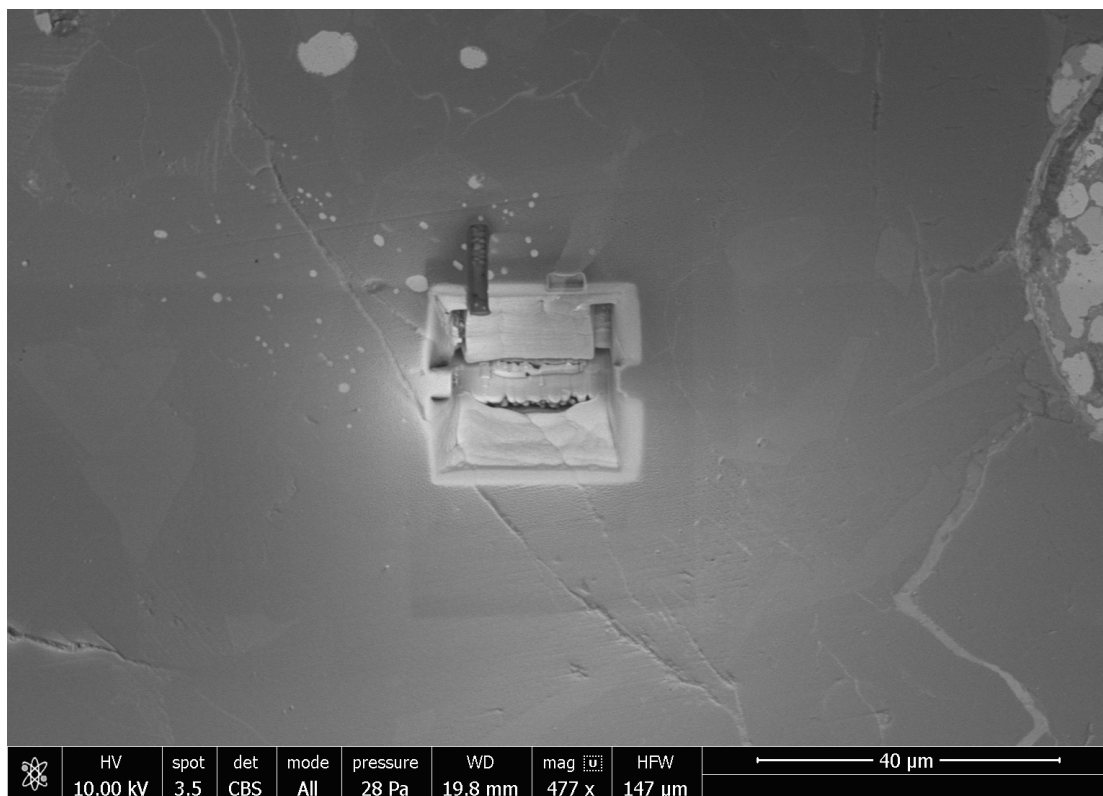


Figure 4.6: An image taken in the focused ion beam scanning electron microscope (FIB/SEM) at Imperial College London of the FIB-milling site of a lamella lifted out of Bishunpur for transmission electron microscopy.

and sample electron wave will be recorded, in addition to the bright-field image (Fig. 4.7) (Midgley and Dunin Borkowski, 2009; Kasama et al., 2011). Also present in Fig. 4.7, and not typical of standard TEM is a Lorentz lens, which is a high strength mini-lens, used to allow magnetic field-free conditions with high magnification when analysing magnetic materials; the objective lens is typically inactive when imaging as it generates significant (> 1.5 T) magnetic fields (Midgley and Dunin Borkowski, 2009; Kasama et al., 2011).

Samples for holography were prepared by FIB-milling lamellae from a polished section of the Bishunpur meteorite onto a Cu Omniprobe grid for room temperature analysis, and onto the windows of a silicon nitride EMheaterchip for in-situ heating with a DENSSolutions double-tilt holder. (S)TEM imaging, chemical analysis and holography experiments were conducted at the Department of Materials, Imperial College London, the Imaging and Analysis Centre, Natural History Museum, London, and the Ernst-Ruska Centre for Microscopy and Spectroscopy with Electrons,

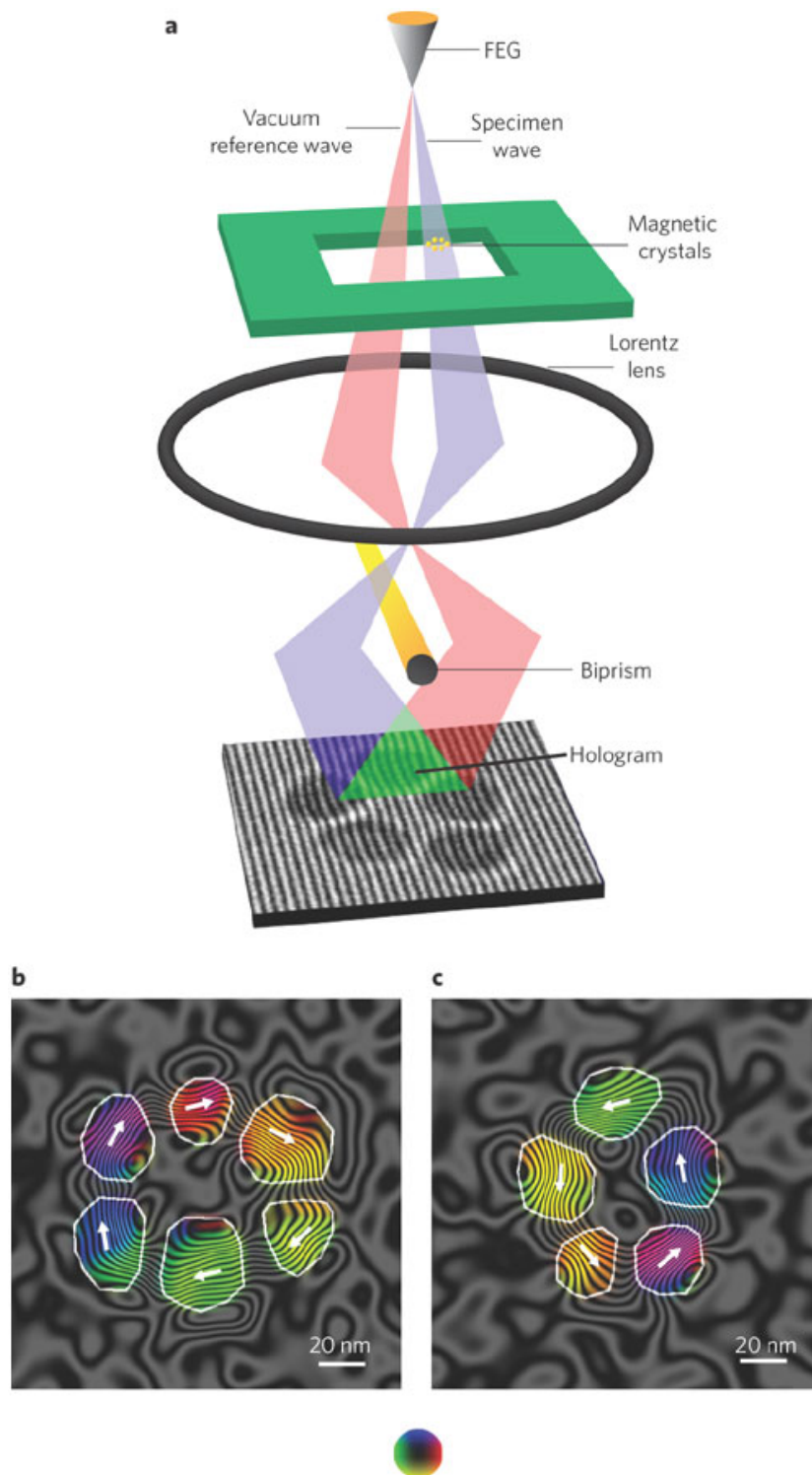


Figure 4.7: (a) A schematic diagram of a transmission electron microscope (TEM) equipped with an electrostatic biprism and Lorentz lens used to produce interference fringes that correspond to the phase shift of the electron beam due to the sample. By isolating the magnetic contribution to the phase shift, magnetic induction maps (b, c) of cobalt nanoparticles are calculated. The contour spacing indicates the intensity of magnetisation, and the arrows and the colour wheel on the nanoparticles indicate the direction of magnetic induction. Red is right, yellow is down, green is left, and blue is up. From Midgley and Dunin Borkowski (2009)

Forschungszentrum Jülich, Germany. Electron holograms were acquired using a FEI Titan 80-300 TEM imaging in Lorentz mode at 300 kV using a charge-coupled device (CCD) camera and an electron biprism typically at 50 V. In-plane magnetic induction maps were obtained by tilting the sample to 70° in a field of > 1.5 T, applied by activating the objective lens, to record images with reversed magnetisation of the sample. An evaluation of half of the difference between phase images recorded with opposite magnetization directions in the sample was used to remove the mean inner potential contribution to the phase. The mean inner potential was subtracted from the unwrapped total phase shift in order to construct magnetic induction maps that were representative of the magnetic remanence (Midgley and Dunin Borkowski, 2009).

Image processing

The holograms were processed whilst imaging using the Gatan Digital Micrograph package HoloWorks to assess the quality of the holograms for phase reconstruction, adjusting the instrument settings accordingly to achieve the best interference fringe resolution possible by maximising fringe contrast, minimising diffraction contrast, and minimising fringe spacing. Closely spaced fringes increase spatial resolution, however also reduces fringe contrast and signal-to-noise ratio, resulting in a lower resolution phase reconstruction. Once holograms were acquired, final processing was conducted with the Semper image processing program. Semper was used to convert the holograms of the sample (Fig. 4.8a) and the vacuum reference (Fig. 4.8b) to Fourier space (Fig. 4.8c). In Fourier space (i.e. Fig. 4.8c), the central peak is representative of the vacuum reference image and conventional bright-field TEM image (Kasama et al., 2011). The sideband in Figure 4.8d represents the complex conjugate of the wave that has passed through the sample (Kasama et al., 2011). A sideband is selected and isolated with a mask, and Fresnel fringes can be removed by selecting streaks originating from the central peak that extend to the sideband (e.g. Fig 4.8e). An inverse Fourier transform of the sideband produces a complex

image of the phase (Fig. 4.8f). Phase unwrapping algorithms incorporated into Semper are then used to generate a phase image (Fig. 4.8g), and then oppositely magnetised phase images (Fig. 4.8h) are used to remove the electrostatic potential contribution to the phase. The cosine of the phase produces a magnetic induction map (Fig. 4.8i). Semper is used to colourise the magnetic induction map to indicate direction of magnetic induction (Fig. 4.8i (inset)).

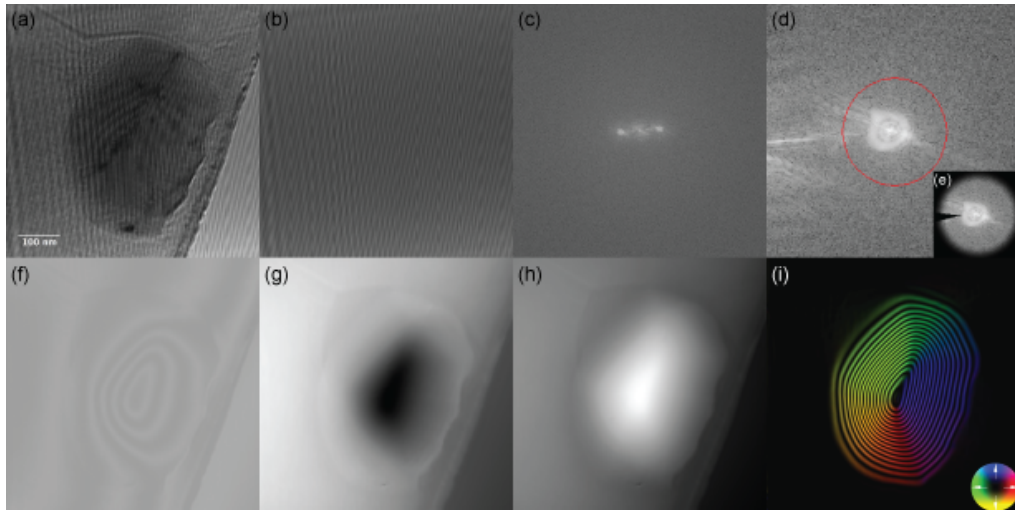


Figure 4.8: The procedure for creating magnetic induction maps using the Semper image processing program. (a) Hologram acquired in the TEM of a dusty olivine kamacite grain. (b) Reference hologram acquired in the TEM of the vacuum a short distance away from the lamella. (c) Fourier transform of the hologram showing the centralband, two sidebands. (d) Sideband, which contains the phase information, is circled, containing also some of the diagonal streak due to Fresnel fringes in the hologram. (e) A mask is applied to radially smooth values to zero, and the streak is also selected and given a zero value. (f) After inverse Fourier transform, the complex phase image is acquired, which is then unwrapped (g) with phase unwrapping algorithms in Semper. (h) The unwrapped phase of the oppositely magnetised hologram to that in (a). (i) A magnetic induction map produced by subtracting the phase images (g) and (h) to isolate magnetic contribution to phase, amplifying the cosine of the remaining phase, and applying colouration to indicate direction of induction ((i) inset).

Temperature-dependent holography

In situ temperature-dependent electron holography was conducted following the methods developed by Almeida et al. (2014a, 2016a). To determine the change in magnetic induction with respect to heating, the sample (Fig. 4.5d) was initially magnetised with a saturating field applied with the objective lens. Holograms were acquired at room temperature, then heated to 100°C, and then to 800°C in 100°C intervals, and the same in reverse for cooling; this is the initial SIRM heating and cooling sequence. The ramp for heating was 50°Cmin⁻¹, and each temperature interval was maintained for 10 minutes to allow sufficient time for imaging. The

process was repeated except with magnetisation reversals in order to determine the electrostatic contribution to the phase shift at each temperature interval.

The repeat heating and cooling sequence was conducted to remove the electrostatic potential from the initial SIRM heating and cooling sequence, as no reversals at high-temperature are recorded on the initial sequence. Thermochemical alteration occurring to the sample at temperatures above 500°C resulted in this second heating and cooling sequence of reversals being unrepresentative of the sample's electrostatic potential, and the room-temperature electrostatic phase contribution was used isolate the high-temperature magnetic phase contributions.

4.2.5 Numerical modelling

Micromagnetic modelling will be expanded upon in the following chapter, however, in this chapter a micromagnetic solution is presented to detail the magnetic structure observed in the temperature-dependent holography. The grain was meshed using Cubit as a tetrahedral mesh modelled after the width and length dimensions observed with the TEM, and the thickness estimated as 60 nm from EELS data of Bish02. Micromagnetic models of the heated grain were conducted at the University of Edinburgh by Prof Wyn Williams using the MERRILL micromagnetic modelling package (Conbhuí et al., in prep).

4.3 Results

4.3.1 Chemical analysis

Chemical analysis of the dusty olivine lamellae prepared for electron holography showed a forsteritic olivine composition with metallic precipitates of almost pure iron composition ($> 99\%$ Fe) (Fig. 4.9). Bish01 has amorphous silica phases associated with the metallic iron precipitates. These associated silica phases have been found before both in chondrule dusty olivine and synthetic dusty olivine, and are a by-product of the sub-solidus reduction process that precipitates the metallic iron

(Leroux et al., 2003). Bish02, Bish03, and Bish04, prepared from a different chondrule from Bishunpur, did not have silica phases associated with the metallic iron precipitates. The STEM EDX analysis of the chondrule that Bish02 and Bish03 originated from showed a similar forsteritic olivine and kamacite of near-pure iron composition as seen in Bish01.

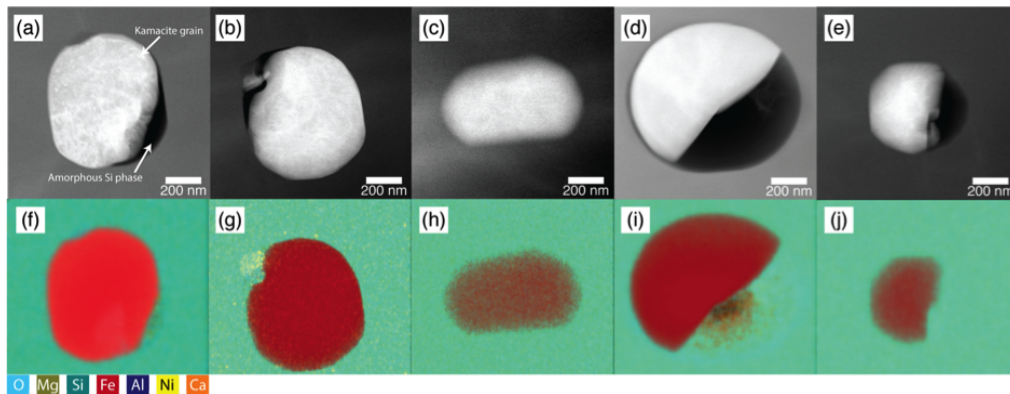


Figure 4.9: High-angle annular dark field images (a-e) of kamacite grains in a forsteritic olivine matrix from Bish01 with elemental maps (f-j) produced by energy dispersive X-ray spectroscopy (EDX) with a scanning transmission electron microscope (STEM) with a spot size of 2 nm. Elements displayed on the maps are in the colour key at the bottom of the figure.

Kamacite grains are also observed to bear associated Al- and Cr-oxide grains, agreeing with previous analyses of chondrule dusty olivine (e.g. Zanda et al. (1994); Leroux et al. (2003)); these phases associated with the metal/silica precipitates are not found in synthetically produced dusty olivine, and are thought to be exsolved during chondrule cooling or thermal metamorphism owing to the metal-silicate equilibration within chondrules (Zanda et al., 1994; Leroux et al., 2003).

The average axial ratio (length/width) of the dusty olivine kamacite grains is 1.5. The grains were 150 to 600 nm in size.

The metal phase alignment seen in the dusty olivine grain that Bish03 and Bish04 sample (Fig. 4.4, 4.5) suggests that the metal precipitates are crystallographically aligned with their host olivine grain, as has been previously found for Bishunpur (Jones and Danielson, 1997; Boland and Duba, 1981, 1986; Lemelle et al., 2000; Leroux et al., 2003).

4.3.2 Room-temperature off-axis electron holography

During the initial holography training period, only a single kamacite grain from Bish01 could be analysed, as the rest were too far from the edge of the lamella such that interference with the vacuum electron beam was not possible. A magnetic induction map for this grain is presented in Figure 4.10. The size of this grain resulted in a high-quality hologram being difficult to produce due to excessive diffraction contrast related to grain thickness variation. Successive attempts to further thin the lamella with a Fischione Nanomill were made, however a new, higher-quality lamella was necessary. Bish02, Bish03, and Bish04 were prepared by Doris Meertens at the ER-C in Jülich during my five-month stay to do the holography experiments, as the FIB in ER-C has strict user requirements.

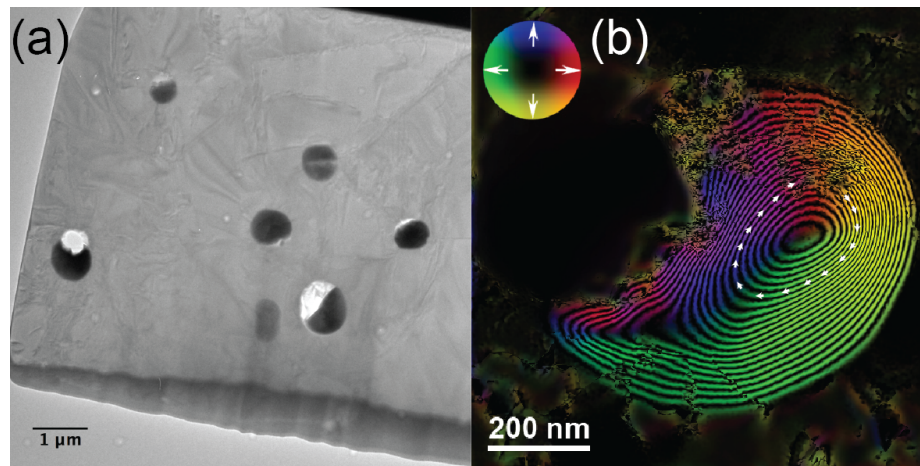


Figure 4.10: (a) Bright field TEM image of lamella Bish01, with one grain sufficiently close to the edge of the lamella for hologram acquisition (boxed in red). The rest of the grains are too far from the vacuum to produce interference fringes. (b) Magnetic induction map of Bishunpur dusty olivine kamacite reconstructed from holograms acquired at room-temperature. Direction of magnetic induction is indicated by the arrows, which correspond to the colour-wheel.

Room-temperature magnetic induction maps for 20 kamacite grains from Bish02 and Bish03 are presented in Figure 4.11. The kamacite grains were typically found to have well-defined single-vortex magnetisations with their vortex cores aligned out-of-plane along $[001]$ axes with little-to-no external stray magnetic-fields (Fig. 4.11). Single-vortex magnetisation is also well-defined in the largest grains tested (450 x 750 nm, Fig. 4.11f,g). Phase reconstruction artefacts for this grain are due to the size and thickness (thickest end of the wedge-like lamella) limiting fringe spacing

and contrast and greater diffraction contrast. These single-vortex magnetisation structures are in accordance with previous holography analyses of chondrule and synthetic dusty olivine (Lappe et al., 2013; Einsle et al., 2016). Deviations from single-vortex structures are typically due to crystallographic variation, e.g. Figure 4.11b, where an inclusion of Cr_3O_2 has split the magnetisation structure into three vortices. The grain in Figure 4.11j has been reshaped through the FIB-milling process, resulting in a multi-vortex structure with magnetostatic interactions. The lack of a magnetisation structure in the upper left grain in Figure 4.11b is due to the magnetisation not reversing, so the magnetic contribution to the phase shift could not be isolated to generate a magnetic induction map.

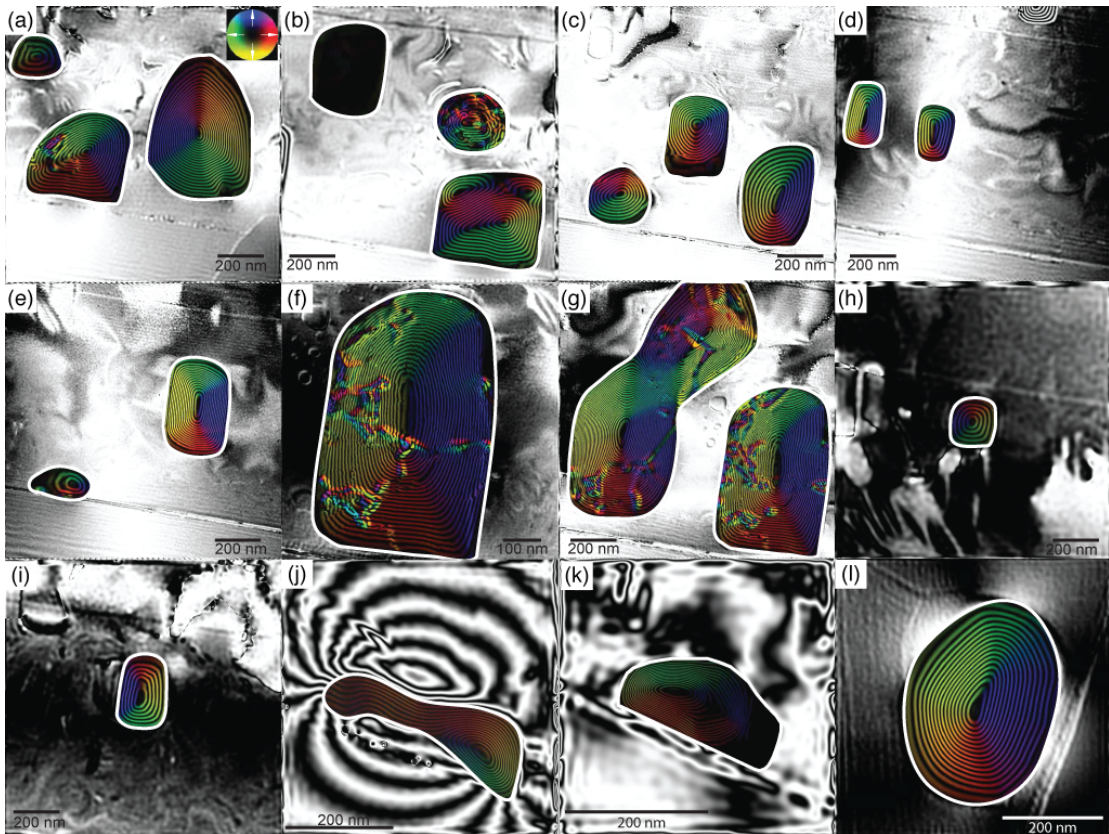


Figure 4.11: Magnetic induction maps of kamacite grains in dusty olivine reconstructed from electron holograms recorded at room temperature. The contour spacing is π radians. The direction of the projected in-plane magnetic induction is indicated by a colour wheel in (a). One of the grains in (b) did not reverse its magnetization direction in the TEM, and a magnetic induction map could not be produced. The defects to the magnetic induction maps for the grains in (a), (f), and (g) are phase reconstruction artefacts due to diffraction contrast (typically a result of grain thickness variations) present in the recorded electron holograms.

4.3.3 Temperature-dependent off-axis electron holography

In-situ temperature-dependent holography (see Methods) for four kamacite particles from Bish04 (Fig. 4.5) was attempted, and it was possible to reconstruct a heating sequence with one grain (Fig. 4.12). The axial ratio of the kamacite grain (Fig. 4.12) is 4.5, with the ratio likely increased by the FIB-milling process. Its saturated remanent magnetisation state at room temperature appears to resemble that of a uniform magnetisation or an in-plane vortex-core magnetisation (Fig. 4.12); the calculations conducted to distinguish between these possibilities are explained below. This structure is maintained as the grain is heated up to 500°C (Fig. 4.12). At 600°C, the grain underwent chemical alteration (Fig. 4.13), likely with the surrounding olivine as the TEM operates in a high-vacuum. Chemical alteration prevents an accurate determination of the magnetic structure beyond 600°C due to the difficulty of removing the phase contribution of the newly mineralized phases.

High-temperature micromagnetic modelling

It is not clear whether the large grain observed using temperature-dependent electron holography is in uniform or in-plane vortex structure (Fig. 4.12a-g). To determine whether the grain is in uniform or in-plane vortex state, a finite element method (FEM) micromagnetic algorithm (MERRILL (Conbhui et al., in prep), see Chapter 5) was used to model the 3D magnetisation structures expected for the grain. The lowest energy magnetisation states of the 1000 total solutions calculated for the grain are the most likely to occur in nature; calculating the energy barrier between these low energy states can determine the stability of the magnetisation structure, i.e., if magnetisation can be retained on Solar System timescales.

The micromagnetic finite-element model builds the geometry of the magnetic grain from a large number of tetrahedral elements, with the magnetization defined in terms of a constant length vector at each node of each element. Stable micromagnetic states were then found by optimizing the free magnetic energy calculated from the magnetostatic, crystalline, and exchange forces within the grain (See Chapter 5

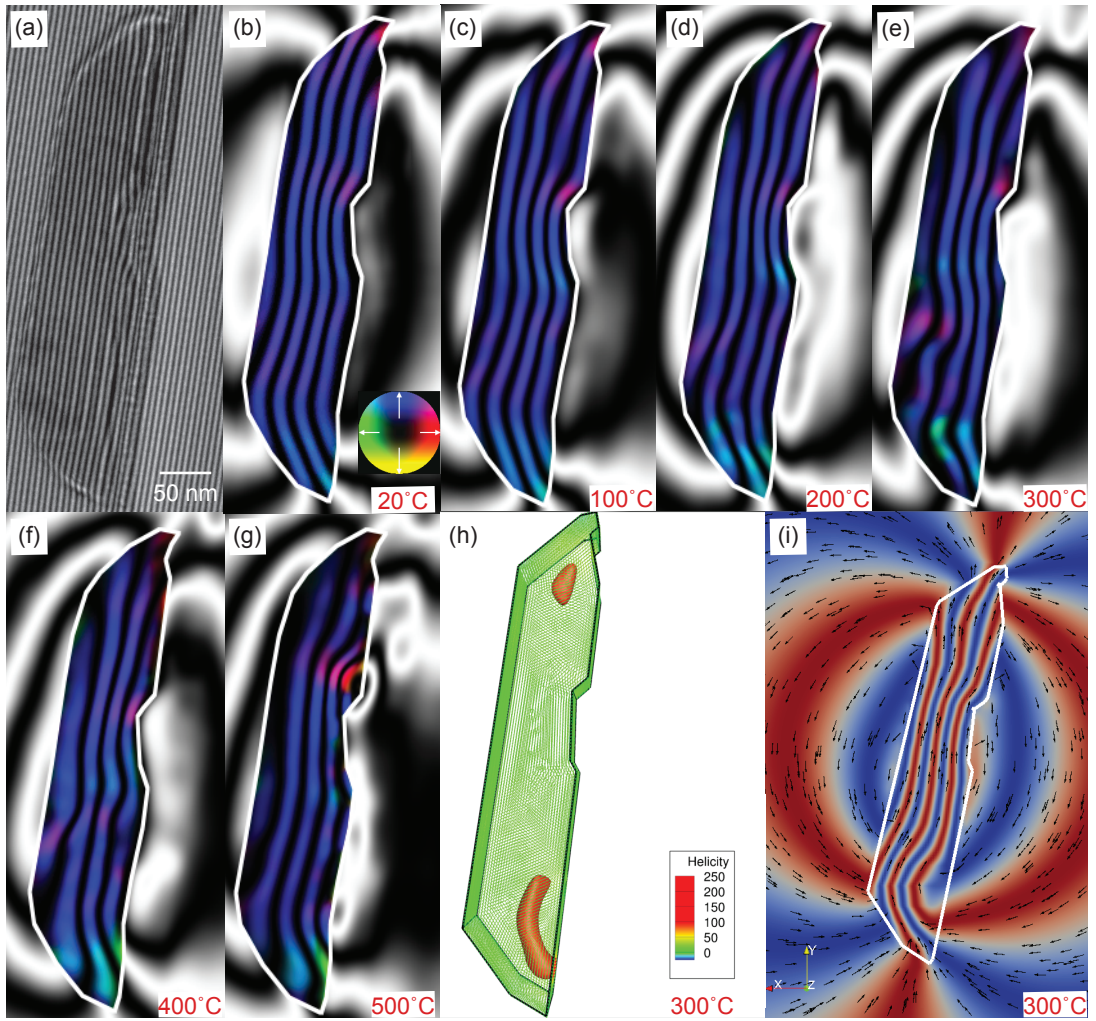


Figure 4.12: (a) Electron hologram of a Bishunpur dusty olivine kamacite grain before heating. The fringes due to electron beam interference are used to determine the phase shift of the electron beam passing through the sample. (b-g) Magnetic induction maps reconstructed from holograms of the kamacite grain heated in-situ from 20-500°C (the grain underwent chemical alteration above 500°C). (h) Micromagnetic model of a minimum energy state magnetization distribution at 300°C for an Fe tetrahedral mesh modelled after the grain in (a-g). Curie temperature for Fe is 760°C and peak temperature of Bishunpur is 300°C (Rambaldi and Wasson, 1981). The regions of high helicity (red) are highlighted by a contour plot to display the vortex cores in the modelled kamacite grain. (i) Electron holography-style magnetic induction map simulated from the micromagnetic solution in (h). The contour spacing for (b-g) is 1.57 radians. The direction of the projected in-plane magnetic induction in (b-g) is indicated by the arrows and the colour wheel in (b).

for more information). The material constants that scale each of these forces were taken to be those for pure Fe at 300°C ($A = 1.52 \times 10^{-11} \text{ Jm}^{-1}$, $K_1 = 2.2 \times 10^4 \text{ Jm}^{-3}$, and $M_s = 1.61 \times 10^6 \text{ Am}^{-1}$). The chosen magnetic constants reflect the chemical composition of the grains that was determined by EDS analysis to be near-pure metallic Fe. A temperature of 300°C was chosen to determine the magnetic domain states and their thermal stability at the maximum temperature to which these magnetic grains are predicted to have been exposed since the time of their formation

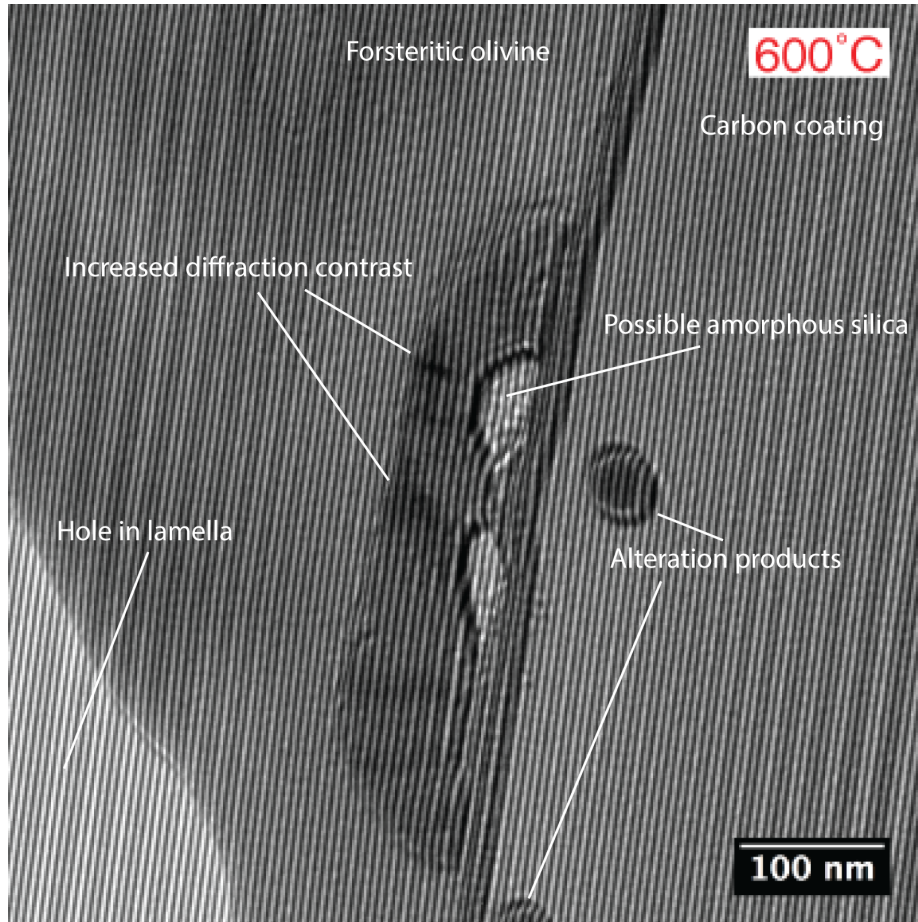


Figure 4.13: Hologram of a Bishunpur dusty olivine kamacite grain at 600°C on the first heating cycle. The fringes due to electron beam interference are used to determine the phase shift of the electron beam due to passing through the sample. The grain is visibly altered compared to its initial grain morphology in Figure 4.12a. Newly mineralised phases have formed on the lamella's carbon coating, and two amorphous phases have replaced iron in the grain.

approximately 4.6 billion years ago (Rambaldi and Wasson, 1981).

I made a tetrahedral mesh of the grain to the approximate dimensions of the heated grain (458 x 98 x 60 nm, and an element size of 3 nm, equal to the exchange length for Fe) using Cubit. Collaborating with Professor Wyn Williams at the University of Edinburgh, we conducted 1000 domain state calculations with the use of ARCHER (www.archer.ac.uk) high-performance computing facility funded by the National Environmental Research Council (NERC). Two domain states, which were examined in detail, are shown in Figure 4.14. Both states produce simulated magnetic induction maps that are consistent with our observations and both have energies near the minimum of the energy distribution, i.e., likely to occur in nature. Despite the superficial similarity of these domain states, the low helicity regions

(coloured green) are oriented in opposite directions, with domain states LEM3 and LEM4 having a normalized x-component of the magnetization (aligned with the grain elongation) of 0.76 and -0.75, respectively (Fig. 4.14).

Due to the similarity of the simulated magnetic induction maps for LEM3 and LEM4 (Fig. 4.14) to those observed experimentally (Fig. 4.12a-g), the nudged elastic band (NEB) method with a convergence constraint of minimum action (Berkov, 1998; Fabian and Shcherbakov, 2017) was used to determine the minimum energy path and thus the energy barrier between two such domain states. In this method, a series of domain states was constructed along an initial guess of the path and these domain states were then optimized so that they were on the optimal minimum energy path.

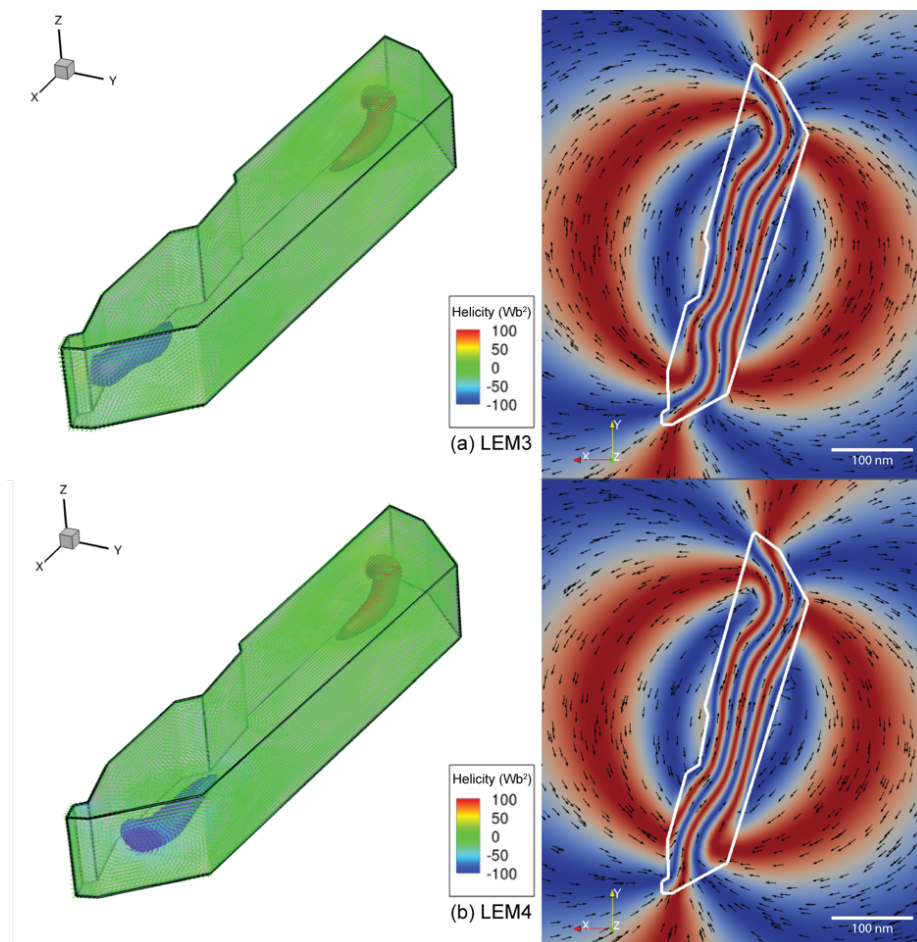


Figure 4.14: (a, b) Magnetic domain states LEM 3 and LEM4 and corresponding electron holographic magnetic induction maps similar to those observed experimentally, with energies of (a) 1.5405×10^{-16} J and (b) 1.5383×10^{-16} J.

The result of NEB optimisation between domain states LEM3 and LEM4 is shown in Figure 4.15. A highly complex path is observed, compared to those reported in this study for much smaller grains. The path is characterized by a multitude of intermediate minima, but has a maximum energy barrier along the path of 4.64×10^{-17} J. At a temperature of 300°C , for which these domain states were calculated, Néel’s equation (See Chapter 5) yields a relaxation time that is of many orders of magnitude greater than the age of the Solar System.

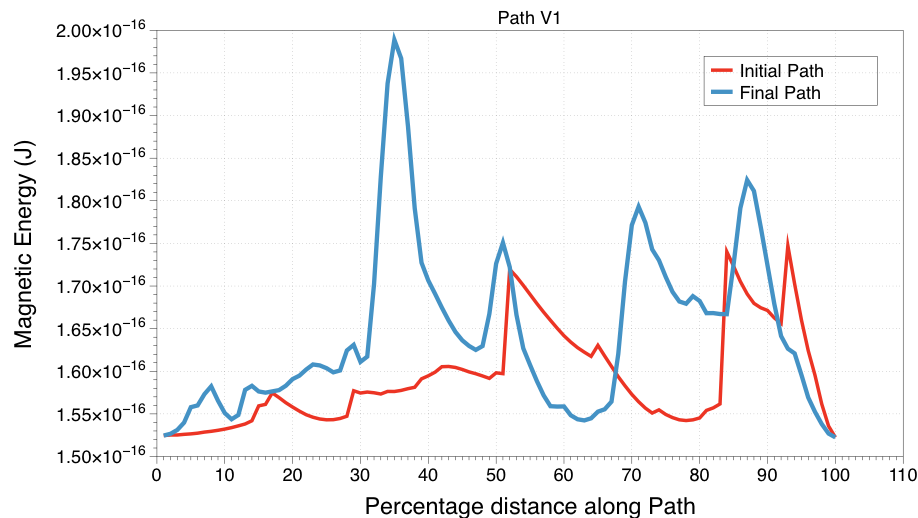


Figure 4.15: Initial guess and optimised minimum energy path between magnetisation states LEM3 and LEM4.

Using a NEB numerical algorithm (Berkov, 1998; Fabian and Shcherbakov, 2017) I found that the grain is in multi-vortex state with cores aligned with the long-axis (also the saturation axis), and that it can carry stable magnetisation for many orders of magnitude longer than the age of the Universe (10^8 Ga) at 300°C , the highest temperature reached by Bishunpur chondrules since formation 4.6 Ga.

4.4 Discussion

Palaeomagnetic data such as palaeointensities and palaeodirections can be estimated due to the widely-accepted theoretical understanding of single domain (uniform) magnetisation structures (Néel, 1949). The behaviour of uniformly magnetised grains can be used to understand ancient magnetic fields (Eq. 1.4) (Koenigs-

berger, 1930), however, the kamacite grains found in dusty olivine may be too large to exhibit uniform magnetisation structures. For grains above the uniform magnetisation size threshold, non-uniform magnetisation structures are the most energetically favourable state (Gatel et al., 2015). A similar underpinning theory for non-uniformly magnetised grains does not exist, and the stability of these non-uniform magnetisation structures is unknown. Non-uniform magnetisation structures are ubiquitous in both meteorites and terrestrial lithologies, however, their stability is not known. A key aim of this study was to determine whether the kamacite found in dusty olivine grains of Bishunpur chondrules is of uniform (single domain) or non-uniform (pseudo-single domain) magnetisation structure, and whether non-uniform magnetisation structures are stable carriers of magnetic remanence. To analyse the magnetisation structures of chondrule dusty olivine kamacite and their temperature-dependent behaviour, two thick-sections of ordinary chondrite Bishunpur were analysed by optical and electron microscopy. A total of six lamellae were prepared by FIB-milling: two Cu Omniprobe grid room-temperature lamellae (Bish01, Bish02), and four EMHeaterChip high-temperature lamellae, of which, one was used at room-temperature (Fig. 4.11) before it was broken during handling (Bish03), and one was used for the temperature-dependent experiment (Fig. 4.12) (Bish04). The rest of the EMHeaterChips had no kamacite grains close enough to the vacuum to produce interference fringes. High-temperature micro-magnetic simulations were conducted to complement the temperature-dependent holography.

4.4.1 Chemical and physical properties of Bishunpur dusty olivine

Bish01 sampled dusty olivine from a different chondrule to the dusty olivine grains sampled by Bish02, Bish03, and Bish04. Abundant glass silica phases associated with the metallic iron precipitates in Bish01 and the lack of glass silica phases observed in Bish02, Bish03, and Bish04 may owe to inhomogeneous reduction con-

ditions in the Solar Nebula at the time of dusty olivine formation. Lemelle et al. (2000) propose a coupled reduction and volatilisation reaction that would result in the production of SiO gas rather than glass, and Leroux et al. (2003) propose a reduction reaction accounting for the presence of SiO₂ glass; both reactions assume some degree of volatilisation of SiO gas to account for the excess metal to silica ratio typically observed.

4.4.2 Electron holography

A key finding of the holography analysis of the chondrule dusty olivine kamacite grains is that all grains analysed are of non-uniform magnetisation state. The lack of any uniform magnetisation structure observed may be due to the large grain sizes observed, however, this is in itself owing to the distribution of grain sizes in natural rock samples (Robertson and France, 1994; Krüver et al., 2001). The electron holography analysis of synthetic dusty olivine by Lappe et al. (2011) found some grains classified as uniformly magnetised. These grains may be naturally uniformly magnetised, or their uniform structure could be due to unnatural elongation (\gg the 1.5 AR average for dusty olivine kamacite) (e.g. through synthesis or sample preparation) or potentially these may have been misinterpreted in-plane vortex magnetisation (i.e. non-uniform) structures, as was determined for the grain shown in (Fig. 4.12h).

The magnetisation structure in the heated kamacite grain resembles that of a uniform magnetisation, which would be unrepresentative of the rest of the sample set exhibiting non-uniform structures, and uniform magnetisation structures already have a well-developed underpinning theoretical framework describing their thermal stability (Néel, 1949). However, upon numerical analysis of a grain of iron meshed to the approximate dimensions of the heated grain, more than 1000 energy minimised solutions exhibit non-uniform magnetisation structures, with the lowest energy solutions producing simulated holography-style magnetic induction maps (Fig. 4.14) that closely resemble the experimental magnetic induction maps (Fig. 4.12b-g). The

non-uniform magnetisation structure observed in the heated kamacite grain is stable with heating up to the point of chemical alteration at 600°C (Fig. 4.12, 4.13). There is no visible change in its direction upon heating, and only minor decrease in intensity (Fig. 4.12b-g). It is not possible to test stability up to the Curie temperature of 760°C due to the chemical alteration, as the change in phase and grain morphology prevents an accurate removal of electrostatic contribution to the phase. A second heating and cooling cycle was also conducted with magnetisation reversals at every temperature step to remove the temperature-dependent mean inner potential from the phase of the initial heating cycle. However, the alteration resulted in the second heating cycle not corresponding to the mean inner potential of the first heating cycle; holograms after heating to 600°C were not used. Instead the method employed by Almeida et al. (2014a), which removes the room-temperature electrostatic potential determined prior to heating was used to process the data.

Stability of non-uniform remanence structures has previously only been observed using temperature-dependent electron holography in synthetic magnetite (Almeida et al., 2016a), which is a mineral that is particularly important for terrestrial palaeomagnetism. Metallic iron is often the primary magnetic carrier in extraterrestrial lithologies; its thermal stability is of great importance with regards to recovering magnetic field information from the Solar Nebula or meteorite parent bodies.

Bishunpur chondrules have not been heated to temperatures greater than 300 to 350°C since accretion (Rambaldi, 1981). This is typical for the majority of un-equilibrated chondrites, and Semarkona, which experienced lower temperatures than Bishunpur since accretion (Sears et al., 1980). Semarkona dusty olivine was used in a palaeomagnetic investigation, in which the palaeointensity was estimated using the ARM normalisation method with a superconducting quantum interference device (SQUID) microscope and a nitrogen-vacancy (NV) quantum diamond microscope for high resolution magnetic measurements (10^{-15} Am²) (Fu et al., 2014b; Glenn et al., 2015; Lima and Weiss, 2016). Fu et al. (2014b) found the palaeointensity to be 54 ± 21 μ T, ruling out a number of theories for chondrule formation, which require

significantly stronger magnetic fields (e.g. electric current sheets and X-wind (Shu et al., 1996; Levy and Araki, 1989; McNally et al., 2013)). The palaeofield estimate suggests that planetesimal collisions or nebular shocks are likely to be the chondrule forming mechanisms early in the Solar System (Desch and Connolly, 2002; Wakita et al., 2017), and the estimate is being used widely constrain models for these processes and for early Solar System mass and momentum transport (Gressel et al., 2015; Bai et al., 2016). The finding in this chapter, that the magnetisation carried by these grains is thermally stable, suggests that the remanence carried by Semarkona dusty olivine is very likely to originate from the early Solar System.

The nudged elastic band (NEB) numerical algorithm (Berkov, 1998; Fabian and Shcherbakov, 2017) was applied to the micromagnetic model solutions of the heated kamacite at 300°C to determine the energy barrier between different magnetisation states, which can be related to temporal stability. The magnetisation structures were found to be stable for timescales far greater than that of the Universe ($> 10^8$ Ga). A more in-depth NEB algorithm micromagnetic study of metallic iron in uniform and non-uniform magnetisation structures is presented in the following chapter.

4.5 Conclusions

This chapter experimentally considers the credibility of chondrule dusty olivine kamacite as a recorder of magnetic fields from the early Solar System using the advanced transmission electron microscope (TEM) technique of off-axis electron holography (electron holography) and temperature-dependent electron holography with some complementary micromagnetic modelling.

The preparation of TEM samples from natural rocks is a time-consuming, costly, and error-prone process, as focused ion beam (FIB) milling is necessary. Six FIB lamellae were prepared from Bishunpur, an ordinary chondrite not heated to temperatures greater than 350°C since accretion. Two of the lamellae were prepared for room-temperature analysis, two prepared for temperature-dependent analysis, and

two did not contain any features of interest.

The room-temperature lamellae were chemically analysed with a scanning-TEM (STEM) using the energy dispersive X-ray spectroscopy technique (EDX) to produce elemental maps that indicate near-pure iron ($> 99\%$ Fe) kamacite encased in a forsteritic olivine matrix. Different chondrules had variable amounts of glassy phases associated with the kamacite, perhaps owing to slight heterogeneities in the chondrule forming environment where reduction and production of dusty olivine occurred.

All of the grains analysed with electron holography showed non-uniform magnetisation structures. This may owe to the large size of the grains analysed, however this is in itself representative of the grain size distribution in natural samples. Therefore, it is imperative to understand the behaviour of non-uniform magnetisation structures, which occupy such a large majority of the magnetic carriers in rocks. The magnetisations observed were typically single-vortex, with the vortex core aligned out-of-plane, and departures from single-vortex structure were typically due to anhedral grain morphology due to the FIB-milling process or non-magnetic inclusions (e.g. Cr_3O_2).

The temperature-dependent holography demonstrated the thermal stability of non-uniform magnetisation structures up to at least 500°C , as chemical alteration occurred at 600°C , contaminating the dataset at higher temperatures. This is higher than the temperatures experienced by Bishunpur or Semarkona, the meteorite used for palaeointensity estimation of the Solar Nebula, suggesting that the remanence carried by the dusty olivine in these meteorites is representative of the Solar Nebula.

Micromagnetic modelling of an iron grain meshed to the approximate dimensions of the heated kamacite grain confirms the experimentally determined magnetic induction map, and indicates that it is due to an in-plane vortex magnetisation. A nudged elastic band numerical algorithm implemented into a micromagnetic model with the solutions generated for the heated kamacite grain determined that the grain is capable of carrying a stable remanence for timescales many magnitudes greater

than the age of the Universe.

4.5.1 Acknowledgements and contributions

I conducted the room-temperature and temperature-dependent off-axis electron holography experiments. I analysed the room-temperature electron holography data, and Trevor P. Almeida helped to analyse the temperature-dependent electron holography data. Trevor P. Almeida and Andras Kovács assisted with electron holography experiments and analysis. I created the mesh for the high-temperature micromagnetic simulations of the large particle. Wyn Williams and Karl Fabian wrote the micromagnetic code MERRILL used for numerical analysis. Wyn Williams and Lesleis Nagy conducted the high-temperature micromagnetic simulations of the large Bishunpur kamacite grain. Wyn Williams helped with the analysis of the high-temperature micromagnetic simulations. Adrian R. Muxworthy had the original idea for the study and led the direction of the study. I wrote this chapter with the help of Adrian R. Muxworthy, Wyn Williams, Trevor P. Almeida, and Rafal E. Dunin-Borkowski.

I would like to thank Doris Meertens for FIB lamellae preparation. Meteorites were provided by the Natural History Museum, London. This work was funded by the STFC (grant number grant number ST/N000803/1). The research leading to these results has received funding from the European Research Council under the European Union's Seventh Framework Programme (FP7/2007-2013)/ ERC grant agreement number 320832.

Chapter 5

Micromagnetic modelling of dusty olivine

5.1 Introduction

The previous chapter analysed the magnetisation structures of kamacite grains found in Bishunpur chondrule dusty olivine, finding that non-uniform (pseudo-single domain) magnetisation structures, which are prominent in dusty olivine kamacite (Fig. 4.11), are capable of retaining magnetic remanence on Solar System timescales (Fig. 4.12, 4.15). With a numerical approach, this chapter focuses on the uniform (single domain) magnetisation to non-uniform magnetisation transition size. The stability of non-uniformly magnetised structures and uniformly magnetised structures is also calculated to more rigorously determine whether these ubiquitous non-uniform structures are capable of retaining remanent magnetisation from the early Solar System. It is important to determine the stability of these non-uniform magnetisation vortex and multi-vortex structures, as they have no underpinning theoretical framework, and are the states occupied by the majority of magnetic remanence carriers in rocks and meteorites (Robertson and France, 1994; Kruiver et al., 2001; Muxworthy and Williams, 2015).

Currently, the estimate of the magnetic field present in the chondrule forming

region of the protoplanetary disk 2 to 3 Myr after the first CAI is $54 \pm 21 \mu\text{T}$, and was obtained from dusty olivine kamacite (Fu et al., 2014b). This estimate suggests that magnetic fields have a significant role in accreting planetary systems, and is being widely incorporated into models to constrain early Solar System conditions for chondrule formation, accretion, and momentum transport. Therefore, it is necessary to determine whether the vortex magnetisation structures that are so abundant in dusty olivine are capable of carrying a stable remanence for Solar System timescales (i.e. 4.6 billion years). Previous studies by Uehara and Nakamura (2006) and Lappe et al. (2011) hailed synthetic dusty olivine grains for their low-maximum metamorphic temperatures (250 to 350°C) and encasing olivine protecting from alteration. Uehara and Nakamura (2006) also considered the relaxation time for single-domain dusty olivine kamacite, finding that it is capable of preserving remanence. However, as these calculations were achieved using Néel's single domain theory (Néel, 1949), they are only applicable to single domain grains.

Typically iron oxides such as magnetite receive the most attention owing to their abundance in terrestrial lithologies. The analytical calculations of the uniform to non-uniform size threshold for various axial ratios of magnetite ellipsoids made by Evans and McElhinny (1969) (based on the methods of Morrish and Yu (1955)) crucially indicated that rocks do contain grains of the uniform size range when considering elongation increases the size threshold. As a result, the observed stable high-coercivity thermoremanence in igneous rocks found by Stacey (1967), Dunlop (1968) and Strangway et al. (1968) was thought to be due to the presence of uniformly magnetised magnetite, dispelling initial concerns that the grain sizes of natural rocks are too large to be uniformly magnetised (Néel, 1955b; Stacey, 1963).

In order to explain the experimental palaeomagnetic observations of rocks, micro-magnetic researchers have endeavoured to define the critical single-domain (referred to in this thesis as uniform magnetisation), size threshold, and the switching field necessary to reverse the magnetisation of these grains, e.g., Morrish and Yu (1955), Evans and McElhinny (1969), Schabes and Bertram (1988), Williams and Dunlop

(1989), Winklhofer et al. (1997), Gatel et al. (2015), and Muxworthy and Williams (2015). Recent studies have supplemented and supported micromagnetic observations with experimental electron holography observations to confirm the structures that are numerically determined, for example the domain state transitions for iron nanocubes of increasing size observed in both electron holography and micromagnetic models (Fig. 5.1) (Gatel et al., 2015). The combination of electron holography and micromagnetic modelling is becoming a standard procedure in the field of nanomagnetism (e.g. Einsle et al. (2016)), hence the complementary micromagnetic study in the previous chapter (see Section 4.3.3) and the micromagnetic analysis of metallic iron in this chapter. However, there is now much evidence that the dominant remanence carriers in natural systems are non-uniformly magnetised.

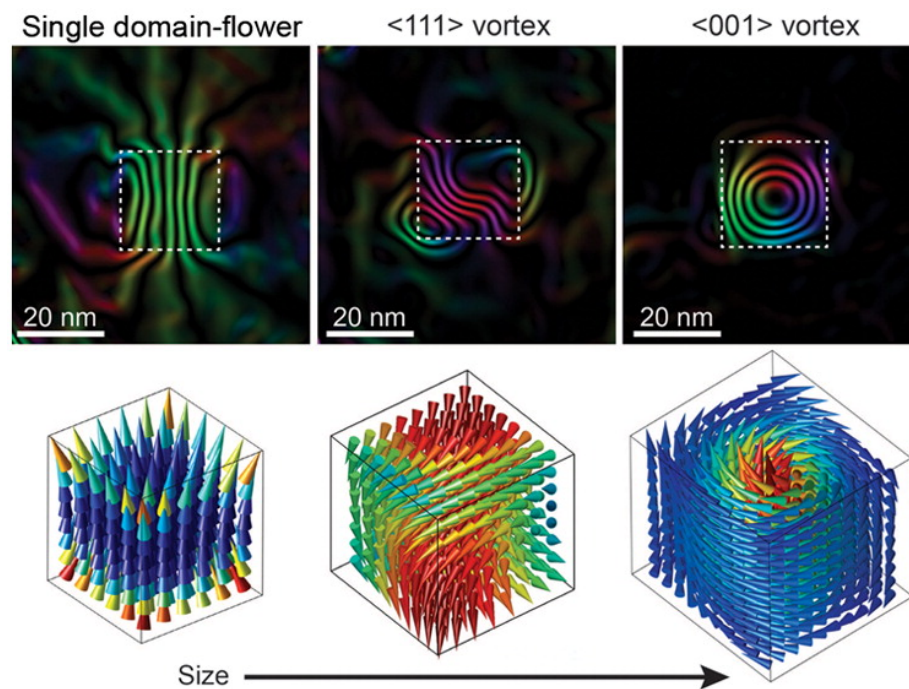


Figure 5.1: Room-temperature magnetic induction maps and micromagnetic solutions of 25, 26 and 27 nm iron nanocubes displaying the transition between easy-axis uniform magnetisation, hard-axis vortex magnetisation and easy-axis vortex magnetisation structures. From Gatel et al. (2015).

The abundance of metallic iron in lunar rocks instilled the motivation to analytically determine the superparamagnetic (SP) to uniform and uniform to non-uniform grain size boundaries for iron for the first time (Butler and Banerjee, 1975). Analysis of the domain state transitions in iron showed that there is a range for uniform mag-

netisation of spherical grains, and stability in the uniform state was only observed for prolate ellipsoids of 1.67 axial ratio between 15 and 35 nm. This supported the apparent low uniformly magnetised grain content observed in lunar samples (Fuller, 1974; Butler and Banerjee, 1975).

The analytical calculations of Butler and Banerjee (1975) were the primary reference point for iron domain state and stability (Lappe et al., 2011; Gattacceca et al., 2014) until estimates were recently improved by a robust micromagnetic determination (Muxworthy and Williams, 2015). The domain state transitions were determined using a finite difference model and a combination of a conjugate gradient algorithm (Williams and Dunlop, 1989) to generate an initial energy-minimised magnetic structure and a dynamic algorithm that solves the Landau-Lifschitz-Gilbert equation (Suess et al., 2002) to determine the local energy minimum (LEM) states for parallelepipeds of a range of sizes and axial ratios (Fig. 5.2) (Muxworthy and Williams, 2015). The redefined domain state transitions by Muxworthy and Williams (2015) agree with experimental observations (Snoeck et al., 2008; Lappe et al., 2011), are larger than those found previously by Butler and Banerjee (1975). The boundaries are sensitive to the material constants assigned; accurate experimental determination of material parameters is crucial to model the magnetic properties of materials.

In the previous chapter a nudged elastic band (NEB) numerical algorithm was implemented into a finite element method (FEM) micromagnetic algorithm to determine the energy barrier for the 458 x 98 x 60 nm multi-vortex low-Ni kamacite grain for the first time, finding that the multi-vortex structure is capable of retaining remanence for many magnitudes longer than the age of the Universe. Further rigorous testing of whether non-uniformly magnetised grains can retain remanence over Solar System timescales is required. In this chapter, the local energy minimum (LEM) magnetisation states are determined for iron parallelepipeds to define the uniform to non-uniform magnetisation size threshold, and an NEB numerical algorithm implemented to determine the stability of these LEM states, and to better characterise

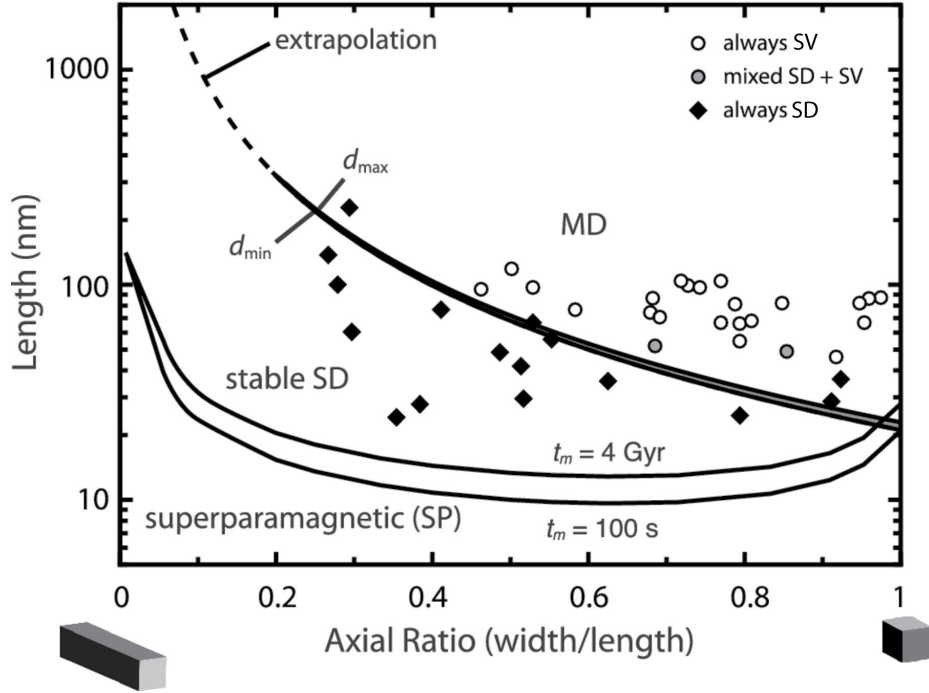


Figure 5.2: The domain state phase diagram for parallelepipeds of metallic iron modelled at various axial ratios using the finite difference method from Muxworthy and Williams (2015). Points plotted on the graph are experimental observations made by electron holography of synthetic dusty olivine kamacite from Lappe et al. (2011), agreeing well with the model for states in single-domain (SD), mixed SD and single-vortex (SV), and always in SV.

our understanding of non-uniform magnetisation stability and switching.

5.2 Methods

Magnetic domain states are grain size dependent: at very small grain sizes, grains are typically uniformly magnetised, and at larger grain sizes, a non-uniform structure is the most energetically favourable state (Schabes and Bertram, 1988; Muxworthy and Williams, 2015). The structures associated with various grain sizes and elongations of iron parallelepipeds were determined by finite element method (FEM) micromagnetic simulation to determine the uniform to non-uniform domain structure transition sizes. Tetrahedral meshes were produced for this using MESHRRILL, a command-line-based meshing software developed by Pádraig Ó Conbhuí at the University of Edinburgh, and FEM models were performed using MERRILL (Conbhuí et al., in prep). The magnetic free energy was determined for each of the tetrahedra and summed over all to determine E_{tot} , which the FEM discretised for the

minimization of an initial state, \mathbf{m} , where the magnetization at each node of each element was given a random direction (m_x, m_y, m_z) , for the particle of volume V in question, Ω ,

$$E_{tot} = \int_{\Omega} [A|\nabla\mathbf{m}| + K_1[m_x^2m_y^2 + m_x^2m_z^2 + m_y^2m_z^2] - M_s[\mathbf{H}_z \cdot \mathbf{m}] - \frac{M_s}{2}[\mathbf{H}_d \cdot \mathbf{m}]] dV \quad (5.1)$$

where the material can be defined by the temperature-dependent parameters: A , the exchange constant; K_1 , magnetocrystalline anisotropy; and M_s , saturation magnetisation. H_z and H_d are the external and self-demagnetising fields respectively. The first term in equation 5.1, $\int_{\Omega} A|\nabla\mathbf{m}| dV$, calculates the exchange energy over the volume of the particle. The second term, $\int_{\Omega} K_1[m_x^2m_y^2 + m_x^2m_z^2 + m_y^2m_z^2] dV$, calculates the magnetic anisotropy energy over the volume of the particle. The fourth term, $\int_{\Omega} M_s[\mathbf{H}_z \cdot \mathbf{m}] dV$, calculates the interaction energy between the magnetisation and the external field. The fifth term, $\int_{\Omega} \frac{M_s}{2}[\mathbf{H}_d \cdot \mathbf{m}] dV$, calculates the energy of the self-demagnetising field. The material parameter constants used in this study are for room-temperature iron (Muxworthy and Williams, 2015): $A = 2 \times 10^{-11} Jm^{-1}$, $K_1 = 4.8 \times 10^4 Jm^{-3}$, and $M_s = 1.72 \times 10^6 Am^{-1}$. External fields were set to zero for all energy minimisations.

Local energy minimum (LEM) magnetisation structures were found by minimizing E_{tot} using a modified-conjugate gradient method (Fabian and Shcherbakov, 2017). For each shape and size for which the relaxation time was evaluated, 100 minimisations were performed to observe the most favourable LEM states. Two different magnetisation structures of the lowest energy were then selected to be used as the initial and final points, for which the NEB method was used to determine the energy barrier (Fabian and Shcherbakov, 2017). For non-uniform vortex states, two LEM states with the same sense of vortex-core rotation were selected, as unwinding of the core is energetically unlikely (Nagy et al., 2017). The NEB method first determines a path between the two initial states, and then minimizes energy along the path to determine a least energy transition between LEM states for the grain. The energy required for this transition can be related to relaxation time by

the Néel-Arrhenius equation (Néel, 1949):

$$\tau = \frac{1}{C} e^{\frac{\Delta E}{k_B T}} \quad (5.2)$$

where C is the atomic switching frequency ($10^{-9}s$), k_B is Boltzmann's constant, T is the temperature, and E is the energy barrier determined by the NEB method. The relaxation time is directly related to the stability of the magnetisation state, and thus, whether dusty olivine can theoretically be stable over Solar System timescales.

Micromagnetic modelling was conducted on an iMac (27-inch, Late 2013) with a 3.2 GHz Intel Core i5 and 16 GB 1600 MHz DDR3 RAM at Imperial College London. The modelling of the much larger grain, meshed from the temperature-dependent holography experiment discussed in the previous chapter, was conducted at the University of Edinburgh by Professor Wyn Williams using the ARCHER (www.archer.ac.uk) high-performance computing (HPC) facility.

5.3 Results

5.3.1 Local energy minima for iron

I determined the global energy minimum (GEM) states for iron parallelepipeds of axial ratio 1, 1.1, 1.2, 1.5 and 1.7, with 1 nm resolution across domain state transitions, and up to 50 nm total, by performing 100 energy minimisations per morphology by finite element method micromagnetic models and finding the least energy local energy minimum magnetisation state. The maximum size of 50 nm was typically due to computational limitation.

Iron nanocubes

For the smaller grain sizes, i.e. < 23 nm, the GEM states display uniform magnetic structures aligned with the easy magnetocrystalline axis for the equant grains with 'flowering' (Schabes and Bertram, 1988; Williams and Dunlop, 1989) at the grain

edges (Fig. 5.3a). As the grain sizes increase towards 23 nm, there is increased flowering (Fig. 5.3a). Above 23 nm for equant Fe particles, vortex structures with cores aligned along the hard magnetocrystalline axis [111] are the GEM state (Fig. 5.3b, Table 5.1), agreeing with the holography observations and modelling of Gatel et al. (2015) and the recent findings of Bonilla et al. (2017). Above 27 nm, the GEM state is a single-vortex with its core aligned with the easy magnetocrystalline axis (Fig. 5.3c, Table 5.1).

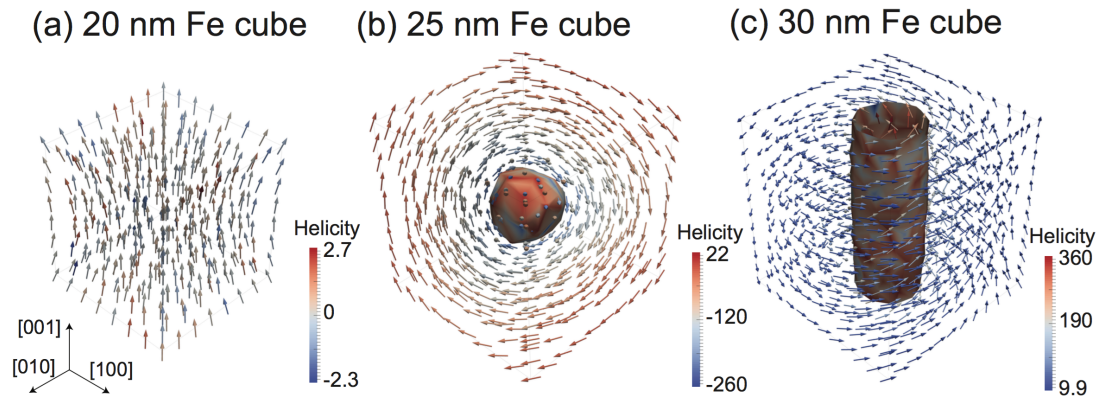


Figure 5.3: Global energy minimum (GEM) magnetization states for cubes of iron determined by finite element method (FEM) micromagnetic algorithm. (a) 20 nm cube in uniform magnetization structure through the easy-axis, (b) 25 nm cube in non-uniform hard-axis magnetization structure, and (c) 30 nm cube in non-uniform easy-axis magnetization structure.

Elongated iron parallelepipeds

Parallelepiped sizes are related to their cube face-length volume equivalent (i.e. a 25 nm parallelepiped of axial ratio 1.5 has the equivalent volume of a cube with faces of 25 nm length). Flower states along the long-magnetocrystalline-easy-axis are the LEM states for elongated parallelepipeds up to 25 nm, 26 nm, 30 nm, and 34 nm for axial ratios of 1.1, 1.2, 1.5, and 1.7 respectively (Table 5.1). Magnetisation structures display increased flowering as grain volume increases as seen with equant grains (Fig. 5.4a). The long-axis magnetisation structures approaching the transition to vortex magnetisation exhibit slight vorticity along the long-axis (Fig. 5.5), referred to hereafter as the ‘twisted flower’ structure (Table 5.1, (Fig. 5.5)). The hard-axis vortex is only seen as a GEM state in parallelepipeds of 1.1 AR of 25 nm size, above which the GEM state is a single-vortex through the short-magnetocrystalline-

easy-axis (Table 5.1, (Fig. 5.4b)). The vortex core alignment with the short-axis is consistent with the out-of-plane vortex cores in the electron holography observations Fig. 4.11; as the kamacite particles embedded in the lamella are thinned to electron transparency, the short axis is out-of-plane.

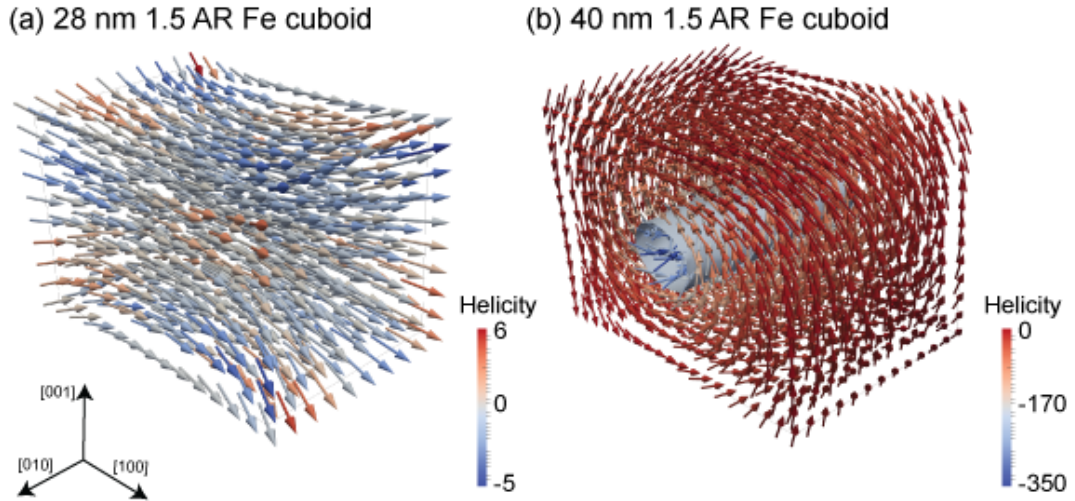


Figure 5.4: Global energy minimum (GEM) magnetization states for parallelepipeds of iron elongated to 1.5 axial ratio determined by finite element method (FEM) micromagnetic algorithm. Sizes relate to the volume of a cube with equivalent face-length. (a) 28 nm cuboid in uniform (flower) magnetization structure through the long-axis, (b) 40 nm cuboid in single-vortex magnetisation through the short-axis.

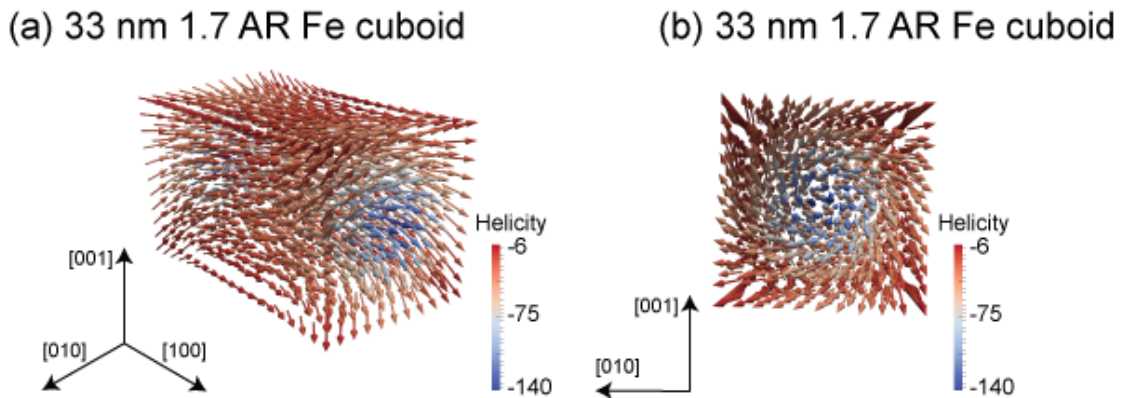


Figure 5.5: Global energy minimum (GEM) magnetisation state for a 33 nm parallelepiped of iron elongated to 1.7 axial ratio in determined by finite element method (FEM) micromagnetic algorithm in (a) three-axis view and (b) view along the [010] long-axis. Size relates to the volume of a cube with 33 nm face-length. There is slight vorticity along the long-axis, but a distinct vortex-core is not formed; this is referred to as the 'twisted flower' state that exists in the size range between the flower state and the easy-axis vortex state.

Table 5.1: A table of the relaxation times (in years), (τ), and global energy minima (GEM) for parallelepipeds of iron of varying size and axial ratio (AR) numerically determined using a finite element method (FEM) numerical algorithm and a nudged elastic band (NEB) numerical algorithm. ‘*F*’ refers to the flower state, ‘*TF*’ refers to the twisted flower state, ‘*SV(H)*’ refers to the single-vortex state through the hard-axis [111], ‘*SV(E)*’ refers to the single-vortex state through the easy-axis [100]. ‘...’ indicates that a path between LEM states was not calculated.

Size	τ 1.0AR (yr)	LEM 1.0AR	τ 1.1AR (yr)	LEM 1.1 AR	τ 1.2AR (yr)	LEM 1.2AR	τ 1.5AR (yr)	LEM 1.5AR	τ 1.7AR (yr)	LEM 1.7AR
10	1.7E-15	F	1.0E-10	F	1.1E-07	F	1.8E+08	F	2.2E+14	F
11	3.5E-14	F	2.8E-10	F	6.8E-03	F	1.2E+16	F	3.1E+26	F
12	9.5E-14	F	6.2E-06	F	6.0E+04	F	4.2E+25	F	4.5E+38	F
13	5.2E-12	F	4.6E-05	F	7.3E+10	F	2.5E+40	F	1.4E+55	F
14	1.0E-10	F	2.0E+01	F	5.9E+14	F	5.3E+54	F	2.5E+73	F
15	5.7E-09	F	4.5E+05	F	2.9E+23	F	7.7E+66	F	2.4E+93	F
16	1.1E-07	F	3.6E+09	F	2.1E+34	F	7.3E+86	F	...	F
17	4.6E-05	F	2.4E+17	F	F	...	F
18	2.7E+00	F	2.9E+23	F	3.6E+52	F	...	F	...	F
19	1.1E+03	F	1.7E+28	F	1.4E+65	F	...	F	...	F
20	6.0E+04	F	2.3E+37	F	3.7E+75	F	4.4E+167	F	4.8E+213	F
21	1.4E-13	F	3.0E+46	F	5.0E+74	F	...	F	...	F
22	1.9E-12	F	2.3E+37	F	1.4E+65	F	...	F	...	F
23	9.5E-14	SV(H)	1.1E+23	F	1.8E+51	F	...	F	1.7E+233	F
24	1.9E-12	SV(H)	5.5E+01	F	1.4E+32	F	...	F	...	F
25	1.0E-10	SV(H)	3.8E-11	SV(H)	1.1E+03	TF	1.1E+132	F	3.9E+217	F
26	2.8E-10	SV(H)	1.2E-04	SV(E)	1.2E+06	SV(E)	...	F	...	F
27	1.2E-04	SV(E)	1.6E+05	SV(E)	2.4E+17	SV(E)	6.6E+126	F	...	F
28	1.2E+06	SV(E)	5.9E+14	SV(E)	8.5E+26	SV(E)	1.9E+97	F	9.7E+171	F
29	2.4E+17	SV(E)	1.6E+25	SV(E)	4.1E+35	SV(E)	6.2E+70	F	...	F
30	4.2E+25	SV(E)	2.3E+37	SV(E)	2.2E+47	SV(E)	3.9E+55	SV(E)	2.0E+120	F
31	2.3E+37	SV(E)	6.0E+47	SV(E)	1.1E+56	SV(E)	5.0E+74	SV(E)	...	F
32	8.1E+46	SV(E)	3.2E+59	SV(E)	8.4E+69	SV(E)	1.3E+85	SV(E)	1.1E+79	TF
33	2.9E+56	SV(E)	3.4E+72	SV(E)	9.0E+82	SV(E)	...	SV(E)	1.5E+121	TF
35	2.8E+76	SV(E)	1.2E+92	SV(E)	1.3E+105	SV(E)	7.5E+152	SV(E)	4.0E+121	SV(E)
40	1.0E+142	SV(E)	6.2E+189	SV(E)	5.2E+216	SV(E)	1.5E+197	SV(E)	4.4E+167	SV(E)
50	...	SV(E)	...	SV(E)	3.90E+293	SV(E)	4.6E+342	SV(E)	1.2E+287	SV(E)

5.3.2 Nudged elastic band modelling iron

Using the NEB algorithm I next determined the transition paths and energy barriers associated with switching between the LEM states of least energy (global energy minimum (GEM)) (Fig. 5.6) to determine their stability on Solar System timescales (Table 5.1, Fig. 5.7).

Structure coherent rotation

The transition paths between non-uniform vortex LEM states were found to be ‘structure coherent rotations’ of the vortex-core from LEM state to another (Fig. 5.6), agreeing with observations of magnetite vortex-core switching (Nagy et al. 2017). Although the individual moments do not rotate coherently, the rotation of the vortex-core itself is similar to the coherent rotation of magnetization vectors observed in uniform LEM states.

Iron nanocubes

The transition energy barriers between uniform states are very low for equant Fe particles ((Table 5.1, Fig. 5.3a, Fig. 5.7)). Equant grains < 29 nm are essentially

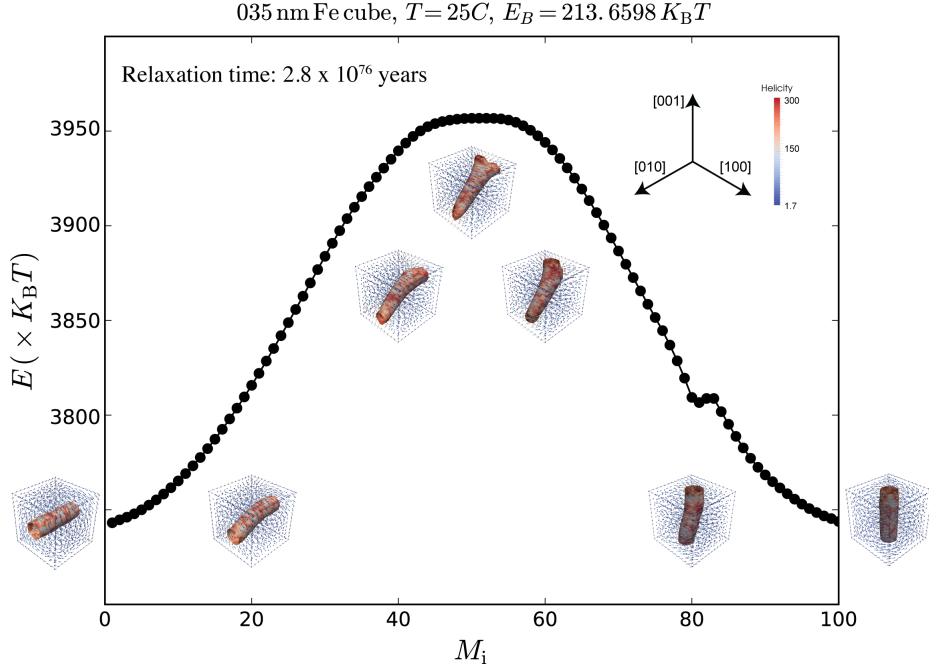


Figure 5.6: A plot of the energy along the path between two global energy minimum (GEM) magnetisation states for a 35nm sized Fe cube determined by a nudged elastic band (NEB) numerical algorithm within a micromagnetic algorithm. The initial and final states of magnetisation are single-vortexes through [010] and [001] respectively, and inset are the calculated magnetisation structures along the path (M_i) demonstrating the structure coherent rotation of the vortex core at $M_i = 1, 20, 40, 50, 60, 80, 100$. The rotation of the vortex core is analogous to that of a uniformly magnetised grain.

unstable on Solar System timescales, that is, flower states in equant grains are unstable at this timescale, and it is only the vortex states with their core aligned along the easy-axis that are capable of retaining magnetisations on Solar System timescales. We find that the vortex-core aligned along the easy magnetocrystalline axis is stable for all equant cubes with grain sizes > 29 nm up to at least 50 nm, the largest grain size modelled (Table 5.1).

Iron parallelepipeds

Elongating the grain increases the uniform to non-uniform transition size as expected (Muxworthy and Williams, 2015), and increases the stability of the magnetization state ((Table 5.1, Fig. 5.7)). Slight elongation to 1.1 AR results in uniform-LEM being stable on Solar System timescales for grain sizes 16 nm to 23 nm (cube volume equivalent). An increase in size of the 1.1 AR cuboid to 24 nm introduces slight vorticity aligned with the long-axis; this twisted flower (Nagy et al., 2017) state

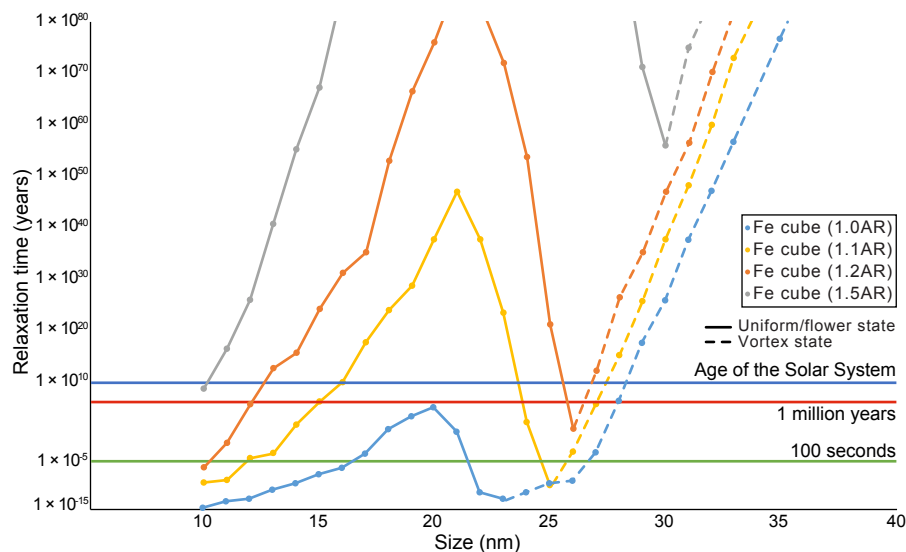


Figure 5.7: A graph displaying the relaxation time (i.e. stability) for a range of axial ratios (AR) and sizes of iron cuboids determined by the nudged elastic band (NEB) method for global energy minimum (GEM) magnetization states determined by finite element method (FEM) numerical algorithm. Size relates to the volume of the equivalent diameter cube (e.g. the volume of the 20 nm cuboid with either 1.1, 1.2, or 1.5 axial ratio is equivalent to the volume of a 20 nm cube). The green line marks 100 seconds of stability, and the blue line marks the age of the Solar System. The solid line indicates that the LEM state is uniform magnetization, and the development of flowering and vorticity results in a reduction in stability. The increase in stability marks the grain magnetization assuming a non-uniform vortex structure (dashed line) through $\langle 100 \rangle$, which increases in stability with increasing grain size. Chondrule dusty olivine kamacite has been observed to be approximately 1.5 in axial ratio, which is observed to be stable over Solar System timescales irrespective of magnetization structure for all sizes tested (10 to 60 nm).

(e.g. Fig. 5.5) is stable for 55 years. For 25 nm, the LEM is an unstable vortex-core aligned with the hard magnetocrystalline axis (e.g. Fig. 5.3b). A further increase in size to 26 nm sees the GEM transition to non-uniform magnetization with a vortex core aligned along the easy magnetocrystalline axis (e.g. Fig. 5.4a), this LEM state is stable for just an hour ((Table 5.1, Fig. 5.7)).

Elongation of the grain increases the stability of the magnetization state and increases the uniform to non-uniform transition size (Table 5.1, Fig. 5.7). Uniform magnetization states increase in energy barrier with increasing size, whereby a flowering of the magnetization vectors at the grain edges further increases the structural stability up to a peak close to 20 nm (Table 5.1, Fig. 5.7). Beyond this peak a vortex is formed during the magnetization reversal, which leads to an intermediate decrease in the energy barrier with increasing grain size (Winklhofer et al., 1997) up to a trough at 25-35 nm (Fig. 5.7). For larger grain sizes, the easy axis vortex state is the LEM, increasing in stability with increasing grain size (Table 5.1, Fig. 5.7).

Typically, low-Ni kamacite particles found in chondrules have AR values of 1.5

(Einsle et al., 2016). Such elongations carry stable magnetization for all grain sizes modelled (10 to 50 nm), whether in a uniform or non-uniform state (Table 5.1, Fig. 5.4, Fig. 5.7).

5.4 Discussion

The local energy minima magnetisation states and their stability were tested in this chapter for a comprehensive distribution of iron parallelepipeds (Table 5.1). The transition between uniform magnetisation state and non-uniform (typically single-vortex e.g. (Fig. 5.6) state was modelled at 1 nm resolution. The vortex state, which is typical for dusty olivine kamacite as observed in the holography (Fig. 4.11) was modelled for its stability using the NEB algorithm (Table 5.1, Fig. 5.7), by determining the energy barriers at room-temperature; the lower temperatures experienced in space would almost certainly increase the calculated stability. The energy barrier determination for the heated grain in Chapter 4.3.3 suggests that multi-vortex magnetisation structures are stable ($\tau > 10^8$ Ga at least). Therefore, the NEB modelling strongly indicates that remanence imparted during dusty olivine formation in the Solar Nebula would remain stable to the present day (Table 5.1, Fig. 5.7). However, current palaeointensity protocols and the palaeointensity estimation made by Fu et al. (2014b) assume that grains contain uniform magnetic structures, as the protocols employed are based on Néel's theory of uniform magnetic states (Néel, 1949). The evidence in this chapter and the previous chapter shows that most of the remanence in dusty olivines will be carried by single- or multi-vortex magnetic states. The thermal and temporal stability of non-uniform magnetization structures is poorly understood, and until this study and that of Nagy et al. (2017) they were considered to be poor magnetic recorders. Therefore, whilst it is correct to say that Semarkona retains a Solar Nebular field, palaeofield estimates are open to debate (Fu et al., 2014b). It is now clear that accurate palaeointensities estimated from meteorites, and thus a more detailed understanding of early Solar System

conditions, can only be obtained with a more comprehensive understanding of the thermomagnetic characteristics of vortex states.

5.4.1 Uniform magnetisation

It has been known since the 1970s that iron has a low uniform to non-uniform magnetisation threshold size (Butler and Banerjee, 1975), and found here to be between 22 and 35 nm depending on elongation, compared to approximately > 64 nm for magnetite (e.g., Muxworthy and Williams 2006). For magnetite, it is believed that approximately 20% of the grains in natural rock samples such as volcanics are in the uniform magnetisation size range (Robertson and France, 1994; Krüver et al., 2001). It is therefore likely that an even smaller fraction of dusty olivine remanence carrying kamacite is in uniform magnetisation state, given that the average size of dusty olivine kamacite was found to be $353 \pm 147 \times 250 \pm 110$ nm (thickness ranges from 60 to 200 nm) in this study, and $242 \pm 94 \times 199 \pm 80 \times 123 \pm 58$ nm found by Einsle et al. (2016). An average axial ratio of 1.5 for dusty olivine kamacite was observed in Bishunpur in the previous chapter, and by Einsle et al. (2016) in Semarkona. No magnetisation state was found to be truly uniform in the experimental electron holography analysis in the previous chapter (Chapter 4.3.3), and the observations of Semarkona dusty olivine by Einsle et al. (2016). While uniformly magnetised grains at 1.5 axial ratio are stable for Solar System timescales (Table 5.1, Fig. 5.7) the maximum size threshold for them is 33 nm; it is unlikely that uniformly magnetised grains are abundant in dusty olivine. Uehara and Nakamura (2006) stated that only single-domain (i.e. uniformly magnetised) dusty olivine kamacite grains with blocking temperature above 490°C can retain remanence from the early Solar System. The uniformly magnetised kamacite grains reported by Lappe et al. (2011) in synthetic dusty olivine could be a result of to the difference between the synthetic and natural formation processes, or in-plane vortex structures as seen in Chapter 4.3.3, that are interpreted as uniform magnetisation structures; micromagnetic modelling to supplement holography observations

is now becoming standard procedure (Gatel et al., 2015; Muxworthy and Williams, 2015; Einsle et al., 2016). These uniform magnetisation observations and the high-unblocking temperatures of uniformly magnetised kamacite analytically determined by Garrick-Bethell and Weiss (2010) were the bases of and justification for Fu et al. (2014b)'s assumption that Semarkona bears uniformly magnetised kamacite in its dusty olivine grains that carry early Solar System remanence.

It has become increasingly clear that uniformly magnetised grains are, although well understood and stable carriers of remanence (in elongated grains, Fig. 5.7), too small to be abundant in meteoritic dusty olivine.

5.4.2 Non-uniform magnetisation

The non-uniformly magnetised 'single-vortex' state appears to be the most abundant magnetisation state for the kamacite grains in dusty olivine (Figure 4.11). The understanding of the thermomagnetic behaviour of single-vortex states is poor, however, and they have until the temperature-dependent holography studies of Almeida et al. (2016a) and the micromagnetic NEB models of Nagy et al. (2017) been assumed to be unstable and poor recorders of magnetic remanence compared to SD grains (Levi, 1977). The results of the NEB calculations here for iron indicate that larger single-vortex magnetisation structures are in fact more stable than their smaller volume uniform magnetisation counterparts (Fig 5.7). The stability of single-vortex magnetisation structures increases with increasing grain size (Fig. 5.7), and experimental evidence of large kamacite grains maintaining a single-vortex structure (rather than splitting into multi-vortexes) up to 600 nm grain size (Fig. 4.11f) suggests that the majority of euhedral dusty olivine kamacite grains are likely to be in single-vortex structure; departures from euhedral grain morphology (and the single-vortex state) have been observed to be typically due to chemical impurities and reshaping grains during sample preparation (Fig. 4.11b,j). It is likely that the single-vortex to multi-vortex transition occurs at a larger grain size for iron than that observed for magnetite (Nagy et al., 2017) due to iron's

much larger saturation magnetisation compared to the anisotropy and exchange constants; the system for iron is simpler than that of magnetite. More complex multi-vortex structures may be assumed to be unstable, however, NEB calculations for the multi-vortex structure of the grain presented in Figure 4.12 in Chapter 4.3.3 indicate that it is stable for timescales greater than the age of the Universe, and the temperature-dependent hysteresis displays its thermomagnetic stability.

The only non-uniform state that does not demonstrate stability is the single-vortex through the magnetocrystalline hard-axis $[111]$ observed in cubes (23 to 26 nm) and 1.1 AR parallelepipeds (25 nm) (Table 5.1, Fig. 5.3b). This LEM state has been previously observed in models and experimentally (Fig. 5.1) (Gatel et al., 2015; Bonilla et al., 2017), and found here through NEB calculations to be unstable. Bonilla et al. (2017) observed this state in cubes and elongated parallelepipeds up to 1.2 AR. Here, it was only observed in a narrow grain size range between the LEM being uniform and the LEM being an easy-axis single-vortex (Table 5.1). At the grain sizes that this state occurs in, the energy surface is flat, i.e., the available LEM states have similar energies, so only a small amount of energy is required to switch states, leading to instability.

Structure coherent rotation

The magnetic coupling required to the bulk magnetic system to facilitate a structure coherent rotation may result in the high energy barriers observed for single- and multi-vortex states. The path transition from one LEM to another cannot transition through intermediate minima due to the coherent vortex-core structure, so it is likely that the energy barrier must be larger for such transitions. The coherence of the vortex-core structure, which is maintained throughout the magnetisation state transitions as determined by the NEB method (Fig. 5.6), is why transitions require large energies, and why vortex states are stable.

5.4.3 Dusty olivine as a credible recorder of pre-accretionary remanence

As stated in the above sections, the bulk remanence carried by dusty olivine is largely by non-uniformly magnetised grains. These grains are capable of carrying stable magnetisations for timescales far in excess of the age of the Universe, let alone the age of the Solar System (Table 5.1, Fig. 5.7). A detailed understanding of the thermomagnetic behaviour of non-uniform magnetisation structures is still lacking, however. An exhaustive investigation into the acquisition and demagnetisation mechanics of thermoremanence by non-uniform magnetisation structures is required, as well as investigation into effects such as shock and chemical alteration, e.g., the effects of oxidation on single-vortex magnetite grains has been seen to alter the directional and intensity information stored (Almeida et al., 2014b). Understanding acquisition and demagnetisation of remanence would help to potentially develop a palaeointensity estimation protocol that fully incorporates, and ideally isolates single-vortex magnetisation for accurate palaeofield determination; current palaeointensity protocols, e.g., Thellier-Thellier, REM, and Preisach, typically assume an assemblage of uniformly magnetised SD grains (Thellier, 1959; Coe, 1967; Gattacceca and Rochette, 2004; Muxworthy and Heslop, 2011). For example, a comparison study of non-heating palaeointensity estimation protocols found that the Preisach method (Muxworthy and Heslop, 2011), which was otherwise found to be the most accurate non-heating method, fails to accurately model samples dominated by single-vortex grains, as they are not incorporated into the input Preisach distribution, and acquisition of thermoremanence is not accurately modelled by the single-domain thermal relaxation theory that forms the basis of palaeointensity estimation protocols (Néel, 1949; Lappe et al., 2013).

5.4.4 Implications for protoplanetary disk magnetic fields

While it is now certain that dusty olivine carries pre-accretionary remanence, the estimation made recently by Fu et al. (2014b) should be approached with caution until a robust estimation protocol that fully incorporates thermoremanence acquisition by single-vortex grains is developed and applied to dusty olivine. The estimation, $54 \pm 21 \mu\text{T}$ was published with large error to account for the 40% uncertainty of the ARM (anhysteretic remanent magnetisation) estimation protocol observed in the non-heating palaeointensity protocol calibration study on synthetic dusty olivine samples by Lappe et al. (2013). Depending on whether the chondrules were precessing as they were rotating and cooling through the Curie Temperature, estimates ranging from $27 \pm 8 \mu\text{T}$ to $108 \pm 42 \mu\text{T}$ are also given. Although the error associated with the natural grain assemblage being unrepresentative of the model assemblage may be understated, the estimate is significantly weaker than the remanence that would have been recorded had magnetic reconnection flares and current sheets (Levy and Araki, 1989) been the chondrule forming mechanism in the protoplanetary disk ($> 500 \mu\text{T}$). However, the X-wind model (Shu et al., 1997) is associated with magnetic fields of 80 to 400 μT in the chondrule forming region, which although stronger than the estimate, cannot be completely ruled out from a palaeomagnetic perspective. The X-wind theory has many inconsistencies, however, and is considered unlikely to have been a chondrule forming mechanism (Desch et al., 2010).

The nebular shock or planetesimal collision mechanisms of chondrule formation are currently the prominent theories for chondrule formation (Desch and Connolly, 2002; Mann et al., 2016; Johnson et al., 2015; Wakita et al., 2017). These mechanisms are typically associated with magnetic fields $< 100 \mu\text{T}$, and a recent experiment successfully formed chondrules bearing dusty olivine, with conditions fulfilled by shock heating (Imae and Isobe, 2017). The exact magnitude of the nebular field estimated by Fu et al. (2014b) from six dusty olivine grains is being implemented into models for chondrule formation, accretion, and momentum transport mechanisms

of the early Solar System (Gressel et al., 2015; Bai et al., 2016; Matsumoto et al., 2017; Wakita et al., 2017). The chondrule formation theories are supported by both experimental evidence and predicted magnetic field conditions (Fu et al., 2014b; Johnson et al., 2015; Wakita et al., 2017). However, uncertainty in the palaeointensity estimation due to an inaccurately modelled grain assemblage (assuming uniform magnetisation rather than non-uniform) would introduce error into the models of these momentum transport dynamics, e.g., degree of magnetorotational instability (MRI) compared to streaming instability to drive early accretion could be over or underestimated. More estimations, and estimations that incorporate single-vortex magnetisation are essential to accurately constrain the magnetic fields present in the protoplanetary disk.

5.5 Conclusions

This chapter follows the experimental analysis of meteoritic dusty olivine in the previous chapter to numerically determine the magnetic recording fidelity of the kamacite grains within dusty olivine. A finite element method (FEM) micromagnetic algorithm was used to determine the local energy minimum (LEM) magnetisation states (i.e. the magnetisation states expected to be naturally occurring) for a range of iron parallelepipeds through the transition between uniform and non-uniform magnetisation behaviours. LEM determinations were made for cubes and parallelepipeds from 10 to 50 nm in size, and at 1 nm resolution across the transition boundary (Table 5.1, Fig. 5.3). This is the first determination of the uniform to non-uniform transition for iron with the FEM micromagnetic algorithm, using a newly modified conjugate gradient algorithm for energy minimisation (Fabian and Shcherbakov, 2017). The ‘uniform’ magnetisation state is observed to always be in a flower state (Fig. 5.3a). As grain volumes approach the uniform to non-uniform transition, the flower state becomes ‘twisted’, and there is minor vorticity through the core along the long-axis, in what is named the ‘twisted flower’ state (Fig. 5.5).

Above the uniform magnetisation threshold, a transitory hard-axis vortex state is an LEM for near equant iron cubes approximately 23 to 25 nm in size (Fig. 5.3b). Above this size, and for the largest grain volumes tested, magnetisation is in a single-vortex state through the magnetocrystalline easy-axis, and short-axis for elongated parallelepipeds, consistent with the electron holography observations reported in the previous chapter.

For the range of parallelepiped elongations tested (1.0 to 1.7), the uniform to non-uniform transition is 22 to 35 nm. The transition for iron occurs in grains more than three times smaller than that calculated for magnetite (e.g. Muxworthy and Williams (2006)). It is evident that dusty olivine kamacite is unlikely to contain assemblages abundant in uniformly magnetised grains, with the average size of kamacite much larger at $353 \pm 147 \times 250 \pm 110$ nm (Chapter 4) and $242 \pm 94 \times 199 \pm 80 \times 123 \pm 58$ nm (Einsle et al., 2016); the average axial ratio of kamacite was found to be 1.5, which is non-uniformly magnetised above 30 nm. The nudged elastic band numerical algorithm applied here, however, contradicts previous assumptions that uniform, i.e., single-domain, magnetisation in iron is the most stable state, as single-vortex magnetisation was found to have greater relaxation times than uniform magnetisation states (Table 5.1, Fig. 5.7).

5.5.1 Acknowledgements and contributions

I conducted the micromagnetic simulations and analysis of the 10 to 50 nm Fe grains. Wyn Williams and Karl Fabian wrote the micromagnetic code MERRILL used for numerical analysis. M.V.-G. wrote bash scripts that helped to streamline the numerical analysis and assisted with the presentation of the numerical data. Adrian R. Muxworthy had the original idea for the project and led the direction of the study. I wrote this chapter with the help of Adrian R. Muxworthy, Wyn Williams, Trevor P. Almeida, Karl Fabian, and Rafal E. Dunin-Borkowski. This work was funded by the STFC (grant number grant number ST/N000803/1).

Chapter 6

Conclusions and future research

6.1 Conclusions and summary

This thesis has focused on the origin of magnetic remanence in chondritic meteorites to determine the type of remanence imparted and the capabilities of retaining remanence to the present day. Key findings reflect upon chondrite heating processes; possible evidence for parent body magnetic dynamos on chondrite parent bodies; and the remarkable fidelity of magnetic carriers within meteorites to retain remanence. A credible palaeomagnetic record held within dusty olivine kamacite indicates that we can significantly develop our understanding of the conditions of the protoplanetary disk with experimental data.

The primary goal of Chapter 2 was to determine whether any magnetic remanence is present and measurable with modern day magnetometers in the medium to higher portion of the coercivity spectrum of Karoonda, as reports for no palaeomagnetic significance in the higher end of the coercivity spectrum and palaeointensity estimates exist in the literature for Karoonda. The rock magnetic measurements presented for Karoonda agree with those previously published (Acton et al., 2007), and indicate that a magnetic remanence, if imparted, could be recorded and preserved to the present day. The sub-samples of Karoonda may have been remagnetised when they were cut using non-magnetic equipment at the Natural History Museum in

London. The demagnetisation of the natural remanence suggests that there is no remanence carried by the medium to high end of the coercivity spectrum, agreeing with previous studies (Sugiura, 1977; Acton et al., 2007).

A study that analysed Karoonda's matrix and chondrules at high resolution using TEM found evidence for heterogeneous partially melted olivines recrystallised as vesicular olivines with inclusions of fine grained magnetite (Ohnishi et al., 2007). The vesicular olivines suggest that the matrix and chondrules have been heterogeneously heated up to 1600°C and then rapidly cooled; this is not the bulk heating temperature. Thermally annealed dislocations indicate that a shock event formed dislocations subsequent to the formation of vesicular olivine. These dislocations also show evidence for thermal annealing, indicating that a final heating event separate to the formation of vesicular olivine and the dislocations occurred (Ohnishi et al., 2007).

The lack of high coercivity magnetic remanence suggests that no ambient field was recorded, or the magnetic remanence was not retained, from the event that resulted in the formation of vesicular olivine and associated fine-grained magnetite (Ohnishi et al., 2007).

The magnetic remanence of Karoonda suggests that it was heated in the absence of an ambient magnetic field, which supports a solar radiative heating mechanism for CV-CK metamorphism. These events could have taken place on the CK parent body in the absence of a magnetic dynamo.

A new micron-scale method for the palaeomagnetic conglomerate test that utilizes micro-CT scanning to generate a rotation matrix for disaggregated sub-millimetre clasts from a conglomerate is presented in Chapter 3. The method was developed to aid the accuracy and reproducibility of mutually oriented palaeomagnetic measurements of small-sized samples. The method was applied to two chondritic meteorites (Bjurböle (L/LL4) and Vigarano (CV3)) to understand the origin of the magnetisation of the chondrules. The alignment of the reoriented low-coercivity components of Vigarano's chondrules' magnetisations demonstrates that the reorientation protocol

was successful. We estimate that the reorientation is accurate to $< 1^\circ$, that is, the directional error in this protocol is the same as that of a standard palaeomagnetic measurement (e.g. a 1-inch core).

Both Bjurböle and Vigarano were found to have random magnetisation distribution amongst their chondrules. We argue that the chondrules in Bjurböle would have lost its pre-accretionary remanence as a result of thermal metamorphism on the parent body, and acquired a phase-transformation remanent magnetisation (PhTRM) on the parent body after cooling from peak-metamorphism to 320°C over 80 to 140 Ma. The scattered palaeodirections of the PhTRM could be due to an ambient field being recorded by the highly anisotropic tetrataenite. However, the variable palaeointensities, scatter in palaeodirections and previously found chemical anomalies suggest Bjurböle formed as a breccia from a brecciated precursor chondrite. Given the demagnetisation behaviour of Vigarano's chondrules and that it is a regolith breccia formed by re-accreting chondrules and matrix material that had been brecciated by 10 to 20 GPa impacts on the parent body, it is most likely that its NRM is a shock remanence overprint due to impacts. The harder, non-viscous component of remanence (MC), suggests these brecciating impacts occurred in the presence of an ambient field prior to the accretion of the Vigarano breccia 4558 Myr ago.

Vigarano chondrules evidence the early-stage magnetic activity (ca. 10 Myr after Solar System formation) on asteroid bodies driven by their thermal structure, and the remanences in the Bjurböle chondrules are an indication of late-stage parent body magnetism (> 80 to 140 Myrs after Solar System formation) likely due to core solidification. The results of our study support earlier findings of Elkins-Tanton et al. (2011) and Gattacceca et al. (2016) that primitive chondrites originate from asteroids that must have sustained a magnetic field. It seems ever more evident that primitive chondrites need not to have originated from entirely primitive, never molten and/or differentiated parent bodies. Rather, parent bodies of primitive meteorites consisted of a differentiated interior, encrusted by a layer of incrementally

accreted primitive meteoritic material. This incremental chondrule accretion model is currently favoured by numerical and analytical analyses of protoplanetary disk accretion, and is supported by this study. Recent palaeomagnetic studies of meteorites have indicated that asteroids can, therefore, sustain at least three periods of magnetic dynamo activity: (i) one early stage dynamo active < 50 Myr, (ii) a period of quiescence or potentially impact-driven magnetism and (iii) a later dynamo once the body has cooled sufficiently. The difference in magnetic activity between the carbonaceous chondrite Vigarano and the ordinary chondrite Bjurböle might indicate a general difference between carbonaceous and ordinary chondrite parent bodies, and/or formation location in the Solar Nebula (e.g. Budde et al. (2016)). However, this needs to be confirmed by additional studies.

Chapters 4 and 5 are combined studies that focused on determining the magnetic properties and recording fidelity of likely the oldest magnetic record in our Solar System, dusty olivine found within unequilibrated chondrites. Dusty olivine has been dated to have formed within the first three million years of our Solar System. However, because the vast majority of the kamacite grains that carry magnetic remanence within dusty olivine are magnetically non-uniform, their ability to retain four-billion-year-old magnetic recordings cannot be estimated by previous theories, which assume only uniform magnetic behaviour. Understanding the reliability of such remanence records is important, as palaeomagnetic data from dusty olivine grains are used to inform and constrain astrophysical numerical models for chondrule formation processes and momentum transport mechanisms that can govern accretion mechanisms in the protoplanetary disk.

The study in Chapter 5, coupled with the experimental electron holography observations and large NEB calculation of multi-vortex magnetisation stability in Chapter 4, demonstrates unequivocally that the majority of kamacite grains in dusty olivines are capable of retaining magnetic field information from the early Solar System, however, this remanence is largely carried by non-uniformly magnetised grains. Understanding of the thermomagnetic properties of vortex-state grains must

be developed, e.g., acquisition of thermoremanence, in order to accurately model the remanence recorded by these grains in the first few million years of the Solar System's existence. Accurate determination of the magnetic fields present during this time is essential to reliably model the chondrule formation processes and mechanisms of momentum transport in the protoplanetary disk.

The studies presented in Chapters 2 to 5 present the importance of palaeomagnetic data for understanding protoplanetary disk processes and conditions as well as parent body conditions, yet the most important finding of this thesis is the remarkable stability of magnetic vortex states in iron, which are the most abundant type of magnetisation state found within natural rock and meteorite samples, yet usually ignored by theories that interpret palaeomagnetic data. Up until now, uniform magnetisations have been the basis and focus of palaeomagnetism, with samples rich in 'single domain' grains considered as ideal. Here, single and multi-vortex magnetic states have been shown to be thermomagnetically stable over timescales greater than the age of the Universe. These grains are so abundant in natural rocks that if their thermomagnetic properties can be fully understood, palaeomagnetic protocols and the resulting datasets are likely to be far more reliable, and our understanding of magnetic fields from the protoplanetary disk to the present day will vastly improve. As a result, the picture of our protoplanetary disk for example, which is presently so poorly understood and populated with postulations, will become clear and well constrained as a result of reliable and accurate palaeomagnetic data.

6.2 Future research

This thesis has inspired many avenues for future research. The palaeomagnetic record of Karoonda, presented in Chapter 2, suggests that Karoonda may not have recorded a significant ambient field. The lack of high coercivity remanence suggests the heating and shock event that formed the vesicular olivine did not occur in the presence of an ambient magnetic field. Further study to determine the age of

the vesicular olivine and the age and peak temperature of the thermal annealing would help to determine whether these events took place on the CK parent body or interplanetary orbit.

Sugiura (1977) and Nagata (1979) report that Karoonda may have recorded a partial thermoremanent magnetisation (pTRM) corresponding to heating up to 300°C in a 89 μT ambient magnetic field, however, this estimate is only based upon one sample estimate and the study did not incorporate pTRM checks, which are now common practise to demonstrate chemical stability during the repeated heatings of the experimental protocol. Such a pTRM, however, may be consistent with the thermal annealing evidenced in Karoonda's matrix and chondrules. Given that Karoonda is likely to be thermomagnetically stable, as suggested by Herndon et al. (1976) and Sugiura (1977), a new Thellier-type experiment to obtain a reliable palaeointensity estimate would be worthwhile.

The micro-CT method for the conglomerate test presented in Chapter 3 opens up much opportunity with regards to mutually oriented small-sized sample analysis. For example, Gattacceca et al. (2016) were not able to mutually orient their subsamples of Kaba. Although they do not state the reason for this beyond curation limitations, modern curatorial practise has begun to incorporate the non-destructive technique of micro-CT scanning meteorites to begin more targeted sampling of meteorites and limiting wasted material. With a volumetric record, secondary micro-CT scans of subsamples facilitates accurate $< 1^\circ$ mutually oriented experiments. Mutual orientation of subsamples of meteorites adds the directional significance to palaeomagnetic data, which is otherwise, without a reference frame, typically meaningless. The technique at the moment is limited to chondrules, however, it may be possible to mutually orient bulk matrix samples given sufficient scanning resolution. As such, further experiments following the methods presented in Chapter 3 could feasibly be applied to any meteorite to determine timing and origin of magnetic remanence acquisition.

The studies in Chapters 4 and 5 motivate further research into the magnetic

recording properties of vortex magnetisation states. They have been shown to be thermomagnetically stable, and capable of carrying remanence for sufficiently long timescales to resolve magnetic fields imparted at the beginning of the Solar System. The electron holography experiments in Chapter 4 observed the saturation isothermal remanent magnetisation (SIRM) stability to high temperature, and SIRM has been shown to be less stable than thermoremanent magnetisation (TRM) for grain assemblages; however, observations of individually magnetised grains should behave identically irrespective of TRM or SIRM. Nevertheless, their thermoremanence acquisition dynamics remain to be well understood. The thermochemical alteration of the kamacite grains presented in the temperature-dependent electron holography experiment in Chapter 4 prevented the acquisition of thermoremanence as a result of cooling from beyond the Curie temperature (760°C) from being observed. The experiment was repeated with synthetic iron nanoparticles deposited directly onto the TEM EMHeaterChip, however reversal of the magnetisation of the particles could not be achieved, so magnetic induction maps could not be produced. Due to the time consuming and costly nature of TEM experiments on natural rock samples, further attempts should be made with iron nanoparticles, as electron holography on them has been achieved before (Gatel et al., 2015). The thermoremanence analysis conducted by electron holography should be accompanied with supporting micromagnetic simulations. The micromagnetic simulations of the large grain meshed after the dimensions of the temperature-dependent electron holography grain demonstrate that modern micromagnetic algorithms are sufficiently advanced to model realistic magnetisation structures. These calculations can be used to determine the thermal relaxation properties, i.e., stability, of the magnetisation states that are likely to occur in nature, thereby calculating the physical possibility for magnetic remanence to represent past magnetic fields. Further micromagnetic modelling (independent of electron holography imaging) would be desirable at high temperature. Temperature-dependent micromagnetic modelling could accurately determine the blocking temperature of magnetic vortex states, which has previously

been attempted analytically for uniformly magnetised grains, however, as has been emphasised in this thesis, greater understanding of the thermomagnetic properties of vortex states is essential to accurately model past magnetic fields from the protoplanetary disk to the present.

Bibliography

- Acton, G., Yin, Q.Z., Verosub, K.L., Jovane, L., 2007, Micromagnetic coercivity distributions and interactions in chondrules with implications for paleointensities of the early solar system: *J. Geophys. Res.*, vol. 112, no. B3, pp. 2156–2202.
- Alexander, C.M.O., Grossman, J.N., Ebel, D.S., Ciesla, F.J., 2008, The Formation Conditions of Chondrules and Chondrites: *Science*, vol. 320, no. 5883, pp. 1617–1619.
- Almeida, T.P., Kasama, T., Muxworthy, A.R., Williams, W., Nagy, L., Dunin Borkowski, R.E., 2014a, Observing thermomagnetic stability of nonideal magnetite particles: Good paleomagnetic recorders?: *Geophys. Res. Lett.*, vol. 41, no. 20, pp. 7041–7047.
- Almeida, T.P., Kasama, T., Muxworthy, A.R., Williams, W., Nagy, L., Hansen, T.W., Brown, P.D., Dunin Borkowski, R.E., 2014b, Visualized effect of oxidation on magnetic recording fidelity in pseudo-single-domain magnetite particles: *Nat. Commun.*, vol. 5.
- Almeida, T.P., Muxworthy, A.R., Kovács, A., Williams, W., Brown, P.D., Dunin-Borkowski, R.E., 2016a, Direct visualization of the thermomagnetic behavior of pseudo-single-domain magnetite particles: *Sci. Adv.*, vol. 2, no. 4.
- Almeida, T.P., Muxworthy, A.R., Kovács, A., Williams, W., Nagy, L., Conbhuí, P.Ó., Frandsen, C., Supakulopas, R., Dunin Borkowski, R.E., 2016b, Direct observation of the thermal demagnetization of magnetic vortex structures in nonideal magnetite recorders: *Geophys. Res. Lett.*, vol. 43, no. 16, pp. 8426–8434.
- Anders, E., 1964, Origin, age, and composition of meteorites: *Space. Sci. Rev.*, vol. 3, no. 5-6, pp. 583–714.
- Anders, E., Goles, G.C., 1961, Theories on the origin of meteorites: *J. Chem. Educ.*, vol. 38, no. 2, p. 58.
- Bai, X.N., Stone, J.M., 2010, Dynamics Of Solids In The Misplane Of Protoplanetary Disks: Implications For Planetesimal Formation: *Astrophys. J.*, vol. 722, no. 2, pp. 1437–1459.
- Bai, X.N., Ye, J., Goodman, J., Yuan, F., 2016, Magneto-thermal disk winds from protoplanetary disks: *Astrophys. J.*, vol. 818, no. 2, p. 152.
- Baker, J., Bizzarro, M., Wittig, N., Connelly, J., Haack, H., 2005, Early planetesimal melting from an age of 4.5662 Gyr for differentiated meteorites: *Nature*, vol. 436, no. 7054, pp. 1127–1131.
- Balbus, S.A., Hawley, J.F., 1991, A powerful local shear instability in weakly magnetized disks. I - Linear analysis. II - Nonlinear evolution: *Astrophys. J.*, vol. 376, pp. 214–233.
- Banerjee, S.K., Mellema, J.P., 1974, A new method for the determination of paleointensity from the A.R.M. properties of rocks: *Earth Planet. Sci. Lett.*, vol. 23, no. 2, pp. 177–184.
- Bean, C.P., Livingston, J.D., 1959, Superparamagnetism: *J. Appl. Phys.*, vol. 30, no. 4, pp. S120–S129.
- Berkov, D.V., 1998, Numerical calculation of the energy barrier distribution in disordered many-particle systems: the path integral method: *J. Magn. Magn. Mater.*, vol. 186, no. 1-2, pp. 199–213.
- Berndt, T., Muxworthy, A.R., Fabian, K., 2016, Does size matter? Statistical limits of paleomagnetic field reconstruction from small rock specimens: *Journal of Geophysical Research*, vol. 121, no. 1, pp. 15–26.

- Bertotti, G., 1998, *Hysteresis in Magnetism*, Gulf Professional Publishing.
- Biggin, A.J., de Wit, M.J., Langereis, C.G., Zegers, T.E., Vouite, S., Dekkers, M.J., Drost, K., 2011, Palaeomagnetism of Archaean rocks of the Onverwacht Group, Barberton Greenstone Belt (southern Africa): Evidence for a stable and potentially reversing geomagnetic field at ca. 3.5Ga: *Earth Planet. Sci. Lett.*, vol. 302, no. 3-4, pp. 314–328.
- Biggin, A.J., Paterson, G.A., 2014, A new set of qualitative reliability criteria to aid inferences on palaeomagnetic dipole moment variations through geological time: *Frontiers in Earth Science*, vol. 2, p. 24.
- Bischoff, A., Scott, E., Metzler, K., 2006, Nature and origins of meteoritic breccias, in: *Meteorites and the Early Solar System II*, University of Arizona Press, pp. 679–712.
- Bischoff, A., Stöfler, D., 1992, Shock metamorphism as a fundamental process in the evolution of planetary bodies: information from meteorites: *European journal of mineralogy*, vol. 4, no. 4, pp. 707–755.
- Bland, P.A., Collins, G.S., Davison, T.M., Abreu, N.M., Ciesla, F.J., Muxworthy, A.R., Moore, J., 2014, Pressure–temperature evolution of primordial solar system solids during impact-induced compaction: *Nat. Commun.*, vol. 5, p. 5451.
- Bland, P.A., Cressey, G., Menzies, O.N., 2004, Modal mineralogy of carbonaceous chondrites by X-ray diffraction and Mössbauer spectroscopy: *Meteorit. Planet. Sci.*, vol. 39, no. 1, pp. 3–16.
- Blandford, R.D., Payne, D.G., 1982, Hydromagnetic flows from accretion discs and the production of radio jets: *MNRAS*, vol. 199, no. 4, pp. 883–903.
- Blum, J., Wurm, G., 2008, The Growth Mechanisms of Macroscopic Bodies in Protoplanetary Disks: *Annu. Rev. Astron. Astrophys.*, vol. 46, no. 1, pp. 21–56.
- Böhlner, H., Michalk, D., Nowaczyk, N., 2009, The use of mini-samples in palaeomagnetism: *Geophys. J. Int.*, vol. 179, pp. 35–42.
- Böhlner, H., Schnepf, E., 2014, Precision of the paleomagnetic method: An example from the Quaternary Eifel volcanics (Germany): *Earth, Planets and Space*, vol. 51, no. 6, pp. 403–412.
- Boland, J.N., Duba, A., 1981, Solid-state reduction of iron in olivine—planetary and meteoritic evolution: *Nature*, vol. 294, no. 5837, pp. 142–144.
- Boland, J.N., Duba, A.G., 1986, An electron microscope study of the stability field and degree of nonstoichiometry in olivine: *J. Geophys. Res.*, vol. 91, no. B5, pp. 4711–4722.
- Boley, A.C., Morris, M.A., Desch, S.J., 2013, High-Temperature Processing Of Solids Through Solar Nebular Bow Shocks: 3D Radiation Hydrodynamics Simulations With Particles: *Astrophys. J.*, vol. 776, no. 2, p. 101.
- Bonilla, F.J., Lacroix, L.M., Blon, T., 2017, Magnetic ground states in nanocuboids of cubic magnetocrystalline anisotropy: *J. Magn. Magn. Mater.*, vol. 428, pp. 394–400.
- Boss, A.P., 2002, Evolution of the Solar Nebula. V. Disk Instabilities with Varied Thermodynamics: *Astrophys. J.*, vol. 576, no. 1, pp. 462–472.
- Boss, A.P., Durisen, R.H., 2005, Chondrule-forming Shock Fronts in the Solar Nebula: A Possible Unified Scenario for Planet and Chondrite Formation: *Astrophys. J.*, vol. 621, no. 2, pp. L137–L140.
- Bozorth, R.M., 1951, *Ferromagnetism*, Van Nostrand.
- Brauer, F., Dullemond, C.P., Henning, T., 2007, Coagulation, fragmentation and radial motion of solid particles in protoplanetary disks: *Astronomy & Astrophysics*, vol. 480, no. 3, pp. 859–877.
- Brecher, A., Arrhenius, G., 1974, The paleomagnetic record in carbonaceous chondrites: Natural remanence and magnetic properties: *J. Geophys. Res.*, vol. 79, pp. 2081–2106.
- Bryson, J., Church, N.S., Kasama, T., 2014, Nanomagnetic intergrowths in Fe–Ni meteoritic metal: The potential for time-resolved records of planetesimal dynamo fields: *Earth Planet. Sci. Lett.*, vol. 388, pp. 237–248.
- Bryson, J.F.J., Nichols, C.I.O., Herrero-Albillos, J., Kronast, F., Kasama, T., Alimadadi, H.,

- van der Laan, G., Nimmo, F., Harrison, R.J., 2015, Long-lived magnetism from solidification-driven convection on the pallasite parent body: *Nature*, vol. 517, no. 7535, pp. 472–475.
- Budde, G., Burkhardt, C., Brennecka, G.A., Fischer-Gdde, M., Kruijer, T.S., Kleine, T., 2016, Molybdenum isotopic evidence for the origin of chondrules and a distinct genetic heritage of carbonaceous and non-carbonaceous meteorites: *Earth Planet. Sci. Lett.*, vol. 454, pp. 293–303.
- Butler, R.F., 1972, Natural remanent magnetization and thermomagnetic properties of the Allende meteorite: *Earth Planet. Sci. Lett.*, vol. 17, no. 1, pp. 120–128.
- Butler, R.F., 1998, *Paleomagnetism: Magnetic domains to geologic terranes*, Electronic edition.
- Butler, R.F., Banerjee, S.K., 1975, Single-domain grain size limits for metallic iron: *J. Geophys. Res.*, vol. 80, no. 2, pp. 252–259.
- Butterworth, A.L., Aballain, O., Chappellaz, J., Sephton, M.A., 2004, Combined element (H and C) stable isotope ratios of methane in carbonaceous chondrites: *MNRAS*, vol. 347, no. 3, pp. 807–812.
- Cameron, A.G.W., 1966, The accumulation of chondritic material: *Earth Planet. Sci. Lett.*, vol. 1, no. 3, pp. 93–96.
- Cameron, A.G.W., 1973, Accumulation processes in the primitive solar nebula: *Icarus*, vol. 18, no. 3, pp. 407–450.
- Carporzen, L., Fu, R., Andrade Lima, E., Weiss, B.P., 2011a, A secondary origin of chondrule magnetization in the Allende CV carbonaceous chondrite: *AGU Fall Meeting Abstracts*.
- Carporzen, L., Gilder, S.A., Hart, R.J., 2005, Palaeomagnetism of the Vredefort meteorite crater and implications for craters on Mars: *Nature*, vol. 435, no. 7039, pp. 198–201.
- Carporzen, L., Weiss, B.P., Elkins-Tanton, L.T., Shuster, D.L., Ebel, D., Gattacceca, J., 2011b, Magnetic evidence for a partially differentiated carbonaceous chondrite parent body: *PNAS*, vol. 108, no. 16, pp. 6386–6389.
- Carporzen, L., Weiss, B.P., Gilder, S.A., Pommier, A., Hart, R.J., 2012, Lightning remagnetization of the Vredefort impact crater: No evidence for impact-generated magnetic fields: *J. Geophys. Res.*, vol. 117, no. E1, p. 737.
- Chaumard, N., Devouard, B., 2016, Chondrules in CK carbonaceous chondrites and thermal history of the CV–CK parent body: *Meteorit. Planet. Sci.*, vol. 51, no. 3, pp. 547–573.
- Chaumard, N., Devouard, B., Bouvier, A., Wadhwa, M., 2014, Metamorphosed calcium-aluminum-rich inclusions in CK carbonaceous chondrites: *Meteorit. Planet. Sci.*, vol. 49, no. 3, pp. 419–452.
- Chaumard, N., Devouard, B., Delbo, M., Provost, A., Zanda, B., 2012, Radiative heating of carbonaceous near-Earth objects as a cause of thermal metamorphism for CK chondrites: *Icarus*, vol. 220, no. 1, pp. 65–73.
- Cisowski, S.M., Collinson, D.W., Runcorn, S.K., Stephenson, A., 1983, A review of lunar paleointensity data and implications for the origin of lunar magnetism: *J. Geophys. Res.*, vol. 88, no. S02, pp. A691–A704.
- Cisowski, S.M., Fuller, M., 1978, The effect of shock on the magnetism of terrestrial rocks: *Journal of Geophysical Research*, vol. 83, no. B7, pp. 3441–3458.
- Clarke, R.S., Scott, E.R.D., 1980, Tetrataenite; ordered FeNi, a new mineral in meteorites: *Am. Mineral.*, vol. 65, no. 7-8, pp. 624–630.
- Clayton, R.N., Mayeda, T.K., 1978, Multiple parent bodies of polymict brecciated meteorites: *Geochim. Cosmochim. Acta*, vol. 42, no. 3, pp. 325–327.
- Clayton, R.N., Mayeda, T.K., 1999, Oxygen isotope studies of carbonaceous chondrites: *Geochim. Cosmochim. Acta*, vol. 63, no. 13-14, pp. 2089–2104.
- Clayton, R.N., Onuma, N., Grossman, L., Mayeda, T.K., 1977, Distribution of the pre-solar component in Allende and other carbonaceous chondrites: *Earth Planet. Sci. Lett.*, vol. 34, no. 2, pp. 209–224.
- Coe, R.S., 1967, Paleo-intensities of the Earth's magnetic field determined from Tertiary and

- Quaternary rocks: *J. Geophys. Res.*, vol. 72, no. 12, pp. 3247–3262.
- Collinson, D.W., 1989, The Magnetism of Ordinary Chondrites and SNC Meteorites: Possible Implications for Ancient Solar System Magnetic Fields, in: *Geomagnetism and Palaeomagnetism*, Springer Netherlands, Dordrecht, pp. 279–295.
- Connelly, J.N., Bizzarro, M., Krot, A.N., Nordlund, A., Wielandt, D., Ivanova, M.A., 2012a, The Absolute Chronology and Thermal Processing of Solids in the Solar Protoplanetary Disk: *Science*, vol. 338, no. 6107, pp. 651–655.
- Connelly, J.N., Bizzarro, M., Nordlund, A., Wielandt, D., Ivanova, M.A., 2012b, The Absolute Chronology and Thermal Processing of Solids in the Solar Protoplanetary Disk: *Science*, vol. 338, no. 6107, pp. 651–655.
- Connolly Jr., H.C., Hewins, R.H., Ash, R.D., Zanda, B., Lofgren, G.E., 1994, Carbon and the formation of reduced chondrules: *Nature*, vol. 371, no. 6493, pp. 136–139.
- Cottrell, R.D., Tarduno, J.A., 1999, Geomagnetic paleointensity derived from single plagioclase crystals: *Earth Planet. Sci. Lett.*, vol. 169, no. 1, pp. 1–5.
- Cournede, C., Gattacceca, J., Gounelle, M., Rochette, P., Weiss, B.P., Zanda, B., 2015, An early solar system magnetic field recorded in CM chondrites: *Earth Planet. Sci. Lett.*, vol. 410, pp. 62–74.
- Crawford, D.A., Schultz, P.H., 1999, Electromagnetic properties of impact-generated plasma, vapor and debris: *International Journal of Impact Engineering*, vol. 23, no. 1, pp. 169–180.
- Dauphas, N., Pourmand, A., 2011, Hf-W-Th evidence for rapid growth of Mars and its status as a planetary embryo: *Nature*, vol. 473, no. 7348, pp. 489–492.
- Day, R., Fuller, M., Schmidt, V.A., 1977, Hysteresis properties of titanomagnetites: grain-size and compositional dependence: *Phys. Earth Planet. Int.*, vol. 13, no. 4, pp. 260–267.
- Desch, S.J., Connolly, H.C., 2002, A model of the thermal processing of particles in solar nebula shocks: Application to the cooling rates of chondrules: *Meteorit. Planet. Sci.*, vol. 37, no. 2, pp. 183–207.
- Desch, S.J., Morris, M.A., Connolly, H.C., Boss, A.P., 2010, A Critical Examination Of The X-Wind Model For Chondrule And Caesium-Rich, Aluminum-Rich Inclusion Formation And Radionuclide Production: *Astrophys. J.*, vol. 725, no. 1, pp. 692–711.
- Desch, S.J., Morris, M.A., Connolly, H.C., Boss, A.P., 2012, The importance of experiments: Constraints on chondrule formation models: *Meteorit. Planet. Sci.*, vol. 47, no. 7, pp. 1139–1156.
- Dodd, S.C., Mac Niocaill, C., Muxworthy, A.R., 2015, Long duration (>4 Ma) and steady-state volcanic activity in the early Cretaceous Paraná–Etendeka Large Igneous Province: New palaeomagnetic data from Namibia: *Earth Planet. Sci. Lett.*, vol. 414, pp. 16–29.
- Dos Santos, E., Gattacceca, J., Rochette, P., Fillion, G., Scorzelli, R.B., 2015, Kinetics of tetrataenite disordering: *J. Magn. Magn. Mater.*, vol. 375, pp. 234–241.
- Doyle, P.M., Jogo, K., Nagashima, K., Huss, G.R., Krot, A.N., 2016, Mn–Cr relative sensitivity factor in ferromagnesian olivines defined for SIMS measurements with a Cameca ims-1280 ion microprobe: Implications for dating secondary fayalite: *Geochim. Cosmochim. Acta*, vol. 174, pp. 102–121.
- Dunin Borkowski, R.E., McCartney, M.R., Frankel, R.B., Bazylinski, D.A., Pósfai, M., Buseck, P.R., 1998, Magnetic Microstructure of Magnetotactic Bacteria by Electron Holography: *Science*, vol. 282, no. 5395, pp. 1868–1870.
- Dunlop, D.J., 1968, Monodomain Theory: Experimental Verification: *Science*, vol. 162, no. 3850, pp. 256–258.
- Dunlop, D.J., 1977, The Hunting of the ‘Psark’, in: *Origin of Thermoremanent Magnetization*, Springer Netherlands, Dordrecht, pp. 61–86.
- Dunlop, D.J., Argyle, K.S., 1997, Thermoremanence, anhysteretic remanence and susceptibility of submicron magnetites: Nonlinear field dependence and variation with grain size: *Journal of*

- Geophysical Research: Solid Earth, vol. 102, no. B9, pp. 20199–20210.
- Dunlop, D.J., Özdemir, Ö., 2001, *Rock Magnetism*, Fundamentals and Frontiers, Cambridge University Press.
- Dunlop, D.J., West, G.F., 1969, An experimental evaluation of single domain theories: Reviews of Geophysics, vol. 7, no. 4, pp. 709–757.
- Dunn, T.L., Gross, J., Ivanova, M.A., Runyon, S.E., Bruck, A.M., 2016, Magnetite in the unequilibrated CK chondrites: Implications for metamorphism and new insights into the relationship between the CV and CK chondrites: Meteorit. Planet. Sci., vol. 51, no. 9, pp. 1701–1720.
- Ebel, D.S., 2006, Condensation of rocky material in astrophysical environments, in: *Meteorites and the Early Solar System II*, University of Arizona Press, pp. 253–278.
- Einsle, J.F., Harrison, R.J., Kasama, T., Conbhuí, P.Ó., Fabian, K., Williams, W., Woodland, L., Fu, R.R., Weiss, B.P., Midgley, P.A., 2016, Multi-scale three-dimensional characterization of iron particles in dusty olivine: Implications for paleomagnetism of chondritic meteorites: Am. Mineral., vol. 101, no. 9, pp. 2070–2084.
- Elangovan, P., Hezel, D.C., Howard, L., Armstrong, R., Abel, R.L., 2012, Phasequant: A tool for quantifying tomographic data sets of geological specimens: Computers & geosciences, vol. 48, pp. 323–329.
- Elkins-Tanton, L., 2010, Chondrites as samples of differentiated planetesimals: EGU General Assembly Conference Abstracts, vol. 12, p. 13683.
- Elkins-Tanton, L.T., Weiss, B.P., Zuber, M.T., 2011, Chondrites as samples of differentiated planetesimals: Earth Planet. Sci. Lett., vol. 305, no. 1-2, pp. 1–10.
- Elliott, J.C., Dover, S.D., 2011, X-ray microtomography: Journal of Microscopy, vol. 126, no. 2, pp. 211–213.
- Emmertson, S., Muxworthy, A.R., Hezel, D.C., Bland, P.A., 2011, Magnetic characteristics of CV chondrules with paleointensity implications: J. Geophys. Res., vol. 116, no. E12, p. E12007.
- Evans, M.E., McElhinny, M.W., 1969, An Investigation of the Origin of Stable Remanence in Magnetite-bearing Igneous Rocks: Journal of Geomagnetism and Geoelectricity, vol. 21, no. 4, pp. 757–773.
- Fabian, K., Shcherbakov, V.P., 2017, Energy barriers in three-dimensional micromagnetic models and the physics of thermo-viscous magnetization in multidomain particles: <https://arxiv.org/abs/1702.00070>.
- Feigelson, E.D., Broos, P., Gaffney III, J.A., Garmire, G., Hillenbrand, L.A., Pravdo, S.H., Townsley, L., Tsuboi, Y., 2002, X-Ray-emitting Young Stars in the Orion Nebula: Astrophys. J., vol. 574, no. 1, pp. 258–292.
- Feigelson, E.D., Montmerle, T., 1999, High-energy processes in young stellar objects: Annu. Rev. Astron. Astrophys., vol. 37, no. 1, pp. 363–408.
- Feinberg, J.M., Harrison, R.J., Kasama, T., Dunin Borkowski, R.E., Scott, G.R., Renne, P.R., 2006, Effects of internal mineral structures on the magnetic remanence of silicate-hosted titanomagnetite inclusions: An electron holography study: J Geophys. Res., vol. 111, no. B12.
- Feinberg, J.M., Scott, G.R., Renne, P.R., Wenk, H.R., 2005, Exsolved magnetite inclusions in silicates: Features determining their remanence behavior: Geology, vol. 33, no. 6, pp. 513–516.
- Fieber-Beyer, S.K., Gaffey, M.J., 2014, Near-infrared spectroscopy of 3:1 Kirkwood Gap asteroids II: Probable and plausible parent bodies; primitive and differentiated: Icarus, vol. 229, pp. 99–108.
- Fieber-Beyer, S.K., Gaffey, M.J., Kelley, M.S., Reddy, V., Reynolds, C.M., Hicks, T., 2011, The Maria asteroid family: Genetic relationships and a plausible source of mesosiderites near the 3:1 Kirkwood Gap: Icarus, vol. 213, no. 2, pp. 524–537.
- Fish, R.A., Goles, G.G., Anders, E., 1960, The Record in the Meteorites. III. on the Development of Meteorites in Asteroidal Bodies.: Astrophys. J., vol. 132, p. 243.
- Fu, R.R., Lima, E.A., Weiss, B.P., 2014a, No nebular magnetization in the Allende CV carbona-

- ceous chondrite: *Earth Planet. Sci. Lett.*, vol. 404, pp. 54–66.
- Fu, R.R., Weiss, B.P., Lima, E.A., Harrison, R.J., Bai, X.N., Desch, S.J., Ebel, D.S., Suavet, C., Wang, H., Glenn, D., Le Sage, D., Kasama, T., Walsworth, R.L., Kuan, A.T., 2014b, Solar nebula magnetic fields recorded in the Semarkona meteorite: *Science*, vol. 346, no. 6213, pp. 1089–1092.
- Fuller, M., 1974, Lunar magnetism: *Reviews of Geophysics*, vol. 12, no. 1, pp. 23–70.
- Funaki, M., Syono, Y., 2010, Acquisition of shock remanent magnetization for demagnetized samples in a weak magnetic field ($7 \mu\text{T}$) by shock pressures 5–20 GPa without plasma-induced magnetization: *Meteorit. Planet. Sci.*, vol. 43, no. 3, pp. 529–540.
- Gabor, D., 1949, Microscopy by Reconstructed Wave-Fronts: *Proceedings of the Royal Society A: Mathematical, Physical and Engineering Sciences*, vol. 197, no. 1051, pp. 454–487.
- Gaffey, M.J., Gilbert, S.L., 1998, Asteroid 6 Hebe: The probable parent body of the H-type ordinary chondrites and the IIE iron meteorites: *Meteorit. Planet. Sci.*, vol. 33, no. 6, pp. 1281–1295.
- Gaffey, M.J., Reed, K.L., Kelley, M.S., 1992, Relationship of E-type Apollo asteroid 3103 (1982 BB) to the enstatite achondrite meteorites and the Hungaria asteroids: *Icarus*, vol. 100, no. 1, pp. 95–109.
- Garrick-Bethell, I., Weiss, B.P., 2010, Kamacite blocking temperatures and applications to lunar magnetism: *Earth Planet. Sci. Lett.*, vol. 294, no. 1–2, pp. 1–7.
- Gatel, C., Bonilla, F.J., Meffre, A., Snoeck, E., Warot-Fonrose, B., Chaudret, B., Lacroix, L.M., Blon, T., 2015, Size-Specific Spin Configurations in Single Iron Nanomagnet: From Flower to Exotic Vortices: *Nano Letters*, vol. 15, no. 10, pp. 6952–6957.
- Gattacceca, J., Berthe, L., Boustie, M., Vadeboin, F., Rochette, P., de Resseguier, T., 2008, On the efficiency of shock magnetization processes: *Phys. Earth Planet. Int.*, vol. 166, no. 1–2, pp. 1–10.
- Gattacceca, J., Boustie, M., Hood, L., Cuq-Lelandais, J.P., Fuller, M., Bezaeva, N.S., de Resseguier, T., Berthe, L., 2010a, Can the lunar crust be magnetized by shock: Experimental groundtruth: *Earth Planet. Sci. Lett.*, vol. 299, no. 1–2, pp. 42–53.
- Gattacceca, J., Boustie, M., Lima, E., Weiss, B.P., de Resseguier, T., Cuq-Lelandais, J.P., 2010b, Unraveling the simultaneous shock magnetization and demagnetization of rocks: *Phys. Earth Planet. Int.*, vol. 182, no. 1–2, pp. 42–49.
- Gattacceca, J., Rochette, P., 2004, Toward a robust normalized magnetic paleointensity method applied to meteorites: *Earth Planet. Sci. Lett.*, vol. 227, no. 3–4, pp. 377–393.
- Gattacceca, J., Rochette, P., Denise, M., Consolmagno, G., Folco, L., 2005, An impact origin for the foliation of chondrites: *Earth Planet. Sci. Lett.*, vol. 234, no. 3–4, pp. 351–368.
- Gattacceca, J., Suavet, C., Rochette, P., Weiss, B.P., Winklhofer, M., Uehara, M., Friedrich, J.M., 2014, Metal phases in ordinary chondrites: Magnetic hysteresis properties and implications for thermal history: *Meteorit. Planet. Sci.*, vol. 49, no. 4, pp. 652–676.
- Gattacceca, J., Weiss, B.P., Gounelle, M., 2016, New constraints on the magnetic history of the CV parent body and the solar nebula from the Kaba meteorite: *Earth Planet. Sci. Lett.*, vol. 455, pp. 166–175.
- Geiger, T., Bischoff, A., 1991, The CK chondrites-Conditions of parent body metamorphism, in: *Meteoritics*, p. 337.
- Ghosh, A., McSween Jr., H.Y., 1998, A Thermal Model for the Differentiation of Asteroid 4 Vesta, Based on Radiogenic Heating: *Icarus*, vol. 134, no. 2, pp. 187–206.
- Glenn, D.R., Lee, K., Park, H., Weissleder, R., Yacoby, A., Lukin, M.D., Lee, H., Walsworth, R.L., Connolly, C.B., 2015, Single-cell magnetic imaging using a quantum diamond microscope: *Nature Methods*, vol. 12, no. 8, pp. 736–738.
- Goldstein, J., Newbury, D.E., Echlin, P., Joy, D.C., Fiori, C., Lifshin, E., 2013, *Scanning Electron Microscopy and X-Ray Microanalysis*, A Text for Biologists, Materials Scientists, and Geologists,

Springer Science & Business Media.

- Grady, M.M., 2000, *Catalogue of Meteorites*, Cambridge University Press.
- Graham, J.W., 1949, The stability and significance of magnetism in sedimentary rocks: *J Geophys. Res.*, vol. 54, no. 2, pp. 131–167.
- Greenwood, R.C., Franchi, I.A., Kearsley, A.T., Alard, O., 2010, The relationship between CK and CV chondrites: *Geochim. Cosmochim. Acta*, vol. 74, no. 5, pp. 1684–1705.
- Gressel, O., Turner, N.J., Nelson, R.P., McNally, C.P., 2015, Global simulations of protoplanetary disks with ohmic resistivity and ambipolar diffusion: *Astrophys. J.*, vol. 801, no. 2, p. 84.
- Griffin, L.D., Elangovan, P., Mundell, A., Hezel, D.C., 2012, Improved segmentation of meteorite micro-ct images using local histograms: *Computers & geosciences*, vol. 39, pp. 129–134.
- Harrison, R.J., Dunin-Borkowski, R.E., Putnis, A., 2002, Direct imaging of nanoscale magnetic interactions in minerals: *PNAS*, vol. 99, no. 26, pp. 16556–16561.
- Hasegawa, Y., Turner, N.J., Masiero, J., Wakita, S., Matsumoto, Y., Oshino, S., 2016, Forming chondrites in a Solar Nebula with magnetically induced turbulence: *Astrophys. J.*, vol. 820, no. 1, p. L12.
- Hayashi, C., 1981, Structure of the Solar Nebula, Growth and Decay of Magnetic Fields and Effects of Magnetic and Turbulent Viscosities on the Nebula: *Progr. Theoret. Phys. Suppl.*, vol. 70, pp. 35–53.
- Heider, F., Dunlop, D.J., 1987, Two types of chemical remanent magnetization during the oxidation of magnetite: *Phys. Earth Planet. Int.*, vol. 46, no. 1-3, pp. 24–45.
- Henke, S., Gail, H.P., Tieloff, M., Schwarz, W.H., 2013, Thermal evolution model for the H chondrite asteroid-instantaneous formation versus protracted accretion: *Icarus*, vol. 226, no. 1, pp. 212–228.
- Herndon, J.M., Rowe, M.W., Larson, E.E., Watson, D.E., 1976, Thermomagnetic analysis of meteorites, 3. C3 and C4 chondrites: *Earth Planet. Sci. Lett.*, vol. 29, no. 2, pp. 283–290.
- Hewins, R.H., Radomsky, P.M., 1990, Temperature conditions for chondrule formation: *Meteorit. Planet. Sci.*, vol. 25, no. 4, pp. 309–318.
- Hezel, D.C., Elangovan, P., Viehmann, S., Howard, L., 2013, Visualisation and quantification of CV chondrite petrography using micro-tomography: *Geochim. Cosmochim. Acta*, vol. 116, pp. 33–40.
- Hood, L.L., Horanyi, M., 1991, Gas dynamic heating of chondrule precursor grains in the solar nebula: *Icarus*, vol. 93, no. 2, pp. 259–269.
- Hood, L.L., Weidenschilling, S.J., 2012, The planetesimal bow shock model for chondrule formation: A more quantitative assessment of the standard (fixed Jupiter) case: *Meteorit. Planet. Sci.*, vol. 47, no. 11, pp. 1715–1727.
- Howard, K.T., Benedix, G.K., Bland, P.A., Cressey, G., 2010, Modal mineralogy of CV3 chondrites by X-ray diffraction (PSD-XRD): *Geochim. Cosmochim. Acta*, vol. 74, no. 17, pp. 5084–5097.
- Hughes, D.W., 1978, A disaggregation and thin section analysis of the size and mass distribution of the chondrules in the Bjurböle and Chainpur meteorites: *Earth Planet. Sci. Lett.*, vol. 38, no. 2, pp. 391–400.
- Huss, G.R., Rubin, A.E., Grossman, J.N., 2006, Thermal metamorphism in chondrites, in: *Meteorites and the Early Solar System II*, University of Arizona Press, pp. 567–586.
- Hutchinson, R., Alexander, C.M.O., Barber, D.J., 1987, The Semarkona meteorite: First recorded occurrence of smectite in an ordinary chondrite, and its implications: *Geochim. Cosmochim. Acta*, vol. 51, no. 7, pp. 1875–1882.
- Imae, N., Isobe, H., 2017, An experimental study of chondrule formation from chondritic precursors via evaporation and condensation in Knudsen cell: Shock heating model of dust aggregates: *Earth Planet. Sci. Lett.*, vol. 473, pp. 256–268.
- Jackson, M., Aubourg, C., 1992, Rock magnetism and the interpretation of anisotropy of magnetic

- susceptibility: *Reviews of Geophysics*, vol. 30, no. 3, pp. 209–226.
- Jogo, K., Nakamura, T., Noguchi, T., Zolotov, M.Y., 2009, Fayalite in the Vigarano CV3 carbonaceous chondrite: Occurrences, formation age and conditions: *Earth Planet. Sci. Lett.*, vol. 287, no. 3-4, pp. 320–328.
- Johansen, A., Low, M.M.M., Lacerda, P., Bizzarro, M., 2015, Growth of asteroids, planetary embryos, and Kuiper belt objects by chondrule accretion: *Sci. Adv.*, vol. 1, no. 3, pp. e1500109–e1500109.
- Johansen, A., Youdin, A., 2007, Protoplanetary Disk Turbulence Driven by the Streaming Instability: Nonlinear Saturation and Particle Concentration: *Astrophys. J.*, vol. 662, no. 1, pp. 627–641.
- Johansen, A., Youdin, A., Klahr, H., 2009, Zonal Flows And Long-Lived Axisymmetric Pressure Bumps In Magnetorotational Turbulence: *Astrophys. J.*, vol. 697, no. 2, pp. 1269–1289.
- Johnson, H.P., Merrill, R.T., 1972, Magnetic and mineralogical changes associated with low-temperature oxidation of magnetite: *J. Geophys. Res.*, vol. 77, no. 2, pp. 334–341.
- Johnson, H.P., Merrill, R.T., 1974, Low-temperature oxidation of a single-domain magnetite: *J. Geophys. Res.*, vol. 79, no. 35, pp. 5533–5534.
- Johnson, B.C., Minton, D.A., Melosh, H.J., Zuber, M.T., 2015, Impact jetting as the origin of chondrules: *Nature*, vol. 517, no. 7534, pp. 339–341.
- Jones, R.H., Danielson, L.R., 1997, A chondrule origin for dusty relict olivine in unequilibrated chondrites: *Meteorit. Planet. Sci.*, vol. 32, no. 6, pp. 753–760.
- Kasama, T., Dunin-Borkowski, R.E., Beleggia, M., 2011, Electron Holography of Magnetic Materials, in: *Holography—Different Fields of Application*, InTech, pp. 53–80.
- Ketcham, R.A., 2005, Computational methods for quantitative analysis of three-dimensional features in geological specimens: *Geosphere*, vol. 1, no. 1, pp. 32–41.
- Kirschvink, J.L., 1980, The least-squares line and plane and the analysis of palaeomagnetic data: *Geophys. J. Int.*, vol. 62, no. 3, pp. 699–718.
- Kita, N.T., Nagahara, H., Togashi, S., Morishita, Y., 2000, A short duration of chondrule formation in the solar nebula: evidence from ²⁶Al in Semarkona ferromagnesian chondrules: *Geochim. Cosmochim. Acta*, vol. 64, no. 22, pp. 3913–3922.
- Kittel, C., 1949, Physical Theory of Ferromagnetic Domains: *Reviews of Modern Physics*, vol. 21, no. 4, pp. 541–583.
- Kletetschka, G., Kohout, T., 2003, Magnetic remanence in the Murchison meteorite: *Meteorit. Planet. Sci.*, vol. 38, no. 3, pp. 399–405.
- Kletetschka, G., Zila, V., Wasilewski, P.T., 2010, Magnetic Effects of Allende and Bjurböle Chondrules Moving from Space to Terrestrial Environments: *Lunar and Planetary Science Conference*, vol. 41, p. 1273.
- Kneller, E.F., Luborsky, F.E., 1963, Particle Size Dependence of Coercivity and Remanence of Single-Domain Particles: *J. Appl. Phys.*, vol. 34, no. 3, pp. 656–658.
- Koenigsberger, J.G., 1930, Ueber die magnetische Eigenschaft von Gesteinen: *J. Geophys. Res.*, vol. 35, no. 3, pp. 145–148.
- Kojima, T., Tomeoka, K., Takeda, H., 1993, Unusual dark clasts in the Vigarano CV3 carbonaceous chondrite: Record of parent body process: *Meteoritics*, vol. 28, no. 5, pp. 649–658.
- Krot, A.N., Meibom, A., Keil, K., 2000, A clast of Bali-like oxidized CV material in the reduced CV chondrite breccia Vigarano: *Meteorit. Planet. Sci.*, vol. 35, no. 4, pp. 817–825.
- Krot, A.N., Scott, E.R.D., Zolensky, M.E., 1995, Mineralogical and chemical modification of components in CV3 chondrites: Nebular or asteroidal processing?: *Meteorit. Planet. Sci.*, vol. 30, no. 6, pp. 748–775.
- Krot, A.N., Zolensky, M.E., Wasson, J.T., Scott, E.R.D., Keil, K., Ohsumi, K., 1997, Carbide-magnetite assemblages in type-3 ordinary chondrites: *Geochim. Cosmochim. Acta*, vol. 61, no. 1,

pp. 219–237.

- Kruiver, P.P., Dekkers, M.J., Heslop, D., 2001, Quantification of magnetic coercivity components by the analysis of acquisition curves of isothermal remanent magnetisation: *Earth Planet. Sci. Lett.*, vol. 189, no. 3-4, pp. 269–276.
- Lambrechts, M., Johansen, A., 2012, Rapid growth of gas-giant cores by pebble accretion: *Astronomy & Astrophysics*, vol. 544, p. A32.
- Laneuville, M., Wieczorek, M.A., Breuer, D., Aubert, J., Morard, G., Rckriemen, T., 2014, A long-lived lunar dynamo powered by core crystallization: *Earth Planet. Sci. Lett.*, vol. 401, pp. 251–260.
- Lanoix, M., Strangway, D.W., 1978, The primordial magnetic field preserved in chondrules of the Allende meteorite: *Geophys. Res. Lett.*, vol. 5, no. 1, pp. 73–76.
- Lappe, S., Church, N.S., Kasama, T., Bromiley, G., Dunin Borkowski, R.E., Feinberg, J.M., Russell, S.S., Harrison, R.J., 2011, Mineral magnetism of dusty olivine: A credible recorder of pre-accretionary remanence: *Geochem Geophys.*, vol. 12, no. 12, p. Q12Z35.
- Lappe, S.C.L.L., Feinberg, J.M., Muxworthy, A., Harrison, R.J., 2013, Comparison and calibration of nonheating paleointensity methods: A case study using dusty olivine: *Geochem Geophys.*, vol. 14, no. 7, pp. 2143–2158.
- Lee, D.C., Halliday, A.N., 1996, Hf-W Isotopic Evidence for Rapid Accretion and Differentiation in the Early Solar System: *Science*, vol. 274, no. 5294, pp. 1876–1879.
- Lee, M.R., Hutchinson, R., Graham, A.L., 1996, Aqueous alteration in the matrix of the Vigarano (CV3) carbonaceous chondrite: *Meteorit. Planet. Sci.*, vol. 31, no. 4, pp. 477–483.
- Lemelle, L., Guyot, F., Fialin, M., Pargamin, J., 2000, Experimental study of chemical coupling between reduction and volatilization in olivine single crystals: *Geochim. Cosmochim. Acta*, vol. 64, no. 18, pp. 3237–3249.
- Lerner, G.A., Smirnov, A.V., Surovitekkii, L.V., Piispa, E.J., 2017, Nonheating methods for absolute paleointensity determination: Comparison and calibration using synthetic and natural magnetite-bearing samples: *Journal of Geophysical Research*, vol. 112, no. E6, pp. 323–1633.
- Leroux, H., Libourel, G., Lemelle, L., Guyot, F., 2003, Experimental study and TEM characterization of dusty olivines in chondrites: Evidence for formation by in situ reduction: *Meteorit. Planet. Sci.*, vol. 38, no. 1, pp. 81–94.
- Levi, S., 1977, The effect of magnetite particle size on paleointensity determinations of the geomagnetic field: *Phys. Earth Planet. Int.*, vol. 13, no. 4, pp. 245–259.
- Levison, H.F., Kretke, K.A., Duncan, M.J., 2015, Growing the gas-giant planets by the gradual accumulation of pebbles: *Nature*, vol. 524, no. 7565, pp. 322–324.
- Levy, E.H., Araki, S., 1989, Magnetic reconnection flares in the protoplanetary nebula and the possible origin of meteorite chondrules: *Icarus*, vol. 81, pp. 74–91.
- Libourel, G., Chaussidon, M., 1995, Experimental constraints on chondrule reduction: *Meteoritics*, vol. 30, no. 5, p. 536.
- Lima, E.A., Weiss, B.P., 2016, Ultra-high sensitivity moment magnetometry of geological samples using magnetic microscopy: *Geochem Geophys.*, vol. 17, no. 9, pp. 3754–3774.
- Lindsley, D.H., Andersen, D.J., 1983, A two-pyroxene thermometer: *J. Geophys. Res.*, vol. 88, no. S02, p. A887.
- Louzada, K.L., Stewart, S.T., Weiss, B.P., 2007, Effect of shock on the magnetic properties of pyrrhotite, the Martian crust, and meteorites: *Geophys. Res. Lett.*, vol. 34, no. 5, p. 790.
- Lovering, J.F., 1959, The magnetic field in a primary meteorite body: *American Journal of Science*, vol. 257, no. 4, pp. 271–275.
- Lovering, J.F., Parry, L.G., Jaeger, J.C., 1960, Temperatures and mass losses in iron meteorites during ablation in the earth's atmosphere: *Geochim. Cosmochim. Acta*, vol. 19, no. 3, pp. 156–167.

- Lurcock, P.C., Wilson, G.S., 2012, Puffinplot: A versatile, user-friendly program for paleomagnetic analysis: *Geochemistry, Geophysics, Geosystems*, vol. 13, no. 6.
- Mann, C.R., Boley, A.C., Morris, M.A., 2016, Planetary Embryo Bow Shocks As A Mechanism For Chondrule Formation: *Astrophys. J.*, vol. 818, no. 2, p. 103.
- Mason, B.H., Wiik, H.B., 1962, Descriptions of two meteorites: Karoonda and Erakot: *American Museum Novitates*, vol. 2115, pp. 1–10.
- Matsumoto, Y., Oshino, S., Hasegawa, Y., Wakita, S., 2017, Chondrule Accretion with a Growing Protoplanet: *Astrophys. J.*, vol. 837, no. 2, p. 103.
- Mayergoyz, I.D., 1986, Mathematical models of hysteresis: *IEEE Trans. Magn.*, vol. 22, no. 5, pp. 603–608.
- McCord, T.B., Adams, J.B., Johnson, T.V., 1970, Asteroid Vesta: Spectral Reflectivity and Compositional Implications: *Science*, vol. 168, no. 3938, pp. 1445–1447.
- McNally, C.P., Hubbard, A., Mac Low, M.M., Ebel, D.S., D'Alessio, P., 2013, Mineral Processing By Short Circuits In Protoplanetary Disks: *Astrophys. J.*, vol. 767, no. 1, p. L2.
- McSween, H.Y.J., 1977, Chondrules as condensation products: *IAU Colloq. 39: Comets, Asteroids, Meteorites: Interrelations, Evolution and Origins*, pp. 365–373.
- Menzies, O.N., Bland, P.A., Berry, F.J., Cressey, G., 2005, A Mössbauer spectroscopy and X-ray diffraction study of ordinary chondrites: Quantification of modal mineralogy and implications for redox conditions during metamorphism: *Meteorit. Planet. Sci.*, vol. 40, no. 7, pp. 1023–1042.
- Midgley, P.A., Dunin Borkowski, R.E., 2009, Electron tomography and holography in materials science: *Nat. Mater.*, vol. 8, no. 4, pp. 271–280.
- Miura, H., Nakamoto, T., 2005, A shock-wave heating model for chondrule formation II. Minimum size of chondrule precursors: *Icarus*, vol. 175, no. 2, pp. 289–304.
- Morris, M.A., Boley, A.C., Desch, S.J., Athanassiadou, T., 2012, Chondrule Formation In Bow Shocks Around Eccentric Planetary Embryos: *Astrophys. J.*, vol. 752, no. 1, p. 27.
- Morrish, A.H., Yu, S.P., 1955, Dependence of the Coercive Force on the Density of Some Iron Oxide Powders: *J. Appl. Phys.*, vol. 26, no. 8, pp. 1049–1055.
- Mothé-Diniz, T., Carvano, J.M., Bus, S.J., Duffard, R., Burbine, T.H., 2008, Mineralogical analysis of the Eos family from near-infrared spectra: *Icarus*, vol. 195, no. 1, pp. 277–294.
- Muxworthy, A.R., Bland, P.A., Davison, T.M., Moore, J., Collins, G.S., Ciesla, F.J., 2017, Evidence for an impact-induced magnetic fabric in Allende, and exogenous alternatives to the core dynamo theory for Allende magnetization: *Meteorit. Planet. Sci.*, vol. 112, p. B03S90.
- Muxworthy, A.R., Dunlop, D.J., Williams, W., 2003, High-temperature magnetic stability of small magnetite particles: *J. Geophys. Res.*, vol. 108, no. B5, p. 7602.
- Muxworthy, A.R., Heslop, D., 2011, A Preisach method for estimating absolute paleofield intensity under the constraint of using only isothermal measurements: 1. Theoretical framework: *J. Geophys. Res.*, vol. 116, no. B4, p. B04102.
- Muxworthy, A.R., Williams, W., 2006, Critical single-domain/multidomain grain sizes in non-interacting and interacting elongated magnetite particles: Implications for magnetosomes: *J. Geophys. Res.*, vol. 111, no. B12.
- Muxworthy, A.R., Williams, W., 2015, Critical single-domain grain sizes in elongated iron particles: implications for meteoritic and lunar magnetism: *Geophys. J. Int.*, vol. 202, no. 1, pp. 578–583.
- Nagahara, H., 1981, Evidence for secondary origin of chondrules: *Nature*, vol. 292, no. 5819, pp. 135–136.
- Nagashima, K., Krot, A.N., Komatsu, M., 2017, 26 Al-26 Mg systematics in chondrules from Kaba and Yamato 980145 CV3 carbonaceous chondrites: *Geochim. Cosmochim. Acta*, vol. 201, pp. 303–319.
- Nagata, T., 1979, Meteorite magnetism and the early solar system magnetic field: *Phys. Earth Planet. Int.*, vol. 20, no. 2-4, pp. 324–341.

- Nagata, T., Funaki, M., 1982, Magnetic properties of tetrataenite-rich stony meteorites: National Institute Polar Research Memoirs, vol. 25, pp. 222–250.
- Nagy, L., Williams, W., Muxworthy, A.R., Fabian, K., Almeida, T.P., Conbhuí, P.Ó., Shcherbakov, V.P., 2017, Stability of Equidimensional Pseudo-Single Domain Magnetite Over Billion Year Time-Scales: PNAS, vol. In press.
- Nakamoto, T., Hayashi, M.R., Kita, N.T., Tachibana, S., 1996, Chondrule-forming shock waves in the solar nebula by X-ray flares, in: *Chond. Proto. Disk. ASP Conf. Series.*, Cambridge University Press, p. 883.
- Néel, L., 1949, Influence of thermal fluctuations on the magnetization of ferromagnetic small particles: C. R. Acad. Sci. Paris, vol. 228, no. 8, pp. 664–666.
- Néel, L., 1955a, Some theoretical aspects of rock-magnetism: *Advances in Physics*, vol. 4, no. 14, pp. 191–243.
- Néel, L., 1955b, Some theoretical aspects of rock-magnetism: *Advances in Physics*, vol. 4, no. 14, pp. 191–243.
- Nichols, C.I.O., Bryson, J.F.J., Herrero-Albillos, J., Kronast, F., Nimmo, F., Harrison, R.J., 2016, Pallasite paleomagnetism: Quiescence of a core dynamo: *Earth Planet. Sci. Lett.*, vol. 441, pp. 103–112.
- Noguchi, T., 1993, Petrology and mineralogy of CK chondrites: Implications for the metamorphism of the CK chondrite parent body, in: *Proc. NIPR Symp. Antarct. Meteorites*, pp. 204–233.
- Nyquist, L., Lindstrom, D., Mittlefehldt, D., Shih, C.Y., Wiesmann, H., Wentworth, S., Martinez, R., 2001, Manganese-chromium formation intervals for chondrules from the Bishunpur and Chainpur meteorites: *Meteorit. Planet. Sci.*, vol. 36, no. 7, pp. 911–938.
- Ohnishi, I., Tomeoka, K., Ishizaki, N., 2007, Microinclusion-rich vesicular olivine in the Karoonda CK4 chondrite: transmission electron microscopy: *Journal of Mineralogical and Petrological Sciences*, vol. 102, no. 6, pp. 346–351.
- Orchowski, A., Rau, W.D., Lichte, H., 1995, Electron holography surmounts resolution limit of electron microscopy: *Phys. Rev. Lett.*, vol. 74, no. 3, pp. 399–402.
- Özdemir, Ö., Dunlop, D.J., 1985, An experimental study of chemical remanent magnetizations of synthetic monodomain titanomaghemites with initial thermoremanent magnetizations: *J. Geophys. Res.*, vol. 90, no. B13, pp. 11513–11523.
- Pickett, B.K., Mejia, A.C., Durisen, R.H., Cassen, P.M., Berry, D.K., Link, R.P., 2003, The Thermal Regulation of Gravitational Instabilities in Protoplanetary Disks: *Astrophys. J.*, vol. 590, no. 2, pp. 1060–1080.
- Pike, C., Fernandez, A., 1999, An investigation of magnetic reversal in submicron-scale Co dots using first order reversal curve diagrams: *J. Appl. Phys.*, vol. 85, no. 9, pp. 6668–6676.
- Pike, C.R., Roberts, A.P., Dekkers, M.J., Verosub, K.L., 2001, An investigation of multi-domain hysteresis mechanisms using FORC diagrams: *Phys. Earth Planet. Int.*, vol. 126, no. 1-2, pp. 11–25.
- Prinz, M., Weisberg, M.K., Nehru, C.E., Delaney, J.S., 1985, ALHA 81189, a highly unequilibrated enstatite chondrite: evidence for a multistage history: *Meteoritics*, vol. 20, p. 731.
- Rambaldi, E.R., 1981, Relict grains in chondrules: *Nature*, vol. 293, no. 5833, pp. 558–561.
- Rambaldi, E.R., Wasson, J.T., 1981, Metal and associated phases in Bishunpur, a highly unequilibrated ordinary chondrite: *Geochim. Cosmochim. Acta*, vol. 45, no. 7, pp. 1001–1015.
- Ramdohr, P., 1963, The opaque minerals in stony meteorites: *J. Geophys. Res.*, vol. 68, no. 7, pp. 2011–2036.
- Rimbert, F., 1959, Contribution à l'étude de l'action des champs alternatifs sur les aimantations remanentes de roches: *Rev. Inst. Fr. Petrole Ann. Combust. Liquides*, vol. 14, p. 17.
- Ringwood, A.E., 1959, On the chemical evolution and densities of the planets: *Geochim. Cosmochim. Acta*, vol. 15, no. 4, pp. 257–283.

- Roberts, A.P., Pike, C.R., Verosub, K.L., 2000, First-order reversal curve diagrams: A new tool for characterizing the magnetic properties of natural samples: *J. Geophys. Res.*, vol. 105, no. B12, pp. 28461–28475.
- Robertson, D.J., France, D.E., 1994, Discrimination of remanence-carrying minerals in mixtures, using isothermal remanent magnetisation acquisition curves: *Phys. Earth Planet. Int.*, vol. 82, no. 3-4, pp. 223–234.
- Rochette, P., Gattacceca, J., Bonal, L., Bourot-Denise, M., Chevrier, V., Clerc, J.P., Consolmagno, G., Folco, L., Gounelle, M., Kohout, T., Pesonen, L., Quirico, E., Sagnotti, L., Skripnik, A., 2008, Magnetic classification of stony meteorites: 2. Non-ordinary chondrites: *Meteorit. Planet. Sci.*, vol. 43, no. 5, pp. 959–980.
- Rochette, P., Gattacceca, J., Bourot-Denise, M., Consolmagno, G., Folco, L., Kohout, T., Pesonen, L., Sagnotti, L., 2009, Magnetic classification of stony meteorites: 3. Achondrites: *Meteorit. Planet. Sci.*, vol. 44, no. 3, pp. 405–427.
- Rochette, P., Sagnotti, L., 2003, Magnetic classification of stony meteorites: 1. Ordinary chondrites: *Meteorit. Planet. Sci.*, vol. 38, no. 2, pp. 251–268.
- Rubin, A.E., 1992, A shock-metamorphic model for silicate darkening and compositionally variable plagioclase in CK and ordinary chondrites: *Geochim. Cosmochim. Acta*, vol. 56, no. 4, pp. 1705–1714.
- Ruzicka, A., Hugo, R., Hutson, M., 2015, Deformation and thermal histories of ordinary chondrites: Evidence for post-deformation annealing and syn-metamorphic shock: *Geochimica et Cosmochimica Acta*, vol. 163, pp. 219–233.
- Sahijpal, S., Gupta, G., 2011, Did the carbonaceous chondrites evolve in the crustal regions of partially differentiated asteroids?: *J. Geophys. Res.*, vol. 116, no. E6, p. B03S90.
- Schabes, M.E., Bertram, H.N., 1988, Magnetization processes in ferromagnetic cubes: *J. Appl. Phys.*, vol. 64, no. 3, pp. 1347–1357.
- Scheinberg, A., Elkins-Tanton, L.T., Schubert, G., Bercovici, D., 2016, Core solidification and dynamo evolution in a mantle-stripped planetesimal: *J. Geophys. Res.*, vol. 121, no. 1, pp. 2–20.
- Scherstén, A., Elliott, T., Hawkesworth, C., Russell, S., 2006, Hf–W evidence for rapid differentiation of iron meteorite parent bodies: *Earth Planet. Sci. Lett.*, vol. 241, no. 3-4, pp. 530–542.
- Scott, E.R.D., 2007, Chondrites and the protoplanetary disk: *Annu. Rev. Earth Planet. Sci.*, vol. 35, no. 1, pp. 577–620.
- Scott, E.R., Keil, K., Stoeffler, D., 1992, Shock metamorphism of carbonaceous chondrites: *Geochimica et Cosmochimica Acta*, vol. 56, no. 12, pp. 4281–4293.
- Scott, E.R.D., Lusby, D., Keil, K., 1985, Ubiquitous brecciation after metamorphism in equilibrated ordinary chondrites: *J. Geophys. Res.*, vol. 90, no. S01, pp. 137–148.
- Sears, D., 2004, *The origin of chondrules and chondrites*, Cambridge University Press, Cambridge.
- Sears, D.W., Grossman, J.N., Melcher, C.L., Ross, L.M., Mills, A.A., 1980, Measuring metamorphic history of unequilibrated ordinary chondrites: *Nature*, vol. 287, no. 5785, pp. 791–795.
- Seitz, H.M., Schoelmerich, M.O., Gaspers, N., Marco, L., Hofer, H.E., Will, S., Zipfel, J., 2016, Duration of Chondrite Parent Body Peak Metamorphic Conditions Deduced from Lithium Partitioning Between Chondrules and Matrix in Unequilibrated and Equilibrated Carbonaceous and Ordinary Chondrites: *Lunar and Planetary Science Conference*, vol. 47, p. 1459.
- Selkin, P.A., Tauxe, L., 2000, Long-term variations in palaeointensity: *Philos. Trans. R. Soc. A-Math. Phys. Eng. Sci.*, vol. 358, no. 1768, pp. 1065–1088.
- Shah, J., Bates, H.C., Muxworthy, A.R., Hezel, D.C., Russell, S.S., Genge, M.J., 2017, Long-lived magnetism on chondrite parent bodies: *Earth Planet. Sci. Lett.*, vol. 475, pp. 106–118.
- Shu, F.H., Shang, H., Glassgold, A.E., Lee, T., 1997, X-rays and fluctuating x-winds from proto-stars: *Science*, vol. 277, no. 5331, pp. 1475–1479.
- Shu, F.H., Shang, H., Lee, T., 1996, Toward an astrophysical theory of chondrites: *Science*, vol.

- 271, no. 5255, pp. 1545–1552.
- Smith, C., Ahmed, F., Sykes, D., Schroeven-Deceuninck, H., 2013, X-ray Microtomography of Martian Meteorites and Implications for Mars Sample Return: EGU General Assembly Conference Abstracts, vol. 15.
- Smith, M.R., Laul, J.C., Ma, M.S., Huston, T., Verkouteren, R.M., Lipschutz, M.E., Schmitt, R.A., 1984, Petrogenesis of the SNC (shergottites, nakhlites, chassignites) meteorites: Implications for their origin from a large dynamic planet, possibly Mars: *J Geophys. Res.*, vol. 89, no. S02, p. B612.
- Snoeck, E., Gatel, C., Lacroix, L.M., Blon, T., Lachaize, S., Carrey, J., Respaud, M., Chaudret, B., 2008, Magnetic Configurations of 30 nm Iron Nanocubes Studied by Electron Holography: *Nano Letters*, vol. 8, no. 12, pp. 4293–4298.
- Stacey, F.D., 1963, The physical theory of rock magnetism: *Advances in Physics*, vol. 12, no. 45, pp. 45–133.
- Stacey, F.D., 1967, The Koenigsberger ratio and the nature of thermoremanence in igneous rocks: *Earth Planet. Sci. Lett.*, vol. 2, no. 1, pp. 67–68.
- Stacey, F.D., 1976, Paleomagnetism of meteorites: *Ann. Rev. Earth Planet. Sci.*, vol. 4, no. 1, pp. 147–157.
- Stacey, F., Banerjee, S.K., 1974, *The Physical Principles of Rock Magnetism*, Elsevier.
- Stacey, F.D., Lovering, J.F., Parry, L.G., 1961, Thermomagnetic properties, natural magnetic moments, and magnetic anisotropies of some chondritic meteorites: *J. Geophys. Res.*, vol. 66, no. 5, pp. 1523–1534.
- Stephenson, A., Collinson, D.W., 1974, Lunar magnetic field palaeointensities determined by an anhysteretic remanent magnetization method: *Earth Planet. Sci. Lett.*, vol. 23, no. 2, pp. 220–228.
- Sterenborg, M.G., Crowley, J.W., 2013, Thermal evolution of early solar system planetesimals and the possibility of sustained dynamos: *Phys. Earth Planet. Int.*, vol. 214, pp. 53–73.
- Stöffler, D., Keil, K., Edward R D, S., 1991, Shock metamorphism of ordinary chondrites: *Geochim. Cosmochim. Acta*, vol. 55, no. 12, pp. 3845–3867.
- Strangway, D.W., Larson, E.E., Goldstein, M., 1968, A possible cause of high magnetic stability in volcanic rocks: *J. Geophys. Res.*, vol. 73, no. 12, pp. 3787–3795.
- Strangway, D.W., Sugiura, N., 1982, Early solar system magnetic fields as recorded in meteorites: *Advances in Space Research*, vol. 2, no. 12, pp. 41–51.
- Suess, D., Tsiantos, V., Schrefl, T., Fidler, J., Scholz, W., Forster, H., Dittrich, R., Miles, J.J., 2002, Time resolved micromagnetics using a preconditioned time integration method: *J. Magn. Mater.*, vol. 248, no. 2, pp. 298–311.
- Sugiura, N., 1977, Magnetic properties and remanent magnetization of stony meteorites: *Journal of Geomagnetism and Geoelectricity*, vol. 29, pp. 519–539.
- Sugiura, N., Lanoix, M., Strangway, D.W., 1979, Magnetic fields of the solar nebula as recorded in chondrules from the Allende meteorite: *Phys. Earth Planet. Int.*, vol. 20, no. 2-4, pp. 342–349.
- Sugiura, N., Strangway, D.W., 1983, A paleomagnetic conglomerate test using the Abee E4 meteorite: *Earth Planet. Sci. Lett.*, vol. 62, no. 1, pp. 169–179.
- Tarduno, J.A., Blackman, E.G., Mamajek, E.E., 2014, Detecting the oldest geodynamo and attendant shielding from the solar wind: Implications for habitability: *Phys. Earth Planet. Int.*, vol. 233, pp. 68–87.
- Tarduno, J.A., Cottrell, R.D., Nimmo, F., Hopkins, J., Voronov, J., Erickson, A., Blackman, E., Scott, E.R.D., McKinley, R., 2012, Evidence for a Dynamo in the Main Group Pallasite Parent Body: *Science*, vol. 338, no. 6109, pp. 939–942.
- Tarduno, J.A., O'Brien, T.M., Smirnov, A.V., 2016, Does the Magnetization of CV Meteorites Record a Parent Body Core Dynamo?: *Lunar and Planetary Science Conference*, vol. 47, p. 2609.

- Tauxe, L., 2010, *Essentials of Paleomagnetism*, University of California Press.
- Thellier, E., 1959, Sur l'intensité du champ magnétique terrestre dans le passé historique et géologique: *Ann. Geophys.*, vol. 15, pp. 285–376.
- Tikoo, S.M., Gattacceca, J., Swanson-Hysell, N.L., Weiss, B.P., Suavet, C., Cournède, C., 2015, Preservation and detectability of shock-induced magnetization: *J. Geophys. Res.*, vol. 120, no. 9, pp. 1461–1475.
- Tikoo, S.M., Weiss, B.P., Buz, J., Lima, E.A., Shea, E.K., Melo, G., Grove, T.L., 2012, Magnetic fidelity of lunar samples and implications for an ancient core dynamo: *Earth Planet. Sci. Lett.*, vol. 337–338, pp. 93–103.
- Tomeoka, K., Ohnishi, I., Nakamura, N., 2001, Silicate darkening in the Kobe CK chondrite: Evidence for shock metamorphism at high temperature: *Meteorit. Planet. Sci.*, vol. 36, no. 11, pp. 1535–1545.
- Tomeoka, K., Tanimura, I., 2000, Phyllosilicate-rich chondrule rims in the vigarano cv3 chondrite: evidence for parent-body processes: *Geochim. Cosmochim. Acta*, vol. 64, no. 11, pp. 1971–1988.
- Tsuchiyama, A., Osada, Y., Nakano, T., Uesugi, K., 2004, Experimental reproduction of classic barred olivine chondrules: Open-system behavior of chondrule formation: *Geochim. Cosmochim. Acta*, vol. 68, no. 3, pp. 653–672.
- Uehara, M., Gattacceca, J., Leroux, H., Jacob, D., van der Beek, C.J., 2011, Magnetic microstructures of metal grains in equilibrated ordinary chondrites and implications for paleomagnetism of meteorites: *Earth Planet. Sci. Lett.*, vol. 306, no. 3–4, pp. 241–252.
- Uehara, M., Gattacceca, J., Rochette, P., Demory, F., Valenzuela, E.M., 2012, Magnetic study of meteorites recovered in the Atacama Desert (Chile): Implications for meteorite paleomagnetism and the stability of hot desert surfaces: *Physics of the Earth and Planetary Interiors*, vol. 200, pp. 113–123.
- Uehara, M., Nakamura, N., 2006, Experimental constraints on magnetic stability of chondrules and the paleomagnetic significance of dusty olivines: *Earth Planet. Sci. Lett.*, vol. 250, no. 1–2, pp. 292–305.
- Urey, H.C., 1955, The cosmic abundances of potassium, uranium, and thorium and the heat balances of the Earth, the Moon, and Mars: *PNAS*, vol. 41, pp. 127–144.
- Verwey, E.J.W., 1939, Electronic Conduction of Magnetite (Fe₃O₄) and its Transition Point at Low Temperatures: *Nature*, vol. 144, no. 3642, pp. 327–328.
- Vilas, F., McFadden, L.A., 1992, CCD reflectance spectra of selected asteroids: *Icarus*, vol. 100, no. 1, pp. 85–94.
- von Tschermak, G., Wood, E.M., 1964, The microscopic properties of meteorites (*Die Mikroskopische Beschaffenheit der Meteoriten*), trans. Wood, J.A.: *Smith. Contr. Astrophys.*, vol. 4, no. 6, pp. 138–239.
- Wahl, W., 1952, The brecciated stony meteorites and meteorites containing foreign fragments: *Geochim. Cosmochim. Acta*, vol. 2, no. 2, pp. 91–117.
- Wakita, S., Matsumoto, Y., Oshino, S., Hasegawa, Y., 2017, Planetesimal collisions as a chondrule forming event: *Astrophys. J.*, vol. 834, no. 2, p. 125.
- Wang, H., Weiss, B.P., Bai, X.N., Downey, B.G., Wang, J., Wang, J., Suavet, C., Fu, R.R., Zucolotto, M.E., 2017, Lifetime of the solar nebula constrained by meteorite paleomagnetism: *Science*, vol. 355, no. 6325, pp. 623–627.
- Wang, H., Weiss, B.P., Downey, B.G., Wang, J., Chen-Wiegar, Y.K., Suavet, C.R., Fu, R.R., Lima, E.A., Zucolotto, M.E., 2015, Onset of a Planetesimal Dynamo and the Lifetime of the Solar Nebular Magnetic Field: *Lunar and Planetary Science Conference*, vol. 46, p. 2516.
- Wasilewski, P.J., 1982, Stable NRM and mineralogy in Allende: Chondrules, in: *Lunar and Planetary Sciences Conference*, pp. 1217–1227.
- Wasilewski, P., 1988, Magnetic characterization of the new magnetic mineral tetrataenite and its contrast with isochemical taenite: *Phys. Earth Planet. Int.*, vol. 52, no. 1–2, pp. 150–158.

- Wasilewski, P., Acuña, M.H., Kletetschka, G., 2002, 443 Eros: Problems with the meteorite magnetism record in attempting an asteroid match: *Meteorit. Planet. Sci.*, vol. 37, no. 7, pp. 937–950.
- Watson, G.S., 1956, A Test for Randomness of Directions: *Geophys. Suppl. MNRAS*, vol. 7, no. 4, pp. 160–161.
- Weiss, B.P., Berdahl, J.S., Elkins-Tanton, L., Stanley, S., Lima, E.A., Carporzen, L., 2008, Magnetism on the Angrite Parent Body and the Early Differentiation of Planetesimals: *Science*, vol. 322, no. 5902, pp. 713–716.
- Weiss, B.P., Carporzen, L., Elkins-Tanton, L.T., Zuber, M.T., Shuster, D.L., Ebel, D.S., Gattacceca, J., 2010a, Magnetic Tests For Partially Differentiated Chondrite Parent Bodies: Chondrules Their Role in Early Solar System History, vol. 8010.
- Weiss, B.P., Elkins-Tanton, L.T., 2013, Differentiated Planetesimals and the Parent Bodies of Chondrites: *Annu. Rev. Earth Planet. Sci.*, vol. 41, no. 1, pp. 529–560.
- Weiss, B.P., Gattacceca, J., Stanley, S., Rochette, P., Christensen, U.R., 2010b, Paleomagnetic Records of Meteorites and Early Planetesimal Differentiation: *Space. Sci. Rev.*, vol. 152, no. 1-4, pp. 341–390.
- Weiss, B.P., Wang, H., Sharp, T.G., Gattacceca, J., Shuster, D.L., Downey, B., Hu, J., Fu, R.R., Kuan, A.T., Suavet, C., Irving, A.J., Wang, J., Wang, J., 2017, A nonmagnetic differentiated early planetary body: *Earth Planet. Sci. Lett.*, vol. 468, pp. 119–132.
- Westphal, M., 1986, Natural remanent magnetization, thermoremanent magnetization and reliability of palaeointensity determinations on H chondrites: *Phys. Earth Planet. Int.*, vol. 43, no. 4, pp. 300–306.
- Whipple, F.L., 1966, Chondrules: Suggestion Concerning the Origin: *Science*, vol. 153, no. 3731, pp. 54–56.
- Williams, W., Dunlop, D.J., 1989, Three-dimensional micromagnetic modelling of ferromagnetic domain structure: *Nature*, vol. 337, no. 6208, pp. 634–637.
- Williams, W., Wright, T.M., 1998, High-resolution micromagnetic models of fine grains of magnetite: *J. Geophys. Res.*, vol. 103, no. B12, pp. 30537–30550.
- Willis, J., Goldstein, J.I., 1982, A revision of metallographic cooling rate curves for chondrites: *Lunar and Planetary Science Conference*, vol. 12B, pp. 1135–1143.
- Windmark, F., Birnstiel, T., Güttler, C., Blum, J., Dullemond, C.P., Henning, T., 2012, Planetesimal formation by sweep-up: how the bouncing barrier can be beneficial to growth: *Astronomy & Astrophysics*, vol. 540, p. A73.
- Winklhofer, M., Fabian, K., Heider, F., 1997, Magnetic blocking temperatures of magnetite calculated with a three-dimensional micromagnetic model: *J. Geophys. Res.*, vol. 102, no. B10, pp. 22695–22709.
- Wood, J.A., 1958, Silicate meteorite structures and the origin of the meteorites, Ph.D. thesis, Massachusetts Institute of Technology.
- Wood, J.A., 1963, On the origin of chondrules and chondrites: *Icarus*, vol. 2, pp. 152–180.
- Wood, J.A., 1996, Processing of chondritic and planetary material in spiral density waves in the nebula: *Meteorit. Planet. Sci.*, vol. 31, no. 5, pp. 641–645.
- Wood, B.E., Müller, H.R., Redfield, S., Edelman, E., 2014, Evidence for a weak wind from the young Sun: *Astrophys. J.*, vol. 781, no. 2, p. L33.
- Yang, C.W., Williams, D.B., Goldstein, J.I., 1997, A new empirical cooling rate indicator for meteorites based on the size of the cloudy zone of the metallic phases: *Meteorit. Planet. Sci.*, vol. 32, no. 3, pp. 423–429.
- Youdin, A.N., Goodman, J., 2005, Streaming Instabilities in Protoplanetary Disks: *Astrophys. J.*, vol. 620, no. 1, pp. 459–469.
- Yu, Y., Doh, S.J., Kim, W., Min, K., 2011, Origin of stable remanent magnetization in LL6 chondrite, St. Séverin: *Phys. Earth Planet. Int.*, vol. 187, no. 3-4, pp. 292–300.

- Yu, Y., Tauxe, L., 2005, Testing the IZZI protocol of geomagnetic field intensity determination: *Geochem Geophys.*, vol. 6, no. 5.
- Zanda, B., 1996, Sodium and Sulfur in Chondrules: Heating Time and Cooling Curves, in: *Chondrules and the Protoplanetary Disk*, Cambridge University Press, pp. 213–219.
- Zanda, B., Bourot-Denise, M., Perron, C., Hewins, R.H., 1994, Origin and Metamorphic Redistribution of Silicon, Chromium, and Phosphorus in the Metal of Chondrites: *Science*, vol. 265, no. 5180, pp. 1846–1849.
- Zeigler, R.A., Almeida, N.V., Sykes, D., Smith, C.L., 2015, Micro Computed Tomography and Micro X-Ray Fluorescence and Tools for the Curation and Scientific Study of Apollo Samples, in: *38th Symp. Ant. Met.*
- Zhao, X., Heslop, D., Roberts, A.P., 2015, A protocol for variable-resolution first-order reversal curve measurements: *Geochem Geophys.*, vol. 16, no. 5, pp. 1364–1377.
- Zijderveld, J.D.A., 1967, AC demagnetization of rocks: analysis of results: *Methods in Paleomagnetism*, pp. 254–286.